

Julia BRUNBAUER

Dissertation

Faber est suae quisque fortunae

"Every man is the artisan of his own fortune"

Appius Claudius Caecus,
quoted by Sallust, 2. letter to Caesar, I.

Julia BRUNBAUER

Dissertation

Fatigue of continuously fibre reinforced composites -

Engineering approaches to fatigue-life prediction

January 2015

Institute of Materials Science and Testing of Polymers

Department Polymer Engineering and Science, Montanuniversitaet Leoben

About the Dissertation

This cumulative Dissertation was authored by

DI Julia BRUNBAUER

born 24. March 1988

in Steyr (Oberösterreich, Austria)

Conducted at

Institute of Materials Science and Testing of Polymers
Department Polymer Engineering and Science
Montanuniversitaet Leoben

Submitted to

Institute of Materials Science and Testing of Polymers
Department Polymer Engineering and Science
Montanuniversitaet Leoben

Academic Supervisor

Univ.-Prof. Dr. Gerald PINTER

Institute of Materials Science and Testing of Polymers
Department Polymer Engineering and Science
Montanuniversitaet Leoben

Part I.

Preamble

Affidavit

I declare in lieu of oath, that I wrote this thesis and performed the associated research myself, using only literature cited in this volume.

Julia Brunbauer

Leoben, January 2015

Acknowledgement

I would like to express my gratitude to all persons supporting me while performing this thesis at this point.

First of all, I want to thank my supervisor Univ.-Prof. Dr. Gerald PINTER (Institute of Materials Science and Testing of Polymers, Department Polymer Engineering and Science, Montanuniversitaet Leoben) for his support during the last years. I am grateful to him for giving me the chance to perform this thesis, for our inspiring discussions and his ability to share his scientific skills and knowledge. Gerald allowed me to work and research on my own without setting explicit boundaries which I enjoyed very much. Thanks to his confidence in my skills I had the chance to find my way through this thesis and to realise my ideas. It was a privilege for me getting supervised by Gerald.

Special thanks go to DI Hannes STADLER and DI Christian BANDION (TCKT – Transfercenter Kunststofftechnik GmbH) who produced the composite plates investigated in this thesis. They provided interesting insights in composite production and supervision of production processes which was very educational for me. I would like to thank them for their help and support in all of my requests and Hannes for acting as co-author.

I would also like to thank Dr. Christian GAIER (Magna Powertrain, Engineering Center Steyr GmbH & CoKG) for sharing his expertise in the field of fatigue-life prediction and for his support as co-author.

I want to thank my colleagues, especially DI Florian ARBEITER, Jürgen GROSSER and DI Steffen STELZER (Institute of Materials Science and Testing of Polymers, Department Polymer Engineering and Science,

Montanuniversitaet Leoben). They were always willing to help when it came to the setup of equipment, getting to know new test machines or just helping with little things which may come across during years of testing in the lab. Thanks to their excellent expertise, the progress of my work was significantly improved. Furthermore, our vivid discussions inspired me and were helpful to keep focused sometimes. I enjoyed the atmosphere at work and in our office very much and would like to thank them for making the years of my thesis such a nice time.

On this occasion, I do not want to miss the opportunity to thank the most important persons in my life, my family. I would like to express my deepest gratitude to my parents, Gertrude and Gottfried, for always supporting and believing in me. Without them, I would not be at this point in my life right now. I want to thank my siblings, Cornelia, Silvia and Gottfried and their partners Andreas, René and Anna. Special thanks go to Silvia, who supported the progress of this thesis as students' colleague in the lab and after work with runs or conversations.

On a final note, I would like to express my love and gratitude to my fiancé Alexander who encouraged and accompanied me in any possible way while performing this thesis.

Kurzfassung

Der durch das hohe Maß an CO₂ Emissionen eingeleitete Klimawandel ist eine der größten globalen Herausforderungen des 21. Jahrhunderts. Möglichkeiten um die notwendige Reduktion der Emissionen zu erzielen sind, unter anderem, die Erhöhung des Anteils erneuerbarer Energien am weltweiten Gesamtenergieverbrauch oder ein Umdenken in emissionsstarken Industriezweigen, wie beispielsweise im Transportwesen. Im Bereich der Transportindustrie, allen voran in der Flugzeug- und Automobilindustrie, wurden in den letzten Jahren bahnbrechende Entwicklungen erzielt. Flugzeuge in bis dato unbekannter Größe revolutionieren den Personenflugverkehr und neuartige Antriebskonzepte bieten im Automobilbau Alternativen zu fossilen Brennstoffen. Um derartige Neuentwicklungen so ressourceneffizient wie möglich zu gestalten, ist die Reduktion des bewegten Gesamtgewichtes eine essentielle Voraussetzung. Faserverbundwerkstoffe bieten für derartige Leichtbauanwendungen einzigartige Eigenschaften. Kohlenstofffaserverstärkte Kunststoffverbunde zählen heute zu den am weitesten verbreiteten Verbundwerkstoffen und besitzen herausragende Kennwerte bei gleichzeitig niedrigem Gewicht.

Um die Performance dieser Hochleistungsmaterialien in höchstbeanspruchten Strukturanwendungen gewährleisten zu können ist die Absicherung des Materialverhaltens von größter Bedeutung. Das inkludiert neben mechanischer Prüfung auch die rechnerische Auslegung. Eine Vielzahl von Versagenskriterien wurde dazu in den letzten Jahrzehnten weltweit entwickelt. Einige der Kriterien sind in der Lage, das anisotrope Materialverhalten der Verbundwerkstoffe korrekt abzubilden und Aussagen darüber zu liefern, unter welchen Lasten welche Art von Versagen zu erwarten ist. Allerdings sind die meisten dieser Versagenskriterien primär für

den quasi-statischen Lastfall entwickelt worden. In jenen Anwendungen, in denen Verbundwerkstoffe ihr Leichtbaupotential voll zur Entfaltung bringen können, treten aber im Normalfall nicht nur statische, sondern auch zyklische Lasten auf. Durch zyklische Beanspruchungen wie mechanische Lasten, Temperatur oder chemische Einwirkung tritt ein Prozess in Kraft, der gemeinhin als Ermüdung bezeichnet wird. Verbundwerkstoffe zeigen unter zyklischer Last nicht nur eine Reduktion der mechanischen Eigenschaften wie Festigkeit und Steifigkeit, sondern auch eine Reihe komplexer Schädigungsmechanismen, die matrix- oder faserdominert sein können, im Laufe der Lebensdauer interagieren und sich schließlich zum Versagen kumulieren können. Auf Grund der komplexen Vorgänge im Material ist eine Lebensdauervorhersage, die auf der tatsächlichen Abbildung der mikro-mechanischen Schädigungsmechanismen beruht, überaus komplex. Darüber hinaus müssen für eine umfassende Lebensdauervorhersage auch die Lastgeschichte und damit verbunden die Schädigungsvorgeschichte im Material mitberücksichtigt werden was dazu führt, dass es noch kein Vorhersagemodell gibt, das die Gesamtheit der wirkenden Einflüsse zufriedenstellend berücksichtigen kann.

Das Ziel der vorliegenden Arbeit war die Untersuchung möglicher Ansätze für die anwendungsorientierte Lebensdauervorhersage von endloskohlenstoff-faserverstärkten Verbundwerkstoffen. Um in der Lage zu sein, Vorhersagen auf fundierte experimentelle Daten zu stützen, wurden zunächst verschiedene Dehnmesssysteme auf ihre Eignung zur Messung zyklischer Dehnungen und der Einfluss verschiedenster Testparameter auf das Materialverhalten untersucht. In umfassenden Vorversuchen wurden dazu die Einflüsse von Faserorientierung, hysteretischer Erwärmung oder oberflächlicher Schädigung auf die Eignung der verwendeten Dehnmesssysteme validiert. Versuchsparameter für die folgende umfassende Materialcharakterisierung wurden definiert. Um darüber hinaus die Schädigungsvorgänge zu studieren, wurden neben dem Effekt der Anisotropie und der mechanischen Mittelspannung, auch der Einfluss des Faservolumengehaltes auf die mechanischen Eigenschaften und die ermüdungsbedingten Schädigungsmechanismen untersucht. Umfangreiche rasterelektronenmikroskopische Untersuchungen an den Bruchflächen getesteter Prüfkörper lieferten schlüssige Erklärungen für das experimentell

gemessene, mechanische Verhalten. Um der in den Versuchen auftretenden anisotropen Dehnratenabhängigkeit des Materials Rechnung zu tragen, wurde eine neue experimentelle Testmethode entwickelt, die es erlaubt die Messung zyklenabhängiger Steifigkeiten von Dehnrateneinflüssen zu entkoppeln. Basierend auf diesen Erkenntnissen wurden in der vorliegenden Arbeit zwei verschiedene Ansätze zur Lebensdauervorhersage verfolgt. Beide Ansätze können als ingenieurstechnisch betrachtet werden, da mikromechanische Effekte und Schädigung nicht explizit von den Modellen abgebildet werden, sondern vielmehr indirekt in den Eingabeparameter inkludiert sind. Als erster Ansatz wurde die klassische Laminattheorie, die für die Berechnung von Steifigkeiten und die schichtweise Spannungsanalyse von Laminaten für quasi-statische Lasten bekannt ist, für Ermüdungslasten erweitert. Durch die Implementierung der mittels der entwickelten Prüfmethode generierten dehnratenunabhängigen, zyklenabhängigen Steifigkeiten unidirektionaler Laminatverbunde konnten die ermüdungsinduzierten Steifigkeitsabfälle eines multidirektionalen Verbundes auf verschiedenen Lastniveaus korrekt vorhergesagt werden. Experimentelle Validierungen bestätigten die gute Übereinstimmung zwischen Experiment und Rechnung. Als zweite Berechnungsvariante wurde eine Adaption des festigkeitsbasierten Ansatzes der Wöhlerlinien, der für metallische Werkstoffe sehr weit verbreitet ist, angewandt. Die in Abhängigkeit der Anisotropie und der Mittelspannungen ermittelten Wöhlerlinien wurden verwendet, um die Lebensdauer eines unidirektionalen und eines multiaxialen Verbundes zu berechnen. Der Vorteil der dazu verwendeten Software besteht darin, dass beispielsweise Last-Zeit-Verläufe oder lokale Spannungsrechnungen aus Finite Elemente Berechnungen in die Lebensdauerabschätzung einfließen. Die Ergebnisse zeigten gute Korrelation mit den experimentellen Messungen und lieferten Anregungen für künftige Weiterentwicklungen um die spezifischen Eigenschaften endlosfaserverstärkter Verbundwerkstoffe in Zukunft noch besser abbilden zu können.

Abstract

The climate change, which has been significantly accelerated by the high amount of carbon dioxide emissions in the last decades, is one of the great challenges of the 21st century. Possibilities to meet the aspired aims and reduce the produced emissions are e.g. the increase of renewable energy fraction of the totally consumed energy or the conversion of big emission causers such as transportation. To revolutionise the transportation industry such as the aircraft or automotive industry, innovative developments have been presented during the last years. Airplanes are being built in new dimensions and novel drive concepts offer alternatives to fossil fuels in the automotive industry. However, to make new airplanes or drive concepts in cars as efficient as possible the reduction of the total weight is of essential importance. Carbon fibre reinforced plastics (CFRP) are among the most widely spread composite materials in these new applications due to their outstanding mechanical properties in relation to weight.

If composite materials are intended to be applied in highly-stressed applications, the assurance of mechanical properties and mechanical behaviour is of tremendous importance. This includes not only the experimental testing of the material but also predictive calculations. Various failure criteria being able to predict composite failure have been developed during the last decades. Some of the proposed criteria are able to take the highly anisotropic material behaviour resulting in fibre or matrix dominated damage modes into account and can predict the load cases causing failure properly. Most of the criteria can provide reasonable predictions for quasi-static loads. However, the high performance structures in which composites are most superior are exactly those in which fatigue is likely to occur. In general, fatigue is concerned with external influences such as mechanical

loading, thermal loading or chemical environments causing loss of properties such as stiffness or strength. The decrease of mechanical properties in composites is caused by complex damage mechanisms which may be fibre or matrix dominated which can interact and finally accumulate to final failure. As a consequence of these progresses, the fatigue-life prediction based on physical damage mechanisms is a very complex issue. The history the material has gone through, such as load or temperature, also has to be taken into account. Furthermore, it has to be considered that for life-time predictions the already damaged material state including the damage history has to be used. Comprehensive fatigue-life prediction theories covering the variety of influences do not exist so far.

The objective of this thesis was to investigate possibilities for application-oriented fatigue-life prediction approaches for continuously carbon fibre reinforced composites. In order to be able to build predictions on sufficient experimental data, a lot of effort was put into the assessment of different strain measurement techniques and the effects of experimental test parameters on the measured material properties. In preliminary fatigue tests the effects of fibre alignment, hysteretic heating or surface cracks on the reliability of the applied strain measurement techniques were assessed. Test set ups for the subsequent material characterisation were defined. Furthermore, it was important to study the unique fatigue-induced damage parameters in detail. Apart from the significant influence of anisotropy and mean stress on the mechanical properties and the damage mechanisms, the effect of fibre volume content was investigated. The fracture surfaces of tested specimens were studied in detail by scanning electron microscopy. The observed damage mechanisms were correlated with the measured mechanical properties and explained the observed correlations and effects. To be able to consider the strain-rate dependent material behaviour measured in the mechanical tests, a new experimental test procedure was developed. This experimental test procedure allowed the uncoupling of cyclic stiffness measurement from strain-rate dependent effects. By implementing this procedure in fatigue tests, a comprehensive mechanical data base reflecting fatigue stiffnesses and strengths of carbon/epoxy materials with different stacking sequences and tested at various angles was created. Based on the experimentally evaluated material properties, two different

approaches to fatigue-life prediction were pursued in this thesis. Both approaches might be considered as engineering approaches, since micro-mechanical effects and damage mechanisms are not taken into account explicitly but are already included in the experimentally measured input parameter. First, the classical laminate theory, which was initially developed for the calculation of composite material's stiffnesses based on the ply's stiffness parameters under quasi-static loads, was adapted for fatigue loads. By implementing the strain-rate independent stiffness properties of unidirectional carbon/epoxy laminates, the fatigue-induced stiffness decreases of multidirectional carbon/epoxy composites were calculated on different load levels. Results proved the good correlation between calculation and experiment. Second, a newly adapted strength-based approach known from classical metal fatigue implemented in a commercially available software tools was used. The advantage of software tools, which are in use for many years now, is the possibility of including load time history or complicated geometries by finite element analysis. The S-N curves of unidirectional laminates reflecting the anisotropy and the effect of fibre volume content were evaluated at different mechanical mean stresses. This input parameter set was used to calculate the fatigues strength of a unidirectional and a multidirectional composite. Predictions showed good correlations with the experimental results. In addition, the necessity of further development for future applications was discussed.

Contents

I	Preamble	V
	Affidavit	VII
	Acknowledgement.....	IX
	Kurzfassung	XI
	Abstract	XV
II	Introduction to the Thesis	1
1.	Motivation and background.....	3
1.1.	Climate change and environmental aims for the 21 st century.....	3
1.2.	Transportation - Composite materials in the aircraft and automotive industry.....	5
1.3.	Continuously fibre reinforced plastics.....	7
1.4.	Composites in service	9
1.5.	Fatigue	11
1.5.1.	Fatigue and damage of composite materials	17
1.6.	Theories describing composite fatigue	19
1.6.1.	Stiffness and residual strength based fatigue-life approaches	19
1.6.2.	Energy based approaches	21
1.6.3.	Fracture mechanical approaches	21
1.6.4.	Approaches based on traditional S-N curves	22
1.7.	Predicting composite failure	24

1.7.1.	Prediction of quasi-static failure	24
1.7.2.	Prediction of composite fatigue failure	27
1.8.	References	31
2.	Objectives	39
2.1.	References	41
3.	Structure of the Thesis	43
3.1.	References	45
III	Measuring techniques in composite fatigue tests	47
4.	Introduction to Publication 1	49
4.1.	References	50
5.	Publication 1	53
5.1.	Bibliographic information	53
5.2.	Abstract	54
5.3.	Introduction.....	54
5.3.1.	Strain gauges	55
5.3.2.	Mechanical extensometers.....	55
5.3.3.	Digital Image Correlation.....	56
5.3.4.	Piston displacement.....	56
5.4.	Experimental work	57
5.5.	Results and Discussion	60
5.5.1.	Quasi-static tensile tests	60
5.5.2.	Tension-tension fatigue tests	63
5.6.	Conclusions and Recommendations	73
5.7.	References	75

IV	Fatigue-induced damage mechanisms in carbon/epoxy laminates	79
6.	Introduction to Publications 2 and 3.....	81
6.1.	References	82
7.	Publication 2	83
7.1.	Bibliographic information	83
7.2.	Abstract	84
7.3.	Introduction	84
7.4.	Experimental work.....	85
7.5.	Results and Discussion	87
7.5.1.	Quasi-static tensile tests	90
7.5.2.	Fatigue tests	92
7.5.3.	Damage mechanisms under fatigue loads.....	96
7.6.	Conclusions.....	102
7.7.	References	103
8.	Publication 3	105
8.1.	Bibliographic information	105
8.2.	Abstract.....	106
8.3.	Introduction	106
8.4.	Experimental work.....	107
8.5.	Results and Discussion	111
8.5.1.	Quasi-static tensile and compression tests	111
8.5.2.	Tension-tension and tension-compression fatigue tests	113
8.5.3.	Damage mechanisms depending on the mean stress and on the fibre volume content.....	118
8.5.3.1.	Epoxy resin	118
8.5.3.2.	UD 90° with 30% and 55% fibre volume content.....	120

8.6.	Conclusions	127
8.7.	References	129
V	Fatigue-life prediction of carbon/epoxy composites with two different approaches	133
9.	Introduction to Publications 4, 5, 6 and 7	135
9.1.	Novel stiffness based fatigue-life prediction of composite materials	135
9.2.	Strength based engineering concept for the fatigue-life prediction of composite materials	138
9.3.	References	141
10.	Publication 4	145
10.1.	Bibliographic information	145
10.2.	Abstract	146
10.3.	Introduction	146
10.4.	Experimental work	148
10.5.	Results and Discussion	149
10.6.	Summary and Outlook	154
10.7.	References	155
11.	Publication 5	157
11.1.	Bibliographic information	157
11.2.	Abstract	158
11.3.	Introduction	158
11.4.	Experimental work	160
11.5.	Results and Discussion	161
11.6.	Conclusions and Outlook	166
11.7.	References	167

12. Publication 6	169
12.1. Bibliographic information	169
12.2. Abstract	170
12.3. Introduction	170
12.4. Experimental work.....	172
12.4.1. Shear moduli in quasi-static and fatigue tests.....	174
12.4.2. Poisson's ratios measured in quasi-static and fatigue tests	175
12.4.3. Fatigue life prediction with CLT	175
12.4.4. Damage mechanisms under fatigue loads.....	178
12.5. Results	179
12.5.1. Quasi-static input parameters for CLT	179
12.5.2. Cycle-dependent moduli and Poisson's ratios as input for CLT ..	181
12.5.3. Calculated stiffness degradation of multidirectional lay-up by CLT vs experiment.....	184
12.5.4. Damage mechanisms as reasons for stiffness degradation.....	187
12.6. Conclusions and Outlook	189
12.7. References.....	190
13. Publication 7	193
13.1. Bibliographic information	193
13.2. Abstract.....	195
13.3. Introduction	195
13.4. Fatigue-Life Prediction Method for Laminates	198
13.5. Experimental Work	201
13.6. Results and Discussion	202
13.6.1. Test Results for Quasi-Static Loading.....	202
13.6.2. Results of Fatigue Tests	204
13.6.3. FE Analysis.....	206

CONTENTS

13.6.4. Fatigue-Life Prediction	207
13.7. Conclusions and Outlook.....	211
13.8. References	212
VI Summary, Conclusions and Outlook	217
Summary	219
Conclusions and Outlook	225
Appendix	229
Symbols	231

Part II.

Introduction to the Thesis

1. Motivation and background

1.1. Climate change and environmental aims for the 21st century

In the 21st century, the world and mankind are meeting extraordinary challenges. The human influence on the climate systems is clear and emissions of greenhouse gases are the highest in history [1,2]. The atmosphere and the ocean have warmed, the amounts of snow and ice have diminished and the sea level has risen [1,2]. Global emissions of carbon dioxide (CO₂) have increased by almost 50 % since 1950 and still continue their upward trend, increasing by 2.6 % between 2010 and 2011 which is a 48.9 % rise above their 1990 level [1,3]. Beyond that, the growth in CO₂ emissions accelerated after 2000, with emissions increasing by 35 % from 2000 to 2011, compared to 10 % from 1990 to 2000 mostly due to the fast growth in emissions from developing regions [3]. To counter this development, the United Nations have proclaimed the insurance of environmental sustainability as one of the eight “Millennium Development Goals” in 2000 [3]. In 2014 the new European Commission has defined its three overall priorities for this term of office [4]. These priorities are:

1. Jobs, Growth and Investment
2. Digital Single Market
3. Energy Union and Climate

The European Commission’s “Energy Union and Climate” program defines the following main objectives in detail [4]:

- Creating an European Energy Union – by pooling resources, connecting networks and uniting the power when negotiating with non EU countries.
- Diversifying the energy sources – so Europe can quickly switch to other supply channels if the financial or political cost of importing from the East becomes too high.
- Helping EU countries become less dependent on energy imports.
- Making the EU the world number one in renewable energy and leading the fight against global warming.

Especially the aim to make the European Union leader with regard to renewable energies is important in order to decrease carbon dioxide emissions. The status quo summarised by the “Renewables 2014 Global Report” lists that the total renewable power capacity (not including hydro power) has increased from 85 Gigawatt in 2004 to 560 Gigawatt in 2013. If hydro power is taken into account as well, 1,560 Gigawatt are produced from renewable sources at the end of 2013 [5]. However, the itemisation of the total energy consumptions is given for the year 2012: In 2012 fossil fuels had the major share of 78.4 %, nuclear power 2.6 % and energy from all renewable sources estimated 19 % with regard to global energy consumptions [5]. A fraction of 9 % of these renewable sources was attributed to traditional biomass (for cooking and heating purposes). Modern renewables (modern biomass, biofuels, geothermal, hydropower, wind and solar) accounted for around 10 %. Wind, solar, modern biomass and geothermal energy together had a share of 1.2 % only in 2012 [5].

These data clarify that in order to meet the demanding aims set by the European Commission a lot of effort still has to be made [1–4,6,7]. The aspired decrease of carbon dioxide emissions can be realised by replacing traditional fossil fuels with renewable energies and consequently decreasing emissions caused by fossil fuels on the one hand. On the other hand, the amount of emissions caused e.g. by industry or transportation has to be reduced by optimising processes. Further development of renewable energy technologies, new concepts in transportation and the use of new materials

enabling weight reduction will be critical to make energy production and energy usage more efficient in the future.

1.2. Transportation - Composite materials in the aircraft and automotive industry

The transportation industry including the aircraft and automotive industry is one of the key producers of CO₂ emissions [6]. In order to meet the aspired environmental aims and to revolutionise transportation, the European Commission has scheduled explicit guidelines for the transportation industry in Europe for the next decades. In 2001, the European “Vision 2020” has set different requirements including quality, affordability, noise reduction, safety and emissions of airplanes until the year 2020 [7]. The environmental demand on the aircraft industry is a 50 % cut in CO₂ per passenger kilometre (which means a 50 % cut in fuel consumption in the new aircraft 2020) and an 80 % in nitrogen oxide emissions until the year 2020, taking the year 2000 as reference [7]. In 2013, 2.6 billion passengers used commercial aircraft for transportation [8]. For the next years, an annual growth of 5 % per year is expected which would increase the number of airplanes in service from 20,000 in the year 2013 to about 40,000 in 2033 [9]. Such growth rates in combination with environmental guidelines set demanding challenges to the construction and production of new airplanes. Beyond that, the fuel consumption is a decisive not only environmental but economic factor: while oil prices were around US\$25 per barrel at the beginning of this century, in 2013 oil prices averaged US\$110 per barrel. This means an increase of 340 % in the short time period between 2000 and 2013 [8]. In combination with increasing number of passengers and the difficulties with fossil fuel in terms of availability and emissions, the reduction of weight in order to reduce fuel consumption is of tremendous importance for the aircraft industry. 1 kg of reduced airframe mass is equivalent to fuel saving of approximately 2000 litre fuel for the complete aircraft life cycle [10].

Furthermore, the “White paper 2011” sets demands not only to the aircraft but to the entire transportation industry [6]. The goals until the year 2050 include:

- No more conventionally-fuelled cars in cities.
- 40 % use of sustainable low carbon fuels in aviation; at least 40 % cut in shipping emissions.
- A 50 % shift of medium distance intercity passenger and freight journeys from road to rail and waterborne transport.
- All of which will contribute to a 60 % cut in transport emissions by the middle of the century.

Due to these ambitious aims, the automotive industry is meeting similar challenges in terms of reduction of fossil fuel consumption. Therefore, the development of new engine systems and car concepts has been forced in the last years. Especially BMW has put a lot of effort in the development and production of the i-Series which is the first car of its kind to be produced in large numbers (figure 1.1) [11]. To make new drive systems such as electric or hybrid systems as efficient as possible, the reduction of car weight is of essential importance also in the automotive industry. The necessary reduction of the entire vehicle weight can be realised by a combination of new design concepts and by the use of materials with lightweight potential offering high mechanical properties at low specific weight. One material class fulfilling these demands are composite materials.



Figure 1.1: Passenger compartment of the BMW i3 made of carbon composites [11].

1.3. Continuously fibre reinforced plastics

Composite materials involve a variety of reinforcing materials such as carbon, glass, aramid, metallic or natural fibres and matrix materials such as resins, thermoplastic materials or different metallic or ceramic matrix systems to name just a few [12–14]. The combination of reinforcing fibres embedded in a surrounding matrix material enables the production of materials and structures with defined properties. In general, the used reinforcing fibres and their orientation within the material influence mechanical properties such as stiffness, strength and fatigue or the impact behaviour. The matrix material on the contrary protects the fibres especially under e.g. temperature influence or chemical environment. The third basic component of composite materials is the finish which is applied on the fibres. Among other functions its main tasks are to act as processing aid and to guarantee the load transfer between fibres and matrix material [12]. Continuously fibre reinforced plastics (CFRP) offer interesting potentials due to their low weight in relation to the obtainable properties. The most commonly used fibres for continuously reinforced polymeric matrix systems are carbon, glass and aramid as illustrated in figure 1.2.

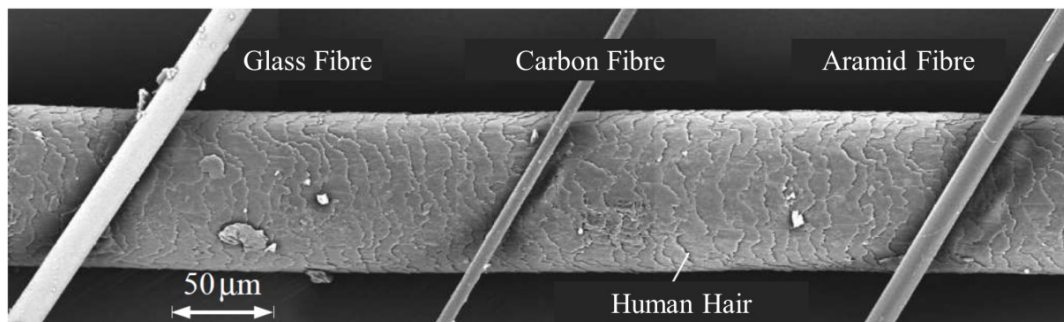


Figure 1.2: Scanning electron microscopy (SEM) photographs of the most widely used reinforcing fibre materials referring to [12].

Apart from the properties of the constituents used, the properties of the composite material are significantly influenced by the production processes and the resulting fibre architectures. Almost all production processes known from the textile industry can be applied to composite manufacturing. A variety of different production concepts is in use in order to create application

tailored composite materials in the industry. Possible fibre architectures are introduced briefly in the following. The easiest structure consisting of fibres arranged only in one direction, unidirectional layers, is schematically illustrated in figure 1.3 a. If unidirectional layers are joined under defined angles, multidirectional lay-ups can be created (figure 1.3 b). One advantage of these fibre arrangements is that fibres can be arranged at a wide range of angles. Furthermore, fibres stay plane within the composite [12]. Woven composites as shown in figure 1.3 c offer different realisable weave architectures and are produced with a variety of material combinations. When creating composite structures with woven materials, it is beneficial that two load directions are automatically covered at the same time. However, as a result of the weaving process, fibres are not plane anymore within the composite which leads to reduced strengths in comparison to multidirectional lay-ups [12]. Continuous fibres may also be processed by braiding in order to create composite pipes or tubular parts (figure 1.3 d).

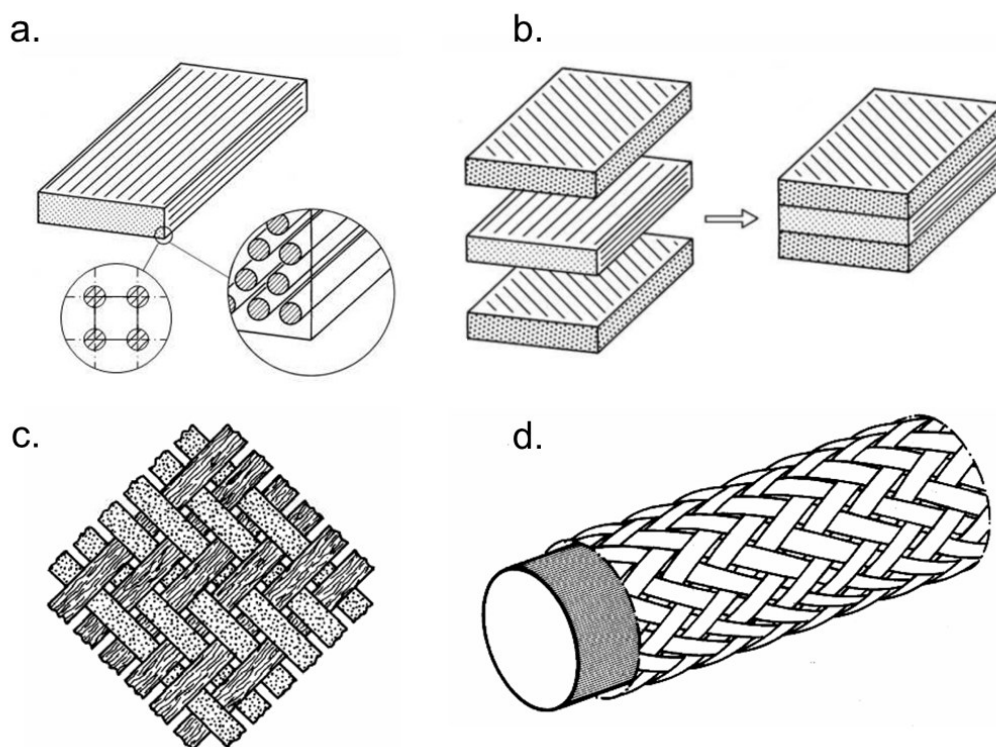


Figure 1.3: Fibre architectures of a. unidirectional layers, b. multidirectional lay-ups, c. woven composites and d. braided composites from [12].

Due to their variable fibre architectures and high properties, composite materials are most superior in structural applications in the aircraft or automotive industry. However, there are still some economic issues determining the success of composite materials. Nowadays, carbon composites are approximately 600 % more expensive than steel [15]. In a study published by McKinsey in 2012, cheaper prices for carbon fibres are expected until the year 2030. It is predicted that until then the price of carbon composites will reduce and be in the price range of aluminium which will be about twice as expensive as steel [15].

1.4. Composites in service

In contrast to metallic materials, which are in industrial use for more than 150 years now, the first use of composite materials started in the 1960s [14]. In a material class, which is as young as composite materials, a lot of practical and experimental experience still has to be gained about the performance under loads. Lightweight structures in the aircraft or automotive industry are highly stressed, usually by mechanical loads. Consequently, the actual testing of physical and mechanical properties is of tremendous importance to ensure the material behaviour and safe application.

As a result of the inhomogeneous inner structure of composite materials consisting of continuous fibres and matrix material, composites behave in an anisotropic way on macroscopic scale. The mechanical behaviour of fibres, matrix and the combined unidirectional composites under a quasi-static tensile load is schematically illustrated in figure 1.4. In general, the tensile strength of the fibres is magnitudes higher than the strength of the matrix material. On the contrary, the deformation reached by the matrix is higher resulting in significantly higher strains to failure. In figure 1.4 a, a tensile load longitudinal to the fibre direction is applied on the unidirectional material. The deformation of the unidirectional composite is limited by the strain to failure of the fibres. In contrast to the unreinforced matrix material, the strain to failure is significantly smaller. In addition, the stiffness of the unidirectional composite is higher than the stiffness of the matrix material. On the contrary, the same unidirectional material is loaded transversal to fibre direction in

quasi-static tensile test in figure 1.4 b. Because the reinforcing fibres are not arranged in direction of the applied load, the reinforcing effect has vanished. Strain at failure of the unidirectional composite is even smaller than strain at failure of the fibres.

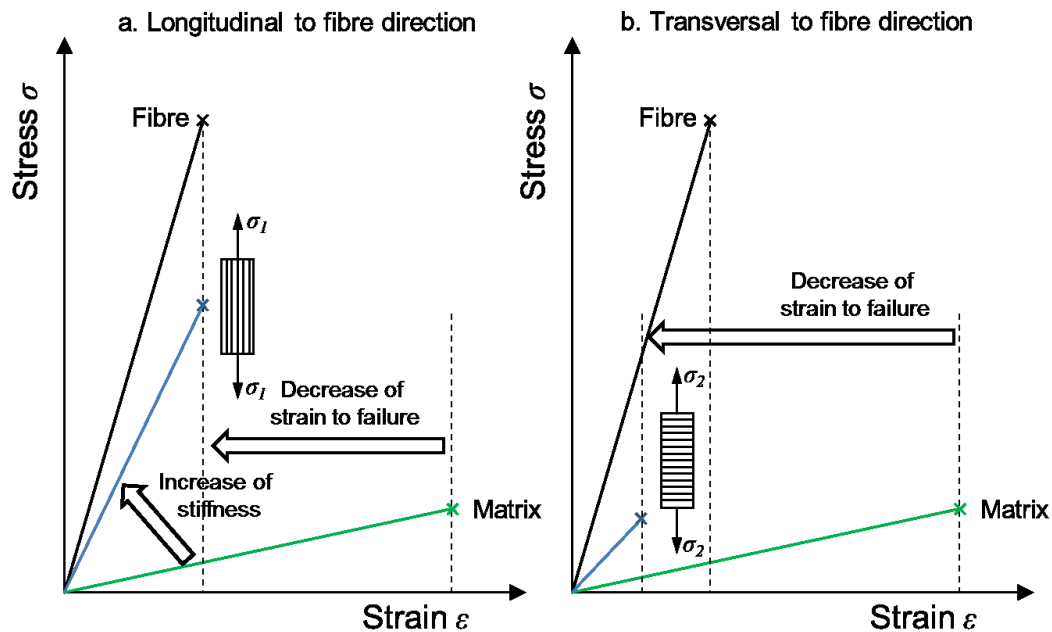


Figure 1.4: Schematic response of unidirectional composites under quasi-static tensile loads applied a. longitudinal to fibre direction and b. transversal to fibre direction according to [16].

In order to take this basic material behaviour influencing the performance of composites in any application into account, material testing is not only concerned with coupon tests investigating the actual material behaviour but also with the performance of entire structures. If a composite part is going to be used in a new application a tremendous number of mechanical tests have to be conducted in advance to validate basic mechanical properties such as strength and stiffness. The schematic test pyramid illustrated in figure 1.5 exemplifies the different levels of mechanical composite tests. Coupon tests characterising the basic behaviour of the material are the tests to start with. Basic material tests usually are quasi-static tensile, compressive or shear tests in which strengths and moduli are evaluated [17]. If strain-rate dependency, temperature dependency or media resistance are of

importance, these influence factors can be included on this level as well. Once the material is characterised, the gained basic knowledge about the material can be used to create small elements such as joining elements which are tested on the next level. Testing of subcomponents and entire components requires even higher test experience and more sophisticated test equipment. At the tip of the pyramid, full scale tests with e.g. an entire airplane can be conducted [18]. The test pyramid fulfils its task if – after considering all lower levels carefully – a full scale test is performed with the expected service load and failure does not occur.

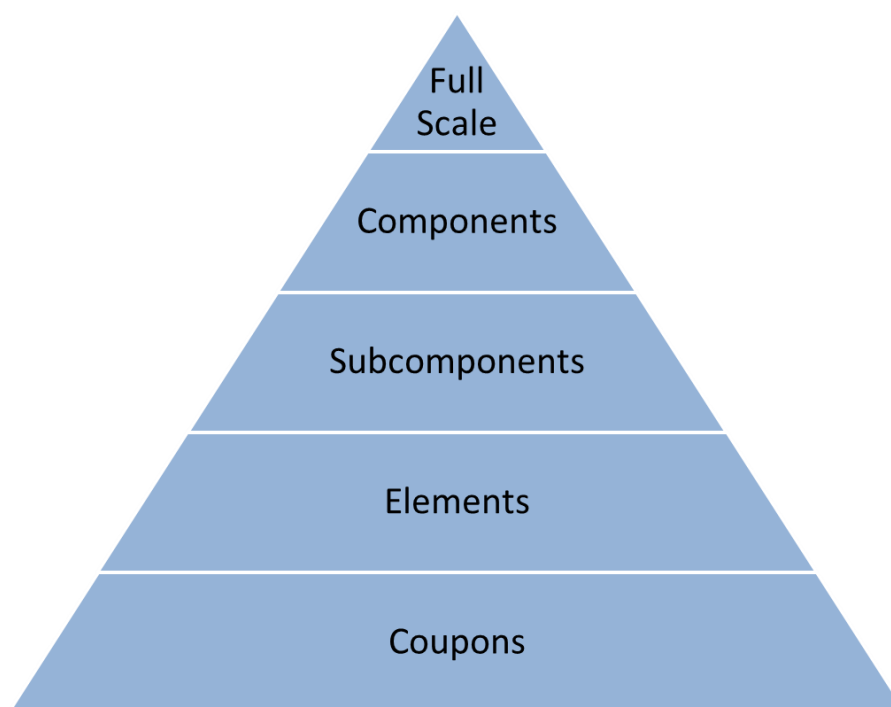


Figure 1.5: Schematic test pyramid for mechanical composite test.

1.5. Fatigue

If the application of a material to an engineering component is contemplated, it is essential to answer not only the fundamental questions regarding strength and stiffness, but also the question of how long the material will last under the conditions applied [19]. In general, fatigue is concerned with the loss of properties and performance caused by external influences such as

mechanical loading, thermal loading or chemical environments [20]. The reduction of strength and the subsequent failure of materials subjected to repeated loading has been identified as a fundamental problem of material science since the early 1800s [19–22]. However, unexpected material failure caused by fatigue can still occur as shown in figure 1.6 or have catastrophic consequences as in the train accident 1998 in Eschede, Germany [22]. The applications for which composite materials are most superior (e.g. high performance structures such as power systems, aircrafts or other vehicles) are precisely those situations in which degradation of strength and life by fatigue processes is most likely to occur [20].



Figure 1.6: Fatigue failure of a composite rotor blade in Conisholme, Lincolnshire, 2009 [23].

The loads inducing fatigue in materials may be deterministic, periodic, aperiodic or stochastic. Cyclic loads with constant amplitudes are often described in relation to a constant or changing mean load by introducing $R = (\text{minimum load} / \text{maximum load})$ (figure 1.7) [21]. The different ratios

between minimum and maximum loads in compression-compression, tension-compression or tension-tension tests have significant influence on the fatigue behaviour and are described in detail by giving the applied R .

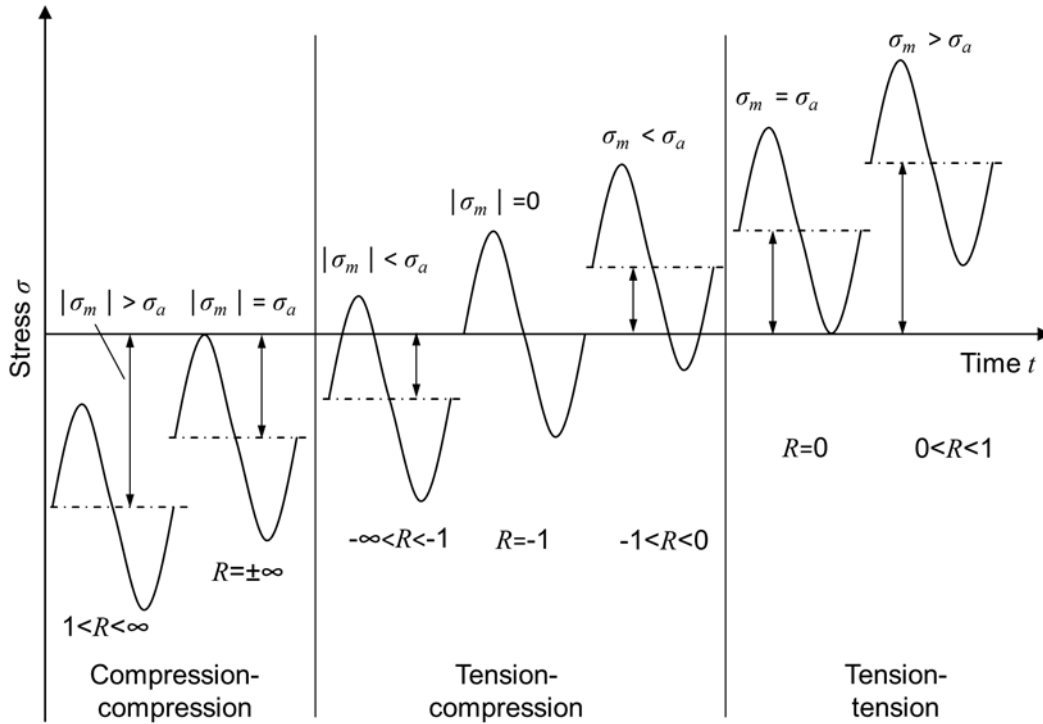


Figure 1.7: Sinusoidal loads for different R according to [21].

The viscoelastic material behaviour known for polymeric materials results in a phase shift between the applied load $\sigma(t)$ and the material response $\varepsilon(t)$ e.g. [13,24–26]. As a consequence, the cyclic stress-strain diagrams show the shape of hysteresis loops (figure 1.8). This correlation can be described by equations (1.1) and (1.2), where ν_c is the number of stress cycles per unit and ω describes the angular frequency (1.3).

$$\sigma(t) = \sigma_{max} * \sin(\omega t) \quad (1.1)$$

$$\varepsilon(t) = \varepsilon_{max} * \sin((\omega t) - \phi) \quad (1.2)$$

$$\omega = 2\pi\nu_c \quad (1.3)$$

The peak values of stress and strain, σ_{max} and ε_{max} , respectively, are related by the complex modulus E^* (1.4).

$$E^* = E' + iE'' = \frac{\sigma_{max}}{\varepsilon_{max}} (\cos \phi + i \sin \phi) \quad (1.4)$$

$$i = \sqrt{-1} \quad (1.5)$$

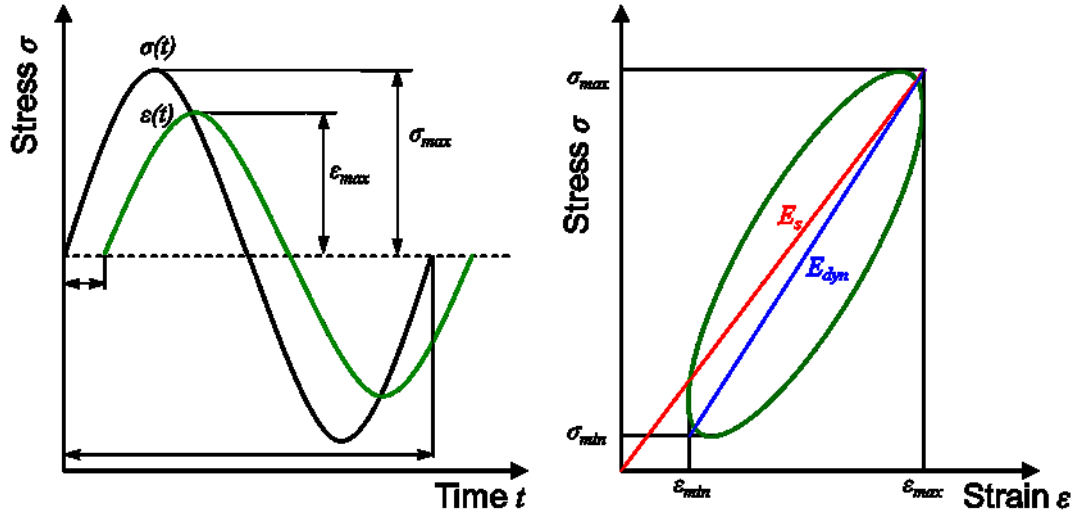


Figure 1.8: Phase shift between applied load and strain response caused by viscoelastic material behaviour.

E' is known as storage modulus and it denotes to the stress in phase with the strain to the strain. The storage modulus correlates to the amount of energy which is stored and regained during each cycle. E'' is the loss modulus and correlates to the ratio of the stress which is 90° out of the phase with stress to the strain. The loss modulus is an indicator for the irreversibly dissipated heat energy. The linear viscous deformation due to sinusoidal fatigue loading can also be characterised in terms of complex compliance D^* (1.6), where analogous to the storage modulus and loss modulus, D' and D'' denote to the storage compliance and loss compliance, respectively. The entity $\tan \delta$ is known as loss tangent (1.7) [13,26].

$$D^* = \frac{1}{E^*} = D' - iD'' \quad (1.6)$$

$$\tan \delta = \frac{E''}{E'} = \frac{D''}{D'} \quad (1.7)$$

For adiabatic heating (i.e. heating in which all the of the heat generated within the polymer is manifested as temperature rise and non is lost to the

surroundings) the time rate change of temperature is given by equation (1.8) where ρ correlates to the mass density, c_p describes the specific heat and \dot{Q} the rate of hysteretic energy dissipated as heat [26]. The maximum stress influences the hysteretic heating by the power of two, which reflects the strong effect of the applied load amplitude.

$$\frac{\Delta T}{dt} = \frac{\dot{Q}}{\rho * c_p} = \frac{\pi * \nu_c * D'' * \sigma_{max}^2}{\rho * c_p} \quad (1.8)$$

The hysteresis loops schematically illustrated in figure 1.8 may be shifted or overturned due to increasing damage progresses. To describe the change of shape and position of hysteresis loops during fatigue tests, two parameters have been introduced (figure 1.9). The secant modulus E_s , which gives the ratio between the maximum stress and the maximum strain (1.9) can be seen as indicator for cyclic creep, hysteretic heating and also progressing material damage. The dynamic modulus E_{dyn} describes the slope of the hysteresis on the contrary and reflects hysteretic heating and material damage (1.10) [27].

$$E_s = \frac{\sigma_{max}}{\varepsilon_{max}} \text{ for } -1 \leq R < 1 \text{ otherwise } E_s = \frac{\sigma_{min}}{\varepsilon_{min}} \quad (1.9)$$

$$E_{dyn} = |E^*| = \frac{\sigma_{max} - \sigma_{min}}{\varepsilon_{max} - \varepsilon_{min}} \quad (1.10)$$

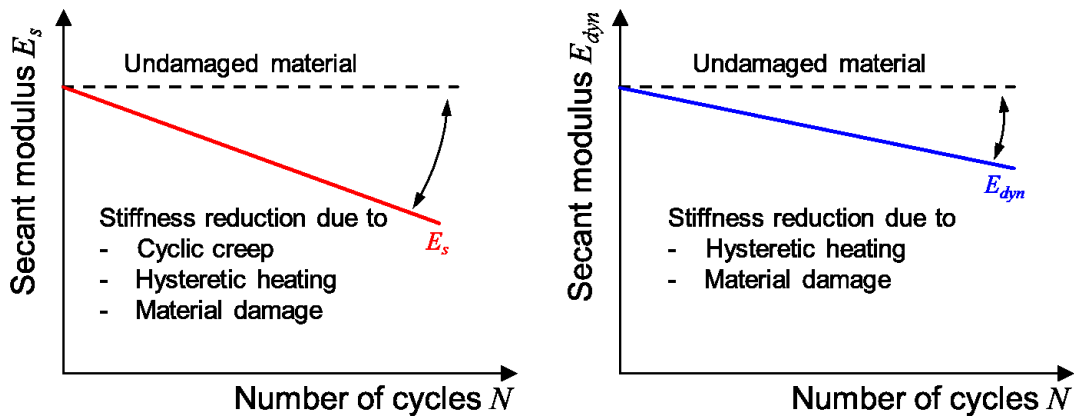


Figure 1.9: Schematic decrease of the secant and the dynamic modulus evaluated from stress-strain hysteresis loops according to [27,28].

The movement of hysteresis loops in cyclic tests depends on whether stress or strain controlled tests are performed. Furthermore, the shape and the location of the hysteresis loops are influenced by the mechanical behaviour of the material and the applied mean stress. The stress response in strain controlled fatigue tests is illustrated according to [25] in figure 1.10 a. While the maximum and the minimum strain are constant during the entire fatigue tests, the load response decreases. This indicates that less load is required to reach to controlled strain limits as a result of progressing material damage. Hysteresis loops for two damaged states during the course of fatigue life show the changes of hysteresis loops in strain controlled tests [25]. If load controlled tests are performed, the maxima and minima of the strain response increase during fatigue life. Again, hysteresis loops for two damaged states are illustrated (figure 1.10 b).

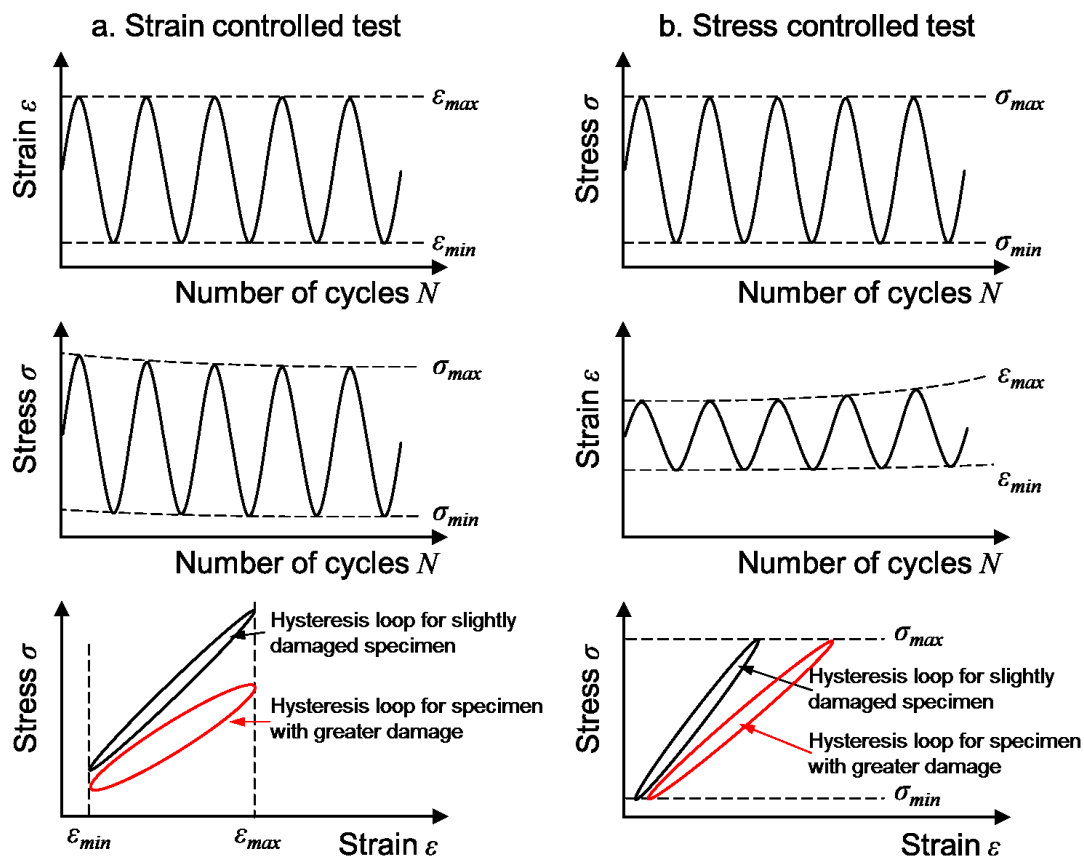


Figure 1.10: Cyclic material response and hysteresis loops for a. strain controlled and b. stress or load controlled fatigue tests referring to [25].

1.5.1. Fatigue and damage of composite materials

The viscoelastic effects within composite materials, especially with resins as matrix materials, are not as significant as for other polymeric materials as a result of the high stiffnesses and small deformations usually obtained in composite materials (figure 1.4). However, the fatigue behaviour is decisively dominated by a series of complex damage mechanisms responsible for the macroscopically observed loss of stiffness and strength.

For the description and analysis of damage development in composite materials under both quasi-static and cyclic loading it is necessary to consider the determination of damage development in composite laminates including damage mechanisms and their chronology and duration of damage events. The general understanding of fatigue as complex combination of damage modes and damage mechanisms resulting in property degradation proposed by Reifsnider, Talreja and others since the 1980s as illustrated in figure 1.11 is well-accepted e.g. [29–36].

The initial state consists of primary matrix cracking along fibres in the plies inclined to the principal load direction. The cracking occurs in a multiple mode while the density of cracks increases. The state of damage given by the saturated and stable matrix cracking pattern in a laminate has been termed the characteristic damage state (CDS) [37,38]. As the primary matrix cracks forms, fibre failure initiates in regions of stress concentration created by the primary cracks. The primary matrix cracks also initiate small secondary cracks which extend short distances away from the interface between the ply. The next event that may occur is delamination in the interior of the laminate. This delamination is caused by a mixed mode of growth of interlaminar cracks which is driven by the strong interlaminar stresses in regions where primary and secondary cracks cross. In compression loading the out-of-plane displacement of plies also influences the delamination growth [37]. The later stage of damage development is typified as a rapidly increasing rate of progression of all damage modes. The terminal event of separation consists usually of large-scale fibre failures in plies aligned with or most nearly aligned with the principal tensile stress [37,38]. However, it is a well-known that the damage development caused by the respective stress

states is significantly dependent on the unique properties of the material (i.e. fibre and matrix material, stacking sequence) [31,39,40].

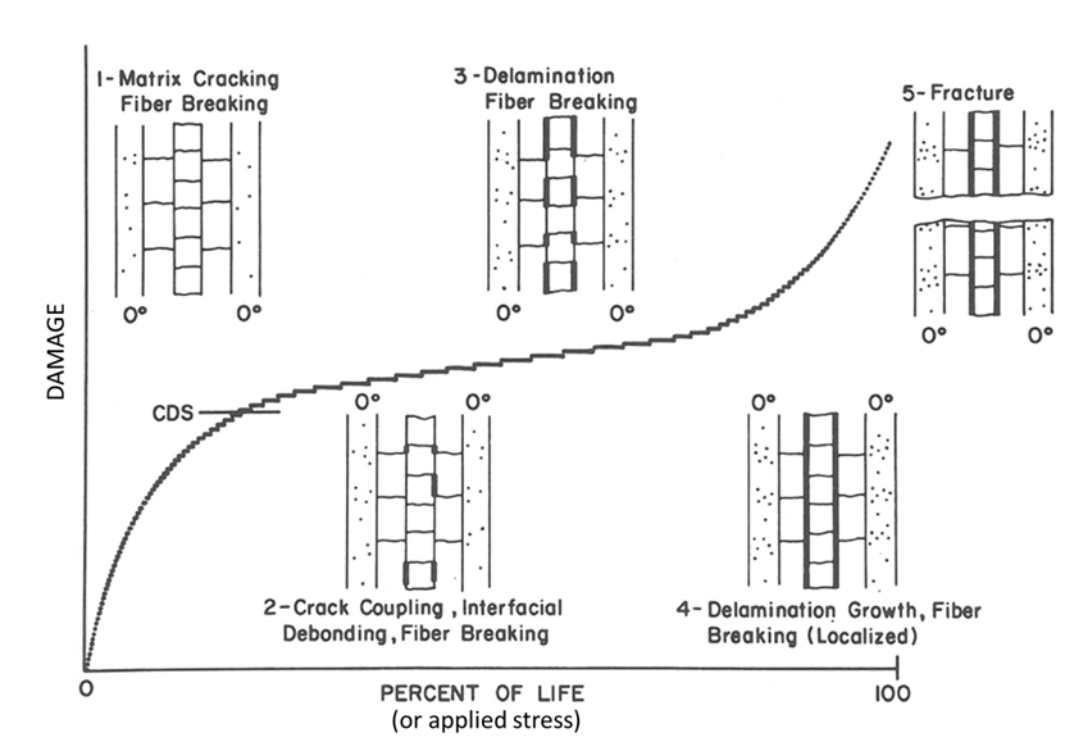


Figure 1.11: Schematic representation of the development of damage and damage modes in fatigue or quasi-static tests with composite laminates according to [38,41,42].

Summarising, the most common damage mechanisms in composite materials which can accumulate, progress and interact, are [19,20,30,31,34,35,38,41–43]:

- Matrix micro-cracking
- Interfacial matrix-fibre debonding
- Delamination
- Fibre rupture

1.6. Theories describing composite fatigue

Many theories describing the fatigue behaviour and the fatigue processes within composite materials have been studied during the last decades. Different approaches have been suggested. While some of them are motivated by the physical progresses occurring on different scales from microscopic damage mechanisms to macroscopic decrease of properties during fatigue life, others characterise fatigue by failure of entire specimens or structures. In the following, four of the most widely spread approaches towards the description of fatigue behaviour of composite materials are introduced. Stiffness and residual strength, energy based approaches, fracture mechanics and traditional fatigue strength based S-N curves are discussed. Of course, this listing does neither assert the claim to be complete nor to discuss all aspects in detail.

1.6.1. Stiffness and residual strength based fatigue-life approaches

In some cases a laminate could be considered to have functionally failed before separation as illustrated in figure 1.11 due to substantial loss of mechanical properties such as residual strength or stiffness [25,37,38]. As figure 1.12 illustrates, both stiffness and residual strength decrease during fatigue life. The fatigue strength, which was added to the chart, represents the strength at failure of a permanently loaded specimen, which is often used to create the well-known Wöhler lines or S-N curves [21,22].

Change in stiffness of composite laminates under long-term, cyclic loading is significant for two important reasons. First, many engineering structures made of composite materials are deformation-limited, or stiffness-critical, structures. Aircraft and aerospace components are aero-elastically designed and tailored for optimum performance. The ability of compressively loaded columns and shell structures to carry load without buckling is directly related to the stiffness of the structure. Changes in stiffness caused by damage alter the response of the component to loads and reduce the performance level of the structure. Fatigue life is thereby determined by a specified stiffness change in a performance-critical component rather than by fracture [25,44]. The second reason for interest in stiffness change in composite laminates is that change in stiffness provides a non-destructive technique for monitoring

damage throughout a loading history. Furthermore, changes in stiffness are directly related to the severity of the damage by the mechanics associated with the subsequent response of the material. Thus, stiffness change can be used, along with appropriate models, to anticipate and predict remaining strength and fatigue-life [25]. The characteristic stages I to III (figure 1.12) of stiffness degradation, which correlate with the damage mechanisms already described in figure 1.11, depend on the cyclic loading and on the respective material. However, the general form of the stiffness change - expended life relationship has been verified for many material systems, including metal matrix composites [25].

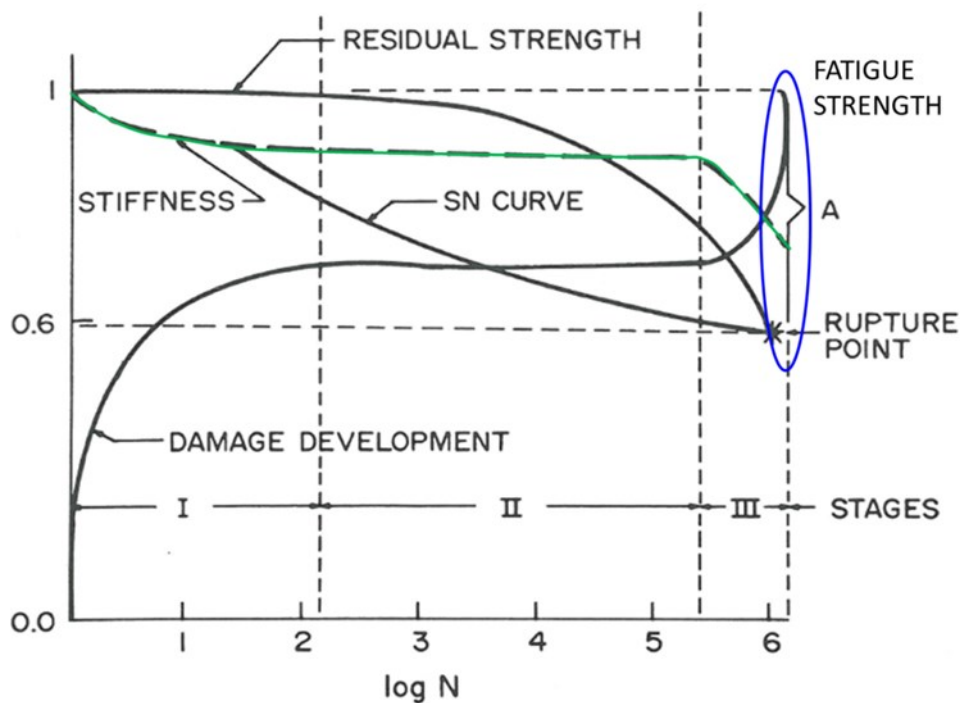


Figure 1.12: Schematic diagram of strength change and stiffness progress during fatigue life of an unnotched laminate referring to [25]

Residual strength of laminates is determined by using a two-stage test. The first stage is a cyclic test in order to create the desired condition in the specimen. The condition could be exposure to a specified number of load cycles, a selected change in a stiffness component, a prescribed state or damage or some condition related to a specific service application [25]. In the

second stage, a monotonic test tensile or compressive test is performed. The strength measured in these monotonic tests represents the residual strength of specimens including the applied load history. Various models using the residual strength as parameter for fatigue-life description have been published [25,45–47].

1.6.2. Energy based approaches

Beyond stiffness and residual strength based models to describe the fatigue-life of composites, another approach – among many others which are not going to be included herein – has been discussed by many researchers. Thermodynamic assumptions or energy based approaches are used to describe the fatigue life of composite materials e.g. [48,49]. In these theories, stress-strain fields and the related anticipated energies are taken into account by analysing the material's hysteresis loops caused by cyclic loads [48]. Shokrieh and Taheri-Behrooz proposed a fatigue life model based on the strain energy concept by assuming an elastic stress-strain relation which can be normalised to the maximum of monotonic strain energy, i.e. the product of maximum monotonic stress and strain [49]. It has to be noted that linear elastic concepts overestimate the actual, usually non-linear material behaviour [48]. Although these concepts are based on the stress-strain behaviour of the material, the possibility of correlating anticipated energies with physical damage mechanisms, as possible for stiffness decreases described by Talreja, Reifsnider, Stinchcomb or many others e.g. [25,37,38], is limited.

1.6.3. Fracture mechanical approaches

Fracture mechanical approaches are based on the assumption that crack growth, initiated by a defined starting crack, void or other imperfection, leads to fracture. Different theories describing the crack tips, plastic zones around the crack tips and evolution laws exist. For polymeric pipe materials for example, fracture mechanical tools can be successfully applied for life-time estimation e.g. [50–52]. With regard to composite materials, fracture mechanics is a useful approach for the understanding and description of delamination, which is a separation of the individual plies weakening the performance of the entire composite e.g. [53–56]. Composite delamination in

structures subjected to in-plane loading can be considered as subcritical failure mode whose effect may be a stiffness loss, a local tensile strain concentration in the load bearing plies that causes tensile failure or a local instability that causes further growth which ends in compressive failure. Some potential delamination sites are common design details that result in discontinuities in the load path such as free edges, hole boundaries, drop-off of the interior plies of a laminate to taper thickness, bonded or co-cured joints or bolted joints [53]. However, in composite structures many possibilities for crack or delamination initiation exist making the fatigue-life prediction based on fracture mechanics a very comprehensive task. Nevertheless, delaminations are one decisive failure mode and have to be taken into account.

1.6.4. Approaches based on traditional S-N curves

While the approaches of stiffness, residual strength, energy and fracture mechanics discussed so far are based on material specific parameters such as physical damage mechanisms and their effect on measurable mechanical properties, the description of fatigue-life by using S-N curves does not take damage mechanisms during fatigue life into account as such. This results mainly from the fact that for the creation of S-N curves one single event (e.g. failure) is used as criterion to assess a specimen and the history prior to this event e.g. stiffness and strength reduction are not evaluated. The creation of S-N curves is schematically illustrated in figure 1.13. For the illustration, stress controlled fatigue tests are chosen and results are drawn in a double-logarithmic way as applied nominal stress amplitude σ_a versus number of cycles N . Specimens are tested experimentally in constant amplitude tests on different stress levels until a previously defined event occurs, e.g. failure of the specimen. Numbers of cycles of each test are recorded. If specimens do not fail within reasonable test times, these specimens may be stopped and marked as run-outs. Depending on the applied load amplitude and consequently on the scales of reached numbers of cycles, S-N curves may be portioned in different regimes. High applied load amplitudes denote the low cycle fatigue (LCF) regime whereas most fatigue tests are performed in the high cycle fatigue (HCF) area. Very low amplitude tests reaching numbers of cycles in scales of 10^8 or 10^9 are usually called ultra high cycle

fatigue (UCHF). The illustrated S-N curve can be described by two data pairs of σ_a and N in combination with the slope k in the double-logarithmic diagram (1.11).

S-N curves are a popular way to describe the fatigue behaviour of materials due to their simplicity in terms of mechanical testing and data evaluation. Since this approach was developed for classical metallic fatigue, a lot of engineering experience for conducting fatigue characterisation properly and many studies on the rating of different influence factors are already available [21,22]. However, a lot of time-consuming material testing is needed especially if anisotropic material behaviour has to be reflected in the fatigue data.

$$N_1 = N_2 * \left(\frac{\sigma_{a,1}}{\sigma_{a,2}} \right)^{-k} \quad (1.11)$$

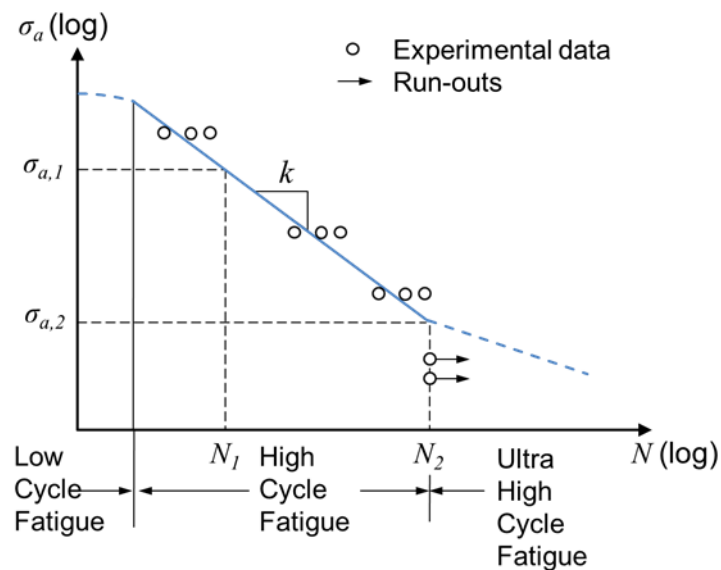


Figure 1.13: Schematic illustration of a S-N curve or Wöhler line. The entity of fatigue life can be divided into the low cycle fatigue (LCF), high cycle fatigue (HCF) and ultra high cycle fatigue (UHF) regime.

1.7. Predicting composite failure

The understanding and description of fatigue-life discussed so far is the first necessary prerequisite for being able to predict the fatigue properties and fatigue life as described above. The second necessity is the definition of failure criteria in order to be able to make assessments about the time when failure will occur in the future. The complex damage mechanisms as illustrated in figure 1.11 do not only describe the evaluation with percentage of fatigue life. In fact, the same mechanisms can be assumed to occur during quasi-static loading in an accelerated way [41]. Prior to the definition of fatigue failure criteria, the failure of composites under quasi-static loads has been studied by many researchers.

1.7.1. Prediction of quasi-static failure

Failure criteria for the prediction of quasi-static composite failure have been developed for more than half a century. Great success was achieved in micromechanics estimates of effective elastic properties, homogenisation, laminate plate theory, etc. [12,57–60]. However, theories for treating failure of composite materials did not succeed to the same extent. In fact, after approximately five decades of research many uncertainties and controversies still remain in predicting composite failure [42]. Numerous failure theories for composites have emerged over the years. Because of the uncertainties of validation of the different failure an exercise named worldwide failure exercise (WWFE) to objectively test how the different theories fare against experimental data [42,61–65]. In the following, two well-known representatives are chosen to discuss the two most accepted theoretical approaches for composite failure criteria, general and physically based approaches. For the discussion of composite failure criteria, the damage progresses illustrated in figure 1.11 – which were initially developed based on observations from tension-tension fatigue tests but have proven to illustrate the failure process in quasi-static loading as well [41,42] – should always be kept in mind.

The first failure theories in the late 1940s were developed by engineers and scientists familiar with the micro-mechanical behaviour of metallic materials. As a consequence, the first criteria started from theories for yielding and

plastic flow of anisotropic metals [42]. The further development for failure of unidirectional composites resulted in the well-known Tsai-Hill [66,67] failure criterion which can be allocated among the general theories and is in essence the yield criterion for thin metal sheets with one preferred orientation lying the plane of the sheet [42]. However, the failure of unidirectional composite materials is not the same under tension, compression or shear loads. Beyond that, due to the anisotropic material behaviour failure depends also on whether loads are applied in longitudinal or transversal direction. Failure under tension normal to the fibres e.g. is initiated by micro-cracks in the matrix or at the fibre/matrix interface, followed by linking of these micro-cracks into macro-cracks that grow unstably to failure [37,38]. In case of failure under axial compression on the contrary, deformation results in the localisation of failure in a kink band e.g. [68]. Based on the increasing knowledge about composite failure, Tsai and Wu further developed their criterion [67]. However, the fact remains that the ellipsoidal representation of the strength of thin sheets of unidirectional composites in the in-plane stress components is not motivated or supported by any physical consideration of failure mechanisms [42].

Puck [69,70] developed his physically based failure mode theories based on Hashin's approach [71,72]. Puck introduced failure modes distinguishing between fibre failure (FF) and inter fibre failure (IFF) caused either by tension, compression, shear or a combination of these load types. The seven parameters for inter fibre fracture (IFF) in Puck's theory are three strength constants and four so-called "inclination parameters" [42]. The normal stresses within a laminate are usually described by the stress longitudinal to the fibre direction σ_1 , the normal stress transversal to the fibre direction σ_2 , the stress perpendicular to the σ_1 - σ_2 plane σ_3 and the shear stresses τ_{12} , τ_{13} , τ_{21} , τ_{23} , τ_{31} and τ_{32} . In addition to that, the inter fibre failure introduced by Puck is influenced by the stress components σ_n , τ_{nb} and τ_{nl} acting on the failure plane along with the inclination angle θ_{fp} (figure 1.14). By reflecting the physical damage behaviour of composites, Puck's theory is able to accurately predict not only the expected stresses causing failure but also the location within the composite where failure will occur [69,70]. However, test data are needed to calibrate those seven constants in Puck's theory.

Both Puck's failure theory and Hashin's approach to developing failure criteria for unidirectional composites consider composites as homogeneous solids. Therefore, fibres are taken into account by distinguishing fibre failure modes from modes that are assumed to occur without affecting the fibres which does not represent the physical progresses of matrix cracks initiating failure [19,30,37,38]. Nevertheless, for unidirectional laminates, the predictions made by physically based theories are more advanced than their more general precursors as comparisons show [42,61–65]. However, a lot of scientific and engineering afford still has to be put in order to face open questions such as inclusion of manufacturing defects, effects of defects, complex fibre structures in woven or braided materials or ductile matrix failure [42].

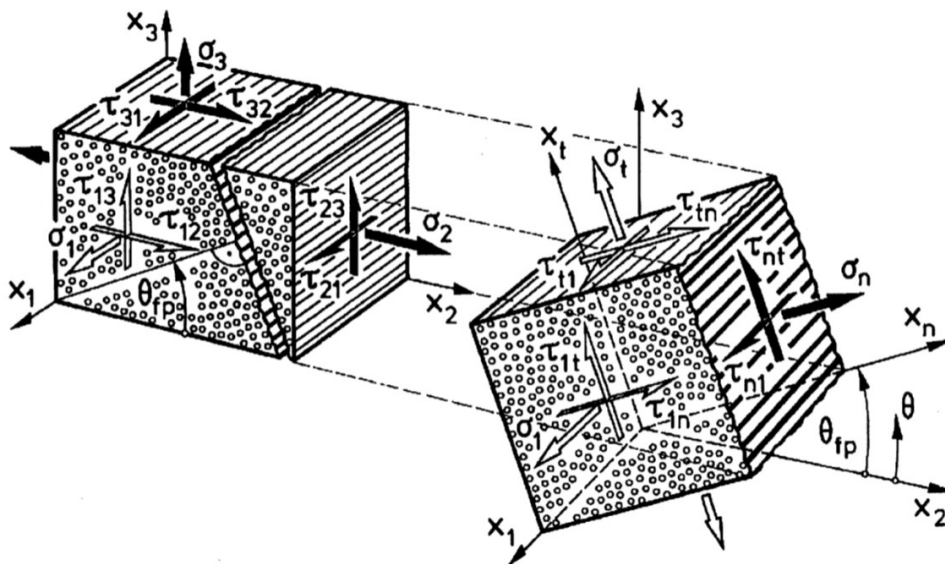


Figure 1.14: Three-dimensional stresses on a unidirectional composite element. (x_1, x_2, x_3) coordinate system is fixed to the fibre direction (x_1) , laminate mid-surface (x_2) and thickness direction (x_3) . The (x_1, x_n, x_t) coordinate system is rotated by an angle θ_{fp} from the x_2 direction to the x_n direction which is normal to the fracture plane. The inter-fibre fracture is influenced by the three stresses $\sigma_n, \tau_{nt}, \tau_{tn}$ only (according to Mohr's strength theory). From Puck and Schürmann [70].

1.7.2. Prediction of composite fatigue failure

Although failure criteria for assessing quasi-static composite failure and also many theories about the progresses during fatigue-life are available, failure criteria for fatigue failure are difficult to define. On the one hand, this is based on the complexity of damage mechanisms depending on the inner structure of each composite and influencing the fatigue behaviour decisively as already discussed. The variety of physical damage mechanisms makes fatigue failure criteria which are able to reflect the actual material damage and damage history way more complex than the introduced quasi-static criteria. Furthermore, since the damage progress is influenced by the specific characteristics such as fibre and matrix material stacking sequence etc., a general failure criterion based on physical damage mechanisms valid for all composite types is not realistic. On the other hand, the overall objective of each fatigue-life prediction should be to meet the real application of a composite structure. However, this aspired aim will probably not be realisable with theories built on effects on microscopic scales due to the quantity of effects which would have to be included into the predictions. Furthermore, the upscaling of theories describing the physical behaviour on microscopic level to prediction of the behaviour of entire structures might not be valid due to different effects on these scales.

As a result of these uncertainties, many theories focus on building on rather technological predictions. Therefore, the prediction of composite fatigue failure nowadays is often based on theories known from metallic materials which are intended to be adapted for composites [73–75]. A lot of effort has been put into accurate description of Haigh or constant life diagrams for composite materials. In general, Haigh diagrams are used to illustrate the correlation between the applied load amplitude σ_a and the mean stress of the cyclic load σ_m in fatigue tests. It is known from metallic materials that the bearable load amplitude σ_a decreases with increasing mean stress σ_m (figure 1.15). This effect is usually described as “mean stress sensitivity” M [21,22]. The Haigh diagram is created based on experimentally evaluated fatigue strengths and usually valid for one defined number of cycles. Different theories describing the shape of the Haigh diagram between the experimentally measured points have been developed for metallic materials.

A common approach for the extension of the Haigh diagram to unknown load ratios R is to use quasi-static values such as tensile strength σ_M or stress at 0.2 % strain $\sigma_{0.2\%}$ as borders for the diagram [22].

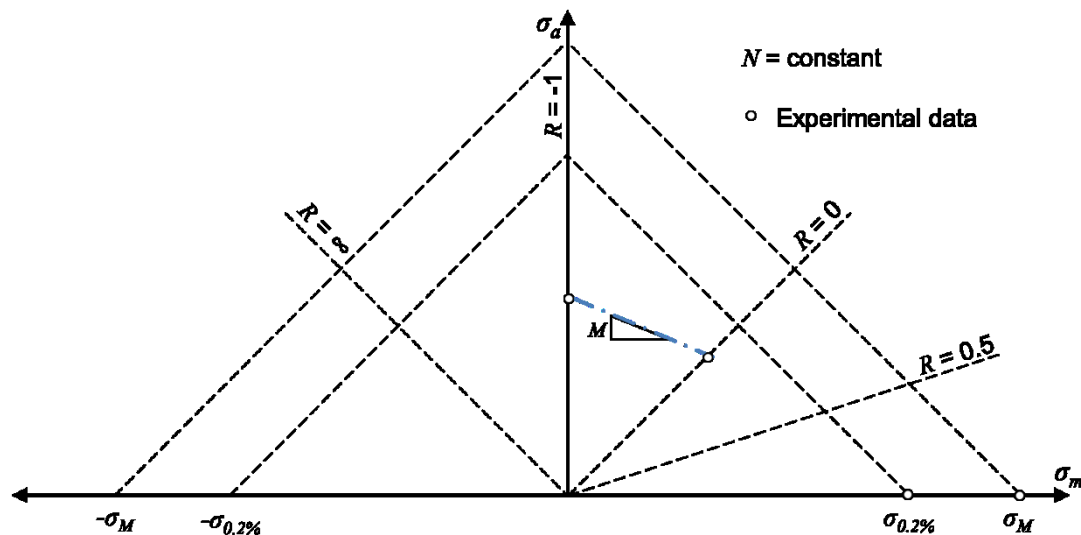


Figure 1.15: Schematic illustration of Haigh or constant life diagrams and the mean stress sensitivity M developed for the description of metallic material behaviour under different load ratios according to [22].

Among others, Kawai [73,74,76] and Vassilopoulos [77–79] published theories and formulations for accurate description of Haigh diagrams for different composite materials. For composite materials, the shape of the Haigh Diagram may appear different from the traditional Haigh diagram as illustrated in figure 1.15 as a result of the significant influences of the e.g. composite type, the fibre architecture and the applied load angle. Furthermore, temperature, load ratio or multiaxial loads determine the material fatigue behaviour. One representative example of experimental data evaluated at different load ratios R and predictive formulations for constant life diagrams of a $[90/0/\pm 45/0]_s$ E-glass/polyester laminate from Vassilopoulos, Manshadi et al. [79] is illustrated in figure 1.16. Accurate predictions of Haigh or constant life diagrams consequently allow statements about the performance of composite materials under unknown load situations.

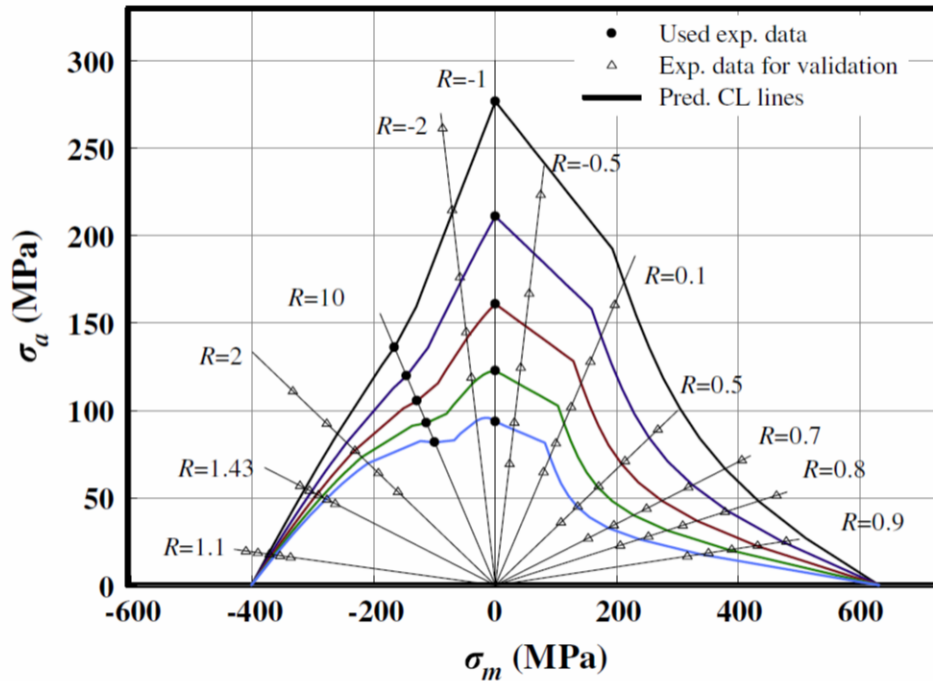


Figure 1.16: Representative example of experimental data and predicted constant life diagrams of a $[90/0/\pm 45/0]_s$ E-glass/polyester laminate from Vassilopoulos, Manshadi et al. [79]. The formulations were based on S-N curves with $R=-1$ and $R=10$.

To assess the effect of load time history, well-known approaches for metallic materials such as rainflow counting may be used [12,21]. One simple but effective way to validate the damage history is the Miner rule, initially developed for metallic materials. The Miner rule accumulates the damage distribution of each single cycle. Therefore, the number of cycles of each load block n_i is set into relation to the theoretically possible number of cycles N_i limited by the S-N curve with the slope k . If the damage sum reaches 1, failure is assumed to occur (1.12). Different ways of counting the applied cycles have been proclaimed: Miner original, Miner modified and Miner elementary according to [22] (figure 1.17). Of course, resulting from the simplicity of theory, crack initiation, crack development or sequence influences in non-constant amplitude fatigue tests are not taken into account [12,21]. However, a technological estimation of expected number of cycles to failure even under multiaxial load channels is possible with this theory. Some studies have shown that the Miner's rule can be applied to composite

materials as well [80,81]. For composite materials, the modification Miner elementary (figure 1.16) refers best to the usually observed material behaviour.

$$D = \sum_i \frac{n_i}{N_i} \quad (1.12)$$

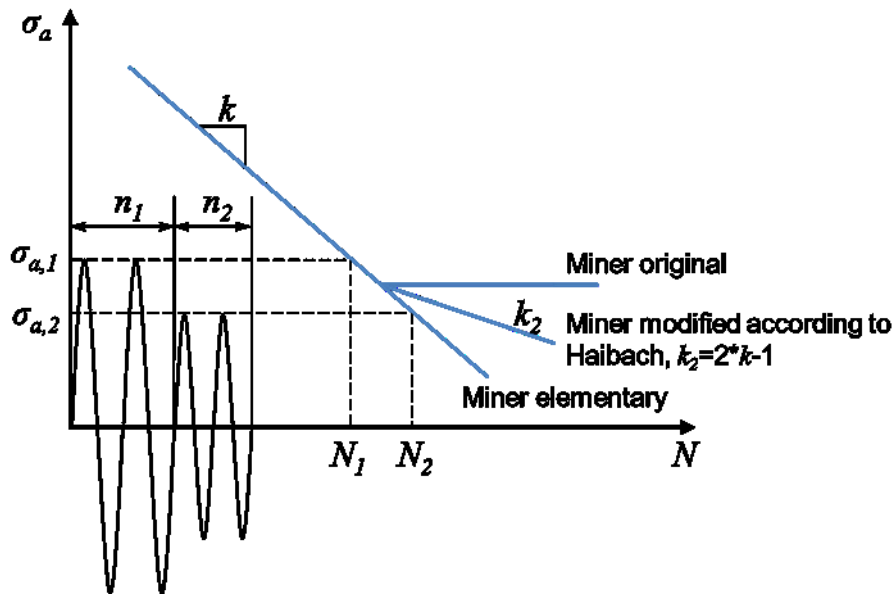


Figure 1.17: Damage calculation developed for metallic materials based on S-N curves according to “Miner original”, “Miner Elementary” and “Miner modified according to Haibach” according to [22].

However, even if strength based fatigue approaches offer the advantage of experience from metallic materials in complex applications, adaptations to meet the unique behaviour of composite materials have to be made. In order to include the damage history, not on microscopic but on macroscopic scale reflected by the mechanical properties, fatigue-life predictions will have to take the decreasing mechanical properties discussed in this chapter into account. Solely strength and damage accumulation based approaches will not provide satisfying results because within these approaches usually only the event of failure is taken into account.

Therefore, tools being able to calculate the stiffness decreases in composite materials based on input parameters will have to be developed in order to

decrease the experimental time effort. Although theories being able to calculate properties of composites based on the properties of the single plies such as the classical laminate theory work well for quasi-static loads, fatigue-induced stiffness decreases describing the events prior to failure can hardly be predicted so far. Additionally, the prediction of the event of failure has to be adapted for fatigue failure. New studies try to combine the benefits of quasi-static failure criteria based on physical considerations with S-N curve based theories developed for metallic fatigue [82].

1.8. References

- [1] IPCC - Intergovernmental Panel on Climate Change. IPCC Fifth Assessment Synthesis Report 'Climate Change 2014': Mitigation of Climate Change; Available from: <http://mitigation2014.org/report/final-draft/final-draft-fgd-17122013>.
- [2] IPCC - Intergovernmental Panel on Climate Change. Climate Change 2014 - Impacts, Adaptation and Vulnerability: Summary for Policymakers; Available from: https://ipcc-wg2.gov/AR5/images/uploads/WG2AR5_SPM_FINAL.pdf.
- [3] United Nations. The Millennium Development Goals Report 2014; Available from: <http://www.un.org/millenniumgoals/2014%20MDG%20report/MDG%202014%20English%20web.pdf>.
- [4] Jean-Claude Juncker. A New Start for Europe: My Agenda for Jobs, Growth, Fairness and Democratic Change: Political Guidelines for the next European Commission; Available from: http://ec.europa.eu/priorities/energy-union/index_en.htm.
- [5] REN21. Renewables 2014: Global Status Report; Available from: http://www.ren21.net/portals/0/documents/resources/gsr/2014/gsr2014_full%20report_low%20res.pdf.
- [6] European Commission. White Paper: Roadmap to a Single European Transport Area - Towards a competitive and resource efficient transport system. Brussels; 2011.

- [7] European Commission. European Aeronautics: A vision for 2020: Report of the Group of Personalities; Available from: <http://ec.europa.eu/research/growth/aeronautics2020/>.
- [8] AIRUBS. Global Market Forecast 2014-2033; Available from: <http://www.airbus.com/company/market/forecast/>.
- [9] Boeing. Long-term forecast 2013-2033; Available from: <http://www.boeing.com/boeing/commercial/cmo/>.
- [10] Breuer U. Efficient CFRP Airframe Manufacturing Technology: Yesterday, Today and Tomorrow. In: Univ.-Prof. Dr.-Ing. Ralf Schledjewski, editor. Schriftenreihe Kunststofftechnik Leoben Band 4: 23. Leobener Kunststoff-Kolloquium; 2014, p. 1–5.
- [11] BMW. i3: Catalogue; Available from: <http://www.bmw.com/com/en/newvehicles/i/i3/2013/showroom/index.html>.
- [12] Schürmann H. Konstruieren mit Faser-Kunststoff-Verbunden: Mit 39 Tabellen. 2nd ed. Berlin, Heidelberg, New York, NY: Springer; 2007.
- [13] Ehrenstein GW. Mit Kunststoffen konstruieren. 3rd ed. München: Hanser; 2007.
- [14] Janda R. Kunststoffverbundsysteme: Grundlagen, Anwendung, Verarbeitung, Prüfung. 1st ed. Weinheim: VCH; 1990.
- [15] Germany Trade and Invest GmbH. Zukunftswerkstoff CFK mit starkem Aufwind; 2012.
- [16] Leitner H. Leichtbau. Leoben; WS 2013/14.
- [17] Hodgkinson JM. Mechanical testing of advanced fibre composites. Boca Raton, FL, Cambridge, England: CRC Press; Woodhead; 2000.
- [18] Flight International. IABG ready to put the A380 through fatigue paces: Aiframe to be subjected to test programme equivalent to 60,000 flight cycles by 2008; Available from: <http://www.flightglobal.com/FlightPDFArchive/2004/2004-09%20-%200685.PDF>.
- [19] Talreja R. Fatigue of Composite Materials. Pennsylvania, U.S.A: Technomic Publishing Inc; 1987.

-
- [20] Reifsnider KL (ed.). *Fatigue of composite materials*. Amsterdam, New York: Elsevier; 1991.
- [21] Radaj D. *Ermüdungsfestigkeit: Grundlagen für Leichtbau, Maschinen- und Stahlbau*. 3rd ed. Berlin [u.a.]: Springer; 2007.
- [22] Haibach E. *Betriebsfestigkeit: Verfahren und Daten zur bauteilberechnung*. Berlin: Springer; 2006.
- [23] The Telegraph. UFO wind turbine 'broke due to mechanical failure not collision with flying object'; Available from: <http://www.telegraph.co.uk/news/newstoppers/howaboutthat/4578998/UFO-wind-turbine-broke-due-to-mechanical-failure-not-collision-with-flying-object.html>.
- [24] Ehrenstein GW. *Faserverbund-Kunststoffe: Werkstoffe, Verarbeitung, Eigenschaften*. 2nd ed. München [u.a.]: Hanser; 2006.
- [25] Stinchcomb W, Bakis CE. Fatigue behaviour of composite materials. In: Reifsnider KL, editor. *Fatigue of composite materials*. Amsterdam, New York: Elsevier; 1991, p. 105–80.
- [26] Suresh S. *Fatigue of materials*. 2nd ed. Cambridge, New York: Cambridge University Press; 1998.
- [27] Zahnt B. *Ermüdungsverhalten von diskontinuierlich glasfaserverstärkten Kunststoffen: Charakterisierungsmethoden, Werkstoffgesetze und Struktur-Eigenschafts-Beziehungen*. Dissertation. Leoben; 2003.
- [28] Mösenbacher A. *Modellentwicklungen zur betriebsfesten Auslegung von Strukturbauteilen aus glasfaserverstärkten Thermoplasten im Motorraum*. Dissertation. Leoben; 2014.
- [29] Ye L. On fatigue damage accumulation and material degradation in composite materials. *Composites Science and Technology* 1989;36(4):339–50.
- [30] Talreja R. Damage development in composites: Mechanisms and modelling. *The Journal of Strain Analysis for Engineering Design* 1989;24(4):215–22.
- [31] Reifsnider K, Talug A. Analysis of fatigue damage in composite laminates. *International Journal of Fatigue* 1980;2(1):3–11.

- [32] Curtis PT. The fatigue behaviour of fibrous composite materials. *The Journal of Strain Analysis for Engineering Design* 1989;24(4):235–44.
- [33] Curtis PT. Tensile fatigue mechanisms in unidirectional polymer matrix composite materials. *International Journal of Fatigue* 1991;13(5):377–82.
- [34] Gamstedt E, Berglund LA, Peijs T. Fatigue mechanisms in unidirectional glass-fibre-reinforced polypropylene. *Composites Science and Technology* 1999;59(5):759–68.
- [35] Gamstedt E, Sjögren B. Micromechanisms in tension-compression fatigue of composite laminates containing transverse plies. *Composites Science and Technology* 1999;59(2):167–78.
- [36] Gamstedt EK, Talreja R. Fatigue damage mechanisms in unidirectional carbon-fibre-reinforced plastics. *Journal of Materials Science* 1999(34):2535–46.
- [37] Talreja R. Damage Characterization. In: Reifsnider KL, editor. *Fatigue of composite materials*. Amsterdam, New York: Elsevier; 1991, p. 79–103.
- [38] Reifsnider KL, Henneke EG, Stinchcomb W, Duke JC. Damage Mechanics and NDE of Composite Laminates. In: Hashin Z, Herakovich CT, editors. *Composite Materials: Recent Advances*: Pergamon Press Inc; 1983, p. 399–420.
- [39] Hessabi ZR, Majidi B, Aghazadeh J. Effects of Stacking Sequence on Fracture Mechanisms in Quasi-isotropic Carbon/Epoxy Laminates under Tensile Loading. *Iranian Polymer Journal* 2005(14 (6)):531–8.
- [40] Correa E, Gamstedt EK, París F, Mantič V. Effects of the presence of compression in transverse cyclic loading on fibre–matrix debonding in unidirectional composite plies. *Composites Part A: Applied Science and Manufacturing* 2007;38(11):2260–9.
- [41] Jamison RD, Schulte K, Reifsnider KL, Stinchcomb WW. Characterization and analysis of damage mechanisms in tension-tension fatigue of graphite/epoxy laminates. In: *Effects of defects in composite materials: A symposium sponsored by ASTM Committees D-30 on High Modulus Fibers and Their Composites and E-9 on Fatigue*,

-
- San Francisco, Calif., 13-14 Dec. 1982. Philadelphia, Pa: ASTM; ©1984, p. 21–55.
- [42] Talreja R. Assessment of the fundamentals of failure theories for composite materials. *Composites Science and Technology* 2014;105:190–201.
- [43] Harris B (ed.). *Fatigue in composites: Science and technology of the fatigue response of fibre-reinforced plastics*. Cambridge: Woodhead; CRC Press; 2003.
- [44] Reifsnider KL, Stinchcomb WW, O'Brien TK. Frequency Effects on a Stiffness-Based Fatigue Failure Criterion in Flawed Composite Specimens. In: Reifsnider KL, Lauraitis KN, editors. *Fatigue of filamentary composite materials: A symposium*. Philadelphia: ASTM; 1977, p. 171–84.
- [45] Shokrieh MM, Lessard LB. Multiaxial fatigue behaviour of unidirectional plies based on uniaxial fatigue experiments - II. Experimental evaluation. *Int. J. Fatigue* Vol. 19 No. 3 1997(Vol. 19 No. 3):209–17.
- [46] Passipoularidis VA, Philippidis T, Bronsted P. Fatigue life prediction in composites using progressive damage modelling under block and spectrum loading. *International Journal of Fatigue* 2010(33):132–44.
- [47] Philippidis T, Passipoularidis V. Residual Strength after fatigue in composites_theory vs experiment. *International Journal of Fatigue* 2007(29):2104–16.
- [48] Naderi M, Khonsari MM. A comprehensive fatigue failure criterion based on thermodynamic approach. *Journal of Composite Materials* 2011;46(4):437–47.
- [49] Shokrieh M, Taheri-Behrooz F. A unified fatigue life model based on energy method. *Composite Structures* 2006;75(1-4):444–50.
- [50] Frank A, Freimann W, Pinter G, Lang RW. A fracture mechanics concept for the accelerated characterization of creep crack growth in PE-HD pipe grades. *Engineering Fracture Mechanics* 2009;76(18):2780–7.

- [51] Frank A, Pinter G, Lang RW. Prediction of the remaining lifetime of polyethylene pipes after up to 30 years in use. *Polymer Testing* 2009;28(7):737–45.
- [52] Arbeiter F, Pinter G, Frank A. Characterisation of quasi-brittle fatigue crack growth in pipe grade polypropylene block copolymer. *Polymer Testing* 2014;37:186–92.
- [53] O'Brien TK. Delamination of composite materials. In: Reifsnider KL, editor. *Fatigue of composite materials*. Amsterdam, New York: Elsevier; 1991, p. 181–98.
- [54] Abdussalam S. Damage and fracture mechanics of composite materials. Dissertation. Winnipeg, Manitoba, Canada; 1999.
- [55] Akshantale N, Talreja R. A mechanistic model for fatigue damage evolution in composite lamiantes. *Mechanics of Materials* 1998(29):123–40.
- [56] Stelzer S, Pinter G, Brunner AJ. Comparison of Quasi-static and Cyclic Fatigue Delamination Resistance of Carbon Fiber Reinforced Polymer-matrix Laminates under Different Mode Loading. *Procedia Materials Science* 2014;3:1087–92.
- [57] Ng Y. Deriving Composite Lamina Properties from Laminate Properties Using Classical Lamination Theory and Failure Criteria. *Journal of Composite Materials* 2005;39(14):1295–306.
- [58] Park CH, Baz A. Comparison between finite element formulations of active constrained layer damping using classical and layer-wise laminate theory. *Finite Elements in Analysis and Design* 2001;37:35–56.
- [59] Chaphalkar P, Kelkar AD. Classical laminate theory model for twill weave fabric composites. *Composites Part A: Applied Science and Manufacturing* 2001;32(9):1281–9.
- [60] Ladevèze P, Lubineau G, Marsal D. Towards a bridge between the micro- and mesomechanics of delamination for laminated composites. *Composites Science and Technology* 2006;66(6):698–712.

-
- [61] Hinton M, Kaddour A, Soden P. Evaluation of failure prediction in composite laminates: background to 'part B' of the exercise. *Composite Science and Technology* 2002(62):1481–8.
- [62] Hinton M, Kaddour A, Soden P. Evaluation of failure prediction in composite laminates: background to 'part C' of the exercise. *Composites Science and Technology* 2004;64(3-4):321–7.
- [63] Kaddour A, Hinton M, Smith P. Damage theories for fibre-reinforced polymer composites: the third world-wide failure exercise (WWFE-III). 16th International Conference on Composite Materials 2007.
- [64] Hinton M, Kaddour A. The second world-wide failure exercise: benchmarking of failure criteria under triaxial stresses for fibre-reinforced polymer composites. 16th International Conference on Composite Materials 2007.
- [65] Soden P, Kaddour A, Hinton M. Recommendations for designers and researchers resulting from the world-wide failure exercise. *Composites Science and Technology* 2004;64(3-4):589–604.
- [66] Azzi VD, Tsai SW. Anisotropic strength of composites. *Experimental Mechanics* 1965;5(9):283–8.
- [67] Tsai S, Wu E. A General Theory of Strength for Anisotropic Materials. *Journal of Composite Materials* 1971(Vol. 5):58–80.
- [68] Argon AS. Fracture of composites. In: Herman H, editor. *Treatise on materials science and technology*. New York: Academic Press; 1972- <1989>, p. 79–114.
- [69] Puck A. *Festigkeitsanalyse von Faser-Matrix-Laminaten: Modelle für die Praxis*. München, Wien: Hanser; 1996.
- [70] Puck A, Schürmann H. Failure analysis of FRP laminates by means of physically based phenomenological models. *Composites Science and Technology* 1998(58):1045–67.
- [71] Vinogradov V, Hashin Z. Probabilistic energy based model for prediction of transverse cracking in cross-ply laminates. *International Journal of Solids and Structures* 2005;42(2):365–92.

- [72] Hashin Z. Failure Criteria for Unidirectional Fiber Composites. *J. Appl. Mech.* 1980;47(2):329.
- [73] Kawai M, Yajima S, Hachinohe A, Takano Y. Off-Axis Fatigue Behavior of Unidirectional Carbon Fiber-Reinforced Composites at Room and High Temperatures. *Journal of Composite Materials* 2001;35(7):545–76.
- [74] Kawai M. A phenomenological model for off-axis fatigue behavior of unidirectional polymer matrix composites under different stress ratios. *Composites Part A: Applied Science and Manufacturing* 2004;35(7-8):955–63.
- [75] Philippidis TP, Vassilopoulos AP. Life prediction methodology for GFRP laminates under spectrum loading. *Composites Part A: Applied Science and Manufacturing* 2004;35(6):657–66.
- [76] Kawai M, Saito S. Off-axis strength differential effects in unidirectional carbon/epoxy laminates at different strain rates and predictions of associated failure envelopes. *Composites Part A: Applied Science and Manufacturing* 2009;40(10):1632–49.
- [77] Philippidis TP, Vassilopoulos AP. Fatigue Strength Prediction under Multiaxial Stress. *Journal of Composite Materials* 1999;33(17):1578–99.
- [78] Philippidis TP, Vassilopoulos AP. Fatigue design allowables for GRP laminates based on stiffness degradation measurements. *Composite Science and Technology* 2000(60):2819–28.
- [79] Vassilopoulos AP, Manshadi BD, Keller T. Piecewise non-linear constant life diagram formulation for FRP composite materials. *International Journal of Fatigue* 2010;32(10):1731–8.
- [80] Nijssen R. Fatigue life prediction and strength degradation of wind turbine rotor blade composites. Dissertation. Delft; 2006.
- [81] Hahne C, Knaust U, Schürmann H. Zur Festigkeitsbewertung von CFK-Strukturen unter Pkw-Betriebslasten*. *MP* 2014;56(7-8):542–9.
- [82] Orth M, Butz M, Gaier C. Durability Assessment of CFRP Components with Static Failure Criteria // Betriebsfestigkeitsanalyse von CFK-Bauteilen mit statischen Versagenskriterien*. *MP* 2014;56(7-8):559–66.

2. Objectives

As outlined in the introductory part, the research issue of composite fatigue is both complex and comprehensive. To make reasonable and detailed scientific investigations possible, it was decided to restrict the experimental studies in this thesis to unidirectional and multidirectional carbon/epoxy composites. The characterisation of the fatigue damage and cyclic behaviour was important in order to understand the unique physical behaviour of the investigated material which may vary as a result of material properties and stacking sequence effects [1–3]. On this experimental and physical basis, possibilities for application-oriented calculation or simulation of material properties should be assessed. Thereby, a comprehensive strategy from experimental testing and material characterisation to fatigue-life prediction should be realised.

In order to sufficiently address those aspects, the objected goals were defined in the following manner:

1. Definition of materials, stacking sequences and fibre volume fractions.
2. Production of epoxy resin plates and carbon/epoxy plates with defined fibre volume fractions.
 - Monitoring and validation of plate quality and fibre fraction with thermo-analytical, thermo-mechanical and microscopic methods.
3. Assessment of test parameters, specimen geometry and applied measurement techniques in preliminary mechanical tests.

- Identification of test frequencies and combined influence of frequency, anisotropy and stacking sequence on hysteretic heating.
 - Application of different strain measurement techniques in fatigue tests.
 - Recommendations for cyclic strain measurement of composite materials.
4. Comprehensive fatigue tests with carbon/epoxy laminates and epoxy resin.
- Quasi-static tension and compression tests in dependency of anisotropy and fibre volume content.
 - Tension-tension and tension-compression fatigue tests in dependency of anisotropy and fibre volume content.
 - Assessment of influence of fibre volume fraction, anisotropy and mechanical mean stress on damage mechanisms.
 - Evaluation of cyclic stress-strain behaviour.
5. Experimental strategy for measuring adequate input parameters for fatigue-life prediction tools.
- Development of a new experimental method in order to uncouple material specific strain-rate effects and fatigue stiffness evaluation.
 - Evaluation of S-N curves.
6. Fatigue-life prediction of a multidirectional carbon/epoxy laminate.
- Development of a stiffness-based fatigue-life prediction tool based on fatigue-induced physical stiffness decreases.
 - Fatigue-life estimation with a newly adapted version of the S-N curve based software tool FEMFAT.
 - Validation and discussion of the obtained results and future potential for optimisation.

2.1. References

- [1] Reifsnider K, Talug A. Analysis of fatigue damage in composite laminates. *International Journal of Fatigue* 1980;2(1):3–11.
- [2] Hessabi ZR, Majidi B, Aghazadeh J. Effects of Stacking Sequence on Fracture Mechanisms in Quasi-isotropic Carbon/Epoxy Laminates under Tensile Loading. *Iranian Polymer Journal* 2005(14 (6)):531–8.
- [3] Correa E, Gamstedt EK, París F, Mantič V. Effects of the presence of compression in transverse cyclic loading on fibre–matrix debonding in unidirectional composite plies. *Composites Part A: Applied Science and Manufacturing* 2007;38(11):2260–9.

3. Structure of the Thesis

According to the objectives outlined above, the thesis presents a series of subsequent publications illustrating the progress in development of fatigue-life prediction tools for carbon/epoxy laminates. The thesis is divided in six parts. The parts are:

1. Preamble
2. Introduction to the thesis
3. Measuring techniques in fatigue tests
4. Fatigue-induced damage mechanisms in carbon/epoxy laminates
5. Fatigue-life prediction of carbon/epoxy composites with two different approaches
6. Summary, conclusions and outlook

The first part presents mandatory (e.g. affidavit) and content related sections (e.g. table of content).

The second part presents an introduction on the political, economic and technological background resulting in the motivation for this thesis. Furthermore the objectives of this thesis are outlined briefly. In the third part, the experimental prerequisites for later fatigue-life prediction are discussed. Based on the investigated mechanical fatigue behaviour of the material, appropriate experimental possibilities for strain measurement in fatigue tests were compared and assessed. The mechanical and hysteretic behaviour of the material in dependency on the stacking sequence and the anisotropy was studied in detail in order to define reliable test parameters for the subsequent material characterisation. Furthermore, a new experimental test procedure

was developed which was designed to meet the anisotropic and strain-dependent nature of the material.

In the fourth part, the unique damage mechanisms and stress-strain behaviour of the investigated material were studied in quasi-static tension and compression and also tension-tension and tension-compression fatigue tests. Apart from the influence of anisotropy and mechanical loads and amplitudes, the effect of fibre volume fraction was investigated in detail. Especially the increasing amount of matrix material, which is known to be the initiator for the damage processes in the material due to the formation of matrix cracks [1,2], is of importance for the general understanding of damage mechanisms in composite materials. The quality and fibre content of the produced carbon/epoxy plates was verified with thermo-analytical and thermo-mechanical methods.

In the fifth part, the new experimental test procedure was used to produce strain-rate independent material stiffnesses progresses reflecting the effects of anisotropy and fibre volume fraction. The experimentally measured results were compared to conventionally used stiffness calculations from stress-strain hysteresis loops in fatigue tests and advantages of the new test procedure were discussed. Furthermore, a stiffness-based fatigue-life prediction procedure was developed and implemented in a software programme. By use of this newly developed routine, the fatigue-induced stiffness decreases of a multiaxial carbon/epoxy composite were successfully calculated and validated with experimental results. As second possibility for fatigue-life prediction, the fatigue strengths of the same multiaxial composite were calculated by using the previously for composites adapted software routine FEMFAT.

The individual parts three, four and five are opened by a brief introduction about the most relevant background information of the specific topic. Thereby, the introduction shall outline the central aspects addressed within the respective paper(s). Furthermore, the major content of the paper(s) is presented. Subsequently, the relevant papers published by the main-author of this thesis along with the co-authors are presented. The individual papers present detailed scientific background and considerations, materials, experimental work, data and conclusions of the scientific work.

In the sixth part the thesis is reviewed briefly and conclusions are drawn from the key findings of the thesis. Finally, the outlook points the future challenges not addressed so far out and outlines recommendations and potential work fields based on the presented findings.

3.1. References

- [1] Reifsnider KL, Henneke EG, Stinchcomb W, Duke JC. Damage Mechanics and NDE of Composite Laminates. In: Hashin Z, Herakovich CT, editors. Composite Materials: Recent Advances: Pergamon Press Inc; 1983, p. 399–420.
- [2] Talreja R. Damage Characterization. In: Reifsnider KL, editor. Fatigue of composite materials. Amsterdam, New York: Elsevier; 1991, p. 79–103.

Part III.

Measuring techniques in composite fatigue tests

4. Introduction to Publication 1

To investigate and develop possibilities for fatigue-life prediction it has to be considered that for all predictive models some sort of experimental input parameters are required. Of course, the quality of predictions depends decisively on the quality of the input parameters. Although the experimental testing of composite materials has been established for decades [1], the anisotropic material behaviour of the material requires practical experience in order to produce reasonable and reproducible results. While for the choice of specimen geometry for quasi-static and fatigue tests different standards or published studies can be consulted e.g. [2–7], for the applicability of strain measurement technique mainly studies for quasi-static load or high-speed load cases have been published [8,9]. If the cyclic stress-strain behaviour or stiffness decreases shall be investigated, for which strain measurement is necessary, little literature exists. The progressing damage mechanisms discussed in chapter 1 and the significant differences of stiffness in and transverse to fibre direction may cause measuring artefacts.

Therefore, an extensive study of strain measurement techniques possibly applicable for fatigue tests with carbon/epoxy laminates has been conducted prior to the actual material tests. Publication 1 includes experimental studies in which strain gauges, mechanical extensometers, digital image correlation and 2 D camera systems were applied on unidirectional and multidirectional carbon/epoxy laminates in quasi-static and fatigue tests. The effect of different stacking sequences on hysteretic heating and the influence of specimen's stiffness on stress-strain data recorded by servo-hydraulic piston were investigated. The influence of strain measurement technique on quasi-static moduli and moduli evaluated from stress-strain hystereses was assessed. Furthermore, effects of surface cracks and anisotropy on the

applicability of the different strain measurement techniques especially in fatigue tests were discussed. Results showed that for the measuring techniques requiring intact specimen surface such as mechanical extensometers, strain gauges and all optical systems, the quality and endurance of strain measurement was determined by the occurrence of surface cracks. Consequently, for specimens such as unidirectional specimens loaded longitudinal to fibre direction the local strain measurement was usually not possible until fracture. On the contrary, for specimens measured transversal to fibre direction, local strain measurement was possible with all applied techniques. In that case, mechanical extensometers might be the technique to be recommended due to the easy application. Depending on the specimen's stiffness the piston displacement, which might be considered as global strain measurement, provided reasonable results as well. In conclusion, recommendations for accurate strain measurement depending on the unique properties of all the investigated fibre lay-ups were provided and the observed effects influencing the material behaviour or measuring artefacts were discussed in detail.

4.1. References

- [1] Hodgkinson JM. Mechanical testing of advanced fibre composites. Boca Raton, FL, Cambridge, England: CRC Press; Woodhead; 2000.
- [2] ASTM International. Standard Test Method for Tensile Properties of Polymer Matrix Composite Materials(ASTM D3039/D3039M-00). West Conshohocken, PA, United States: ASTM International; 2000.
- [3] ASTM International. Standard Test Method for Tension-Tension Fatigue of Polymer Matrix Composite Materials(ASTM D3479/D3479M - 96). West Conshohocken, PA, United States: ASTM International; 2007.
- [4] ASTM International. Standard Test Method for In-Plane Shear Response of Polymer Matrix Composite Materials by Tensile Test of a $\pm 45^\circ$ Laminate(ASTM D3518/D3518M-94). West Conshohocken, PA, United States: ASTM International; 2007.

-
- [5] ASTM International. Standard Test Method for Compressive Properties of Polymer Matrix Composite Materials with Unsupported Gage Section by Shear Loading (ASTM D3410/D3410M-03). West Conshohocken, PA, United States: ASTM International; 2008.
- [6] Baere I de, van Paepegem W, Degrieck J. On the design of end tabs for quasi-static and fatigue testing of fibre-reinforced composites. *Polym. Compos* 2009;30(4):381–90.
- [7] Baere I de, van Paepegem W, Hochard C, Degrieck J. On the tension–tension fatigue behaviour of a carbon reinforced thermoplastic part II: Evaluation of a dumbbell-shaped specimen. *Polymer Testing* 2011;30(6):663–72.
- [8] Frieden J, Cugnoni J, Botsis J, Gmür T, Ćorić D. High-speed internal strain measurements in composite structures under dynamic load using embedded FBG sensors. *Composite Structures* 2010;92(8):1905–12.
- [9] He Y, Makeev A, Shonkwiler B. Characterization of nonlinear shear properties for composite materials using digital image correlation and finite element analysis. *Composites Science and Technology* 2012;73:64–71.

5. Publication 1

5.1. Bibliographic information

- Title: On the strain measurement and stiffness calculation of carbon fibre reinforced composites under quasi-static tensile and tension-tension fatigue loads
- Authors and relevant contributions to this publication:
 - Julia BRUNBAUER¹
Application and implementation of strain measurement techniques, experimental testing, data evaluation, preparation of the publication
 - Gerald PINTER¹
Discussion of experimental data
- Affiliation:
 1. Institute of Materials Science and Testing of Polymers, Montanuniversitaet Leoben, Otto Glöckel-Strasse 2, 8700 Leoben, Austria
- Periodical: Polymer Testing
- DOI: 10.1016/j.polymeresting.2014.09.014

Statement with regard to this publication: The manuscript presented here is an adapted accepted manuscript in order to fit the formatting of the thesis and does not necessarily reflect exactly the actually published version.

5.2. Abstract

The applicability of different strain measurement techniques for carbon/epoxy laminates under quasi-static tensile and tension-tension fatigue loads was studied. Strain gauges, mechanical extensometers, digital image correlation and 2 D camera systems were applied on laminates tested at angles of 0°, 45°, 60°, 90° and $\pm 45^\circ$. In addition, displacements recorded by the servo-hydraulic piston were monitored and compared to local strain measurement techniques. Representative examples that illustrate characteristics and limits of each technique in quasi-static and fatigue tests are discussed. Influences of the respective way of strain measurement, the specimens' surfaces, fibre directions and processes in the specimens during tests on the recorded stress-strain behaviour and on the calculated stiffnesses are presented. Recommendations for accurate strain measurement of anisotropic laminates based on the found results are made.

5.3. Introduction

Carbon fibre reinforced plastics (CFRP) are, compared to metal materials, a relatively young material class. Consequently, comprehensive mechanical tests for assuring safe applications are even more important for these materials. Mechanical composite tests range from coupon level for material characterisation to component tests under realistic load profiles [1–3]. The highly anisotropic properties provide great opportunities for tailored components on the one hand. On the other hand, mechanical and thermal anisotropy issue new challenges to testing [4]. Regarding mechanical tests, material properties are mainly determined under quasi-static or fatigue loads. For both load cases, anisotropic material behaviour has to be considered for load application. Additionally, strains in composites are generally small compared to other materials. Under fatigue loads the associated strains in composites are even smaller [5]. Therefore, the recording of fatigue stress-strain behaviour requires giving attention to test techniques. A variety of methods for strain measurement under mechanical loads is available. However, studies about the choice of strain measurement technique or

accurate strain measurement of composite materials are hardly available in literature.

In this work, the applicability of strain gauges, mechanical extensometer, digital image correlation (DIC) and 2 D camera systems for local strain measurement of carbon/epoxy laminates in quasi-static as well as fatigue tests is investigated. Piston displacement was also recorded in all tests to provide information about global strain behaviour. Stiffnesses of laminates tested at angles of 0° , 45° , 60° , 90° and $\pm 45^\circ$ are calculated according to different standards. Representative results measured with different techniques under quasi-static and fatigue loads are discussed. Limits, characteristics and influences on the measured stress-strain behaviour of each technique are illustrated. In preliminary tests, the tendency of different carbon/epoxy laminates for hysteretic heating in fatigue tests has been investigated, which is also presented. Recommendations for accurate mechanical testing, strain measurement and stiffness calculation under mechanical loads are given in conclusion.

5.3.1. Strain gauges

Strain gauges are one of the oldest and most accepted methods for measuring strains and were initially developed for use on specific metals. Measuring strains with strain gauges is based on changes in electrical resistance. Small resistance changes can be considered and are generally measured by using a Wheatstone bridge circuit [4]. When applying them to composite materials inaccuracies, mainly caused by the anisotropic nature of composite materials, can occur. Measuring accuracy can also be affected by strain gauge misalignment [6]. Beyond the need for calibration [4] and precise strain gauge alignment [6], the amount of time and money when many tests are required often limits the application of strain gauges.

5.3.2. Mechanical extensometers

Extensometers are, as well as strain gauges, a well-known and established technique for measuring strains originally developed for metal testing. Extensometers are easy to apply and available in different sizes and with different blades, depending on the type of test specimen to assure good

contact. Hodgkinson [4] points out one recommendation when using extensometers for strain measurement of composites: since failure in composites can occur suddenly or almost explosively, removing the extensometers prior to failure to avoid damaging of the extensometers is recommended. Another aspect which prevents strain measurement to final failure has been investigated by [7], [8] and [9]. In these three works, unidirectional and braided carbon/epoxy composites were tested under fatigue loads. In all fatigue tests, extensometers lost surface contact with the surfaces of CFRP specimens in the range of 10^4 to 10^5 cycles because of slipping and delamination prior to composite failure.

5.3.3. Digital Image Correlation

Digital Image Correlation (DIC) systems have been developed since the 1980's and have seen continuous improvement to very high levels since then. The main requirement of these systems is a pattern attached to the surface of specimen to track local deformations. During loading, grey scale images of an object are compared with image correlation software. As a first step, the displacement field is calculated tangential to the displacement gradients. Secondly, strains are derived from the displacement gradients [10]. DIC systems provide great opportunities of accurate measurement of strains and strain fields. Longitudinal as well as transversal strains can be evaluated which provides advantage in comparison to other techniques. These systems are popular for different types of mechanical test with very different materials, such as high strain rate tests with glass-polypropylene weaves [11], biaxial tension and shear tests with unidirectional carbon-epoxy [10] or tests with polyoxymethylene [12].

5.3.4. Piston displacement

Piston displacement of test machines can also be used to interpret fatigue tests. In contrast to the local strain measurement techniques of strain gauges, extensometers and optical systems, piston displacement records not only the strain behaviour of the specimen but of the entire specimen–test machine–system. Consequently, data from piston displacement may vary from locally recorded data. Nevertheless, if the global character of the data

measured via piston displacement is kept in mind, it can offer useful information about material fatigue behaviour in addition to local techniques.

5.4. Experimental work

Laminates made of carbon fibre and epoxy resin were studied in quasi-static tensile and tension-tension fatigue tests. EPIKOTE™ Resin MGS® RIMR135 (approved by German Lloyd) with the curing system EPIKURE™ Curing Agent MGS® RIMH1366 by Momentive (Esslingen am Neckar, Germany) and carbon fibres HS 15-50/250 by G. Angeloni srl (Quarto d'Altino, Italy) were used to produce plates in a vacuum assisted resin transfer moulding process. Glass transition temperature T_g of the cured epoxy resin was about 93 °C (measured with differential scanning calorimetry). All carbon/epoxy plates were cured at 80 °C for 5 h. The curing process of carbon/epoxy plates was monitored by dielectric analysis to assure fully cured plates for further specimen production. Carbon fibre volume content was 55 % (measured with thermo gravimetric analysis). Unidirectional (UD) specimens were cut from plates with diamond blades at angles of 0°, 45°, 60° and 90°. Balanced ±45° specimens were also produced. Geometry was 200x10x1 mm (length x width x thickness) for UD 0° and 200x20x2 mm for all other specimens. Aluminium tabs with 1 mm thickness were glued on both sides of all specimens.

Quasi-static as well as fatigue tests were performed on a servo-hydraulic test machine MTS 810 equipped with a load frame and load cell for 100 kN by MTS Systems Corporations (Minnesota, USA). Gauge length for all specimens was 100 mm. Hydraulic wedge pressure of 5 MPa was chosen in order to prevent slipping without damaging the specimen. Quasi-static tensile tests were performed with a test speed of 0.5 mm/min to failure. Tensile moduli of specimens tested at different angles were calculated between 0.0005 and 0.0025 absolute strain according to ISO 527-4 [13] and ISO 527-5 [14] and between 0.001 and 0.003 absolute strain according to ASTM D3039 [15]. Only unidirectional specimens in the fibre direction were evaluated between 10 % and 50 % of the maximum tensile load according to aircraft standards in addition [16]. Fatigue tests were performed at four different stress levels. A minimum of three specimens was tested at each

stress level. All fatigue tests were performed with the R -value (= minimum force / maximum force) of 0.1 and constant load amplitude. Test frequency was chosen between 3 and 10 Hz depending on the test load and the tendency for hysteretic heating of the respective specimens. Temperature of the specimens was monitored with infrared (IR) sensors. Fans were additionally used to control the specimen temperature. Secant moduli E_s (5.1) and dynamic moduli E_{dyn} (5.2) were evaluated from stress-strain hystereses.

$$E_s = \frac{\sigma_{max}}{\varepsilon_{max}} \quad (5.1)$$

$$E_{dyn} = \frac{\sigma_{max} - \sigma_{min}}{\varepsilon_{max} - \varepsilon_{min}} \quad (5.2)$$

In quasi-static and fatigue tests, strains were measured with a variety of methods. Strain gauges by HBM (Darmstadt, Germany) were glued on the specimens' prepared surfaces and electric signals were directly embedded in the servo-hydraulic test machine's software. Extensometers by MTS Systems Corporations (Minnesota, USA) with a gauge length of 50 mm were fixed to the specimens with metallic tension springs. As Digital Image Correlation (DIC) System, ARAMIS 4M by Gom (Braunschweig, Deutschland) was used. Speckle patterns were produced on the specimen with graphite sprays. For analysis, strain fields were chosen in such a way that the measuring size was comparable to other techniques and edge effects could be neglected. Thus, 50x15 mm² were used for strain analysis for specimen dimension 200x20x2 mm, and 50x7 mm² for specimen dimension 200x10x1 mm. Additionally an optical system CV-X100 by Keyence Corporation (Osaka, Japan) was used. This camera system consisted of two cameras, red lights, software for line detection allowing automatic measurement of distances between marks on the specimen's surface. Both, DIC and the camera system were controlled by digital output signals from the MTS test machine.

Different strain measurement tools were installed on one specimen for direct comparison. For example, four strain gauges (two on the front and two on the back side of the specimen measuring strains in and transverse to the load direction), the optical strain measurement and an extensometer were used to measure strain on one specimen. In another configuration, DIC and

extensometer at the front side of a specimen were combined with two strain gauges on the back side (figure 5.1).

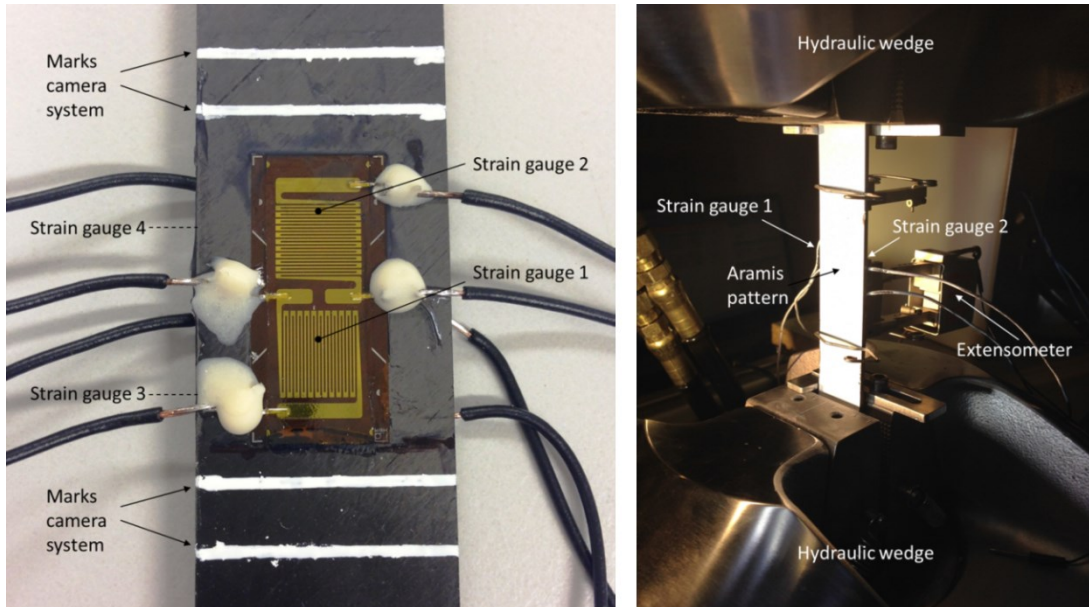


Figure 5.1: Test specimen with strain gauges and camera marks (left), test specimen with mechanical extensometer, strain gauges and DIC pattern fixed in the servo-hydraulic test machine (right).

The use of optical systems in fatigue tests went along with the need for data limitation. Because such systems required saving each picture for further strain processing, the optical systems were triggered by the test machine to control the number of saved pictures. For measurement of hysteresis, the test machine reduced the test speed to 1 Hz for two cycles. During these two measurement cycles, 20 data points were collected by the optical systems. The measurement cycles were repeated each 1000 cycles. Extensometer and piston collected also 20 data points in the same two cycles in order to be able to compare the different techniques.

5.5. Results and Discussion

All presented results of specimens tested in quasi-static and fatigue tests failed within the test length. Failure never occurred in the interface between the aluminium tab and specimen or within the tab length. Good adhesion between aluminium tabs and carbon/epoxy specimens was assured in preliminary tests and microscopic investigations of the interface. For the comparison of the different strain measurement techniques, only longitudinal strains in direction of the tensile load (11-direction) are used in the following.

5.5.1. Quasi-static tensile tests

UD 0°, UD 45° and UD 90° are discussed in detail in the following as representative of strain measurement and stiffness calculation in quasi-static tensile tests. Ultimate tensile strength (UTS), strain at break ϵ_{break} and Young's moduli evaluated according to different standards are presented with their respective standard deviations (SD). For UD 0° specimens (table 5.1), the deviation between "global" piston measurement and "local" measuring devices became obvious. Stress-strain curves recorded by piston were usually flatter in contrast to the locally measured curves. Accordingly, strains to failure measured by the piston were higher and Young's moduli smaller. Contact extensometer and non-contact optical systems measured similar Young's moduli. The extensometer was more sensitive to accurate fixing on the specimen as the higher standard deviation of extensometer data exemplifies. The strain ranges used for calculation [14–16] only made a difference for piston measurements. For locally measured stress-strain curves, the differences were negligible as a result of the highly linear curves.

The quasi-static results analysed with different standards for UD 45° are summarised in table 5.2. Representative stress-strain curves for UD 45° specimens are presented in figure 5.2 in addition. Piston and extensometer on the one hand, and optical systems on the other hand, measured similar Young's moduli E_{45} in the strain ranges between 0.0005 and 0.0025 [14] and between 0.001 and 0.003 absolute strain [15], respectively. Optical systems measured higher moduli in contrast to the extensometer, although all of those systems measured strains locally. An explanation for this observation could be that fibres oriented only under 45° probably had a tendency to align in the

load direction. As a consequence, a contact extensometer would have to follow the fibre movement and could not measure accurate uniaxial material behaviour. Strains at failure were slightly smaller when measured with optical methods.

Table 5.1: Quasi-static tensile mechanical properties of UD 0° measured and calculated with different methods.

	UTS ± SD [MPa]	$\varepsilon_{Break} \pm$ SD [%]	$E_{11} \pm$ SD [GPa] ISO 527-5	$E_{11} \pm$ SD [GPa] ASTM D3039	$E_{11} \pm$ SD [GPa] DIN EN 2561
Piston	1554 ± 64	1.7 ± 0.1	90.8 ± 3.9	91.0 ± 3.7	87.6 ± 4.6
Extensometer		1.2 ± 0.1	105.9 ± 5.5	105.3 ± 3.7	106.1 ± 4.2
DIC		1.3 ± 0.1	106.9 ± 1.8	107.0 ± 1.6	107.5 ± 1.4
Camera system		1.3 ± 0.1	105.1 ± 2.2	106.3 ± 1.9	105.9 ± 2.4

Table 5.2: Quasi-static tensile mechanical properties of UD 45° measured and calculated with different methods.

	UTS ± SD [MPa]	$\varepsilon_{Break} \pm$ SD [%]	$E_{45} \pm$ SD [GPa] ISO 527-5	$E_{45} \pm$ SD [GPa] ASTM D3039
Piston	66 ± 0	1.4 ± 0.1	8.7 ± 0.2	8.4 ± 0.2
Extensometer		1.3 ± 0.1	7.9 ± 0.1	8.0 ± 0.1
DIC		1.1 ± 0.1	9.2 ± 0.0	9.0 ± 0.1
Camera system		1.2 ± 0.1	9.6 ± 0.4	8.9 ± 0.4

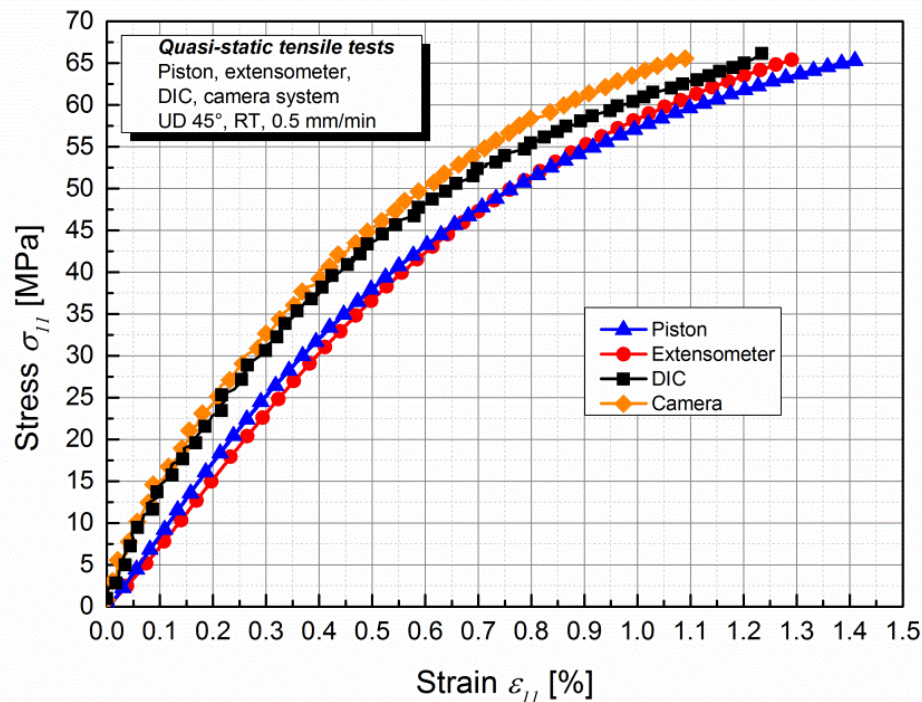


Figure 5.2: Stress-strain curves of a UD 45° specimen measured with the test machine's piston, mechanical extensometer, DIC and a camera system.

UTS, ε_{Break} and Young's moduli for unidirectional plies tested at angles of 90° E_{22} are summarised in table 5.3. For UD 90° laminates, contact extensometer measured higher Young's moduli than the non-contact optical systems. Calculating moduli between 0.0005 and 0.0025 measured with extensometer and optical systems led to similar results as taking the secant between 0.001 and 0.003 absolute strain, which indicated linear material behaviour in this strain range. Strains at break measured with piston and optical systems were on a similar scale.

Strain gauges produced results which were not comparable with other strain measurement methods. The measured strains were not on scales typical for the studied materials and standard deviations were very high. These observations might be due to the following reasons: strain gauge misalignment might have occurred during specimen preparation (especially UD 0° specimens were very sensitive to that) or transmission failures could be caused if the surface contact between specimen and strain gauge was not

ideal. Consequently, it was decided not to include the results measured by strain gauges in the tables. One exemplary fatigue test equipped with strain gauges is discussed in the following.

Table 5.3: Quasi-static tensile mechanical properties of UD 90° measured and calculated with different methods.

	UTS ± SD [MPa]	$\varepsilon_{Break} \pm$ SD [%]	$E_{22} \pm$ SD [GPa] ISO 527-5	$E_{22} \pm$ SD [GPa] ASTM D3039
Piston	33 ± 2	0.6 ± 0.1	5.6 ± 0.1	5.6 ± 0.0
Extensometer		0.5 ± 0.1	6.7 ± 0.1	6.3 ± 0.1
DIC		0.6 ± 0.1	5.4 ± 0.2	5.5 ± 0.5
Camera system		0.6 ± 0.1	5.7 ± 0.4	5.7 ± 0.3

5.5.2. Tension-tension fatigue tests

5.5.2.1. Effect of hysteretic heating

A necessary precondition in fatigue tests was to ensure that hysteretic heating stayed within certain temperature limits to produce comparable results. The choice of test frequency usually was a decision between short test times and hysteretic heating. Therefore, temperature increases of different specimen types under different fatigue loads were investigated in preliminary tests. It became apparent that the lay-ups of the specimens had significant influence on their tendency for hysteretic heating. In unidirectional specimens, on the one hand, the temperature increase was usually not higher than 5 °C during the entire test time. On the other hand, ±45° specimens were very sensitive to the chosen load frequency and the level of applied load. The explanation for this observation might be the higher tendency to inner movement in non-unidirectional specimens. Especially, ±45° layers may tend to align in the load direction in each cycle, which could cause high inner friction. Representative temperature curves for two ±45° specimens tested with the same frequency exemplify hysteretic heating and the benefit of additional fan cooling in figure 5.3. Specimen 1 was tested with

nominal maximum stress of 80 MPa, R 0.1, test frequency of 5 Hz without additional fan cooling. Temperature measured with an IR sensor increased constantly during the entire test time until a last sudden increase up to 63 °C before failure after $2.25 \cdot 10^4$ cycles. Because of the temperature influence, specimens that behaved in such a way were usually not representative for the actual material behaviour. In contrast, specimen 2 was tested at the even higher nominal maximum stress of 85 MPa, R 0.1, test frequency of 5 Hz with additional fan cooling. After a temperature increase from 25 °C to 30 °C during the first 10^3 cycles, the specimen's temperature stayed on a constant level up to 10^5 cycles. To reach a constant temperature level turned out to be very important for the specimen's lifetime. Before final failure after $1.78 \cdot 10^5$ cycles, the temperature increased up to 37 °C. Consequently, specimen 2 reached ten times higher number of cycles despite the applied cyclic load being higher and the test frequency the same in both tests.

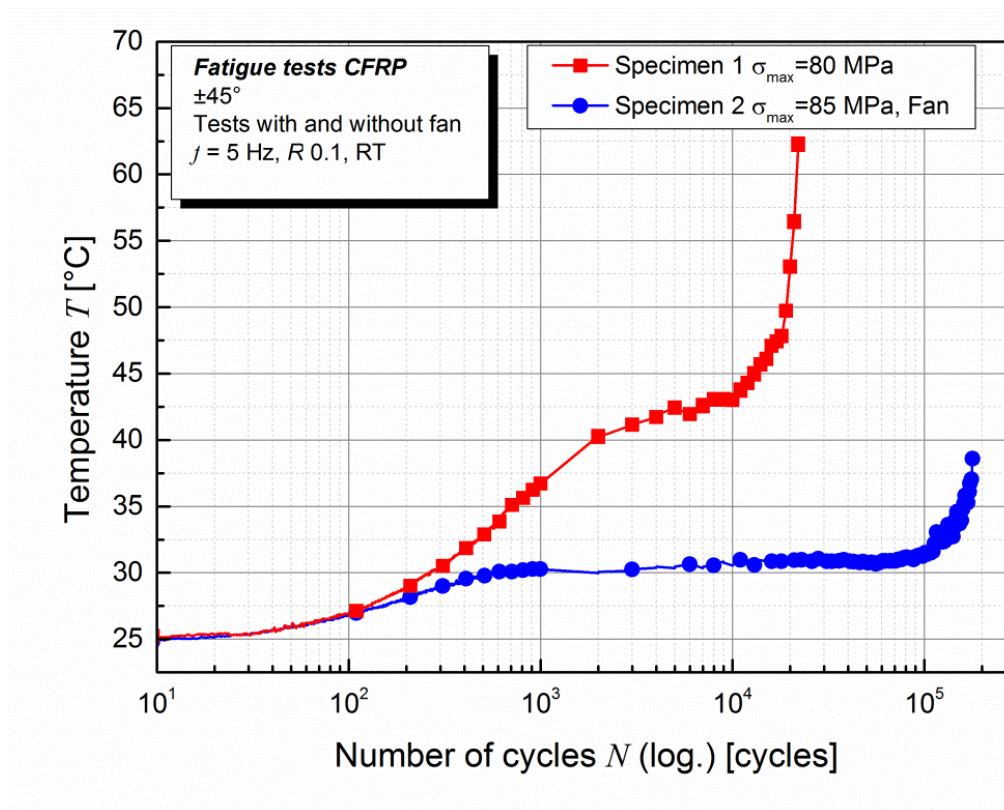


Figure 5.3: Temperature increase in $\pm 45^\circ$ specimens under tension-tension fatigue load due to hysteretic heating.

The significant influence of hysteretic heating on the measured stress-strain behaviour is illustrated in figure 5.4. The normalised dynamic moduli measured with extensometers of the same two specimens as illustrated in figure 5.3 are shown. The modulus decrease of specimen 1 (high hysteretic heating) started earlier and was more sudden compared to specimen 2. As a result of hysteretic heating, not only the number of cycles to failure but also the material's stress-strain behaviour changed. Consequently, test frequencies were chosen in order to avoid mean temperature decreases during the entire test higher than 8 °C. Temperature was monitored in all fatigue tests and non-unidirectional specimens were tested with additional fan cooling.

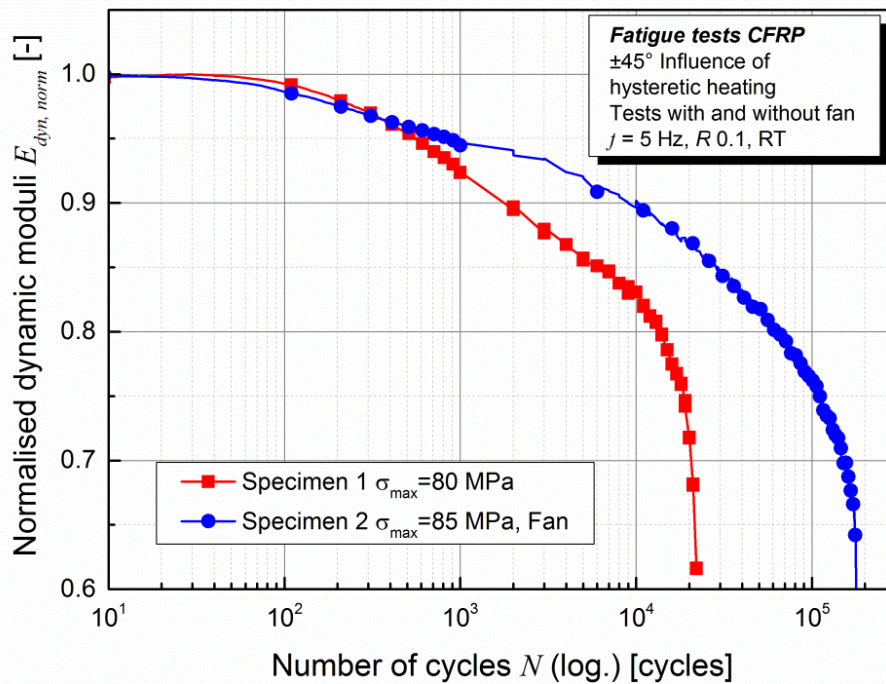


Figure 5.4: Influence of hysteretic heating on the stress-strain fatigue behaviour of $\pm 45^\circ$ specimens.

5.5.2.2. Influence of strain measurement technique on stress-strain hystereses

Stress-strain hystereses were measured with different techniques in cyclic tests. Figure 5.5 illustrates the stress-strain hysteresis of one UD 45° specimen equipped with extensometer, strain gauges and the DIC system. Stress-strain hysteresis after 0, 10^3 , 10^4 , $5 \cdot 10^4$, 10^5 , $2 \cdot 10^5$, $3 \cdot 10^5$ and $3.75 \cdot 10^5$ cycles are drawn. The cyclic test was performed under load control with 10 Hz, R 0.1, maximum stress $\sigma_{max} = 30$ MPa until specimen failure after 375007 cycles. For accurate hysteresis recording with the optical system, the test machine performed two slower cycles at 1 Hz when the optical system was active. Thus, the test procedure consisted of two cycles at 1 Hz followed by 1000 cycles at 10 Hz.

Hysteresis was shifted to higher strains with progressing number of cycles, independent of strain measurement method. Extensometer data resulted in hysteresis with steepest slopes and least deviation. Also, those hysteresis loops were very narrow, which could be expected for materials behaving approximately linear-elastic under strains smaller than 0.3 %, as exemplified in quasi-static tests. Hysteresis recorded by piston displacement possessed slightly flatter slopes but narrow shape. Strain gauges applied in the load direction produced hysteresis loops that were shifted to strains larger than 0.25 % as a whole. Those hysteresis loops possessed a more broaden shape which was not reasonable for UD 45°. The material behaviour was not correctly measured by strain gauges, probably because of contact problems or strain gauge misalignment. Data measured by DIC did not result in hysteresis shaped stress-strain curves and could, consequently, not be used for further moduli calculation. The problematic issue with all optical systems was the need for good adhesion between the pattern and the specimen's surface. Even if the specimen's surface was still intact on the macroscopic scale, movements within the specimens could partially lead to contact problems. Consequently, a surface pattern which was not sufficiently connected with the specimen's surface could not display the actual material behaviour anymore. Optical systems might be more suitable for specimens with symmetric lay-ups.

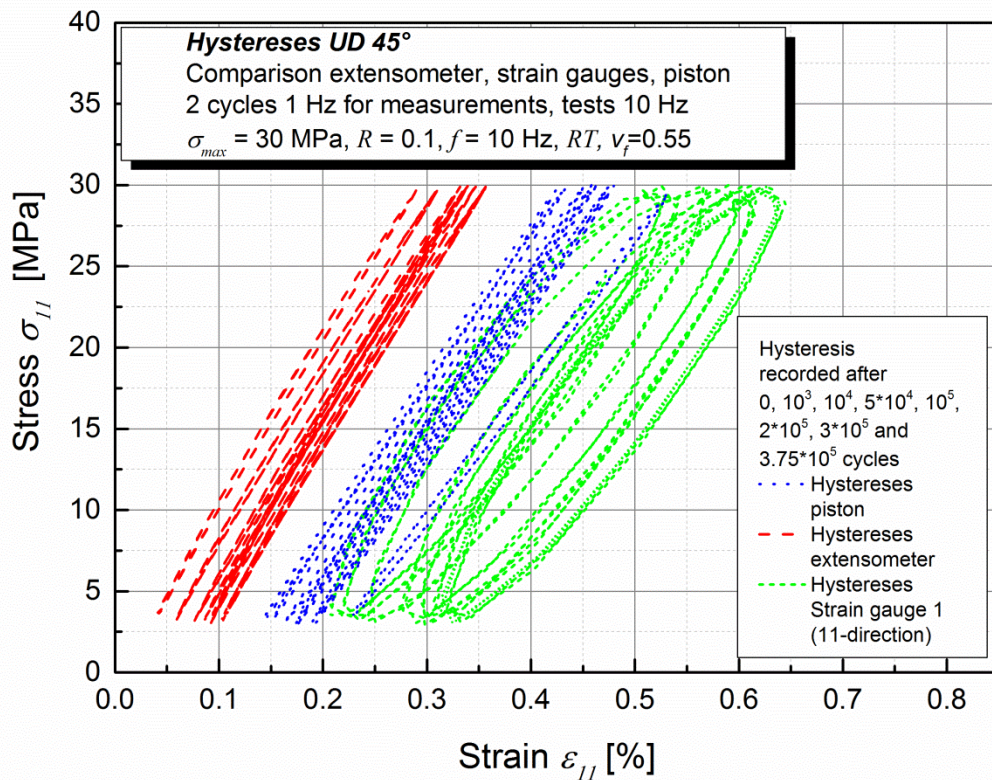


Figure 5.5: Stress-strain hystereses of UD 45° specimen measured by extensometer, strain gauge and piston.

The dynamic moduli E_{dyn} and secant moduli E_s were calculated from presented stress-strain hysteresis loops measured by extensometer, piston and strain gauges (figure 5.6) according to (5.1) and (5.2). The quasi-static Young's modulus of UD 45° measured by extensometer is included in the illustration for comparison. Dynamic moduli measured with all strain measurement methods were higher than the quasi-static modulus. Depending on the strain measurement method, dynamic moduli were scattered between 8600 MPa (strain gauge) and 10600 MPa (extensometer). All dynamic moduli stayed on a constant level during the entire fatigue tests, which indicated no progressive damage but sudden failure occurred in the specimens. Secant moduli measured with extensometer were significantly higher than secant moduli measured with piston and strain gauge, which results from the location of hysteresis in the stress-strain diagram (figure 5.5). The slight degradation of secant moduli could be interpreted as small cyclic creep in the epoxy matrix. Especially, this comparison exemplifies the

complexity of fatigue stiffness measurement. Depending on the strain measurement technique, the results scattered over a wide range. Additionally, the interpretation of absolute values of dynamic and secant moduli was very difficult. Relative values (normalised to e.g. the first measured value) could provide information about damage and cyclic creep. However, although the strain range used for modulus evaluation was similar in quasi-static and fatigue tests (cyclic strain was usually not higher than 0.003 absolute strain as figure 5.5 illustrates), absolute fatigue values higher than quasi-static material parameters did not seem reasonable.

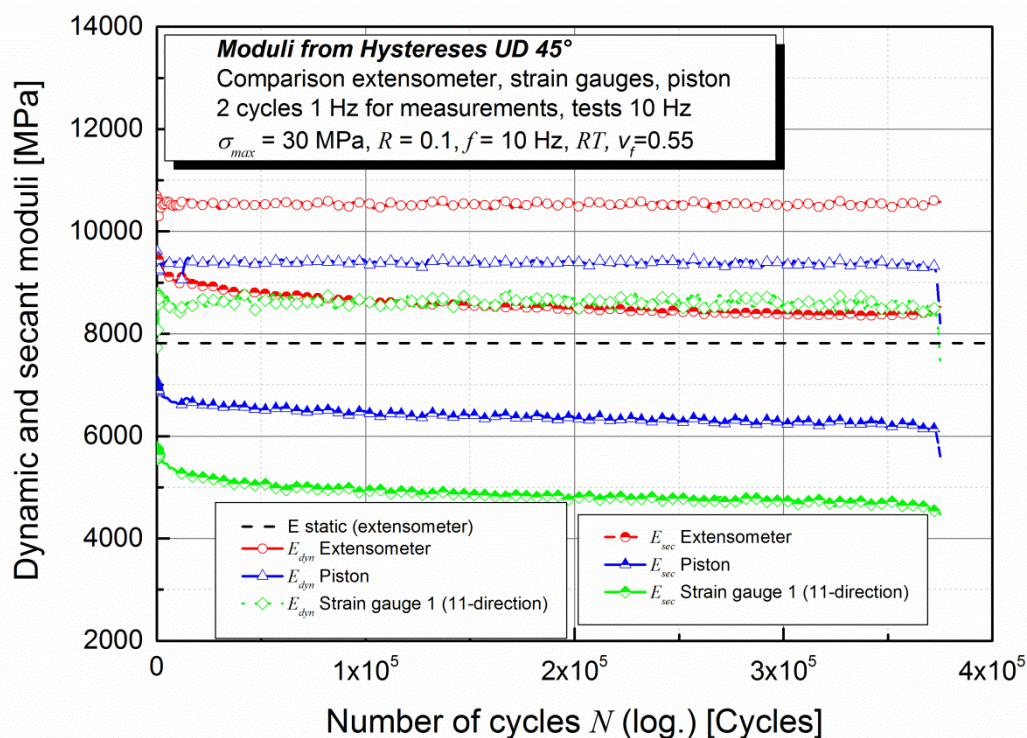


Figure 5.6: Comparison between quasi-static, secant and dynamic moduli of an UD 45° specimen measured by extensometer, strain gauge and piston.

The main reason for the deviation between quasi-static Young's moduli and moduli calculated from hysteresis may be the strain-rate dependent material behaviour of the polymer matrix system [17]. In quasi-static tests, test speeds of 1 mm/min are much slower compared to the load speeds in cyclic tests with usual test frequencies of 5 or even 10 Hz. As a result, moduli from

quasi-static tests and moduli calculated from hystereses are not comparable as such because they describe two very different kinds of material behaviour. However, in some cases it might be interesting to relate fatigue data to the widely spread and almost always used Young's moduli. A simple but effective experimental procedure called "cyclic tensile tests" has been published which allows monitoring the degradation of cyclic material properties starting from quasi-static Young's moduli. In this test procedure, the test machine performs a displacement controlled tensile test with a test speed comparable to quasi-static tests up to mean displacement of the cyclic load after a certain number of load controlled sinusoidal cycles [17,18]. Consequently, this test method provides Young's moduli measured under quasi-static conditions within a fatigue test.

5.5.2.3. Strain measurement phenomena in UD plies

In addition to the influence of strain measurement technique on the measured stress-strain behaviour, the specimen lay-up also affected the applicability. In the following, normalised dynamic moduli $E_{dyn, norm}$ calculated according to (5.2) are presented. In figure 5.7, normalised dynamic moduli of unidirectional specimens tested at angles of 45° and 60° are illustrated. Figure 5.8 includes the normalised dynamic moduli of ±45° specimens and unidirectional specimens tested at an angle of 90°. For all lay-ups, stress-strain hystereses recorded by mechanical extensometer and piston displacement were used for moduli calculation. In UD 45° specimens, dynamic moduli measured with contact extensometer increased during test time, especially in tests lasting longer than 10⁵ cycles. This effect seemed to result from fibres aligning more and more in the load direction. Consequently, moving fibres probably led to measurement artefacts when using contact methods. In UD 60° specimens, this effect was not as strong as for UD 45° specimens. At the very end of the UD 60° test the extensometer measured a peak that was probably an artefact caused by contact problems with the failing specimen.

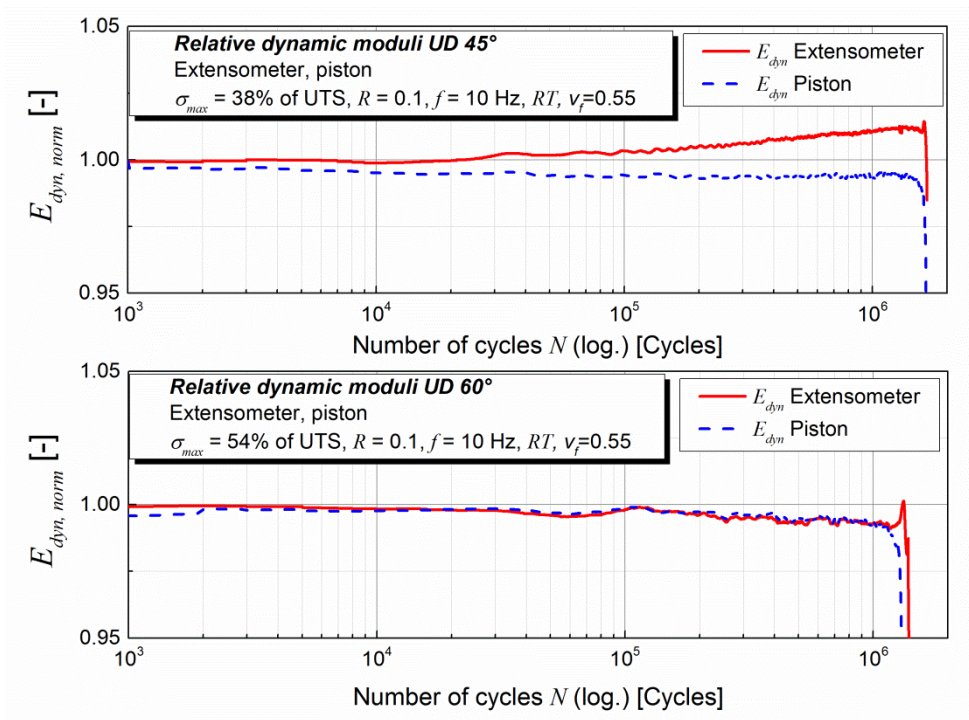


Figure 5.7: Strain measurement effects in UD 45° and UD 60° specimens.

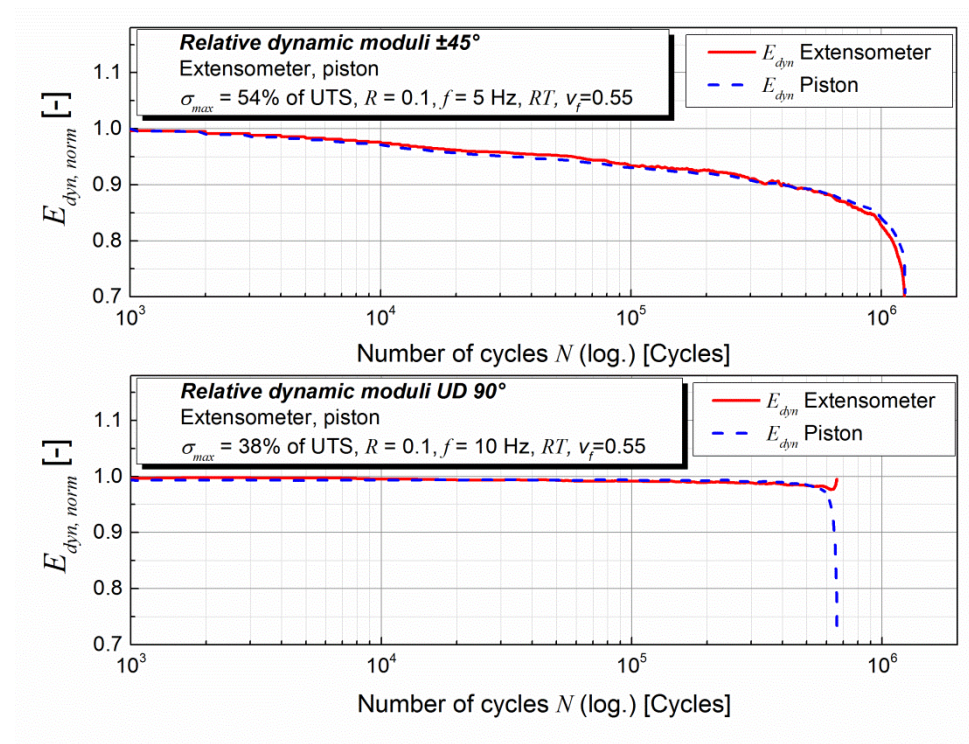


Figure 5.8: Strain measurement effects in ±45° and UD 90° specimens.

In $\pm 45^\circ$ specimens, the relative dynamic modulus progress measured by extensometer and piston decreased constantly during test time. The decreases did not depend on the strain measurement device. However, the absolute values measured with piston and extensometer differed. The behaviour of $\pm 45^\circ$ specimens was very different from the behaviour of the single unidirectional 45° specimen. While moduli of UD 45° stayed on constant level or even increased (figure 5.7), the decreasing moduli in $\pm 45^\circ$ specimens indicated progressive failure [5]. In UD 90° specimens, dynamic moduli stayed on a constant level during test time. This indicated that neither fibre movement nor increasing damage occurred in specimens tested transverse to fibre direction until sudden failure (figure 5.8).

5.5.2.4. Limits for measurement techniques in fatigue tests

In carbon/epoxy laminates, the application of strain measurement techniques was often limited by the requirement of an intact specimen surface. Strain gauges, optical systems such as digital image correlation and camera systems as well as mechanical extensometers depended on good surface quality for accurate measurement. Especially in UD 0° specimens, surfaces were usually not intact at the end of the fatigue test (figure 5.9). The illustrated specimen with camera marks was superficially in good order after $2.5 \cdot 10^5$ cycles. After $2.55 \cdot 10^5$ cycles, cracks in the longitudinal direction became apparent. After that point, reliable strain measurement was impossible. Figure 5.9c illustrates the specimen immediately before final failure at $2.92 \cdot 10^5$ cycles.

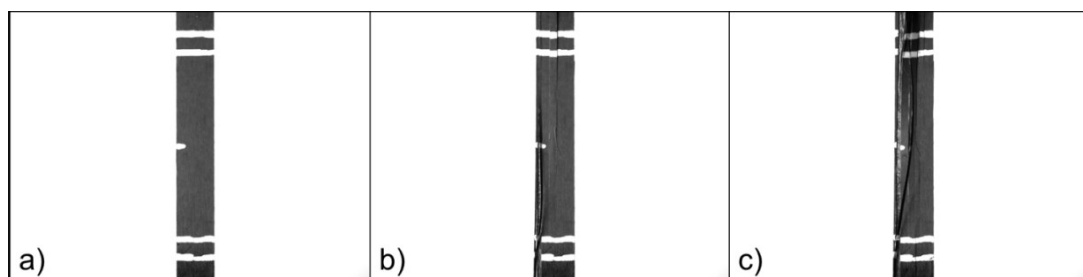


Figure 5.9: UD 0° specimen tested with nominal maximum stress $\sigma_{max} = 1100$ MPa and 5 Hz after a. $2.5 \cdot 10^5$, b. $2.55 \cdot 10^5$ and c. $2.92 \cdot 10^5$ cycles.

Secant and dynamic moduli of the UD 0° specimen illustrated in figure 5.9 are presented in figure 5.10. The qualitative modulus progresses measured with piston and extensometer are similar. However, absolute values of UD 0° depended highly on the method of strain measurement, as discussed by means of quasi-static results. The deviation between quasi-static Young's and dynamic moduli was not significant in contrast to the presented UD 45° specimens. Fibre dominated UD 0° did not show strain-rate dependent behaviour comparable to matrix-dominated off-axis specimens [17]. The monitored surface cracks starting at 2.55×10^5 cycles were reflected in the dynamic modulus measured by extensometer and in the piston displacement. The appearance of the piston displacement suggested that the stiffness of the specimen actually decreased. The secant modulus measured by extensometer was not reasonable but was a sign of slipping of the extensometer on the smooth specimen surface. In this case, piston displacement could provide a great deal of information on whether actual specimen's stiffness changed, while all strain measurement methods depending on the specimen's surface can only provide information about starting surface cracks.

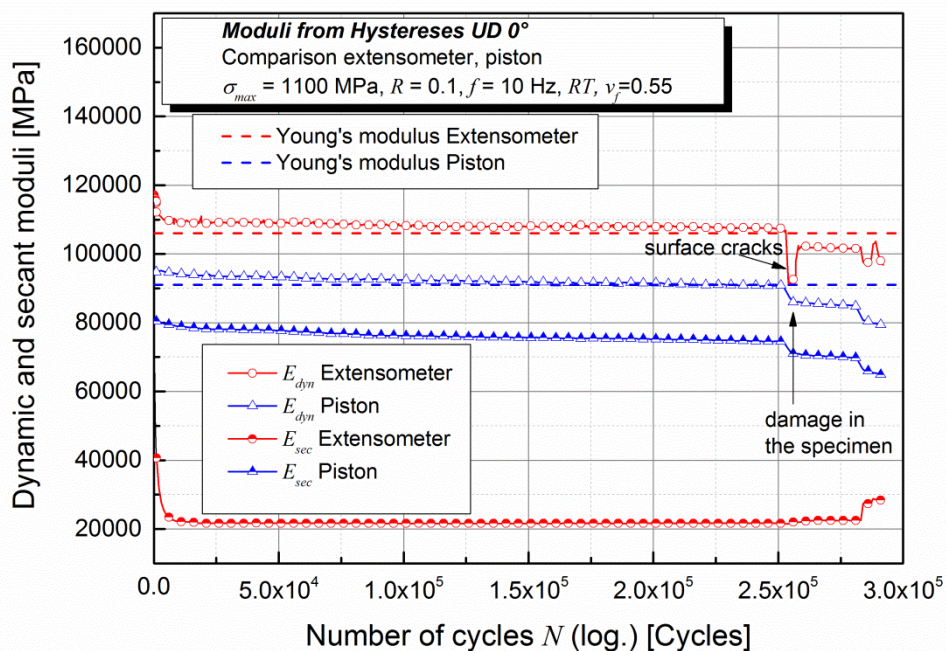


Figure 5.10: Secant and dynamic moduli of UD 0° specimen measured by mechanical extensometer and piston displacement.

Similar behaviour was monitored in multiaxial specimens where the outer layers were aligned in the 0° direction in a previous work [18]. For specimens with a lay-up of [0/+45/-45/90/symm.] tested in tension-tension fatigue tests, the strain measurement was also limited by an intact 0° layer at the surface. It was shown that contact and optical systems could provide useful information in addition to the piston displacement about starting of different cracks on the specimen.

5.6. Conclusions and Recommendations

Strain gauges, mechanical extensometers, piston displacement, digital image correlation and a 2 D camera system were used for strain measurement and stiffness calculation of carbon/epoxy laminates. Specimens were tested at angles of 0° , 45° , 60° , 90° and $\pm 45^\circ$ under quasi-static tensile and tension-tension fatigue loads. Different representative examples illustrating challenges which can occur when measuring strains of carbon/epoxy laminates, especially under fatigue loads, were discussed. The conclusions of this study are as follows;

- The accuracy and choice of strain measurement technique in mechanical tests depends on the test direction in anisotropic unidirectional CFRP. Generally, intact specimens' surfaces are a prerequisite for all surface strain measurements. The surface structure can also have influence on the applicability.
- The deviation between global piston displacement and local strains measured by extensometer and optical systems depends on the specimen's stiffness. The larger the difference between machine stiffness and specimen stiffness, the more accurate are the strains recorded by piston displacement.
- Optical systems are perfectly suitable for strain measurement in quasi-static tests and can be recommended for all investigated laminates. In fatigue tests, data reduction by triggering the optical system with the test machine is necessary. However, the applicability in fatigue tests

might be restricted by the movement of specimen surface affecting the adhesion of the applied pattern.

- Based on the conducted tests, strain gauges cannot be recommended for strain measurement of unidirectional plies because of the influence of misalignment, the high default rate caused by progressing fatigue damage on specimen surfaces and the high deviation of measured strains.
- Hysteretic heating has to be avoided as effectively as possible in fatigue tests to produce reasonable results. Numbers of cycles to failure as well as stress-strain behaviour are affected by hysteretic heating. Non-unidirectional specimens have a higher disposition to hysteretic heating than unidirectional specimens. Specimen temperature may be controlled by adaption of the test frequency or by additional cooling.
- Moduli evaluated from stress-strain hysteresis are not comparable with quasi-static Young's moduli, independent of the strain measurement technique. A reason for this observation is the strain-rate dependent behaviour especially in tests with off-axis specimen. An alternative test procedure to measure fatigue properties under conditions comparable to quasi-static tests has been suggested in previous works [17,18].

In consequence, the following recommendations for strain measurement of carbon/epoxy laminates in fatigue tests can be made:

- UD 0°: Contact extensometer or DIC can be used for first few thousand cycles up to first surface cracks to measure actual local strains. For evaluation of the entire fatigue test, piston displacement should be used and combined with local methods for accurate absolute stiffness values.
- UD 45°, 60°: If unbalanced unidirectional laminates are measured in fatigue tests, alignment of fibres during the test has to be taken into account. For accurate load measurement, a three dimensional load cell would be required as well to take into account the forces in transversal direction. Optical systems can be used for local strain measurement during the first few thousand cycles and then be

removed because of data capacity or contact problems between the surface pattern and, probably, moving fibres. For evaluation of the entire fatigue test, piston displacement should be combined with optical measurements. Contact extensometers are not reliable for unbalanced laminates because of possible fibre movement.

- $\pm 45^\circ$: Contact extensometer is the most simple and effective method for strain measurement of balanced laminates.
- UD 90° : Contact extensometer can be highly recommended for fatigue tests with unidirectional specimens tested transverse to fibre direction.

5.7. References

- [1] Aoki Y, Ishikawa T, Takeda S, Hayakawa Y, Harad A, Kikukawa H. Fatigue test of lightweight composite wing structure. *International Journal of Fatigue* 2006;28(10):1109–15.
- [2] Erkal S, Sayman O, Benli S, Dogan T, Yeni E, Erkal S et al. Fatigue damage in composite cylinders. *Polym. Compos* 2010 // 2009(31):707–713 // NA.
- [3] Mandell J, Samborsky D, Wahl N, Sutherland H. Testing and analysis of low cost composite materials under spectrum loading and high cycle fatigue conditions. ICCM14 2003;SME/ASC(paper 1811).
- [4] Hodgkinson JM. *Mechanical testing of advanced fibre composites*. Boca Raton, FL, Cambridge, England: CRC Press; Woodhead; 2000.
- [5] Talreja R. *Fatigue of Composite Materials*. Pennsylvania, U.S.A: Technomic Publishing Inc; 1987.
- [6] Ajovalasit A, Pitarresi G. Strain Measurement on Composites: Effects due to Strain Gauge Misalignment. *Strain* 2011;47:e84–e92.
- [7] Painold M. *Basischarakterisierung und Untersuchung des Ermüdungsverhaltens Karbonfaserverstärkter RTM-Laminat*. Diplomarbeit. Leoben; 2003.

- [8] Mannsberger G. Experimentelle Ermittlung von Eingangsparametern für ein Versagens-Meso-Modell für die Ermüdungsanalyse von faserverstärkten Laminaten. Studienarbeit. Leoben; 2006.
- [9] Felber S. Bestimmung der Schadenstoleranz und der Ermüdungseigenschaften von kohlestofffaserverstärkten Epoxikharz-Laminaten. Diplomarbeit. Leoben; 2006.
- [10] Willems A, Lomov S, Verpoest I, Vandepitte D. Optical strain fields in shear and tensile testing of textile reinforcements. *Composites Science and Technology* 2008;68(3-4):807–19.
- [11] Koerber H, Xavier J, Camanho P. High strain rate characterisation of unidirectional carbon-epoxy IM7-8552 in transverse compression and in-plane shear using digital image correlation. *Mechanics of Materials* 2010;42(11):1004–19.
- [12] Tscharnuter D, Muliana A. Nonlinear response of viscoelastic polyoxymethylene (POM) at elevated temperatures. *Polymer* 2013;54(3):1208–17.
- [13] DIN EN ISO 527-4. *Plastics - Determination of tensile properties - part 4: Test conditions for isotropic and orthotropic fibre-reinforced plastics composites*(DIN EN ISO 527-4:1997). Brüssel, Belgium: CEN (European Committee for Standardization); 1997.
- [14] DIN EN ISO 527-5. *Plastics - Determination of tensile properties - Part 5: Test conditions for unidirectional fibre-reinforced plastic composites*(DIN EN ISO 527-5-2010). Brüssel, Belgium: CEN (European Committee for Standardization); 2010.
- [15] ASTM International. *Standard Test Method for Tensile Properties of Polymer Matrix Composite Materials*(ASTM D3039/D3039M-00). West Conshohocken, PA, United States: ASTM International; 2000.
- [16] DIN Deutsches Institut für Normung e.V. *Aerospace series - Carbon fibre reinforced plastics - Unidirectional laminates, Tensile tests parallel to fibre direction*;49.040.10(2561). Berlin: Beuth Verlag GmbH; 1995.
- [17] Brunbauer J, Pinter G. Technological approach to fatigue life prediction of CFRP. In: *ECCM16*, editor. 16th European Conference on Composite Materials; 2014.

-
- [18] Brunbauer J, Arbeiter F, Stelzer S, Pinter G. Stiffness Based Fatigue Characterisation of CFRP. AMR 2014;891-892:166–71.

Part IV.

Fatigue-induced damage mechanisms in carbon/epoxy laminates

6. Introduction to Publications 2 and 3

After determining the experimental tools necessary for evaluation of mechanical material properties, the next step towards fatigue-life prediction was to study the physical damage mechanisms of the investigated materials in detail. The general damage mechanisms assumed for composite materials as well as the indication, that damage mechanisms and damage progresses depend on the respective material and the stacking sequence, have already been introduced in chapter 1. Numerous studies have investigated the effect of mechanical mean stress, temperature or angle between the fibres and the applied load on the fatigue properties e.g. [1–3]. In most cases, these data were used as input parameters for S-N curved based fatigue models. However, little effort has been made to verify the influence of fibre volume fraction on the fatigue behaviour and on the fatigue damage mechanisms in detail although cracks emerging from the matrix are known to initiate the damage process [4–6]. Furthermore, the effect of fibre volume fraction on the fatigue behaviour might be of special interest for two reasons. First, in industrially produced parts fibre volume fraction will probably not be constant inside the entire structure due to geometry reasons and production influences. Second, to make generalisation of fatigue-life prediction theories possible, it would be beneficial to be able to generalise the material behaviour, which is significantly influenced by the fibre volume content.

In these two publications carbon/epoxy laminates with different fibre volume fractions and the fatigue behaviour of the unreinforced epoxy material were investigated. All materials were tested in tension-tension and also tension-compression fatigue tests and the fracture surfaces were investigated by scanning electron microscopy (SEM) in detail. In publication 2, the quality of the plates produced for these tests was validated with different thermo-

mechanical and thermo-analytical methods in addition. Detailed investigations of the fracture surfaces showed that the fibre volume content influenced the fatigue strength and damage mechanisms of specimens tested transverse to fibre direction significantly in tension-tension fatigue tests. In publication 3, the damage mechanisms observed in tension-tension fatigue tests were compared to fracture surfaces from tension-compression fatigue tests. Furthermore, stress-strain hysteresis loops from tension-tension and tension-compression tests reflecting progressing damage behaviour were discussed in relation with the respective fracture surfaces in detail.

6.1. References

- [1] Kawai M, Yajima S, Hachinohe A, Takano Y. Off-Axis Fatigue Behavior of Unidirectional Carbon Fiber-Reinforced Composites at Room and High Temperatures. *Journal of Composite Materials* 2001;35(7):545–76.
- [2] Kawai M, Yajima S, Hachinohe A, Kawase Y. High-temperature off-axis fatigue behaviour of unidirectional carbon-fibre-reinforced composites with different resin materials. *Composite Science and Technology*;2001(61):1285–302.
- [3] Kawai M. A phenomenological model for off-axis fatigue behavior of unidirectional polymer matrix composites under different stress ratios. *Composites Part A: Applied Science and Manufacturing* 2004;35(7-8):955–63.
- [4] Talreja R. *Fatigue of Composite Materials*. Pennsylvania, U.S.A: Technomic Publishing Inc; 1987.
- [5] Reifsnider KL, Henneke EG, Stinchcomb W, Duke JC. Damage Mechanics and NDE of Composite Laminates. In: Hashin Z, Herakovich CT, editors. *Composite Materials: Recent Advances*: Pergamon Press Inc; 1983, p. 399–420.
- [6] Reifsnider KL (ed.). *Fatigue of composite materials*. Amsterdam, New York: Elsevier; 1991.

7. Publication 2

7.1. Bibliographic information

- Title: Mechanical properties, fatigue damage and microstructure of carbon/epoxy laminates depending on fibre volume content
- Authors and relevant contributions to this publication:
 - Julia BRUNBAUER¹
Experimental testing, microscopic investigations, data evaluation, preparation of the publication
 - Hannes STADLER²
Specimen production, discussion of experimental results
 - Gerald PINTER¹
Discussion of experimental results
- Affiliations:
 1. Institute of Materials Science and Testing of Polymers, Montanuniversitaet Leoben, Otto Glöckel-Strasse 2, 8700 Leoben, Austria
 2. TCKT – Transfercenter Kunststofftechnik GmbH, Franz-Fritsch-Strasse 11, 4600 Wels, Austria
- Periodical: International Journal of Fatigue
- DOI: 10.1016/j.ijfatigue.2014.08.007

Statement with regard to this publication: The manuscript presented here is an adapted accepted manuscript in order to fit the formatting of the thesis and does not necessarily reflect exactly the actually published version.

7.2. Abstract

This paper investigates the effect of fibre volume fraction on the fatigue behaviour and damage mechanisms of carbon/epoxy laminates. Epoxy resin and unidirectional carbon/epoxy specimens with two different fibre volume fractions are tested under quasi-static tensile and tension-tension fatigue loads at angles of 0°, 45° and 90°. Fracture surfaces are studied with scanning electron microscopy. The results show that stiffness and strength increase with increasing fibre volume fractions. The damage behaviour of off-axis specimens changes with increasing fibre volume content and the height of the applied cyclic load. While matrix cracking and interfacial debonding are dominating damage mechanisms in specimens with low fibre content, fibre bridging and pull out are monitored with increasing fibre content. The higher the applied load in fatigue tests transverse to fibre direction, the more similar behave specimens with different fibre volume fractions.

7.3. Introduction

Carbon fibre reinforced plastics (CFRP) are exposed to mechanical loads, quasi-static as well as fatigue, in most light weight applications. Due to their inner structure consisting of continuous fibres and matrix material the macroscopic properties of composite materials are anisotropic. The interface between the fibre and the matrix resin and its properties influence the performance of the composite as well [1]. When mechanical quasi-static or fatigue loads are applied, a variety of complex damage mechanisms such as matrix micro-cracking, interfacial fibre/matrix debonding, transverse rupture, fibre rupture or delamination occur on microscopic scale [1–3]. The properties of unidirectional (UD) composites transverse to fibre direction are generally low. Under fatigue loads, the matrix is subjected to strain-controlled fatigue due to the constraint provided by the fibres. Additionally, the constraint caused by the embedded fibres results in high local strains and stress concentrations in the matrix material around the fibres [2]. As a consequence, the composites' properties transverse to fibre direction are even lower than the unreinforced matrix material [4]. The different deformation behaviour of fibres and matrix material can cause interfacial

debonding as well. Longitudinal interfacial debonding can be studied in detail by the use of pull out tests [5–7].

In addition to the dependency of complex damage mechanisms on the applied load [2], the properties of composite materials can be affected by the amount of fibres [2,8]. It is well known that higher fibre volume fractions increase mechanical properties such as tensile strength and stiffness in fibre direction [8,9]. Under fatigue loads, the effect of fibre volume fraction on the performance of different materials has been investigated [10–12]. However, the influences of fibre volume fraction on the damage mechanisms of the matrix material, on the fibre/matrix interfaces and on the fatigue properties of unidirectional laminates have not been studied in detail. In this work, the effect of low and high fibre volume fractions on the damage mechanisms caused by fatigue loads was investigated experimentally. The pure epoxy resin was studied as well. Quasi-static tensile and tension-tension fatigue tests were performed with unidirectional carbon/epoxy laminates at angles of 0°, 45° and 90°. The fractured surfaces of the specimens were observed using a scanning electron microscope.

7.4. Experimental work

Epoxy plates were made of EPIKOTE™ Resin MGS® RIMR135 (approved by German Lloyd) with the curing system EPIKURE™ Curing Agent MGS® RIMH1366 by Momentive (Esslingen am Neckar, Germany). The epoxy resin and curing agent mixture was cast into a mould tool. Epoxy plates were cured in three different ways in preliminary tests to examine the optimum process for production of carbon/epoxy plates: curing at 23 °C for 24 h and at 80 °C subsequently, only at 80 °C and at 90 °C. The curing processes were monitored with dielectric analysis (DEA) to measure the time necessary for full curing. Additionally, the effect of subsequent tempering was investigated. Therefore, tensile tests with epoxy resin specimens without tempering and with specimens tempered at 105 °C for 24 h before the mechanical tests were performed. Glass transition temperatures of resin plates were investigated with differential scanning calorimetry (DSC) and dynamic mechanical analysis (DMA). Finally, the thermal, thermo-mechanical and

mechanical properties of the differently cured resins were compared to define the process parameters for subsequent plate production. Unidirectional carbon/epoxy plates were produced in a vacuum assisted resin transfer moulding (vaRTM) process. Two different unidirectional fabric sheets were used to create plates with two specific fibre contents while assuring uniform fibre distribution through thickness. Fabric sheets with mass a per unit area of 80 g/m² were used for the production of plates with an aspired fibre volume content of 30 %. For plates with 55 % fibre volume content, sheets with 250 g/m² were processed. Thermogravimetric analysis (TGA) allowed testing of fibre mass contents of the produced plates. A minimum of six samples was taken from different positions on the plates to assure homogenous fibre content through the plates. In TGA measurements, 20 mg specimens were first heated under nitrogen (N₂) atmosphere from 30 °C to 700 °C with 5 K/min. Second, specimens were cooled, N₂ atmosphere switched to oxygen (O₂) and heated from 200 °C to 800 °C with 5 K/min. By measuring the densities of the composites with the immersion method according to ISO-1183-1 [13], multiplying it with the mass content measured by TGA and dividing it by density of carbon fibres (1.74 g/m³ [8]), fibre volume content was calculated.

For mechanical quasi-static and fatigue tests with epoxy resin, dumbbell specimens based on ISO 527-2 [14] with 2 mm thickness were cut out of resin plates. CFRP specimens were cut with diamond blades at angles of 0°, 45° and 90° to fibre direction out of the produced plates. Dimensions for UD 0° specimens 55 *vf.*% were 200x10x1 mm (length x width x thickness) and 200x10x2 mm for UD 0° specimens 30 *vf.*%. UD 45° and UD 90° specimens of both fibre contents were cut to geometries of 200x20x2 mm. Aluminium tabs with 1 mm thickness were glued on both sides of all specimens.

A servo-hydraulic test machine MTS 810 equipped with a 100 kN load cell by MTS Systems Corporations (Minnesota, USA) was used for quasi-static and fatigue tests at room temperature. Gauge length for all tests was 100 mm. Hydraulic wedge pressure was 5 MPa. Quasi-static tests were evaluated according to ASTM D 3039 [15]. Strains in quasi-static tests were recorded by digital image correlation (DIC) system by GOM (Braunschweig, Germany).

All fatigue tests were performed with the R -value (= minimum / maximum force) of 0.1. Specimens were usually tested at four different stress levels, testing at least three specimens per stress level until fracture of specimens. Test frequency of 5 Hz was applied in low cycle and 10 Hz in high cycle fatigue tests. The obtained fatigue data were evaluated according to ASTM E 739 [16]. Fracture surfaces of specimens with different fibre volume contents tested at all produced angles were investigated with optical methods to get greater insights in influence of fibre volume content on microstructure and on damage behaviour. Light microscopy and scanning electron microscopy (SEM) were used.

7.5. Results and Discussion

Dielectric analysis (DEA) allowed monitoring the different curing progresses while producing epoxy plates. It was observed that the curing processes of all plates were finished at the latest after 5 h. Differential scanning calorimetry (DSC) proved that neither the three different ways of curing nor the subsequent tempering had influence on the glass transition temperature. Glass transition temperature of epoxy resin specimens was about 93 °C in DSC measurements. Dynamic mechanical analysis (DMA) with 3-point-bending load showed that different processes of epoxy plate production used in this work did not result in statistical relevant trends of the thermo-mechanical behaviour (figure 7.1). Glass transition temperatures measured by DMA varied between 97 °C and 102 °C. Results of quasi-static tensile tests with epoxy resin specimens with and without subsequent tempering at 105 °C for 24 h are presented in table 7.1. The different ways of curing and the tempering before the mechanical tests did not result in a significant trend of the Young's moduli, ultimate tensile strengths (UTS) or the tensile strains at UTS either. Based on the thermo-analytical, thermo-mechanical and mechanical results, it was decided to cure all carbon/epoxy plates at 80 °C for 5 h without subsequent tempering.

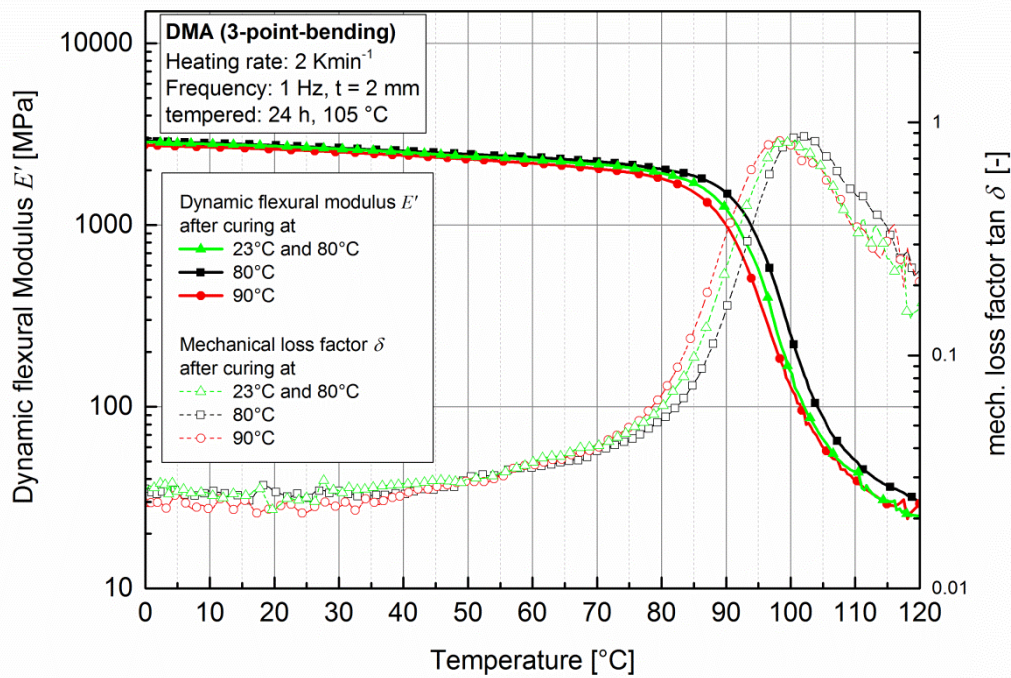


Figure 7.1: Dynamic mechanical analysis of epoxy resins cured either at 23 ° and 80 °C, 80 °C or 90 °C and tempered at 105 °C for 24 h after curing.

Table 7.1: Results of quasi-static tensile tests comparing the Young’s moduli, ultimate tensile strengths (UTS) and strains at UTS of epoxy resins cured and tempered in different ways.

Curing	Tempering	Young’s Modulus [GPa]	UTS [MPa]	Strain at UTS [%]
23 °C for 24 h, 80 °C for 5 h	105 °C for 24 h	2.7±0.1	62±0.3	4.9±0.1
23 °C for 24 h, 80 °C for 5 h	no	2.7±0.1	62±0.5	4.9±0.1
80 °C for 5 h	105 °C for 24 h	2.7±0.1	62±0.6	4.9±0.1
80 °C for 5 h	no	2.7±0.1	62±0.2	4.9±0.1
90 °C for 5 h	105 °C for 24 h	2.7±0.1	62±0.6	4.9±0.1
90 °C for 5 h	no	2.7±0.1	62±0.5	4.9±0.1

Mean normalised weight vs time as results of six thermogravimetric analysis (TGA) measurements each is presented in figure 7.2. Epoxy resin specimens and carbon/epoxy specimens with both fibre contents showed a first mass decrease between 350 °C and 450 °C under nitrogen atmosphere. This temperature range is typical for the pyrolysis of polymeric materials under inert atmosphere [17]. After cooling down of the samples to 200 °C, the atmosphere was switched from nitrogen to oxygen. During heating-up under oxygen atmosphere, a small mass decrease was detected at around 450 °C, which was too low to be a possible temperature range for the pyrolysis of carbon fibres [17]. Because the mass decrease was smaller for specimens with high fibre content it seemed that this effect was caused by the matrix material in the specimens. Therefore, TGA measurements with pure epoxy resin using the same test procedure as for carbon/epoxy plates were done as well. The mass decrease of epoxy resin at around 450 °C could be attributed to oxidation of pyrolysis carbon black which had been formed previously by the resin under N₂ atmosphere. The carbon fibres in carbon/epoxy specimens finally combusted under O₂ atmosphere between 550 °C and 700 °C.

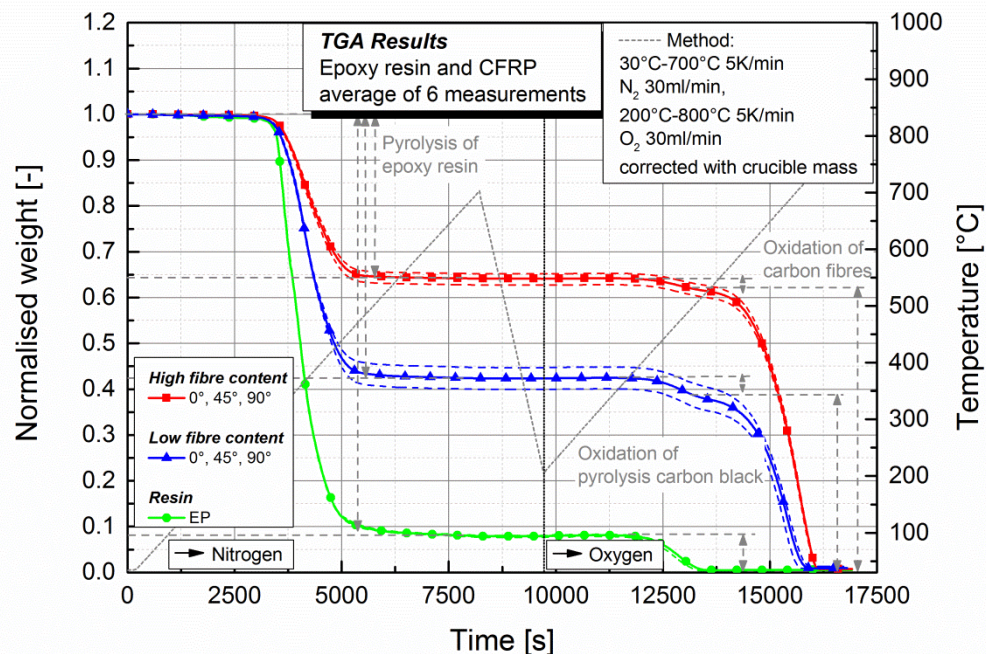


Figure 7.2: TGA results for carbon/epoxy plates with high and low fibre content and pure epoxy resin.

Density measurements provided mean density of 1.5 g/m^3 for composites with high fibre content and 1.3 g/m^3 for low fibre content. By using the average fibre weight contents of 0.63 for high and 0.39 for low fibre content measured with TGA for calculation, the aspired fibre volume contents of 55 % and 30 % could be confirmed.

7.5.1. Quasi-static tensile tests

Results of all quasi-static tensile tests are illustrated in figure 7.3. The stress-strain curves of epoxy resin and UD specimens tested at angles of 45° and 90° are shown in greater detail in figure 7.4. Young's moduli, UTS and the strains at UTS are reported with the respective standard deviations in table 7.2.

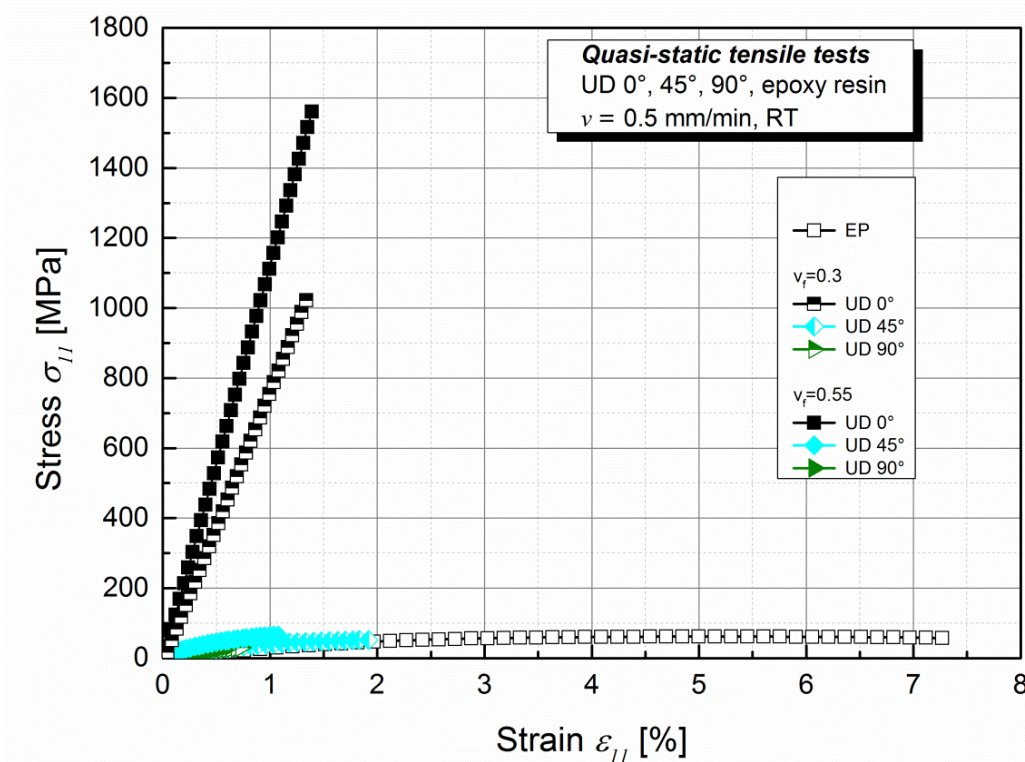


Figure 7.3: Summary of the UD CFRP quasi-static tensile tests with fibre volume contents 0 v_f %, 30 v_f % and 55 v_f % tested at angles of 0° , 45° and 90° .

The generally small scatter of quasi-static results proved the good quality of the produced plates. Young's moduli and ultimate tensile strengths at all test angles were higher for specimens with 55 *vf.*%. Strain at failure was slightly higher for 30 *vf.*% tested at angles of 0° and 90° compared to their counterparts with higher fibre volume content. In UD 45° specimens, the decrease of fibre volume fraction led to significantly higher strains at failure. Pure epoxy resin possessed the smallest stiffness of all tested specimens. However, UTS for epoxy resin was much higher compared to UD 90° as well as UD 45° 30 *vf.*%. Strain at UTS of epoxy resin was magnitudes higher compared to CFRP as result of higher ductility and the possibility of unrestricted transverse elongation. When comparing the matrix dominated specimens – epoxy resin, UD 90° with low and UD 90° with high fibre content – pure epoxy resin possessed higher UTS than UD 90° 55 *vf.*% which corresponded to literature [4].

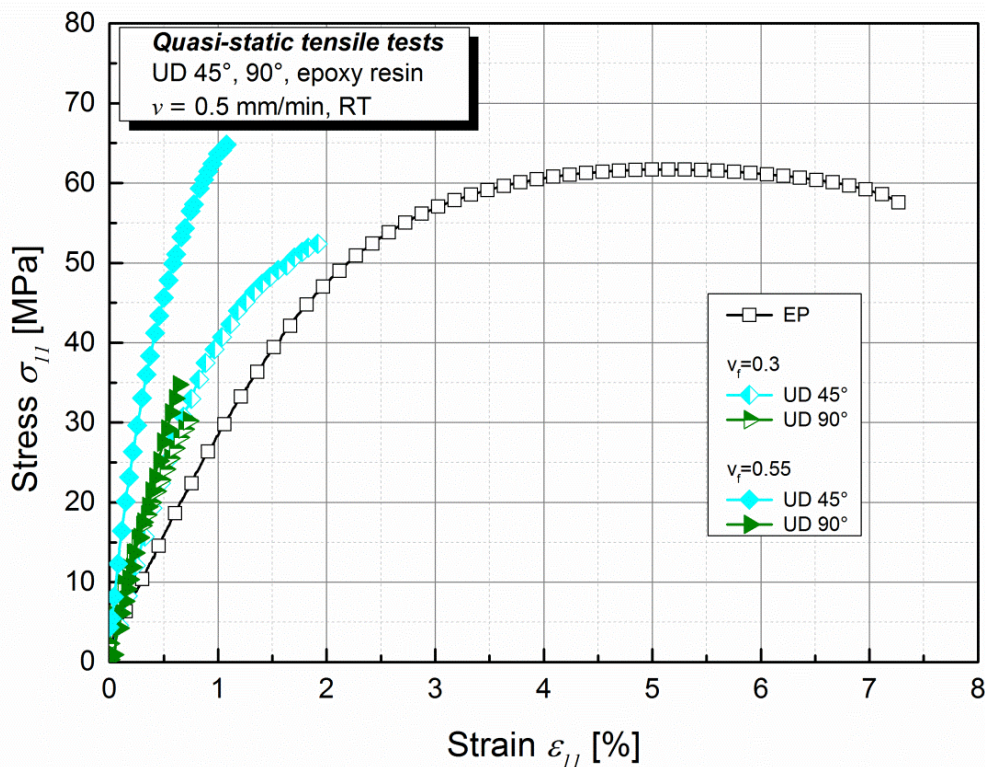


Figure 7.4: Detailed tensile stress-strain curves of epoxy resin and UD specimens with 30 *vf.*% and 55 *vf.*% fibre volume fraction tested at angles of 45° and 90°.

Table 7.2: Young's modulus, ultimate tensile strength (UTS) and strain at UTS with respective standard deviations of UD CFRP quasi-static tests with fibre volume contents 0 *vf.*%, 30 *vf.*% and 55 *vf.*% tested at angles of 0°, 45° and 90°.

	Young's modulus [GPa]	UTS [MPa]	Strain at UTS [%]
UD 0° 55%	107.0±1.6	1554±64	1.3±0.1
UD 0° 30%	72.5±2.7	1026±36	1.4±0.1
UD 45° 55%	9.0±0.1	66±0	1.1±0.1
UD 45° 30%	5.1±0.2	51±5	1.9±0.4
UD 90° 55%	5.5±0.5	33±2	0.6±0.1
UD 90° 30%	4.0±0.2	31±1	0.7±0
Epoxy resin	2.7±0.1	62±0.6	4.9±0.1

Based on this observation it might be expected that the UD 90° 30 *vf.*% specimen including the second highest matrix volume of these three specimen configurations would possess the second highest UTS as well. However, results proved that UTS of UD 90° 30 *vf.*% was even smaller than UTS of UD 90° 55 *vf.*%, which might be ascribed to the following causes: A first explanation could be that during the production process of plates with lower fibre content more imperfections are included in the bigger amount of matrix material. This assumption could be disproved by optical investigations. The second suggestion could be, that failure of UD 90° is not merely matrix dominated. SEM investigations presented in this paper provide explanations.

7.5.2. Fatigue tests

All fatigue data were analysed by the classical stress-life approach referring to ASTM E 739 [16]. In the diagrams shown below, data are drawn in terms of maximum stress σ_{max} versus number of cycles to failure N . Test results are reported in double logarithmic diagrams. Specimens that passed $2 \cdot 10^6$ cycles without failure were usually stopped. These runouts are marked with

arrows in the diagrams. Figure 7.5 illustrates all specimens tested under fatigue loads. For better comparison, specimens tested at angles of 45° and 90° and epoxy resin specimens are shown separately in figure 7.6. Slope k , scatter width T_s and cyclic stress maxima at $5 \cdot 10^6$ cycles σ_{max} at $5 \cdot 10^6$ evaluated according to ASTM E 739 [16] are listed in table 7.3 for all fatigue tests. Specimens tested at same angles were located in the same areas of the S-N diagrams. S-N curves of UD 0° specimens with high and low fibre contents showed similar and very flat slopes k . UD 0° with 55 *vf.*% specimens were shifted to higher fatigue stresses as a result of the higher UTS. The appearance of both UD 0° S-N curves indicated that fibre dominance mainly influenced the fatigue behaviour of specimens in fibre direction with both fibre volume fractions.

Slopes of S-N curves for UD 45° specimens were similar for both fibre volume contents (figure 7.6). UD 45° specimens with low fibre content were shifted to smaller maximum fatigue stresses. Fatigue behaviour of epoxy resin was in similar scales as UD 45° specimens with 55 *vf.*% and consequently clearly higher than UD 90° specimens. Although primarily matrix material was loaded in both UD 90° and epoxy tests, included fibres led to stress concentrations and might act as possibilities for crack initiation and as crack paths. Slopes of UD 90° specimens were different for the two fibre contents. At higher fatigue stresses and number of cycles to failure between 10^3 and 10^4 cycles, the fibre content did not influence the fatigue behaviour significantly. At lower fatigue loads on the contrary, UD 90° specimens with 55 *vf.*% reached at least two times higher number of cycles to failure compared to specimens with 30 *vf.*%. These observations indicated that damage mechanisms might be influenced by both fibre volume content and the applied fatigue load (figure 7.6).

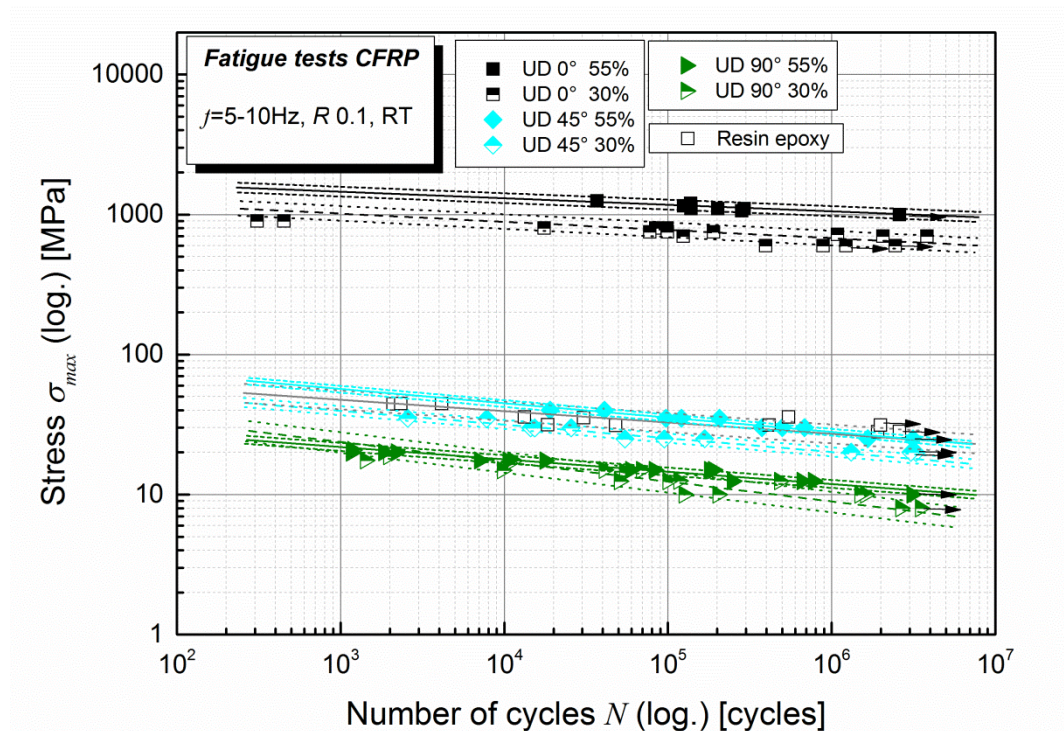


Figure 7.5: Uniaxial fatigue curves of epoxy resin with 0 *vf.*%, 30 *vf.*% and 55 *vf.*% carbon fibre volume content tested at angles of 0°, 45° and 90°, $R = 0.1$ at room temperature.

Scatter widths for specimens with low fibre content were higher compared to specimens with high fibre volume content at all tested angles. Consistently specimens with highest matrix-dominance (epoxy resin specimens and UD 90° specimens with 30 *vf.*%) showed the highest scatter width T_s (table 7.3). Maximum stresses σ_{max} at $5 \cdot 10^6$ cycles of all tested specimens were smaller compared to ultimate tensile strengths. As a consequence of the very flat slopes of the UD 0° S-N curves, decreases of fatigue strength for these materials were smallest (~60 % of UTS at $5 \cdot 10^6$ cycles). For all other specimens fatigue strengths at $5 \cdot 10^6$ cycles decreased significantly to ~30 % of UTS (table 7.3).

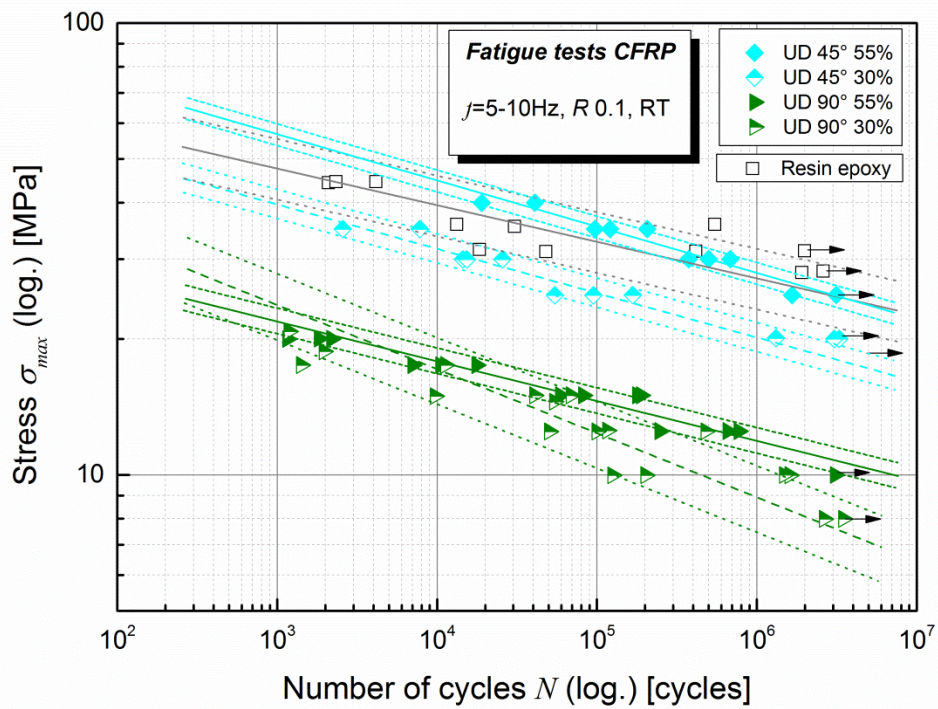


Figure 7.6: Uniaxial fatigue curves of epoxy resin with 0 *vf.*%, 30 *vf.*% and 55 *vf.*% carbon fibre volume content tested at angles of 45° and 90°, $R = 0.1$ at room temperature.

Table 7.3: Evaluation of fatigue curves: slope k , scatter width T_s and fatigue strength after $5 \cdot 10^6$ cycles of specimens with 0 *vf.*%, 30 *vf.*% and 55 *vf.*% carbon fibre volume content tested at angles of 0°, 45° and 90°, $R = 0.1$ at room temperature.

	k [-]	T_s [-]	σ_{max} at $5 \cdot 10^6$ [MPa]
UD 0° 55%	24.9	1/1.14	967.0
UD 0° 30%	16.1	1/1.29	593.3
UD 45° 55%	9.2	1/1.12	23.6
UD 45° 30%	11.0	1/1.15	17.7
UD 90° 55%	11.1	1/1.15	10.7
UD 90° 30%	7.2	1/1.41	7.5
Epoxy resin	12.8	1/1.36	25.1

7.5.3. Damage mechanisms under fatigue loads

Damage mechanisms of specimens with different fibre contents tested at angles of 0°, 45° and 90° were investigated with light microscopy and scanning electron microscopy (SEM) after fatigue tests. In all carbon/epoxy specimens, fibres were consistently distributed across the thickness and all tested specimens were of comparably good quality. In figure 7.7, the representative fracture surface of pure epoxy resin dumbbell specimen is presented ($\sigma_{max} = 31$ MPa, $f = 10$ Hz, $N = 47952$). On the fracture surface, areas of crack initiation, crack growth and residual fracture area could be identified which corresponded to [18]. Microstructure was investigated in greater detail with SEM in areas of residual fracture and crack growth (figure 7.8). Smooth fracture surfaces were characteristic for crack growth in epoxy resin, whereas residual fracture areas showed more structured and rougher appearance. The optical investigations of epoxy resin microstructures after testing on different stress levels (figure 7.6) indicated that fracture behaviour of the investigated epoxy resin did not depend on the applied fatigue stress.

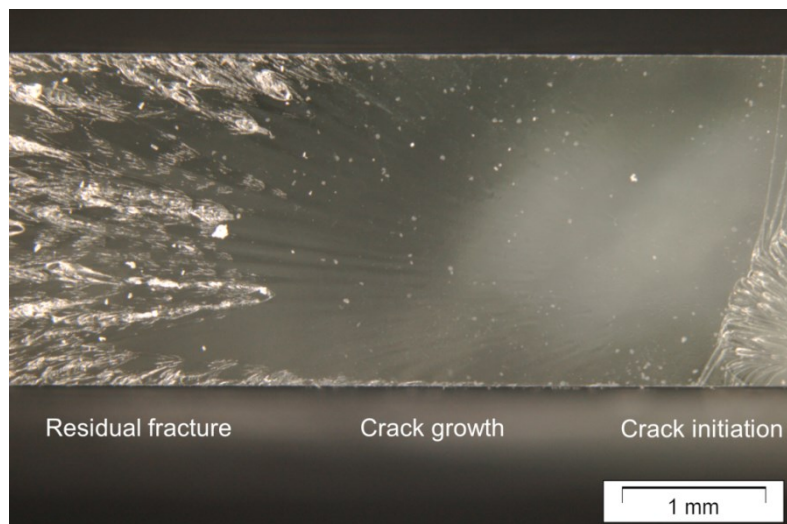


Figure 7.7: Light microscopic photograph of pure epoxy resin fracture surface.

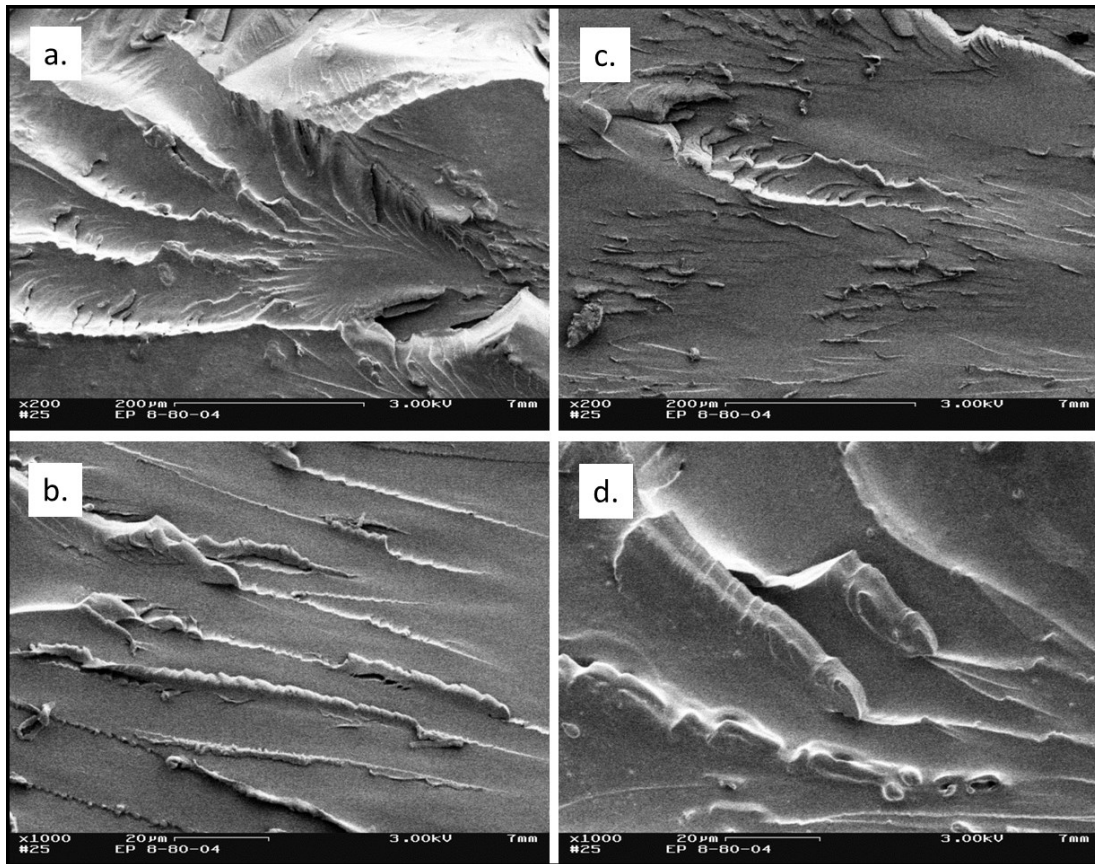


Figure 7.8: Fracture surface of epoxy resin tested at $\sigma_{max} = 31$ MPa, $f = 10$ Hz, $N = 47952$: a. area of residual fracture (200x), b. area of residual fracture (1000x), c. area of crack growth (200x), d. area of crack growth (1000x).

The fracture surfaces of specimens tested at the same angles containing different fibre volume fractions are presented after being tested at the same respective fatigue stress level with R 0.1. To investigate possible influences of the height of the applied load, the effect of fibre volume content was studied in UD 45° and UD 90° at two selected stress levels each. UD 90° specimens containing 30 *vf.*% and 55 *vf.*% carbon fibres were compared at fatigue stresses of 12.5 MPa (figure 7.9) and 15 MPa (figure 7.10), respectively. When applying maximum fatigue stress of 12.5 MPa, the specimen with low fibre content failed after 116350 cycles, the one with high fibre content after 660151 cycles. Fracture behaviour comparing these two specimens was clearly different. The high amount of matrix in specimens with 30 *vf.*% fibres benefited matrix dominated fracture behaviour (figure 7.9a).

Interfacial debonding along the fibres and plane fracture surfaces were observed. In figure 7.9b good fibre matrix adhesion in the fracture plane and smooth fracture behaviour is visible. On the contrary, fracture surfaces of UD 90° specimens with 55 *vf.*% appeared rough. Not only matrix failure, but fibre bridging, pulled out and fractured fibres transverse to fracture plane were studied (figure 7.9c). The pullout of fibres perpendicular to the fracture plane seemed to consume much more failure energy than matrix fracture which might be the explanation for the significant difference in number of cycles to failure.

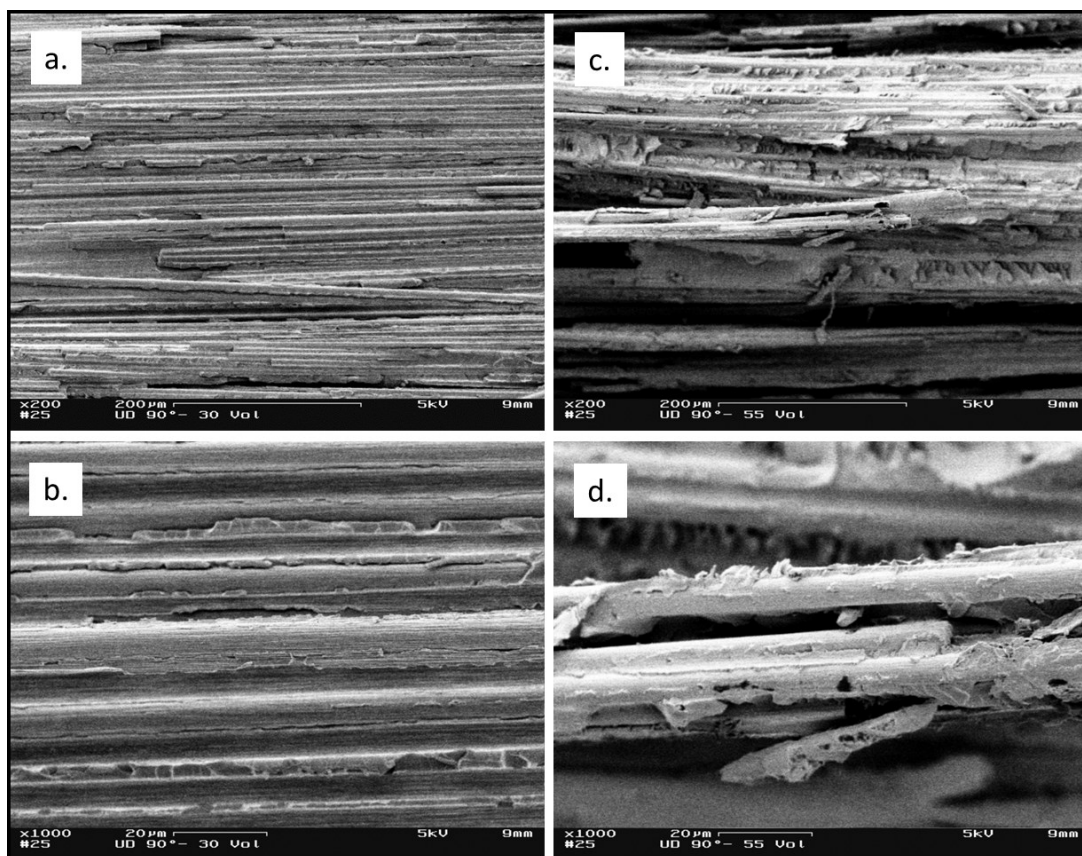


Figure 7.9: Fracture surfaces of two UD 90° specimens both tested at $\sigma_{max} = 12.5$ MPa: a. UD 90° 30 *vf.*%, $N = 116350$ (200x), b. UD 90° 30 *vf.*%, $N = 116350$ (1000x), c. UD 90° 55 *vf.*%, $N = 660151$ (200x), d. UD 90° 55 *vf.*%, $N = 660151$ (1000x).

At the higher applied load of 15 MPa the failure mechanisms monitored in specimens tested at 12.5 MPa were intensified. Higher fatigue load led to increasing number of pulled out fibres not only in 55 *vf.*% specimens (figure 7.10c) but partly in specimens with low fibre content as well (figure 7.10a). These observations of damage mechanisms depending on load level were reasonable in respect of S-N curves for UD 90° specimens. In tests with high maximum loads (number of cycles to failure between 10³ and 10⁴) the influence of different fibre volume contents was vanishing but it became evident at lower load levels. Similar damage mechanisms were observed in UD 90° specimens tested under quasi-static conditions. Fibre pull-out out of the fracture plane in specimens with high fibre content resulted in higher ultimate tensile strengths compared to specimens with low fibre content.

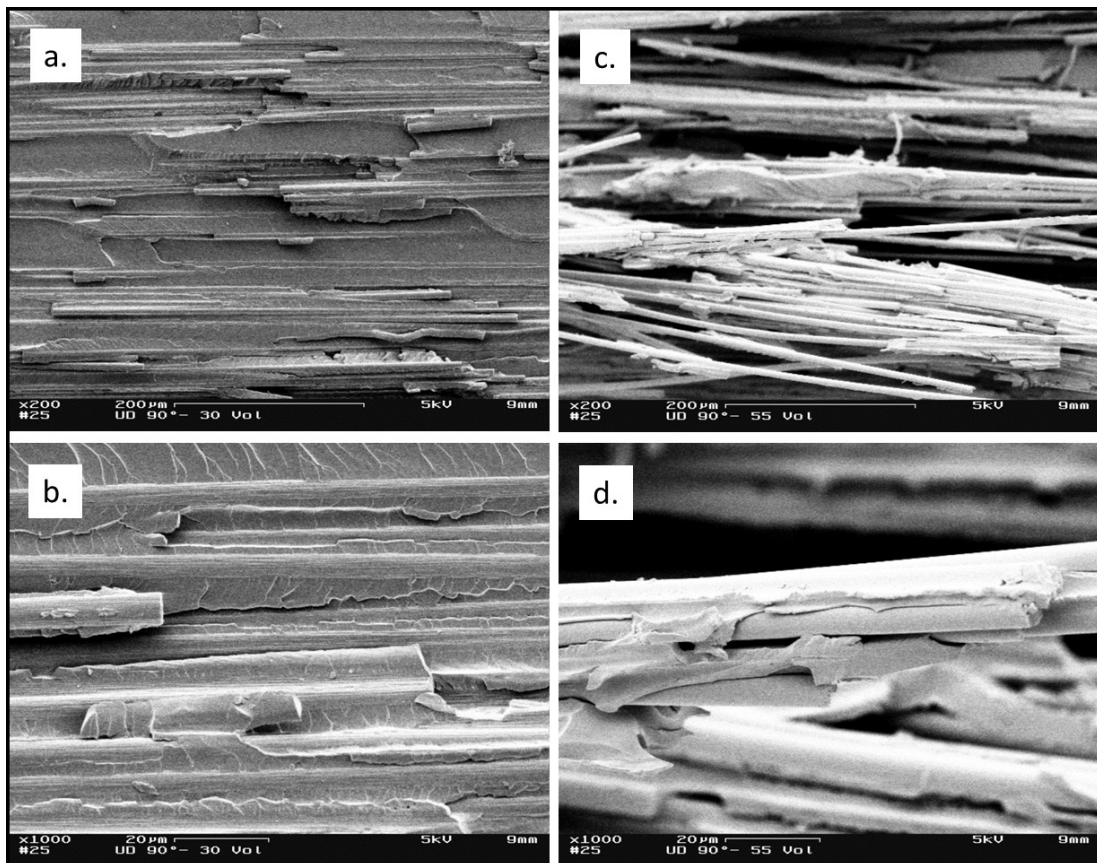


Figure 7.10: Fracture surfaces of two UD 90° specimens both tested at $\sigma_{max} = 15$ MPa: a. UD 90° 30 *vf.*%, $N = 68929$ (200x), b. UD 90° 30 *vf.*%, $N = 68929$ (1000x), c. UD 90° 55 *vf.*%, $N = 189003$ (200x), d. UD 90° 55 *vf.*%, $N = 189003$ (1000x).

Damage mechanisms in UD 45° specimens with low and high fibre content were studied after testing both specimen types at 30 MPa and 35 MPa. Fracture surfaces of UD 45° tested at $\sigma_{max} = 30$ MPa are presented in figure 7.11. At this stress level, UD 45° 30 vf.% tested with 5 Hz failed after 15342 cycles, UD 45° 55 vf.% tested with 10 Hz failed after 683777 cycles. Damage behaviour of specimens with low fibre volume content was matrix-dominated again (figure 7.11a) with single broken fibres which were still aligned in the fracture plane (figure 7.11b). Brittle matrix fracture was clearly visible between and around the carbon fibres (figure 7.11b). Fibre failure was more dominant in specimens with high fibre content (figure 7.11c). In contrast to UD 90° specimens with high fibre content, UD 45° showed fibre breakage but still within the fracture plane.

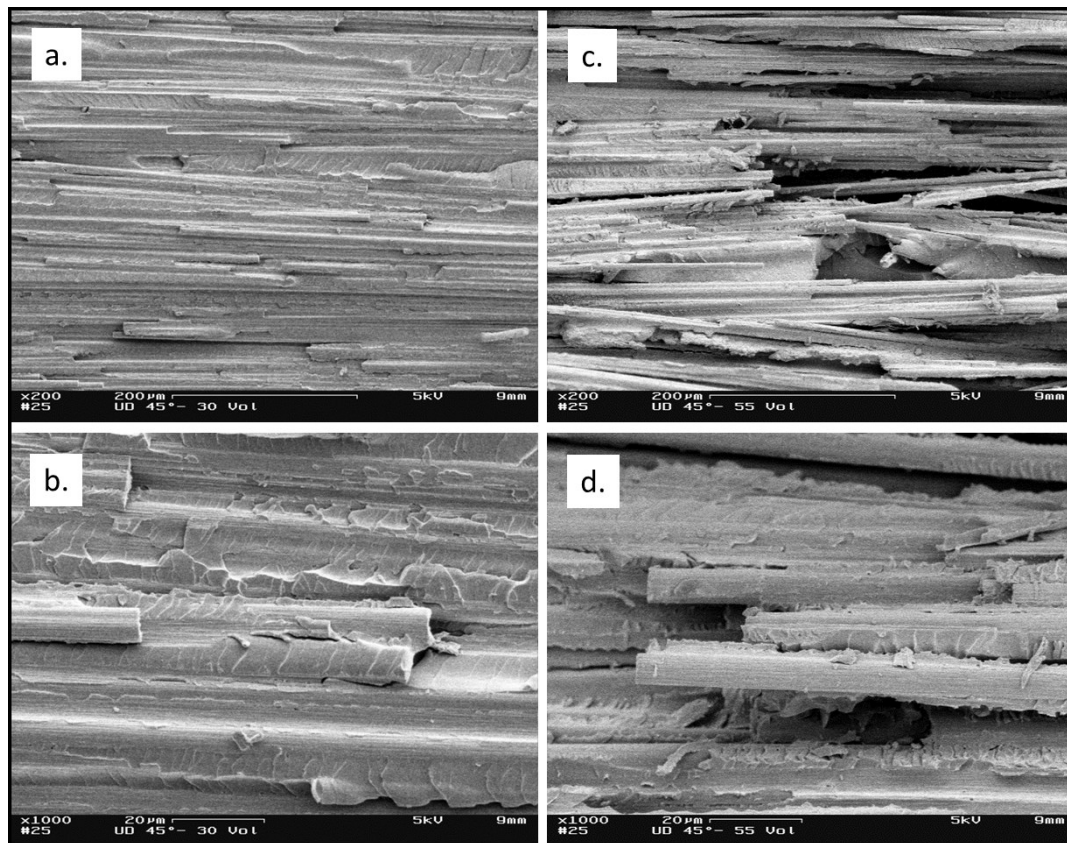


Figure 7.11: Fracture surfaces of two UD 45° specimens both tested at $\sigma_{max} = 30$ MPa: a. UD 45° 30 vf.%, $N = 15342$ (200x), b. UD 45° 30 vf.%, $N = 15342$ (1000x), c. UD 45° 55 vf.%, $N = 683777$ (200x), d. UD 45° 55 vf.%, $N = 683777$ (1000x).

At higher cyclic stress $\sigma_{max} = 35$ MPa more broken fibres appeared in specimens with 30 *vf.*% (figure 7.12a). Fibre pull-outs, which were observed in UD 90° specimens, were not very dominant in UD 45° specimens. Observations indicated that with increase of maximum cyclic load, entire fracture behaviour got rougher in specimens of both fibre contents. More pulled-out fibres, fibre breakage and destroyed fracture surfaces were monitored at $\sigma_{max} = 35$ MPa. These behaviours were reflected in the S-N curves, which showed similar slopes for UD 45° specimens with low and high carbon fibre content but higher fatigue strengths for UD 45° with 55 *vf.*%.

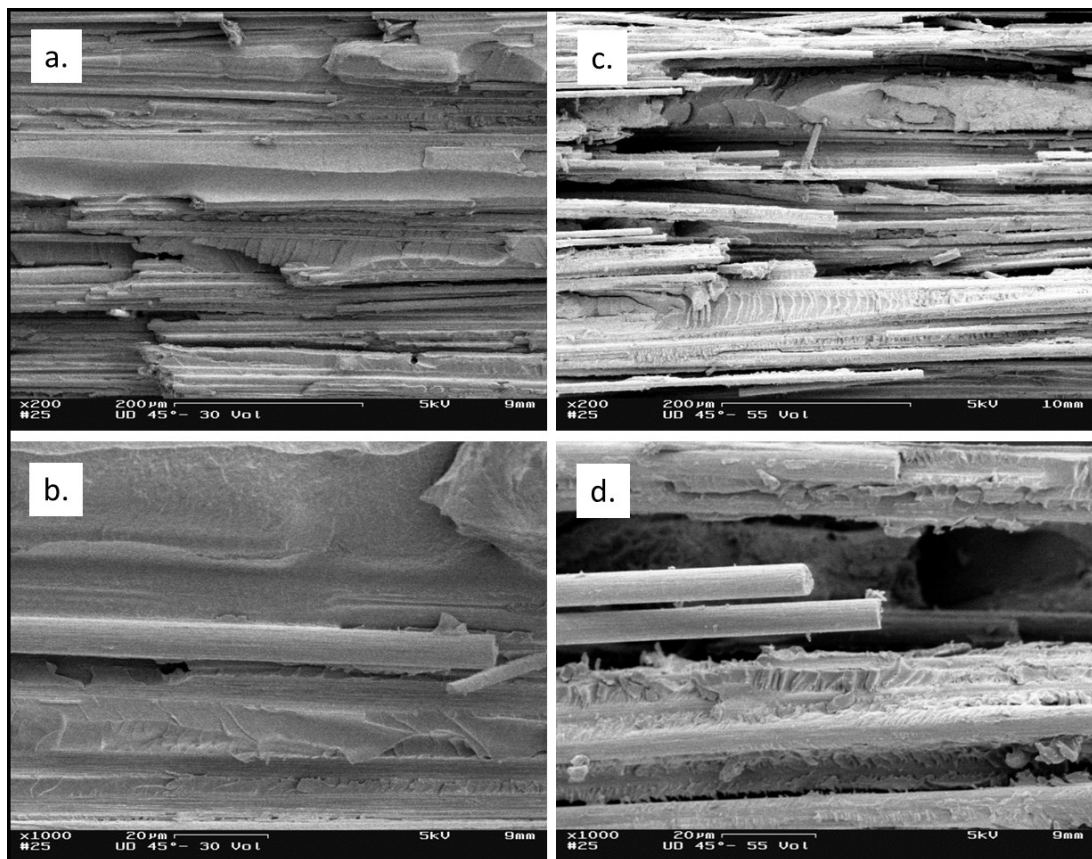


Figure 7.12: Fracture surfaces of two UD 45° specimens both tested at $\sigma_{max} = 35$ MPa: a. UD 45° 30 *vf.*%, $N = 7800$ (200x), b. UD 45° 30 *vf.*%, $N = 7800$ (1000x), c. UD 45° 55 *vf.*%, $N = 121001$ (200x), d. UD 45° 55 *vf.*%, $N = 121001$ (1000x).

Resulting from fibres' high stiffness and strength, which are magnitudes higher than matrix properties, fibre failure was dominant in fatigue tests with UD 0° specimens. Fibre content did not influence damage mechanism of fibre failure. Because all UD 0° failed explosively in mechanical tests, no fracture surfaces as such were left after mechanical tests for investigations by SEM.

7.6. Conclusions

Epoxy resin and unidirectional carbon/epoxy plates with two specific fibre contents were produced to study the influence of carbon fibre content on the mechanical behaviour and on damage mechanisms. Thermo-analytical methods were used to optimise plate production process and to assure quality of the produced specimens. Thermo-gravimetric analysis confirmed the aspired carbon fibre volume fractions of 30 % and 55 % in plates.

Under quasi-static tensile loads specimens with higher fibre content possessed both higher Young's moduli and ultimate tensile strengths. Young's modulus of epoxy resin was lower compared to UD 90° specimens but UTS and strain at UTS were significantly higher. In fatigue tests, specimens with higher fibre volume content always reached higher numbers of cycles to failure when testing at the same stress level. As a consequence of the higher quasi-static strength, epoxy resin possessed higher fatigue strength than UD 90° specimens. The different fibre volume content of UD 90° specimens was more dominant at lower applied fatigue stresses than at high stress levels. The observations made in mechanical tests could be correlated with scanning electron microscopy investigations of the fracture surfaces.

Failure of specimens with low fibre contents tested at angles of 45° and 90° was matrix dominated. Fracture planes were smooth and fracture occurred inside the matrix material or along the fibres. On the contrary, specimens tested at angles of 45° and 90° with high fibre content showed fibre breakage. Especially in 90° specimens with high fibre content fibres were not only broken but pulled out of the fracture plane. Damage mechanisms in

UD 90° with both fibre contents became more similar with increasing applied cyclic loads. As a consequence, the difference between numbers of cycles to failure of UD 90° specimens with high and low fibre contents vanished with increasing applied cyclic stress. In specimens tested in fibre direction, damage mechanisms were exclusively fibre dominated and consequently did not depend on the fibre volume content.

7.7. References

- [1] Talreja R, Singh CV. Damage and failure of composite materials. Cambridge, New York: Cambridge University Press; 2012.
- [2] Talreja R. Fatigue of Composite Materials. Pennsylvania, U.S.A: Technomic Publishing Inc; 1987.
- [3] Reifsnider KL (ed.). Fatigue of composite materials. Amsterdam, New York: Elsevier; 1991.
- [4] Ehrenstein GW. Faserverbund-Kunststoffe: Werkstoffe, Verarbeitung, Eigenschaften. 2nd ed. München [u.a.]: Hanser; 2006.
- [5] Koyanagi J, Yoneyama S, Eri K, Shah PD. Time dependency of carbon/epoxy interface strength. *Composite Structures* 2010;92(1):150–4.
- [6] Kerans RJ, Parthasarathy TA. Theoretical Analysis of the Fiber Pullout and Pushout Tests. *Journal of the American Ceramic Society* 1991(Volume 74, Issue 7):1585–96.
- [7] Shiqiang Deng, Lin Ye, Mai Y. Measurement of interfacial shear strength of carbon fibre/epoxy composites using a single fibre pull-out test. *Advanced Composite Materials* 1998;7(2):169–82.
- [8] Schürmann H. Konstruieren mit Faser-Kunststoff-Verbunden: Mit 39 Tabellen. 2nd ed. Berlin, Heidelberg, New York, NY: Springer; 2007.
- [9] Naik PS, Orangalu SA, Londhe NV. Effect of fiber weight fraction on mechanical properties of carbon-carbon composites. *Polym Compos* 2012;33(8):1329–34.

- [10] Mini KM, Lakshmanan M, Mathew L, Mukundan M. Effect of fibre volume fraction on fatigue behaviour of glass fibre reinforced composite. *Fatigue & Fracture of Engineering Materials & Structures* 2012;35(12):1160–6.
- [11] Allah M, Abdin EM, Selmy AI, Khashaba UA. Effect of fibre volume fraction on the fatigue behaviour of GRP pultruded rod composites. *Composites Science and Technology* 1996;56(1):23–9.
- [12] Fotouh A, Wolodko JD, Lipsett MG. Fatigue of natural fiber thermoplastic composites. *Composites Part B: Engineering* 2014;62:175–82.
- [13] Austrian Standards Institute. *Plastics - Methods for determining the density of non-cellular plastics*;83.080.01(ISO 1183-1:2012); 2013.
- [14] DIN EN ISO 527-2. Bestimmung der Zugeigenschaften(DIN EN ISO 527-2:1996). Brüssel, Belgium: CEN (European Committee for Standardization); 1996.
- [15] ASTM International. *Standard Test Method for Tensile Properties of Polymer Matrix Composite Materials*(ASTM D3039/D3039M-00). West Conshohocken, PA, United States: ASTM International; 2000.
- [16] ASTM International. *Standard Practice for Statistical Analysis of Linear or Linearized Stress -Life (S-N) and Strain-Life (e-N) Fatigue Data*(ASTM E739-91). West Conshohocken, PA, United States: ASTM International; 1991.
- [17] Ehrenstein GW, Riedel G, Trawiel P. *Praxis der thermischen Analyse von Kunststoffen*. 2nd ed. München: Hanser; 2003.
- [18] Williams JG, Patrick TJ. *Fracture Mechanics of Non-Metallic Materials [and Discussion]*. *Philosophical Transactions of the Royal Society A* 1981(Vol. 299 no. 1446):59–72.

8. Publication 3

8.1. Bibliographic information

- Title: Effects of mean stress and fibre volume content on the fatigue-induced damage mechanisms in CFRP
- Authors and relevant contributions to this publication:
 - Julia BRUNBAUER¹
Experimental testing, microscopic investigations, data evaluation, preparation of the publication
 - Gerald PINTER²
Discussion of experimental results
- Affiliation:
 1. Institute of Materials Science and Testing of Polymers, Montanuniversitaet Leoben, Otto Glöckel-Strasse 2, 8700 Leoben, Austria
 2. Polymer Competence Center Leoben GmbH, Roseggerstrasse 12, 8700 Leoben, Austria
- Periodical: International Journal of Fatigue
- Status: accepted for publication

Statement with regard to this publication: The manuscript presented here is an adapted manuscript in order to fit the formatting of the thesis and does not necessarily reflect exactly the actually accepted version.

8.2. Abstract

The effect of the load type (tension and compression) in quasi-static and of the applied mean stress in fatigue tests on the mechanical behaviour and on the damage mechanisms in unidirectional (UD) carbon/epoxy laminates has been studied in combination with the influence of fibre volume content. Results show that the fibre volume content increases the mechanical properties in tension-tension fatigue tests for all tested angles 0° , 45° and 90° . The tensile damage mechanisms of off-axis specimens depend on the fibre volume content and change from matrix cracking and matrix-fibre debonding to fibre-pull out with an increasing amount of fibres as investigated in detail in a previous work. In tension-compression tests, higher fibre volume contents are only beneficial in fatigue tests at angles of 0° and 45° . Fatigue strengths of UD 90° specimens in tension-compression tests are not significantly improved by the fibre volume content which can be ascribed to breakage of entire fibre bundles and crushed fibres on the fracture surfaces.

8.3. Introduction

Continuously fibre reinforced composites offer a wide range of applications due to their high performance properties. If mechanical loads are applied, the macroscopic structure of composite materials consisting of continuous fibres and matrix material causes anisotropic behaviour. Microscopic damage mechanisms are decisively affected by the quality of the interface between fibre and matrix [1–3], the stacking sequence [4] and the mode of the applied load (tension or compression) [5] in addition. If fatigue loads are applied, the occurring mechanisms can progress or interact in composite materials [3,6]. Common damage mechanisms in laminates are e.g. matrix cracking, interfacial fibre/matrix debonding, fibre fracture or delamination [2,7–10]. Under fatigue loads, the mechanical mean stress, which distinguishes between tension-tension, tension-compression or compression-compression fatigue loads, affects the mechanical properties of composite materials [11–13]. Beyond that, damage mechanisms are influenced by the mean stress, the applied load amplitude and the angle between the reinforcing fibres and

the applied load and have been investigated in detail in different studies e.g. [7,9,14,15–18].

It has been shown in a previous work that, in addition to the already mentioned effects, damage mechanisms of unidirectional laminates depend on the fibre volume content in tension-tension fatigue tests [19]. Especially in fatigue tests with off-axis specimens, the monitored fracture mechanisms were different in specimens with low and high fibre contents. While matrix-cracking and interfacial debonding were mainly monitored in specimens with low fibre content, interfacial debonding followed by fibre-pull out was observed in specimens with high fibre content resulting in an increased fatigue strength [19]. To broaden the understanding of composite damage this work investigates the combined effect of mean stress, applied load amplitude and fibre volume content on the mechanical properties and on the damage mechanisms in unidirectional carbon/epoxy laminates tested at angles of 0°, 45° and 90° with fibre volume contents of 30 % and 55 %. Fatigue results of the unreinforced epoxy resin material tested at the same stress ratios are presented as well.

8.4. Experimental work

Carbon/epoxy specimens with 30 % and 55 % fibre volume fraction (measured with thermogravimetric analysis [19]) as well as epoxy resin specimens were produced. EPIKOTE™ Resin MGS® RIMR135 (approved by German Lloyd) with the curing system EPIKURE™ Curing Agent MGS® RIMH1366 by Momentive (Esslingen am Neckar, Germany) and carbon fibres HS 15-80 and HS 15-50/250 by G. Angeloni srl (Quarto d'Altino, Italy), respectively, were used. The reinforcement fibres were adhesively connected by an epoxy-compatible binder in order to make the handling easier and prevent distortion during the manufacturing. The plates were produced in a pressure-driven vacuum assisted resin transfer moulding process. Glass transition temperature T_g of the cured epoxy resin was about 93 °C (measured with differential scanning calorimetry). In all carbon/epoxy plates fibres were aligned in an unidirectional way and plates were cured at 80 °C for 5 h [19]. The curing process of carbon/epoxy plates was monitored by

dielectrical analysis (DEA) to assure fully cured plates for further specimen production. Unidirectional (UD) carbon/epoxy specimens were milled from plates with diamond blades at angles of 0° , 45° and 90° . For epoxy specimens used in quasi-static tensile and tension-tension fatigue tests a dumbbell-geometry was chosen in reference to [20] (figure 8.1). Specimen geometries for mechanical tests with carbon/epoxy specimens were chosen referring to [21] for tensile and according to [22] for compressive loads. Aluminium tabs with 1 mm thickness were glued on both sides of all carbon/epoxy specimens. For tensile loads, usually 1 mm thickness is chosen for specimens with high fibre contents tested in fibre direction and 2 mm thickness for off-axis specimens. In general, the cross-sections are selected in order to cause failure loads in reasonable ranges. The smaller thickness for UD 0° specimens in combination with reduced width is recommended because of the high tensile loads which have to be expected in fibre direction and which have to be properly introduced into the specimens by shear loading [21]. Furthermore, the tab area available for load introduction for UD 0° specimens is smaller due to the smaller tab width which makes the load introduction even more difficult. If the loads cannot be introduced into the specimen by means of the tabs, failure in the area of the tabs' edges or even within the tabs might occur. This would not reflect the actual material behaviour. Consequently, 1 mm thickness for UD 0° instead of 2 mm is beneficial since it divides the upcoming loads during the tests in half. Therefore, for specimens with high fibre contents specimens dimensions were 200x10x1 mm for UD 0° specimens (figure 8.2) and 200x20x2 mm for off-axis specimens. If the fibre content is reduced, the expected loads reachable by UD 0° specimens also decrease [23]. As a consequence, the load introduction by shear becomes less critical. Therefore, specimens' geometries for specimens with low fibre volume fractions were 200x10x2 mm for specimens tested in fibre direction (figure 8.3) and 200x20x2 mm for off-axis specimens (figure 8.4). Compressive tests with unsupported gauge sections in which loads are introduced by shear loading were performed [22]. All specimens for compressive loads were of rectangular shape. Specimens' dimensions were 110x10x2 mm for all UD 0° specimens and 110x20x2 mm for all other specimens including epoxy resin specimens referring to [22]. Free gauge length for all specimens tested under compression loads was 10 mm. For data evaluation, all moduli and strengths were calculated with the

real cross-sections of the respective tested specimens. Moduli were evaluated between 0.001 and 0.003 absolute strain [21,22]

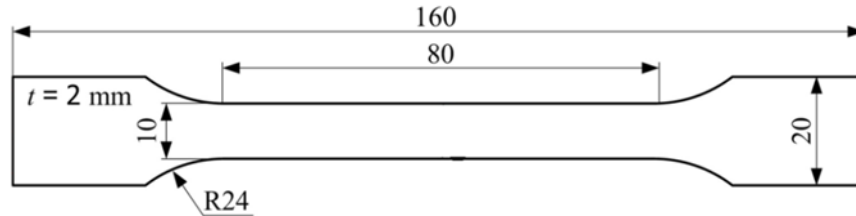


Figure 8.1: Specimen geometry for epoxy resin specimens used in quasi-static tensile and tension-tension fatigue tests.

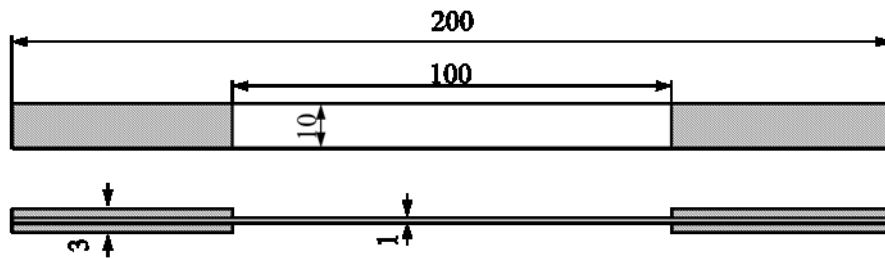


Figure 8.2: Specimen geometry for UD 0° specimens with 55 % fibre volume content used in quasi-static tensile and tension-tension fatigue tests.

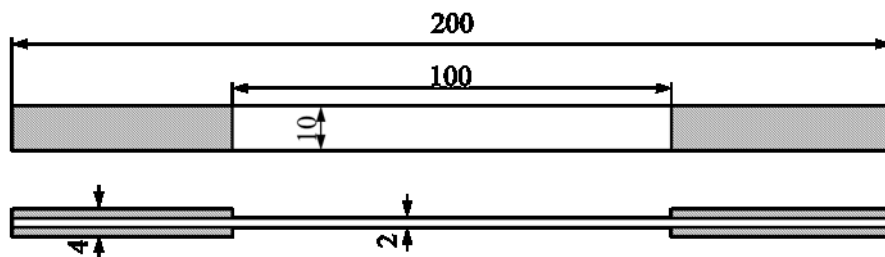


Figure 8.3: Specimen geometry for UD 0° specimens with 30 % fibre volume content used in quasi-static tensile and tension-tension fatigue tests.

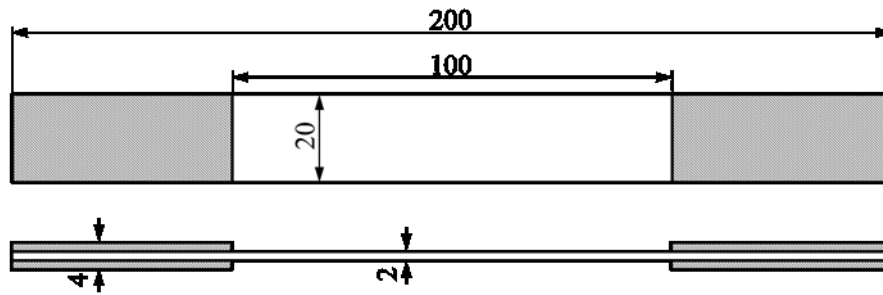


Figure 8.4: Specimen geometry for UD 45° and UD 90° specimens with 30 % and 55 % fibre volume content used in quasi-static tensile and tension-tension fatigue tests, respectively.

All mechanical tests were performed on a servo-hydraulic test machine MTS 810 designed for loads up to 100 kN by MTS Systems Corporations (Minnesota, USA) at room temperature. The test machine was equipped with a 100 kN load cell by MTS Systems Corporations (Minnesota, USA) with an accuracy of 0.5 % within the respective measuring range. In quasi-static tension and compression tests, specimens were loaded in a displacement controlled way with a test speed of 0.5 mm/min. Strains in longitudinal direction were recorded by means of a digital image correlation system by GOM (Braunschweig, Deutschland). Tension-tension fatigue tests were performed with the R -value (= minimum force / maximum force) of 0.1, tension-compression fatigue tests with $R = -1$ until fracture. Maximum cyclic stresses between approximately 80 % and 65 % of the ultimate tensile strengths were chosen as load levels for UD 0° and between 60 % and 35 % for the tested off-axis specimens in tension-tension fatigue tests. In tension-compression fatigue tests, the maximum cyclic tensile stresses applied were between approximately 25 % and 15 % of the ultimate tensile strengths for UD 0° specimens and between approximately 65 % and 25 % for off-axis specimens. For the creation of S-N curves, specimens were tested at four different stress levels. A minimum of three specimens were tested on each stress level. If number of cycles exceeded $2 \cdot 10^6$, tests were usually stopped. Test frequency was chosen between 2 and 10 Hz depending on the test load and the hysteretic heating [24]. Specimens' temperatures were monitored by infrared sensors in all tests. Results of fatigue tests were evaluated statistically to calculate the slope of the S-N curves k , scatter width T_s and the

nominal stress amplitude after $5 \cdot 10^6$ cycles σ_a at $5 \cdot 10^6$ according to [25]. For this statistical evaluation, only failed specimens were taken into account. Additionally, stress-strain hystereses were recorded in all fatigue tests. Due to the small free gauge length of only 10 mm in tension-compression fatigue tests making local strain measurement difficult, the piston displacement recorded by the servo-hydraulic test machine was used to evaluate the representative hysteretic slopes discussed in this work. Preliminary tests showed that the lower the stiffness of the tested specimen, the more accurate the strains measured by the servo-hydraulic piston are [24]. Fracture surfaces were investigated in detail with a scanning electron microscope (SEM). 200x and 1000x magnifications were used for the presented SEM photographs.

8.5. Results and Discussion

8.5.1. Quasi-static tensile and compression tests

Results of quasi-static tensile and compressive tests are presented in figures 8.5 and 8.6. The stress-strain curves measured under tension and compression loads of each specimen type were joined graphically after the tests for better comparison. Due to different stress magnitudes, stress-strain curves of UD 0° specimens are shown in a separate graph (figure 8.6).

Figure 8.5 compares the tension and compression stress-strain curves of unidirectional carbon/epoxy specimens with 30 % and 55 % fibre volume content tested at angles of 45° and 90° with the stress-strain behaviour of the pure epoxy resin. It is apparent that the anisotropic carbon/epoxy laminates behave very differently under tension and compression loads compared to the isotropic resin. The compressive strengths of all tested laminates were significantly higher in relation to the respective tensile strengths. For UD 45° specimens, compressive strength was about twice as high as the tensile strengths. UD 90° reached even three times higher strengths under compression loads. All UD 45° and 90° specimens with 55 % fibre volume content possessed higher tensile and compressive strengths than the respective specimens with 30 % fibre content. Strain at failure was higher for

specimens with low fibre content under both load conditions. In contrast to that, the compressive strength of the isotropic epoxy resin was only slightly higher than the tensile strength. The epoxy resin showed higher strains at failure under tensile loads. The stiffnesses evaluated under tensile and compression loads between 0.001 and 0.003 absolute strain were in similar scales for all tested specimens.

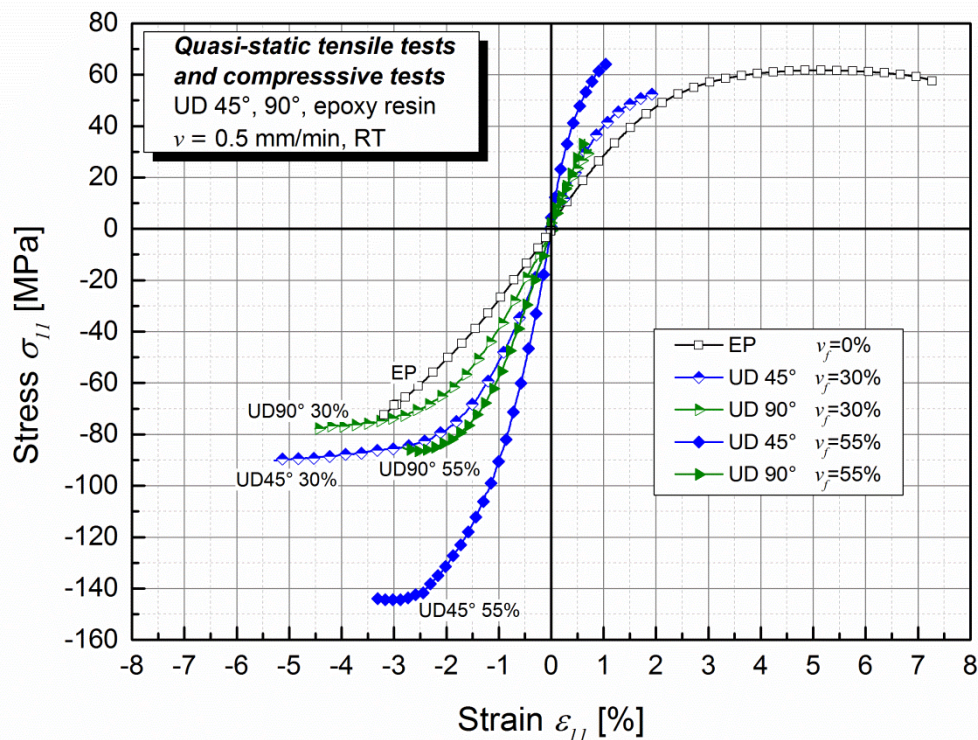


Figure 8.5: Quasi-static tension and compression stress-strain curves for UD laminates tested at angles of 45° and 90° with 30 % and 55 % fibre volume fraction and for epoxy resin specimens.

In UD 0° specimens the increase of the fibre volume content caused both higher strength and stiffness under tension as well as compression loads. Specimens loaded in fibre direction reached higher strengths under tension than under compression loads. Besides, stiffness was similar in the tensile and compression areas of the stress-strain curves of UD 0° $\nu_f = 55\%$. The reduction of fibre volume content to 30 % resulted in reduced stiffness and strength under both load conditions. However, for UD 0° $\nu_f = 30\%$ specimens, stiffnesses under tensile and compression load were different.

Under tensile loads, specimens with low fibre content showed a higher stiffness than in compression tests. The lower fibre volume content led to a higher strain at failure in compression tests.

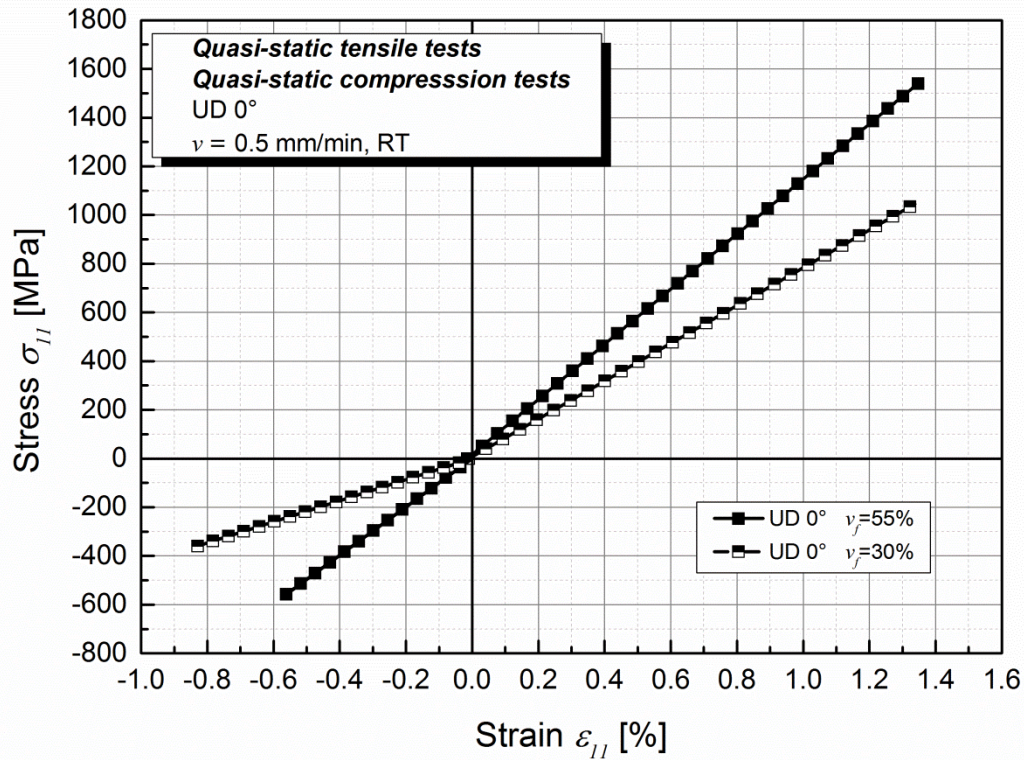


Figure 8.6: Quasi-static tension and compression stress-strain curves for UD 0° laminates with 30 % and 55 % fibre volume content, respectively.

8.5.2. Tension-tension and tension-compression fatigue tests

The results of tension-tension and tension-compression fatigue tests with carbon/epoxy laminates with different fibre volume fractions and epoxy resin are presented in three diagrams. The statistically evaluated slope k , scatter width T_s and the nominal stress amplitude after $5 \cdot 10^6$ cycles, σ_a at $5 \cdot 10^6$, are listed in table 8.1. The fatigue data of epoxy resin specimens and UD 90° specimens with both fibre volume contents are illustrated in figure 8.7.

The S-N curves of epoxy resin specimens were steeper in tension-compression than in tension-tension fatigue tests, which was consistent with

literature [15]. The slope k changed from 12.8 ($R = 0.1$) to 7.2 ($R = -1$). Consequently, epoxy resin specimens were tested at higher nominal stress amplitudes in the low cycle fatigue area at $R = -1$ but reached slightly lower nominal stress amplitudes after $5 \cdot 10^6$ cycles (table 8.1). This indicated different damage mechanisms at the applied stress ratios.

Table 8.1: Evaluation of fatigue curves: slope k , scatter width T_s and calculated nominal fatigue strength after $5 \cdot 10^6$ cycles σ_a at $5 \cdot 10^6$ of specimens with 0 %, 30 % and 55 % carbon fibre volume content tested at angles of 0°, 45° and 90°, $R = 0.1$ and $R = -1$ at room temperature.

Specimen	v_f [%]	R [-]	k [-]	T_s [-]	σ_a at $5 \cdot 10^6$ [MPa]
EP	0	0.1	12.8	1/1.36	11.3
UD 90°	30	0.1	7.2	1/1.41	3.4
UD 90°	55	0.1	11.1	1/1.15	4.8
UD 45°	30	0.1	11.0	1/1.15	8.0
UD 45°	55	0.1	9.2	1/1.12	10.6
UD 0°	30	0.1	16.1	1/1.29	267.0
UD 0°	55	0.1	24.9	1/1.14	435.2
EP	0	-1	7.2	1/1.29	10.4
UD 90°	30	-1	7.8	1/1.14	4.0
UD 90°	55	-1	8.0	1/1.58	4.2
UD 45°	30	-1	6.1	1/1.28	9.4
UD 45°	55	-1	6.0	1/1.49	14.6
UD 0°	30	-1	33.0	1/1.10	187.5
UD 0°	55	-1	13.4	1/1.41	248.4

For UD 90° specimens tested transverse to fibre direction, the fibre volume content affected the slope and fatigue strength mainly in tests with $R = 0.1$. Increasing the amount of fibre from 30 % to 55 % volume content led to an increase of 40 % of σ_a at $5 \cdot 10^6$. This effect could be ascribed to changing damage mechanisms in tension-tension fatigue tests - while in UD 90° specimens with low fibre content matrix cracking and fibre-matrix debonding were dominant damage mechanisms, fibre pull-out was monitored in specimens with high fibre content transverse to the fracture plane resulting in increased fatigue strengths [19]. In tension-compression tests on the contrary, the fatigue results of UD 90° 30 % specimens ($k = 7.8$, σ_a at $5 \cdot 10^6 = 4.0$ MPa) and UD 90° with 55 % fibre content ($k = 8.0$, σ_a at $5 \cdot 10^6 = 4.2$ MPa) were not significantly influenced by the fibre volume content.

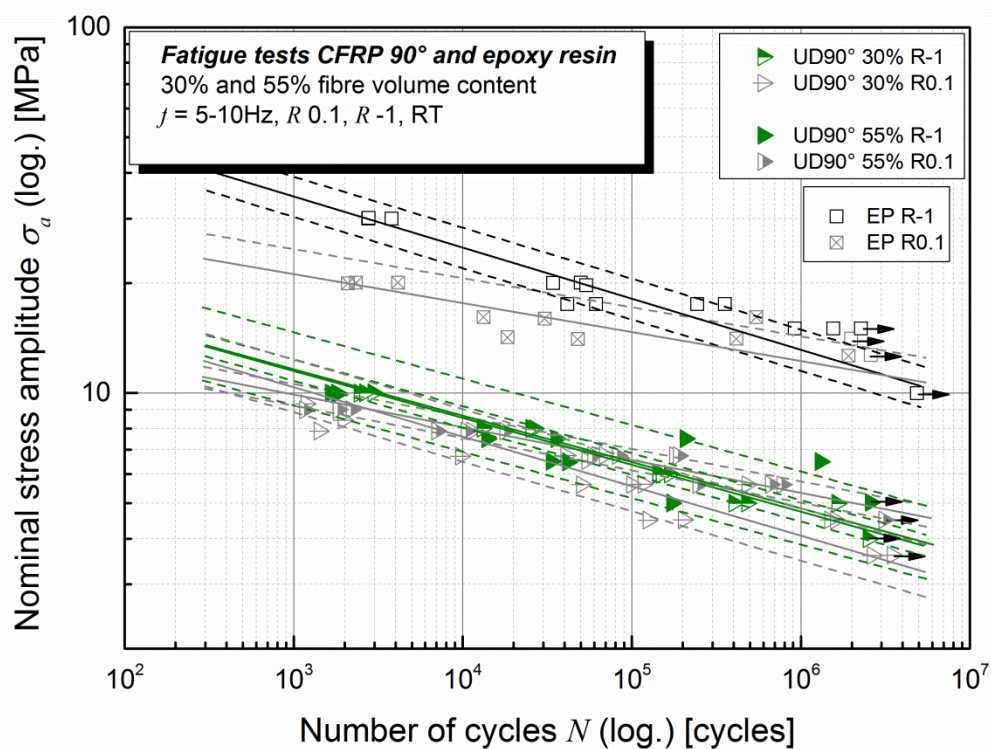


Figure 8.7: S-N curves (nominal stress amplitude versus number of cycles to failure) for UD 90° laminates with 30 % and 55 % fibre volume fraction and epoxy resin specimens tested at $R = 0.1$ and $R = -1$.

In figure 8.8 the S-N curves of all unidirectional specimens tested at an angle of 45° are presented. In tension-tension fatigue tests, specimens with higher fibre content reached higher fatigue strengths due to different damage mechanisms depending on the fibre volume content as described for UD 90° specimens [19]. When comparing all S-N curves presented in figure 8.8, UD 45° tested in tension-compression tests showed different fatigue behaviour than in tension-tension tests. UD 45° with both fibre contents reached higher nominal stress amplitudes σ_a at $5 \cdot 10^6$ when testing with $R = -1$ which was consistent with the quasi-static compressive strengths being higher than the tensile strengths.

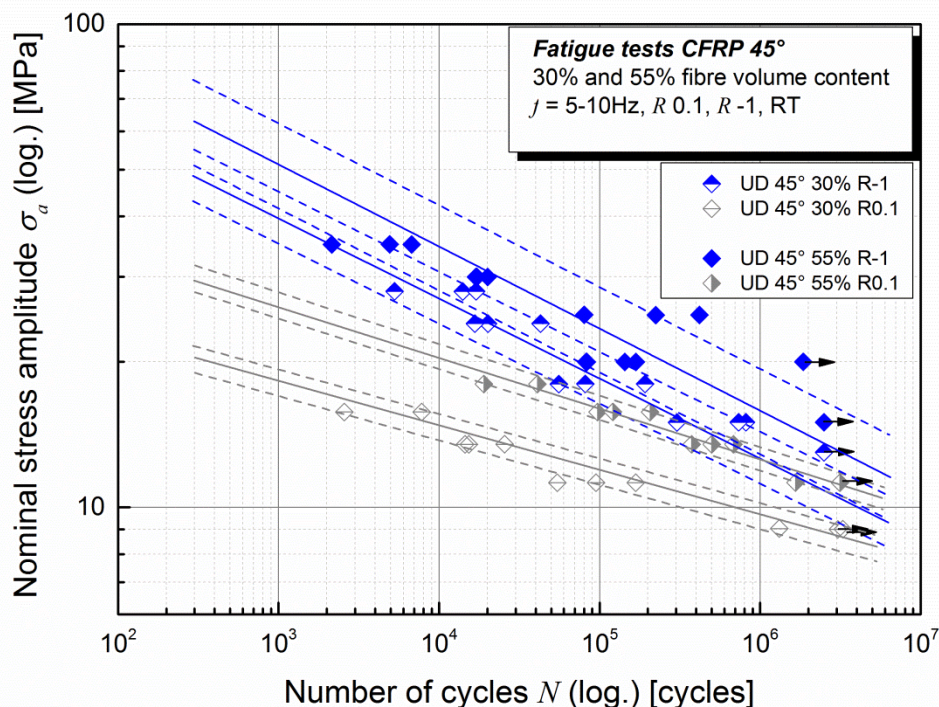


Figure 8.8: S-N curves (nominal stress amplitude versus number of cycles to failure) for UD 45° laminates with 30 % and 55 % fibre volume fraction tested at $R = 0.1$ and $R = -1$.

Again, higher fibre volume content resulted in higher fatigue strengths. However, slopes of S-N curves created in tension-compression tests were significantly steeper than tension-tension curves. These observations indicated that UD 45° with both fibre volume contents showed different

damage mechanisms depending on the applied mean stress. Therefore, fracture surfaces were investigated in detail with SEM.

In figure 8.9 all specimens tested at an angle of 0° are drawn. UD 0° with 30 % and 55 % fibre volume fraction both tested at $R = 0.1$ and $R = -1$ are compared. As a result of the quasi-static ultimate tensile strength being higher than the compressive strengths, UD 0° specimens reached higher nominal stress amplitudes in tension-tension fatigue tests than in tension-compression tests. Consequently, the compression load could be considered critical for failure in tension-compression tests. Due to the higher ultimate tensile strength of UD 0° with high fibre content, UD 0° 55% specimens were shifted to higher amplitudes than their counterparts with lower fibre content in all fatigue tests. Beyond that the S-N curve of UD 0° with 55 % fibre content was significantly steeper at $R = -1$ than all other curves measured in fibre direction. The steepness of the $R = -1$ slopes seemed to be influenced by the fibre volume content.

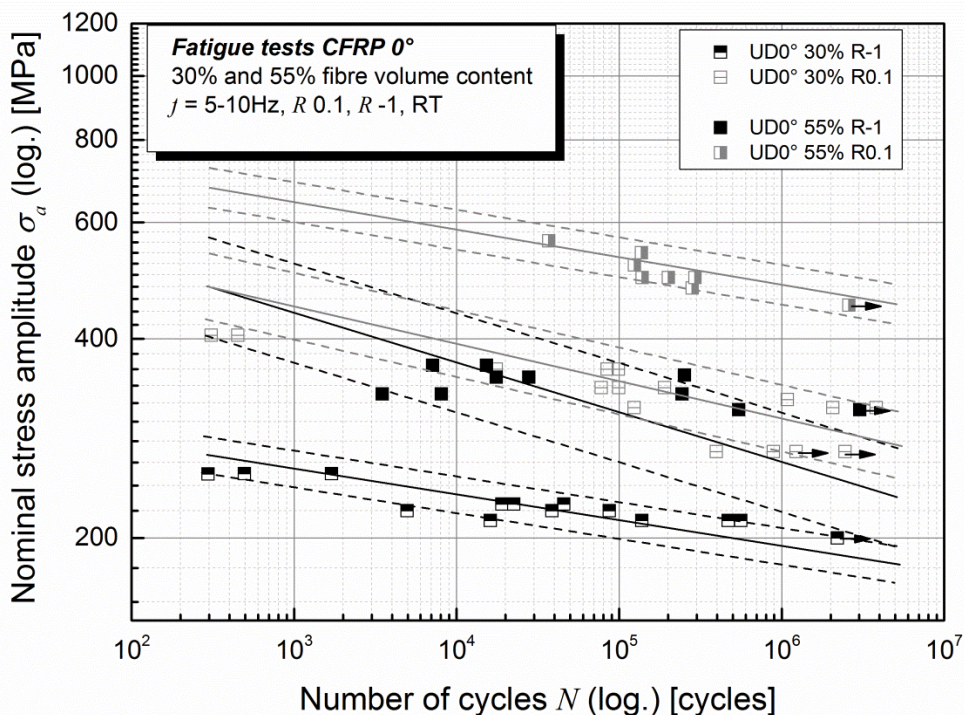


Figure 8.9: S-N curves (nominal stress amplitude versus number of cycles to failure) for UD 0° laminates with 30 % and 55 % fibre volume fraction tested at $R = 0.1$ and $R = -1$.

8.5.3. Damage mechanisms depending on the mean stress and on the fibre volume content

In the following, damage mechanisms investigated in unidirectional carbon/epoxy specimens with 30 % and 55 % fibre volume content and in epoxy resin specimens observed in tension-tension and tension-compression are presented and discussed. Fracture surfaces are compared for similar number of cycles to failure N_f because comparing one material tested with different stress ratios at the same nominal stress amplitude was not possible as figure 8.7, 8.8 and 8.9 illustrate. It has to be considered in the presented comparisons, that higher stress amplitudes usually intensify but not change the observed damage mechanisms [19]. Representative stress-strain hystereses comparing the behaviour of unidirectional specimens with high fibre volume content tested at angles of 0° , 45° , 90° as well as epoxy resin in tension-tension and tension-compression fatigue tests are illustrated. Stress-strain hystereses of specimens with low fibre volume content are not presented in detail because the stress-strain behaviour of specimens with different fibre volume fractions tested at the same angle were similar in principle resulting from similarities in quasi-static tests (figure 8.5 and 8.6).

8.5.3.1. Epoxy resin

To investigate damage mechanisms in epoxy resin specimens tested in tension-tension and tension-compression tests, two fracture surfaces with comparable numbers of cycles to failure N_f were investigated with SEM. As a result of the different slopes of the S-N curves as illustrated in figure 8.7, nominal stress amplitudes applied in tension-compression fatigue tests were higher. Figures 8.10a and 8.10b illustrate an epoxy resin specimen tested with $R = 0.1$ ($\sigma_a = 14$ MPa, $N_f = 4.7 \cdot 10^4$) while figures 8.10c and 8.10d present the fracture surface of a fatigue test with $R = -1$ ($\sigma_a = 20$ MPa, $N_f = 5.0 \cdot 10^4$). The fracture surfaces appeared different at first sight. Tension-tension fatigue loads created rough fracture surfaces (figure 8.10a and 8.10b). Areas of crack initiation, crack growth and residual fracture were found on the investigated surfaces [19]. On the contrary, the fracture surfaces from tension-compression fatigue tests were smooth through the entire surface even on SEM photographs with 1000x magnification. This

observation might be ascribed to the compression forces flattening the fracture surfaces (figure 8.10d).

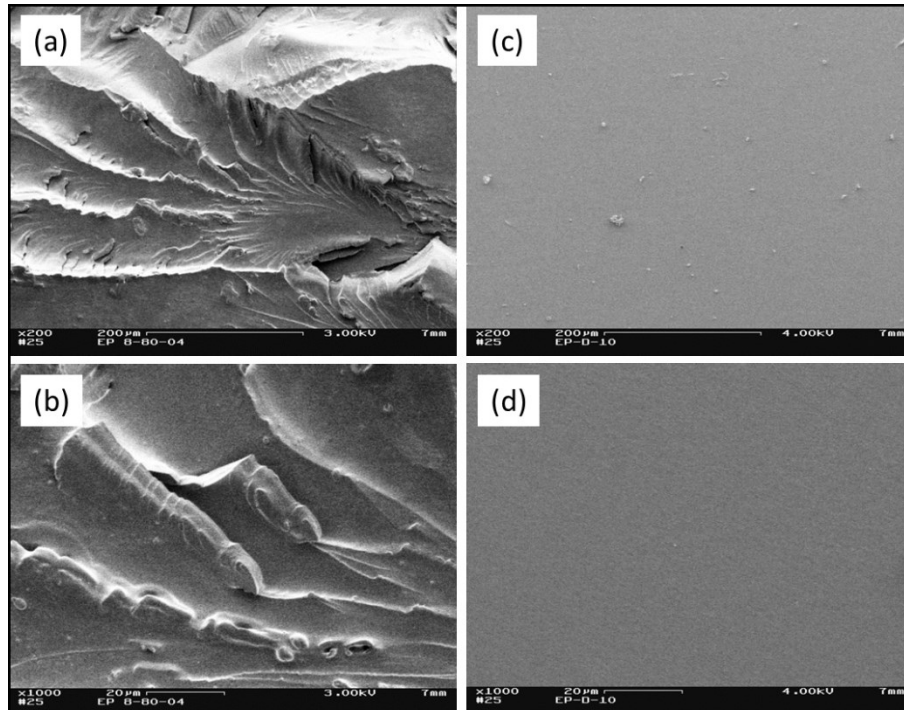


Figure 8.10: Fracture surfaces of epoxy resin specimens tested at $R = 0.1$ ($\sigma_a = 14$ MPa, $N_f = 4.7 \cdot 10^4$) with a. 200x and b. 1000x magnification [19] and at $R = -1$ ($\sigma_a = 20$ MPa, $N_f = 5.0 \cdot 10^4$) with c. 200x and d. 1000x magnification.

To enable greater insight in the cyclic material behaviour until fracture, the stress-strain hystereses corresponding to the specimens investigated with SEM after fracture are presented in figure 8.11. Hystereses curves measured in both tests show only a little shift to higher strains but no significant deformation or buckling of hystereses which indicates sudden failure rather than distinctive damage development.

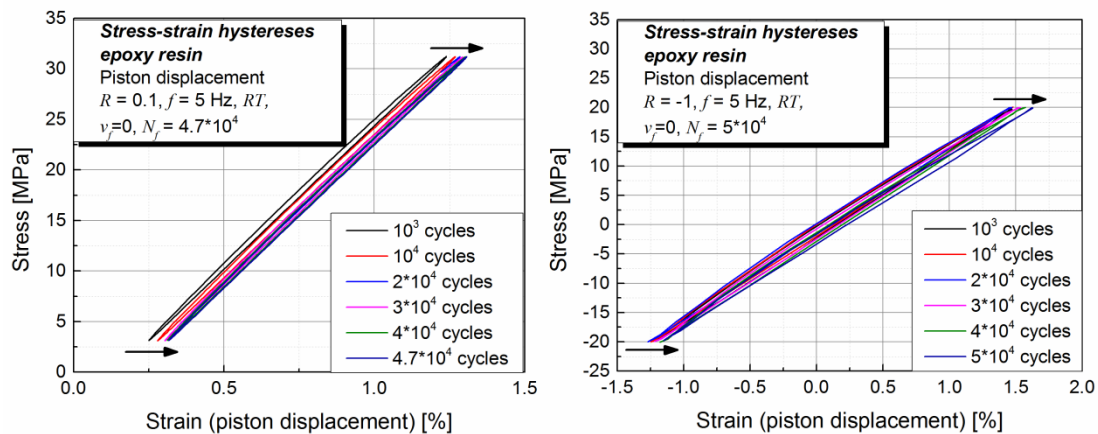


Figure 8.11: Representative stress-strain hystereses of epoxy resin tested with $R = 0.1$ (left) and $R = -1$ (right).

8.5.3.2. UD 90° with 30% and 55% fibre volume content

In figure 8.12, UD 90° specimens with 30 % fibre volume fraction tested with $R = 0.1$ ($\sigma_a = 5.64$ MPa, $N_f = 1.2 \cdot 10^5$) (8.12a and 8.12b) are compared to specimens tested with $R = -1$ ($\sigma_a = 6$ MPa, $N_f = 1.5 \cdot 10^5$) (8.12c and 8.12d). As already indicated in table 8.1, nominal stress amplitudes for specimens tested in tension-compression tests were slightly higher due to the higher quasi-static compressive strength. In specimens tested at both stress ratios, matrix-cracking and matrix-fibre debonding were dominant damage mechanisms. Figure 8.12c indicates that fibre breakage seemed to be more likely in tension-compression test and might be caused by the applied compression load.

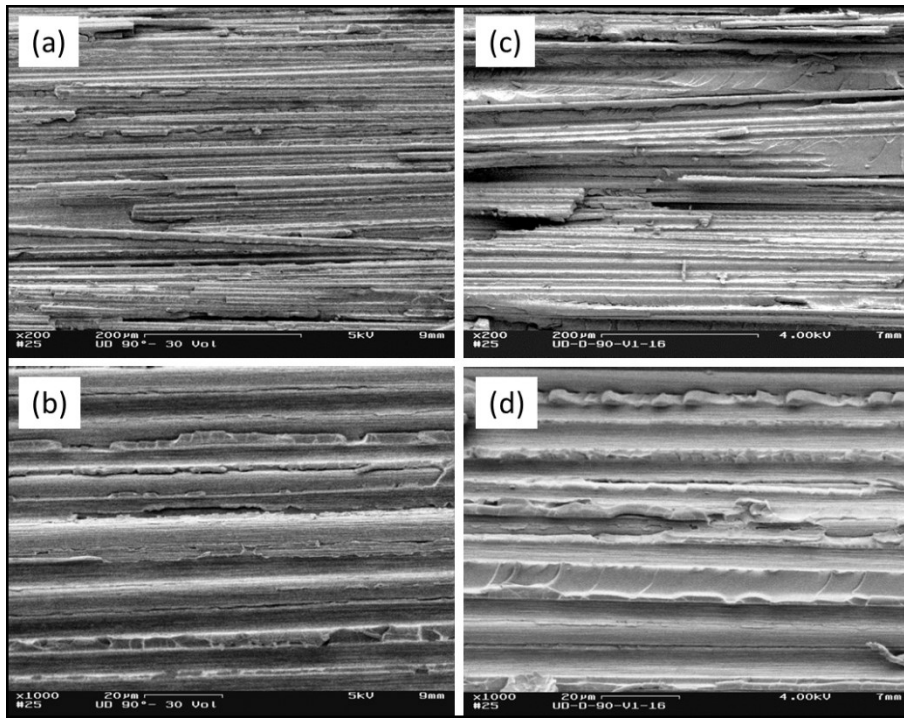


Figure 8.12: Fracture surfaces of UD 90° 30 % specimens tested at $R = 0.1$ ($\sigma_a = 5.64$ MPa, $N_f = 1.2 \cdot 10^5$) with a. 200x and b. 1000x magnification [19] and at $R = -1$ ($\sigma_a = 6$ MPa, $N_f = 1.5 \cdot 10^5$) with c. 200x and d. 1000x magnification.

In figure 8.13, fracture surfaces of UD 90° specimens with 55 % tested in tension-tension ($\sigma_a = 6.75$ MPa, $N_f = 1.9 \cdot 10^5$) (8.13a and 8.13b) and in tension-compression ($\sigma_a = 7.5$ MPa, $N_f = 2.1 \cdot 10^5$) (8.13c and 8.13d) are compared. The different damage behaviours when comparing the specimen with low fibre content (figure 8.12a and 8.12b) to the specimen with high fibre content (figure 8.13a and 8.13b) after being tested in tension-tension fatigue tests are significant as presented in [19]. The fibre volume content affected the fracture surfaces in tension-compression fatigue tests as well, as figure 8.13c and especially figure 8.13d emphasize. In figure 8.13c (200x magnification) a broken fibre bundle and fragments of broken fibres lying on the fracture surface are visible. Figure 8.13d (1000x magnification) presents the fractured fibres in greater detail. The broken fibres were still embedded in the matrix material which was usually not the case with the pulled-out fibres observed in tension-tension tests (figure 8.13b). Besides, the matrix material appeared more damaged in tension-compression tests.

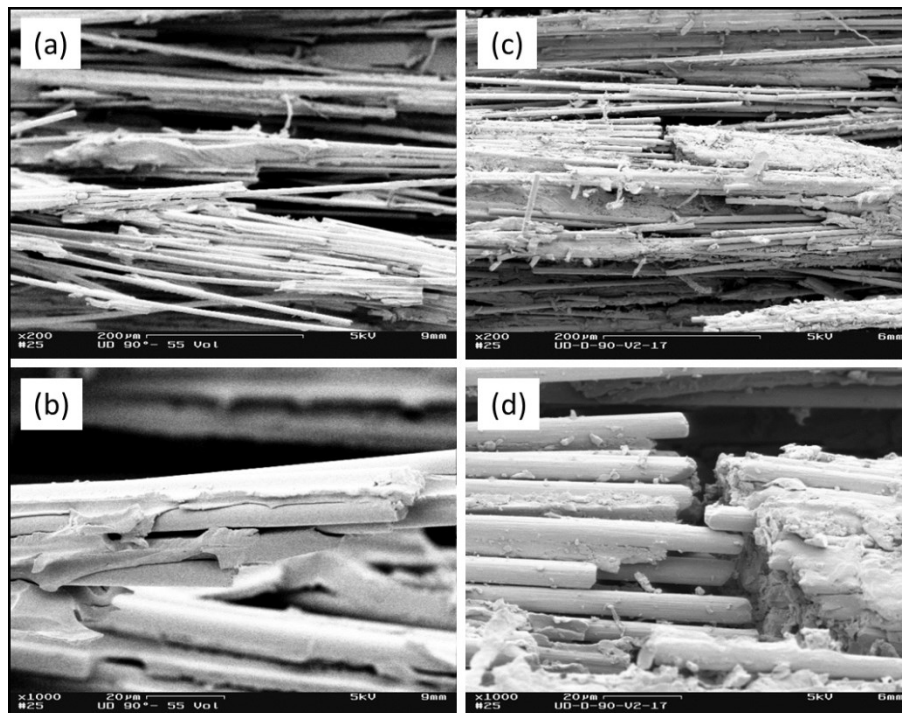


Figure 8.13: Fracture surfaces of UD 90° 55 % specimens tested at $R = 0.1$ ($\sigma_a = 6.75$ MPa, $N_f = 1.9 \cdot 10^5$) with a. 200x and b. 1000x magnification [19] and at $R = -1$ ($\sigma_a = 7.5$ MPa, $N_f = 2.1 \cdot 10^5$) with c. 200x and d. 1000x magnification.

The respective stress-strain hystereses for UD 90° specimens with high fibre content are illustrated in figure 8.14 for stress ratios $R = 0.1$ and $R = -1$. The shapes of the hystereses correlated with the monitored damage mechanisms. In fatigue tests with $R = 0.1$, the last hysteresis slope measured after $1.9 \cdot 10^5$ cycles was shifted to higher strains and indicated clearly progressing damage during the last 10^4 cycles of the fatigue test. The fibre pull-out observed in SEM investigations might be responsible for the shift to higher strains. However, the shape of the hystereses did not change during the fatigue test. In contrast to that, stress-strain hystereses measured in tension-compression fatigue test illustrated a different material behaviour. The last two illustrated hystereses measured after $2 \cdot 10^5$ and $2.1 \cdot 10^5$ in combination with the damage mechanisms presented in figure 8.13c and 8.13d suggested the following damage mechanisms: while tension loads pulled the fibres a little bit out of the fracture plane as monitored in fatigue test with $R = 0.1$, the consequential compression load seemed to press the

fibres either in the more and more damaged matrix material or against other fibres. In this case, in specimens with high fibre content it would be more likely that fibres were pressed against each other which might even result in local bending load and consequently in broken fibre bundles (figure 8.13d). If such a specimen was loaded with tension after that the already broken fibres could not be pulled out anymore and would result in the stress-strain behaviour illustrated in the last hystereses in figure 8.14 where the tensile load was finally critical. Based on these observations, a higher amount of fibres would not necessarily be beneficial in tension-compression tests which might explain the similar fatigue results of UD 90° 30 % and UD 90° 55 % specimens in tension-compression S-N curves.

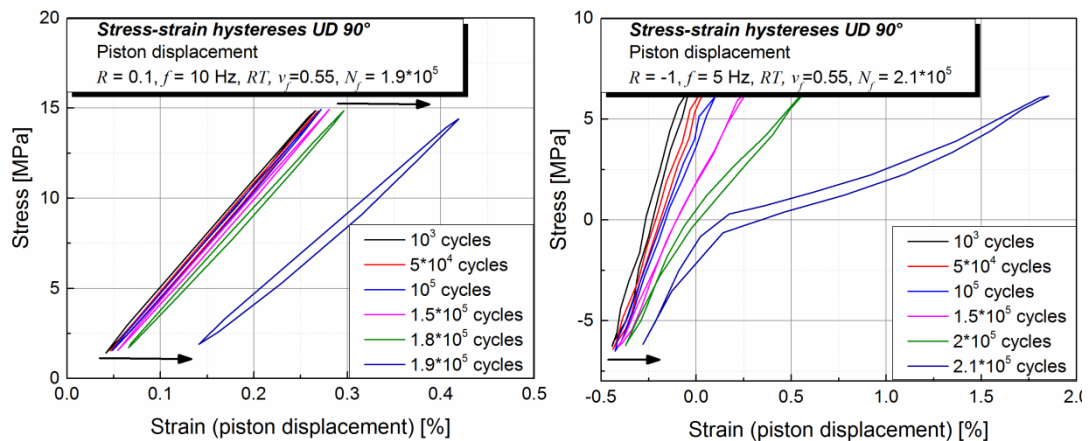


Figure 8.14: Representative stress-strain hystereses of UD 90° 55% tested with $R = 0.1$ (left) and $R = -1$ (right).

8.5.3.3. UD 45° with 30% and 55% fibre volume content

UD 45° specimens of both fibre volume contents reached considerably higher stress amplitudes in tension-compression tests and showed steeper S-N curves than in tension-tension fatigue tests (table 8.1). The comparison between damage mechanisms in UD 45° specimens with 30 % fibre content is presented in figure 8.15. At $R = 0.1$, mainly matrix cracking and fibre matrix debonding were observed at the fracture surfaces. At $R = -1$ on the contrary, broken fibre bundles and fibre fragments as already discussed for UD 90° specimens were observed. The described effects were even more dominant in UD 45° specimens with high fibre volume content (figure 8.16c and 8.16d).

Stress-strain hystereses presented in figure 8.17 showed basically a hysteretic behaviour similar to UD 90° specimens. However, the deformation of the last hysteresis slope in the tension area of the fatigue test was not as significant as in UD 90° specimens. Probably, the breakage of fibre bundles (figure 8.16d) was combined with the fibre pull-out (figure 8.16c) resulting from the inclination of 45° between the fracture plane and the applied load. A “mixed-mode” of these effects would consume more energy than only fibre pull-out as monitored in tension-tension fatigue test and result in higher nominal stress amplitudes in tension-compression tests.

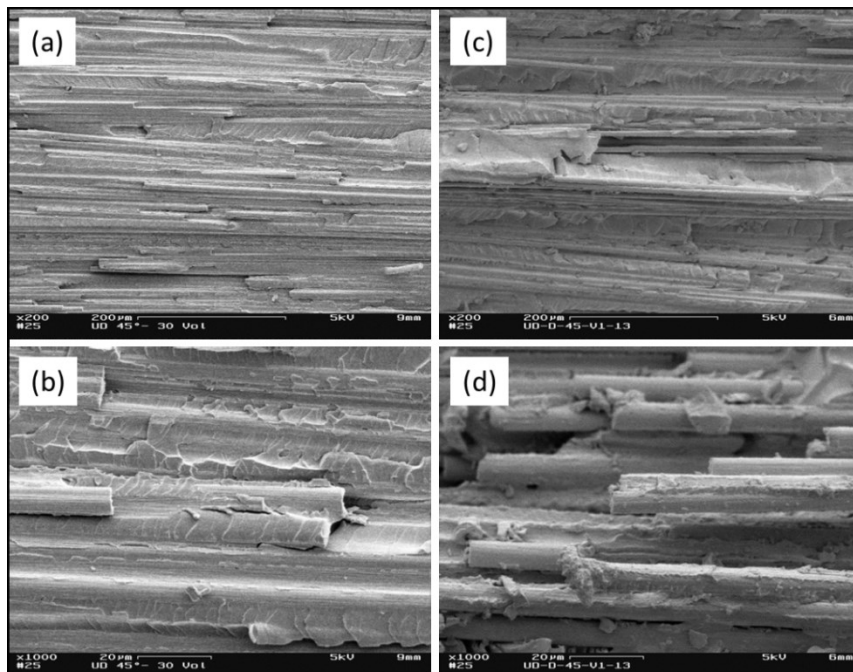


Figure 8.15: Fracture surfaces of UD 45° 30 % specimens tested at $R = 0.1$ ($\sigma_a = 13.5$ MPa, $N_f = 1.5 \cdot 10^4$) with a. 200x and b. 1000x magnification [19] and at $R = -1$ ($\sigma_a = 28$ MPa, $N_f = 1.7 \cdot 10^4$) with c. 200x and d. 1000x magnification.

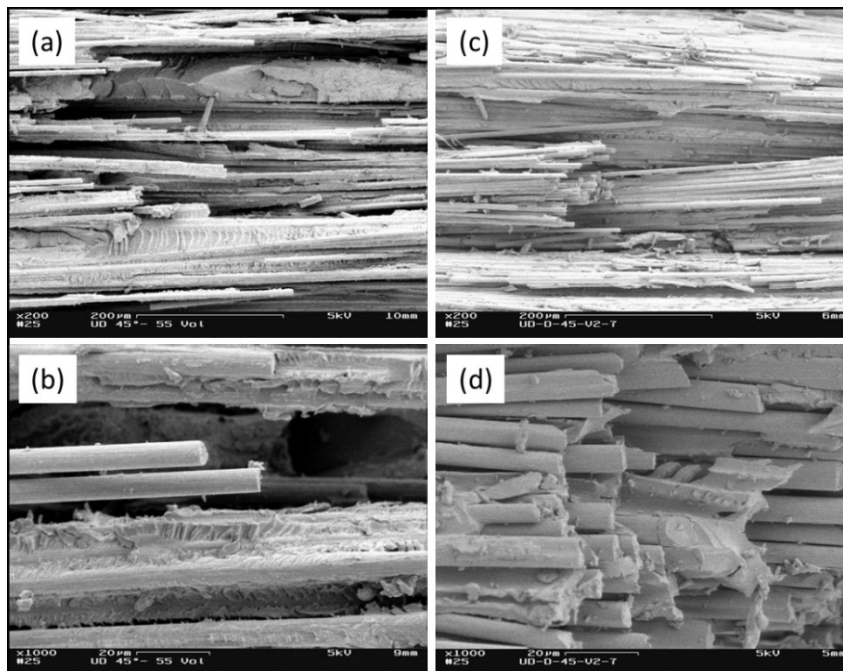


Figure 8.16: Fracture surfaces of UD 45° 55% specimens tested at $R = 0.1$ ($\sigma_a = 15.7$ MPa, $N_f = 1.2 \cdot 10^5$) with a. 200x and b. 1000x magnification [19] and at $R = -1$ ($\sigma_a = 20$ MPa, $N_f = 1.4 \cdot 10^5$) with c. 200x and d. 1000x magnification.

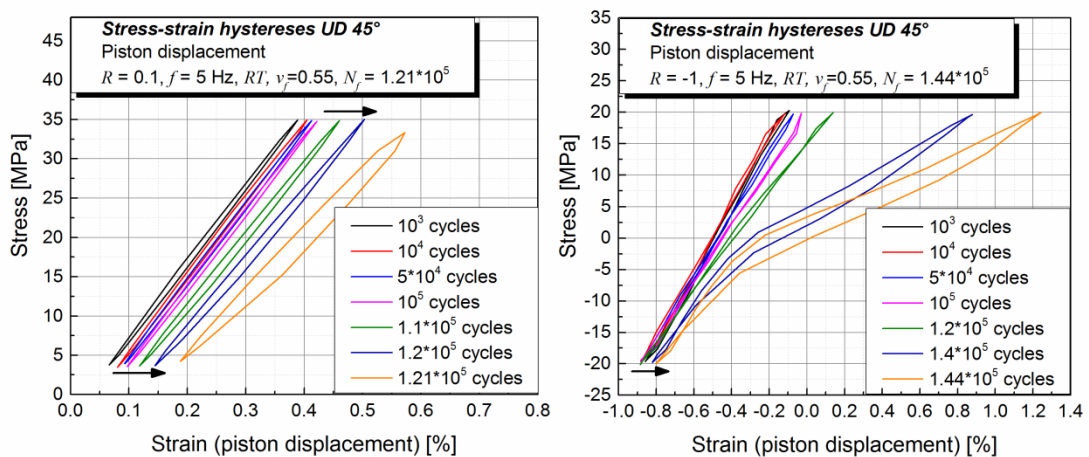


Figure 8.17: Representative stress-strain hystereses of UD 45° 55% tested with $R = 0.1$ (left) and $R = -1$ (right).

8.5.3.4. UD 0° with 30% and 55% fibre volume content

The fracture surfaces of UD 0° with both fibre volume contents were too uneven to be investigated by scanning electron microscopy. Therefore, representative photographs of UD 0° with high fibre volume content are illustrated in figure 8.18 which corresponded to [10,26]. Fracture surfaces of UD 0° with low fibre volume content showed comparable features. After tension-tension fatigue tests pulled out fibres and broken single fibres or fibres bundles were usually observed (figure 8.18a). In UD 0° specimens tested in tension-compression fatigue tests, fibre breakage either in a few fracture planes as shown in figure 8.18b or fibre breakage along only one fracture plane were dominant damage mechanisms. The corresponding stress-strain hystereses are presented in figure 8.19. In tension-tension fatigue tests, the stress-strain hystereses were shifted to higher strains during the first $2.5 \cdot 10^5$ cycles of the fatigue test. Only for the last hysteresis measured after $2.92 \cdot 10^5$ cycles immediately before failure the slope changed as well. In tension-compression fatigue tests on the contrary, the stress-strain hysteresis overturned during the tests. That would indicate that the tensile and compression stiffnesses of the specimen decreased. This observation might be argued by continuously developing fibre breakage in the specimens due to compressive loads weakening the tensile and compressive behaviour of UD 0° specimens finally resulting fracture surfaces as illustrated in figure 8.18b.

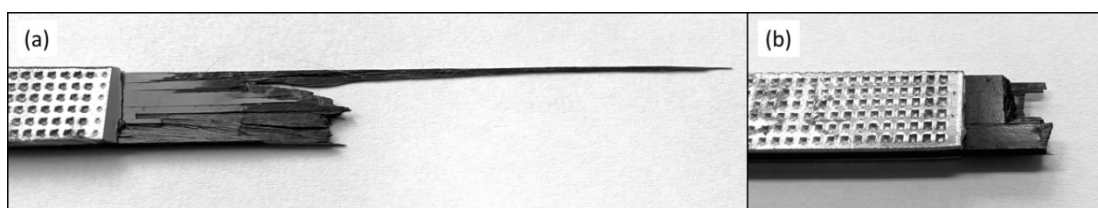


Figure 8.18: UD 0° specimens with 55% fibre volume content tested with stress ratios a. $R = 0.1$ and b. $R = -1$.

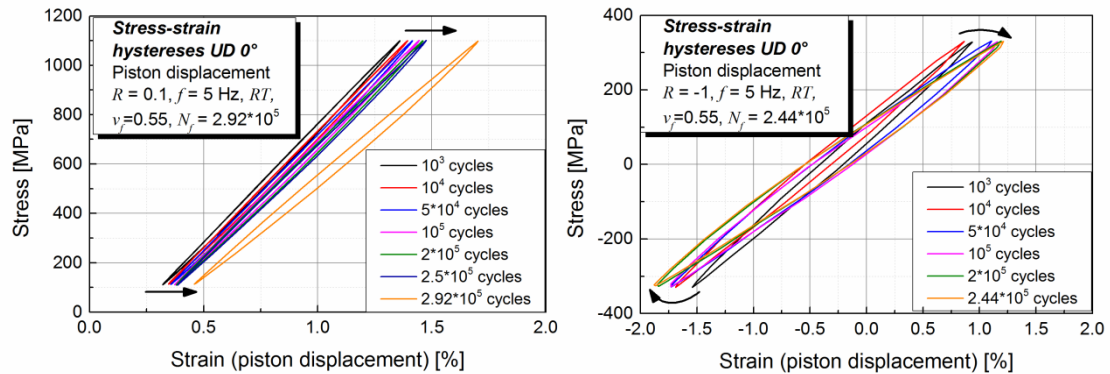


Figure 8.19: Representative stress-strain hystereses of UD 0° 55% tested with $R = 0.1$ (left) and $R = -1$ (right).

8.6. Conclusions

The mechanical behaviour and damage mechanisms in UD 0°, 45° and 90° specimens with two different fibre volume fractions and the pure epoxy resin were investigated in quasi-static and fatigue tests. The effect of load type (tension and compression) in quasi-static and of the mean stress in fatigue tests was studied in addition to the influence of the fibre volume content. In epoxy resin specimens, the load type did not influence the quasi-static mechanical behaviour significantly. In fatigue tests, the slope k of S-N curves was steeper in tension-compression fatigue tests. Very smooth fracture surfaces were observed after tension-compression fatigue tests probably due to flattening effects of the compression loads on the fracture structures. The found results and damage mechanisms of carbon/epoxy laminates are schematically summarised in figure 8.20. In quasi-static tension and compression tests, a higher amount of fibres resulted always in higher tensile and compressive strengths, respectively. For UD 0° specimens, quasi-static compressive strength was about 30 % of the tensile strength. On the contrary, UD 45° and UD 90° possessed twice or three times higher compressive than tensile strengths.

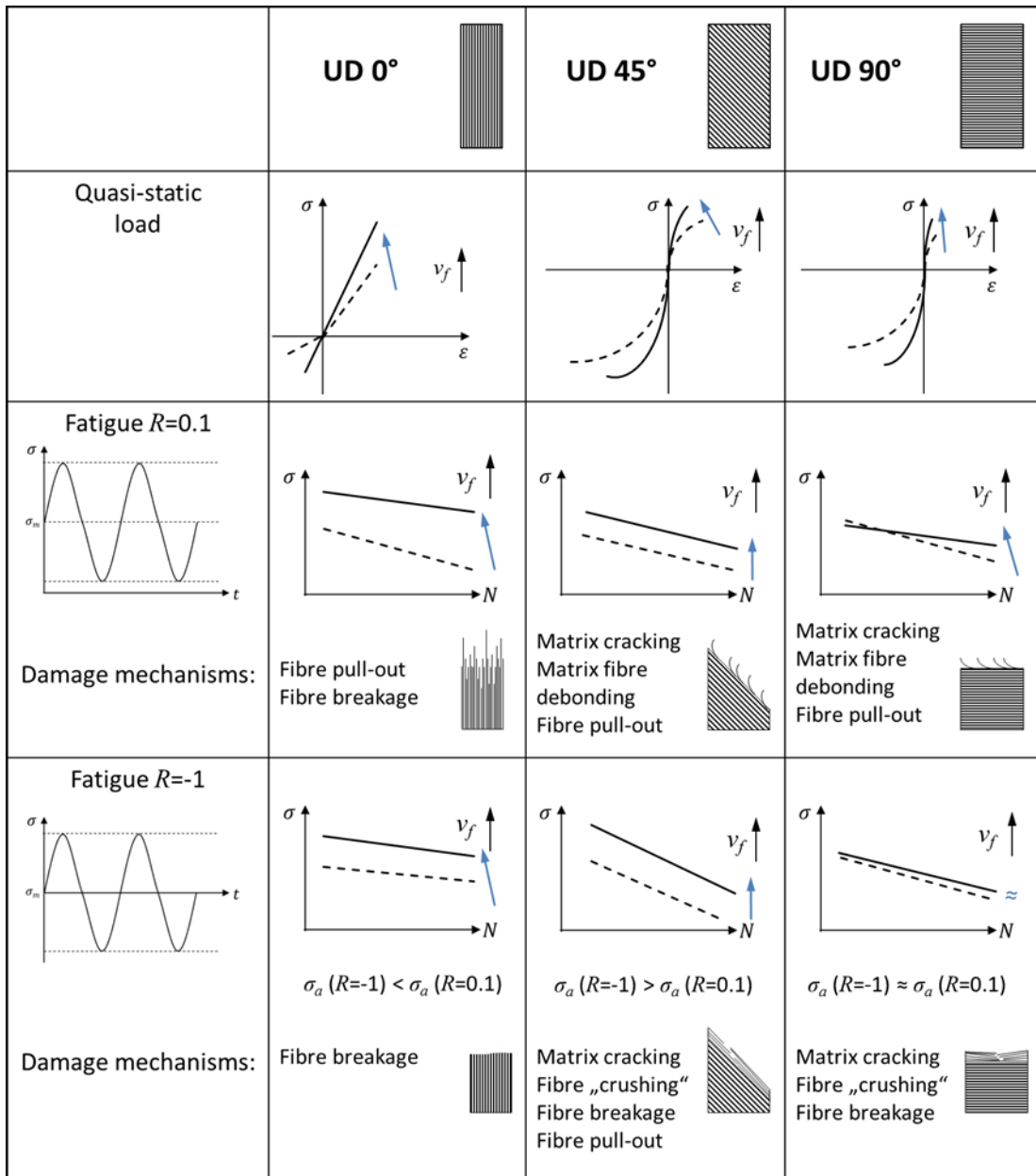


Figure 8.20: Schematic summary of investigated mechanical behaviour and damage mechanisms in unidirectional carbon/epoxy laminates depending on the fibre volume content, the test angle and the applied load type and fatigue mean stress, respectively.

As a consequence of the quasi-static behaviour, nominal stress amplitude σ_a in tension-tension fatigue tests was always higher for specimens with high fibre volume content. In fatigue tests at $R = 0.1$, UD 0° and UD 45° specimens with high fibre volume content were tested at higher nominal stress amplitudes than their counterparts with low fibre content. In UD 90° specimens, the fibre volume content mainly influenced fatigue tests in the high cycle fatigue regime due to damage mechanisms changing from fibre pull-out at high stress levels to matrix cracking at lower levels in specimens with 30 % fibre volume content [19]. In tension-compression fatigue tests, nominal stress amplitudes σ_a for UD 0° were lower and amplitudes for off-axis specimens were higher or similar compared to tension-tension fatigue tests. For UD 90° specimens, the fibre volume content did not influence the fatigue strength in tension-compression fatigue tests significantly. Damage mechanisms in UD 0° changed from pull out and fracture of single fibres at $R = 0.1$ to breakage of fibre bundles at $R = -1$. In off-axis specimens, matrix cracking and fibre pull-out were dominant damage mechanisms in tests with $R = 0.1$. In contrast to that breakage of fibre bundles and fragments of crushed fibres were observed on the fracture surfaces after tension-compression fatigue tests.

8.7. References

- [1] Gamstedt EK, Talreja R. Fatigue damage mechanisms in unidirectional carbon-fibre-reinforced plastics. *Journal of Materials Science* 1999;34):2535–46.
- [2] Gamstedt E, Berglund LA, Peijs T. Fatigue mechanisms in unidirectional glass-fibre-reinforced polypropylene. *Composites Science and Technology* 1999;59(5):759–68.
- [3] Talreja R. Damage development in composites: Mechanisms and modelling. *The Journal of Strain Analysis for Engineering Design* 1989;24(4):215–22.

- [4] Hessabi ZR, Majidi B, Aghazadeh J. Effects of Stacking Sequence on Fracture Mechanisms in Quasi-isotropic Carbon/Epoxy Laminates under Tensile Loading. *Iranian Polymer Journal* 2005(14 (6)):531–8.
- [5] Kawai M, Saito S. Off-axis strength differential effects in unidirectional carbon/epoxy laminates at different strain rates and predictions of associated failure envelopes. *Composites Part A: Applied Science and Manufacturing* 2009;40(10):1632–49.
- [6] Curtis PT. The fatigue behaviour of fibrous composite materials. *The Journal of Strain Analysis for Engineering Design* 1989;24(4):235–44.
- [7] Talreja R. *Fatigue of Composite Materials*. Pennsylvania, U.S.A: Technomic Publishing Inc; 1987.
- [8] Talreja R, Singh CV. *Damage and failure of composite materials*. Cambridge, New York: Cambridge University Press; 2012.
- [9] Reifsnider KL. *Fatigue of composite materials*. Amsterdam, New York: Elsevier; 1991.
- [10] Curtis PT. Tensile fatigue mechanisms in unidirectional polymer matrix composite materials. *International Journal of Fatigue* 1991;13(5):377–82.
- [11] Kawai M. A phenomenological model for off-axis fatigue behavior of unidirectional polymer matrix composites under different stress ratios. *Composites Part A: Applied Science and Manufacturing* 2004;35(7-8):955–63.
- [12] Kawai M, Koizumi M. Nonlinear constant fatigue life diagrams for carbon/epoxy laminates at room temperature. *Composites Part A: Applied Science and Manufacturing* 2007;38(11):2342–53.
- [13] El Khadi H, Ellyin F. Effect of stress ratio on the fatigue of unidirectional glass fibre/epoxy composite laminae. *Composites Part A: Applied Science and Manufacturing* 1994;25(10):917–24.
- [14] Rotem A. Tensile and compressive failure modes of laminated composites loaded by fatigue with different mean stress. *Journal of composites, technology and research* 1990;12(4):201–8.

-
- [15] Gamstedt E, Sjögren B. Micromechanisms in tension-compression fatigue of composite laminates containing transverse plies. *Composites Science and Technology* 1999;59(2):167–78.
- [16] Philippidis T. Fatigue of composite laminates under off-axis loading. *International Journal of Fatigue* 1999;21(3):253–62.
- [17] Plumtree A. Fatigue damage evolution in off-axis unidirectional CFRP. *International Journal of Fatigue* 2002;24(2-4):155–9.
- [18] Correa E, Gamstedt EK, París F, Mantič V. Effects of the presence of compression in transverse cyclic loading on fibre–matrix debonding in unidirectional composite plies. *Composites Part A: Applied Science and Manufacturing* 2007;38(11):2260–9.
- [19] Brunbauer J, Stadler H, Pinter G. Mechanical properties, fatigue damage and microstructure of carbon/epoxy laminates depending on fibre volume content. *International Journal of Fatigue* 2014 // 2015;70:85–92.
- [20] DIN EN ISO 527-2. Bestimmung der Zugeigenschaften(DIN EN ISO 527-2:1996). Brüssel, Belgium: CEN (European Committee for Standardization); 1996.
- [21] ASTM International. Standard Test Method for Tensile Properties of Polymer Matrix Composite Materials(ASTM D3039/D3039M-00). West Conshohocken, PA, United States: ASTM International; 2000.
- [22] ASTM International. Standard Test Method for Compressive Properties of Polymer Matrix Composite Materials with Unsupported Gage Section by Shear Loading(ASTM D3410/D3410M-03). West Conshohocken, PA, United States: ASTM International; 2008.
- [23] Schürmann H. Konstruieren mit Faser-Kunststoff-Verbunden: Mit 39 Tabellen. 2nd ed. Berlin, Heidelberg, New York, NY: Springer; 2007.
- [24] Brunbauer J, Pinter G. On the strain measurement and stiffness calculation of carbon fibre reinforced composites under quasi-static tensile and tension-tension fatigue loads. *Polymer Testing* 2014;40:256–64.

- [25] ASTM International. Standard Practice for Statistical Analysis of Linear or Linearized Stress -Life (S-N) and Strain-Life (e-N) Fatigue Data(ASTM E739-91). West Conshohocken, PA, United States: ASTM International; 1991.
- [26] Gamstedt EK, Berglund LA. Fatigue of thermoplastic composites. In: Harris B, editor. Fatigue in composites: Science and technology of the fatigue response of fibre-reinforced plastics. Cambridge: Woodhead; CRC Press; 2003, p. 315–38.

Part V.

Fatigue-life prediction of carbon/epoxy composites with two different approaches

9. Introduction to Publications 4, 5, 6 and 7

9.1. Novel stiffness based fatigue-life prediction of composite materials

A method was developed to use the decreases of mechanical stiffness resulting from progressing damage within the material [1–3] as introduced in chapter 1 for fatigue-life prediction. It was intended to adapt the well-known stiffness-based classical laminate theory (CLT) [4] for the fatigue loads. The CLT was initially designed to predict stiffness properties of laminates based on the mechanical properties of the single layer and conduct ply-by-ply stress analysis for quasi-static load cases.

In order to describe the necessary linear-elastic stress-strain material behaviour resulting from Hooke's law for quasi-static load cases, 81 material constants would be necessary in the most general form of the material law [4]. Due to simplifications and symmetry relationships of the stress-strain matrices, 13 material constants are necessary for the description of a triaxial anisotropy, 9 constants for an orthotropic material and 5 to describe transversal isotropy [4]. For all following considerations, transversal isotropic material behaviour as schematically illustrated in figure 1 describing the material behaviour of the unidirectional laminate is assumed. Transversal isotropy does not take material behaviour in the third direction into account [4]. Consequently, for performing calculations with the CLT a minimum of five material parameters, the so-called "engineering constants" have to be known: Young's modulus in fibre direction (E_{11}), Young's modulus transverse to fibre direction (E_{22}), the shear modulus (G_{12}) and at least one Poisson's ratio ν_{12} or ν_{21} .

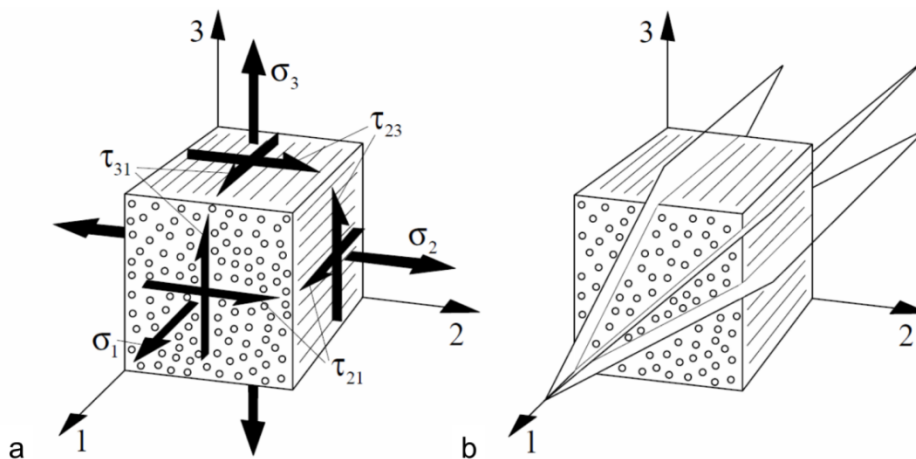


Figure 9.1: a. Volume element of the UD layer, b. Demonstration of the transversal isotropy. Isotropic plane is the 1-plane. All other planes perpendicular to the isotropic plane possess – independent of the rotation of the coordinate system – the same properties from [4].

Basically, the classical laminate theory uses the mechanical material properties to create the stiffness or compliance matrix of the ply in order to describe the relations of the stress-strain behaviour, which is assumed to be linear elastic, as a first step. Subsequently, the created matrix is transformed from the local ply's coordinate system into the global coordinate system of the composite which is to be calculated. By rotating the single plies in the global coordinate system and superimposing the single, rotated plies by considering the single thicknesses into one laminate, the stiffness or compliance matrix of the multidirectional composite can be created. Finally, the matrix is converted and used to calculate the stresses in each single ply of the multidirectional lay-up. By comparing the calculated ply stresses with stress allowables, statements about the behaviour of the composite under applied quasi-static loads can be made [4].

In figure 9.2, the stiffnesses and stresses calculable by the classical laminate theory within the different plies of a multidirectional composite loaded with a quasi-static strain are schematically illustrated. The layered structure of the laminate results in inhomogeneous stiffness and stress distributions across

the ply's thickness. This characteristic has to be taken into account for the design of any composite structure.

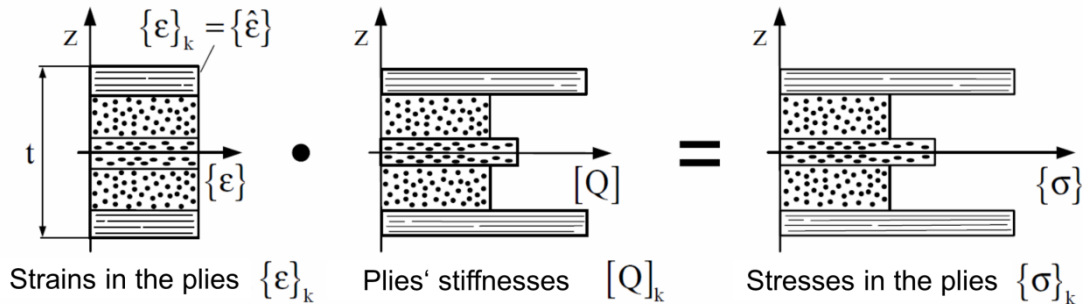


Figure 9.2: Schematic illustration of strains, stiffnesses and stresses across the laminate thickness from [4].

Publications 4, 5 and 6 deal with the adaption of the CLT for fatigue loads. In publication 4, the basic consideration was made that, in order to adapt this theory, the fatigue stiffnesses have to be measured under similar load conditions as the quasi-static Young's moduli. Therefore, a new experimental test procedure called "cyclic tensile tests" was developed. In this test procedure, the servo-hydraulic test machine performed displacement controlled quasi-static tensile tests after certain numbers of load-controlled cycles with constant load amplitude. The repeated included tensile tests were used to evaluate stiffnesses after defined number of cycles. A multiaxial lay-up was investigated in cyclic tests and moduli were evaluated from the new test procedure and from stress-strain hysteresis loops. Because of the high material stiffness, the difference between those two ways of cyclic stiffness calculation was not significant. Furthermore it was shown that in strain measurements with optical systems, occurring artefacts can be correlated with damage mechanisms on the surface.

However, in publication 5 the cyclic moduli of unidirectional laminates tested at different angles were evaluated from cyclic tensile tests and also stress-strain hysteresis loops. Due to the highly anisotropic material behaviour the significant influence of modulus evaluation became apparent. Especially matrix-dominated specimens tested transverse to fibre direction showed strain-rate dependent behaviour influencing the evaluated moduli. The higher the stiffness of the specimens, the lower was the influence of strain-rate and

consequently of cyclic modulus evaluation. Consequently, it could be shown that for reasonable modulus evaluation of laminates with arbitrary angles or stacking sequences, the cyclic tensile test procedure could be used. Furthermore, the number of cycles to failure could be also used for the evaluation of S-N curves since the included tensile tests did not influence the cyclic material behaviour.

Based on the developed experimental procedure, the CLT was adapted for cyclic loads and programmed as software routine in publication 6. The cyclic tensile test procedure was used to generate the cycle-dependent input parameters $E_{11}(N)$, $E_{22}(N)$, $G_{12}(N)$, $\nu_{12}(N)$ and $\nu_{21}(N)$. Based on these input parameters, the cycle-dependent stiffness decreases $E_x(N)$, $E_y(N)$, $G_{xy}(N)$ and Poisson's ratios $\nu_{xy}(N)$ and $\nu_{yx}(N)$ of a multidirectional composite were calculated on different load levels. Experimental validation of the calculations with the investigated multi-axial lay-up proofed the possibility for adapting the CLT for cyclic loads. Fatigue-induced stiffness decreases could be predicted accurately on the different load levels.

Comment to publications 5 and 6: The visibility of the three stages of stiffness degradation caused by progressing damage mechanisms as described in [5] and discussed in chapter 1 which were measured in the experimental parts of this thesis depended on the scale chosen for data illustration. In linear scales, the three stages were clearly visible. However, in the papers 5 and 6 it was chosen to use double logarithmic diagrams in order to be able to show the very different scales of transversal and longitudinal material behaviour in the same graphs. As a result of the logarithmic scale, the first state of stiffness degradation is not clearly visible in these two publications.

9.2. Strength based engineering concept for the fatigue-life prediction of composite materials

Engineering concepts for the life-time prediction of metallic materials are well-known. Some of these technological concepts are the nominal stress concept, the local stress and strain concepts, the structural stress concept and fracture mechanical concepts [6]. All of these approaches – except for

fracture mechanical concepts, which pursue crack propagation in the material – are designed to determine the stresses acting within components, to define critical stresses and strains and to make assumptions about the life-time that can be expected. Usually, the cyclic material behaviour within these concepts is described by fatigue strengths reflected in S-N curves and subsequently by Haigh diagrams as introduced in chapter 1. Damage accumulation theories such as the Miner rule are applied to assess the damage accumulated during the cyclic load (chapter 1). While the nominal stress concept was designed for parts with simple geometries such as pipes or tubes, in more complex geometries the nominal cross-sections are difficult to define. Consequently, the local concepts were developed which allow the calculation of local strains and stresses by finite element analysis [6–8]. While the local strain concept is used for higher deformations in the low cycle fatigue regime, local stress concepts describe the material behaviour in the high cycle fatigue area.

Due to the fact that the mentioned life-time concepts were developed for metallic materials, usually isotropic, linear-elastic material behaviour is assumed. To take the characteristic of anisotropic materials into account, the local stress concept has been successfully adapted for short fibre reinforced plastics during the last years [8–11]. Real part geometries are used to calculate the local stresses acting in a component by finite element analysis. S-N curves are used to describe the cyclic material behaviour and to reflect effects such as stress concentrations, mean stress or temperature [8]. By taking the load time history into account, damage accumulation can be conducted as introduced in chapter 1. This concept has been realised in the commercially available software tool Finite Element Fatigue (FEMFAT) by Magna Powertrain, Engineering Centre Steyr (St. Valentin, Austria).

In order to meet the specific characteristics of orthotropic materials such as short fibre reinforced composites, the anisotropic material behaviour and the fibre orientation caused by the injection moulded process have to be included [8–11]. For short fibre reinforced materials, the simulation of the injection moulded process is used to calculate the orientation tensor of each finite element, which is subsequently implemented to an anisotropic finite element analysis. Based on these specific properties of each element, local S-N curves are created by modifying the material's S-N curve [8]. Damage

accumulation based on the critical plane concept is finally performed with the adapted, local S-N curves [12–14]. The application of the concept is necessary in order to be able to predict the fatigue behaviour for directions within the anisotropic material which have not been determined previously by experimental tests. In order to describe the fatigue strengths as a function of the critical plane angle α , a cosinusoidal relation between the orthogonal fatigue strengths is assumed [8]. Subsequently, the calculated anisotropic S-N curves are compared to the acting forces and the angles of the planes, which may become critical for failure, are identified [7,8] (figure 9.3). This concept is also implemented in the fatigue software tool FEMFAT.

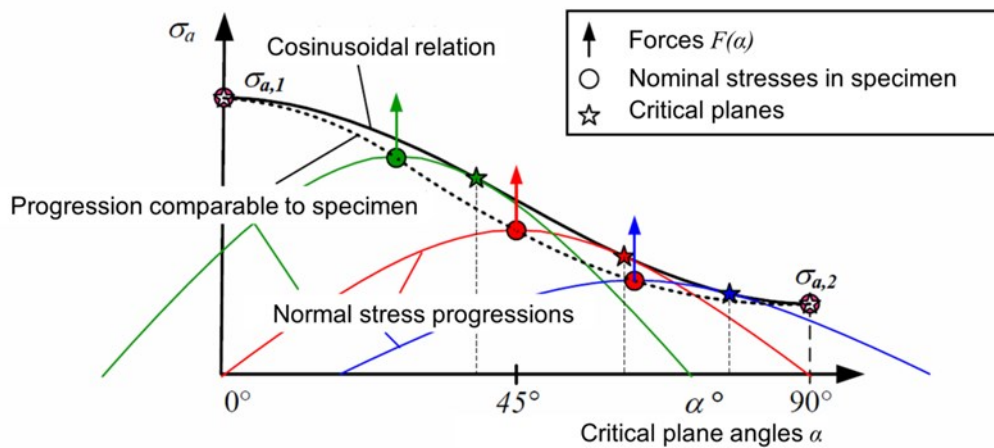


Figure 9.3: Critical plane concept according to [8].

Furthermore, for accurate life-time prediction influences on the local S-N curves such as the mean stress (Haigh diagram), multiaxial load conditions, stress gradients, supporting effects and statistical deviation of experimental results known from metallic fatigue have to be considered [8]. In any case, the relevance of these influencing factors for polymers has to be investigated and assessed. Probably, some of the listed influences will not be useful to describe the fatigue behaviour of polymers.

To address the specific behaviour of composite materials, the fatigue-software FEMFAT has been extended with the tool Laminat. In publication 7, the functional principle of this composite tailored extension is presented. In contrast to the life-time prediction of short fibre reinforced plastics, the orientation of the continuous fibres within the material was clear and given by

the layers of the unidirectional or multidirectional lay-ups. Furthermore, not only the quasi-static and fatigue data longitudinal and transversal to fibre direction were used as input parameters, but also the shear behaviour of the material evaluated with $\pm 45^\circ$ specimens. Because only uniaxial loads were applied on rectangular specimens, stress gradients or supporting effects were not taken into account for the performed estimations. In order to address the different failure modes in continuously fibre reinforced composites introduced in chapter 1, Puck's criterion is included in the extended software version. Experimental quasi-static data and S-N curves measured were implemented in the software tool and Haigh diagrams of the material were created. Damage accumulation according to Miner was performed by using the critical plane concept.

The implemented material data set for carbon/epoxy laminates was used to predict the fatigue-life of a unidirectional 45° laminate and a multiaxial carbon/epoxy lay-up. Results for the predicted UD laminate were very accurate. However, to be able to predict the total failure of a multiaxial lay-up influenced by the different stresses in the respective plies within the composite accurately, modifications of the software tool will be necessary. The conducted calculations, obtained results and potential for future development are discussed in detail.

9.3. References

- [1] Reifsnider KL, Henneke EG, Stinchcomb W, Duke JC. Damage Mechanics and NDE of Composite Laminates. In: Hashin Z, Herakovich CT, editors. Composite Materials: Recent Advances: Pergamon Press Inc; 1983, p. 399–420.
- [2] Talreja R. Damage development in composites: Mechanisms and modelling. *The Journal of Strain Analysis for Engineering Design* 1989;24(4):215–22.
- [3] Talreja R. Damage Characterization. In: Reifsnider KL, editor. *Fatigue of composite materials*. Amsterdam, New York: Elsevier; 1991, p. 79–103.

- [4] Schürmann H. Konstruieren mit Faser-Kunststoff-Verbunden: Mit 39 Tabellen. 2nd ed. Berlin, Heidelberg, New York, NY: Springer; 2007.
- [5] Stinchcomb W, Bakis CE. Fatigue behaviour of composite materials. In: Reifsnider KL, editor. Fatigue of composite materials. Amsterdam, New York: Elsevier; 1991, p. 105–80.
- [6] Radaj D. Ermüdungsfestigkeit: Grundlagen für Leichtbau, Maschinen- und Stahlbau. 3rd ed. Berlin [u.a.]: Springer; 2007.
- [7] Haibach E. Betriebsfestigkeit: Verfahren und Daten zur bauteilberechnung. Berlin: Springer; 2006.
- [8] Mösenbacher A. Modellentwicklungen zur betriebsfesten Auslegung von Strukturbauteilen aus glasfaserverstärkten Thermoplasten im Motorraum. Dissertation. Leoben; 2014.
- [9] Guster C, Pinter G, Mösenbacher A, Eichlseder W. Evaluation of a Simulation Process for Fatigue Life Calculation of Short Fibre Reinforced Plastic Components. *Procedia Engineering* 2011;10:2104–9.
- [10] Mösenbacher A, Brunbauer J, Pichler PF, Guster C, PINTER G. Modelling and validation of fatigue life calculation for short fibre reinforced injection moulded parts. In: ECCM16, editor. 16th European Conference on Composite Materials; 2014.
- [11] Gaier C, Fleischer H, Guster C, Pinter G. Influence of Fiber Orientation, Temperature and Moisture on the Fatigue Behavior of Injection Molded Fiber Reinforced Thermoplastics // Einfluss von Faserorientierung, Temperatur und Feuchtigkeit auf das Ermüdungsverhalten von kurzfaserverstärkten Thermoplasten*. *MP* 2010;52(7-8):534–42.
- [12] Gaier C, Dannbauer H. Ein effizientes kritisches Schmittebenenverfahren für duktile, semi-duktilen und spröden Werkstoffe: 1. Leobener Betriebsfestigkeitstage Planneralm, 8.-10. März 2006:145–57.
- [13] Gaier C, Pramhas G, Steiner W. An Extended Critical Plane Criterion for General Load Situations. In: Blom AF, editor. Proceedings of the 8th International Fatigue Conference June 2-7 2002 Stockholm Sweden // Fatigue 2002: Proceedings of the Eighth International Fatigue Congress

held 3-7 June, 2002, Stockholm, Sweden. Heath, West Midlands, UK: Engineering Materials Advisory Services; 2002, p. 259–66.

- [14] Gaier C, Unger B, Dannbauer H. Multiaxial fatigue analysis of orthotropic materials. *Rev. Metall.* 2010;107(9):369–75.

10. Publication 4

10.1. Bibliographic information

- Title: Stiffness based fatigue characterisation of CFRP
- Authors and relevant contributions to this publication:
 - Julia BRUNBAUER¹
Experimental testing, data evaluation, preparation of the publication
 - Florian ARBEITER¹
Discussion of experimental results
 - Steffen STELZER¹
Discussion of experimental results
 - Gerald PINTER¹
Discussion of experimental results
- Affiliation:
 1. Institute of Materials Science and Testing of Polymers, Montanuniversitaet Leoben, Otto Glöckel-Strasse 2, 8700 Leoben, Austria
- Periodical: Advanced Materials Research
- DOI: [10.4028/www.scientific.net/AMR.891-892.166](https://doi.org/10.4028/www.scientific.net/AMR.891-892.166)

Statement with regard to this publication: The manuscript presented here is an adapted accepted manuscript in order to fit the formatting of the thesis and does not necessarily reflect exactly the actually published version.

10.2. Abstract

This paper investigates the possibility of determining damage under fatigue loading in carbon fibre reinforced plastics (CFRP) by using mechanical stiffness. Therefore, stress-strain-hystereses recorded in fatigue tests under sinusoidal loads are used for moduli calculation. Additionally, a new method for stiffness evaluation called “cyclic tensile tests” is presented. Its results are compared to results from hysteresis analysis and to actual damage mechanisms monitored non-destructively with thermography analysis.

10.3. Introduction

Laminated composites are increasingly used in a wide range of applications due to their outstanding mechanical properties and light weight potential. In many cases machine parts and components made of composites are exposed to cyclic service loads and experience fatigue during their service life. It is known in literature that different damage modes occur during fatigue life of composite materials. According to Reifsnider [1] these damage modes can be classified as follows: the first failure mode under fatigue loading which causes a first, rapid increase of damage in the material is matrix cracking followed by crack coupling and interfacial debonding. When fatigue loading continues, delamination, delamination growth and local fibre breakage occur. In this stage of fatigue life, damage increases slower than at the very beginning. Finally, fibre breakage leads to fracture and a second significant increase of damage. As a consequence of the described damage modes, elastic properties change during fatigue life. This degradation has to be considered as well.

In literature, many models and approaches to fatigue life of composites and description of failure modes exist. One approach based on mechanical testing shows a possible relation between the increase of damage during fatigue life and degradation of stiffness. This would suggest that damage could be monitored in fatigue tests by recording mechanical stiffnesses [2]. However, stiffnesses and moduli are somehow a matter of definition. Quasi-static moduli are calculated as secant moduli based on the recorded stress-

strain curves and measured with a constant test speed. The strain range, which is used for modulus calculation, depends on the used standard e.g. [3,4]. For non-isotropic materials moduli need to be measured in different loading directions. Stiffnesses are then the constants in the stiffness matrix of a non-isotropic but linear-elastic material, which connect the material's stress-strain behaviour under quasistatic conditions [5]. Under fatigue loading by contrast, moduli are often determined by analysing the stress-strain-hysteresis detected under sinusoidal cyclic loads. When evaluating moduli based on stress-strain-hystereses there are mainly two options which are illustrated in figure 10.1: first, to divide maximum of stress by maximum of strain which is defined as secant modulus E_s (10.1). The secant modulus depicts cyclic creep as well as damage during fatigue life. The second option is to analyse only the delta values of the hysteresis, which is defined as dynamic modulus $|E^*|$ [6] or E_{dyn} (10.2). The dynamic modulus can therefore exclude the influence of cyclic creep [7].

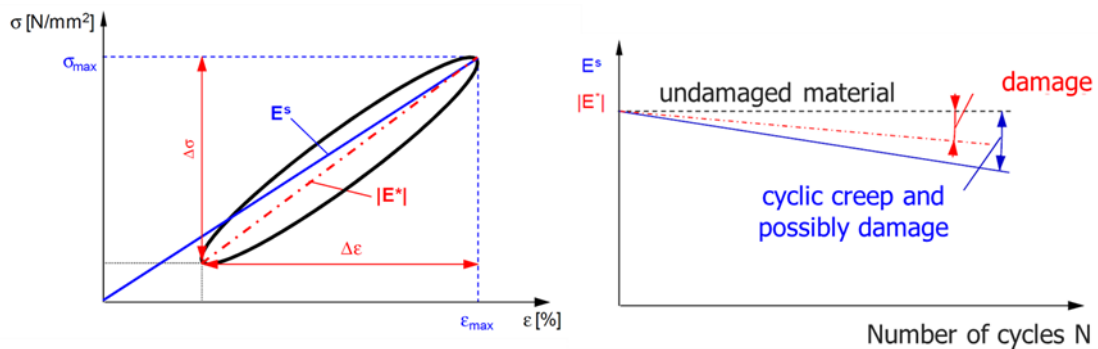


Figure 10.1: Definition of secant and dynamic modulus and their schematic behaviour related to damage progress [6,8].

$$E_s = \frac{\sigma_{max}}{\varepsilon_{max}} \quad (10.1)$$

$$|E^*| = \frac{\Delta\sigma}{\Delta\varepsilon} \quad (10.2)$$

The intention of this work is to evaluate the possibility of detecting damage progress under fatigue loads by the change of fatigue stiffnesses during cyclic tests. Therefore, uniaxial tension-tension fatigue loads were applied to a multiaxial lay-up made of carbon fibres and epoxy resin. On one hand, stiffnesses were evaluated by analysing stress–strain-hystereses. On the

other hand, a new experimental method to measure stiffnesses under fatigue loads was implemented. In these so called “cyclic tensile tests” the servo-hydraulic test machine performed displacement controlled tensile tests after a certain number of load controlled sinusoidal cycles. Additionally, thermography analysis was used to monitor fatigue damage non-destructively.

10.4. Experimental work

In this work a multiaxial lay-up made of carbon fibres and epoxy resin and the stacking sequence $[0/+45/-45/90]_2$ was investigated. The fibre content was 60 % (measured by thermo gravimetric analysis). The specimens' geometry was 200x20x2 mm and Aluminium tabs with 1 mm thickness were glued on both sides of the specimens. Gauge length for all specimens was 100 mm. Quasistatic and cyclic tests were performed on a servo-hydraulic testing machine equipped with a 250 kN load cell by MTS Systems Corporations. All tests were monitored with an optical measurement system and a thermographic analysis system. The test procedure of cyclic tensile tests is illustrated in figure 10.2. All fatigue tests were performed with the R -value (= minimum force / maximum force) of 0.1. The servo-hydraulic test machine started the testing procedure with a defined number of sinusoidal cycles under load control. After that, the servo-hydraulic test machine unloaded the specimen to 0 N, switched to displacement control and performed a tensile test with a speed of 0.5 mm / min. The tensile tests were performed up to the mean displacement of the respective fatigue tests to avoid additional damaging.

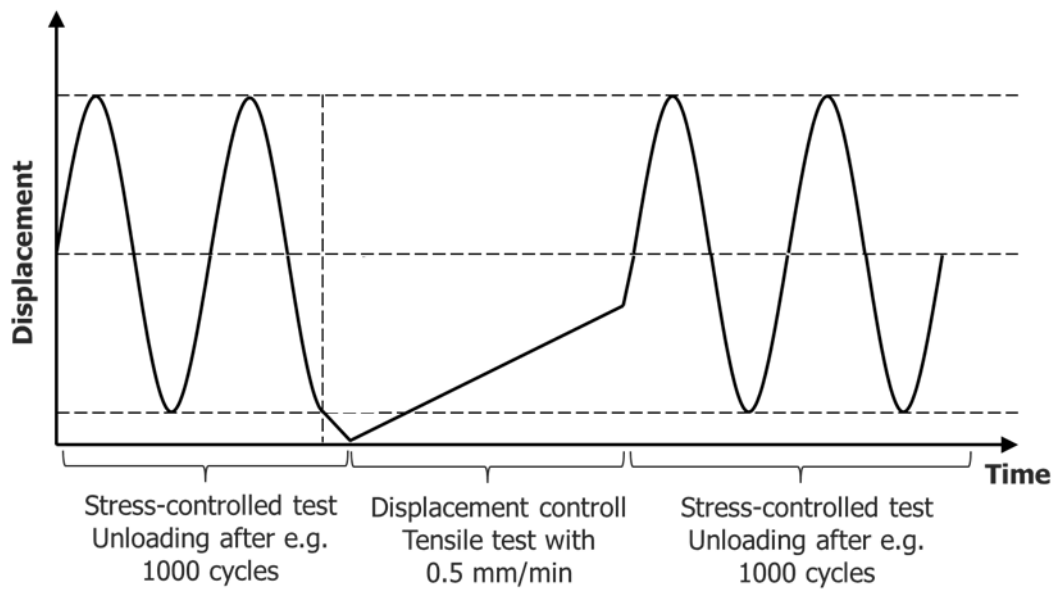


Figure 10.2: Test procedure for cyclic tensile tests.

During these tensile tests, strains in and transverse to fibre direction were recorded by an optical measurement system. Information about force and displacement during the entire test was recorded by the testing machine. Hysteresis data was recorded by the test machine every 1000 cycles with 100 data points each.

10.5. Results and Discussion

The two different methods for measuring stiffnesses in fatigue tests under tension loading are discussed using three representative specimens. Stress-strain hystereses as well as cyclic tensile tests were recorded with the same specimens respectively. The specimens were tested at three different stress levels. Test frequencies were adapted to the stress levels. Stress amplitude, frequency and number of cycles to failure of these three specimens are summarised in table 10.1.

Table 10.1: Nominal stress amplitude, test frequency and number of cycles to failure of the three representative specimens.

Specimen	Stress amplitude [MPa]	Frequency [Hz]	Number of cycles [-]
Specimen 8	180	5	8,569
Specimen 13	157.5	10	59,297
Specimen 14	135	10	1,233,644

Figure 10.3 shows the results of analysing the stress-strain-hystereses recorded by the testing machine. The full symbols represent the secant moduli calculated from maxima of stress and strain. The empty symbols are the dynamic moduli calculated from the delta of stress and strain. The constant line at 35,000 MPa represents the tensile modulus according to [4] from quasi-static tests. All three specimens showed a slow decrease of secant as well as dynamic moduli. The level of dynamic moduli was a bit higher compared to the secant moduli, which was constant with literature. Moduli progressions did not indicate creep tendency of this material. Absolute levels might be shifted if stress-strain-hystereses were measured with optical strain measurement methods. Because of the high material stiffness the stress-strain-hystereses recorded by the test machine show reasonable results nevertheless.

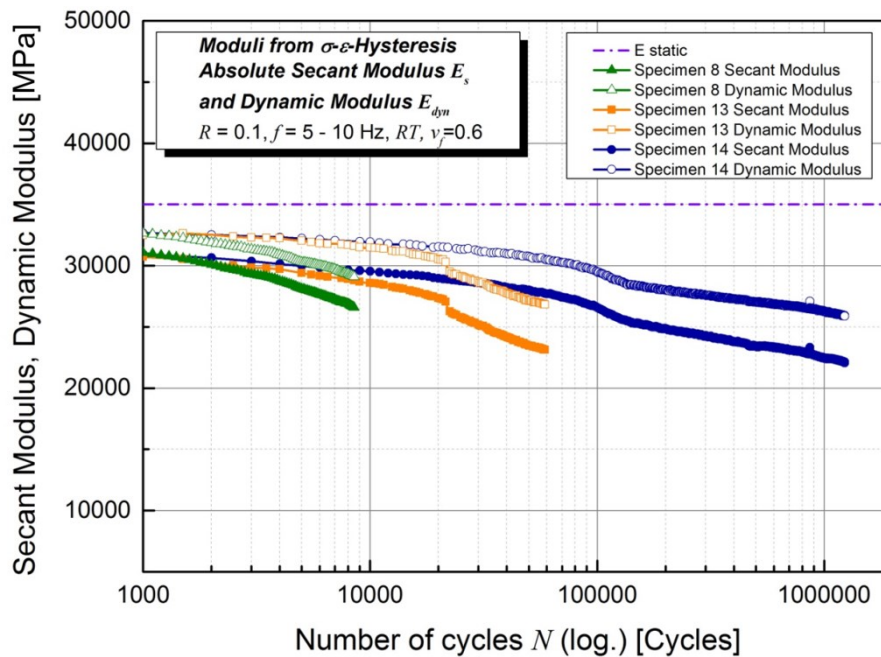


Figure 10.3: Absolute values secant moduli E_s from stress-strain-hystereses.

Regarding life-time prediction, it is not clear which one of these two moduli provides reliable absolute stiffness values. Depending on the stiffness of the test machine, the results of analysing stress-strain-hysteresis can be influenced as well. As a result of these issues, in literature stiffness degradation is very often published in terms of relative secant moduli, normalised to e.g. the Young's modulus or the stiffness at a certain number of cycles [2,8,9].

Figure 10.4 illustrates the results from the cyclic tensile tests measured with exactly the same specimens. Moduli from cyclic tensile tests are superimposed by the illustrated dynamic moduli from stress-strain-hystereses. The two specimens with lower number of cycles to failure tested at higher stress levels showed a slow decrease of stiffness which was almost equivalent to the dynamic modulus progression. In contrast to that, the stiffness progression from cyclic tensile tests measured by optical methods of specimen 14 showed an alternating signal. To clarify possible damage at the surface thermographic photographs are presented for specimen 13 and 14. Selected sections are marked with number 1 to 6 in figure 10.4 and the corresponding thermographic photographs are illustrated in table 10.2.

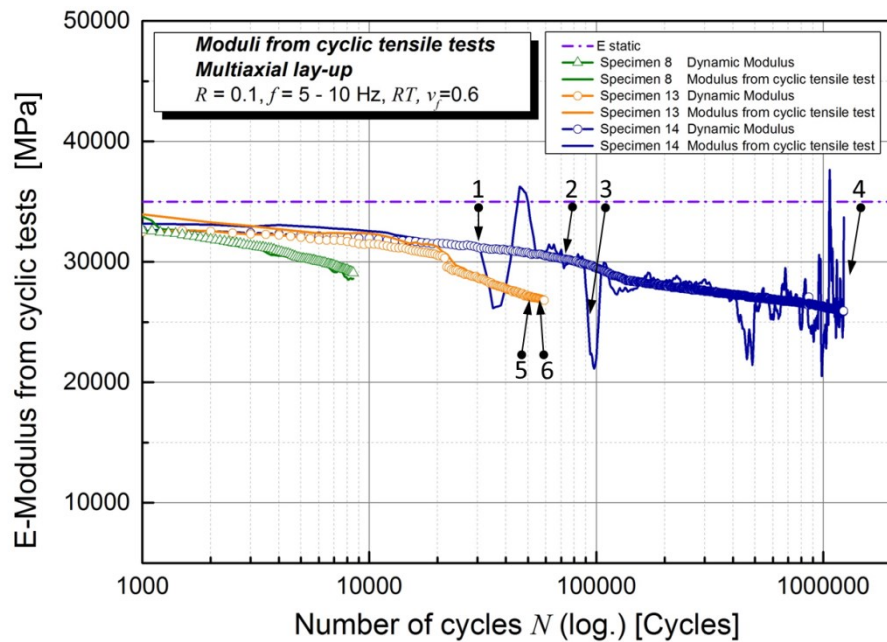
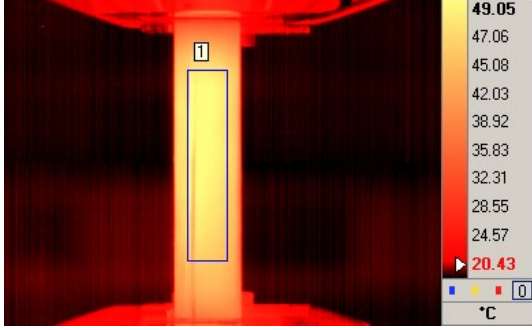
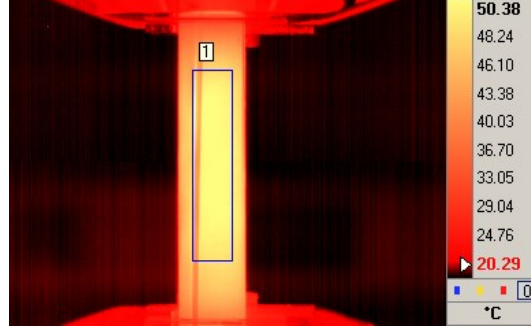
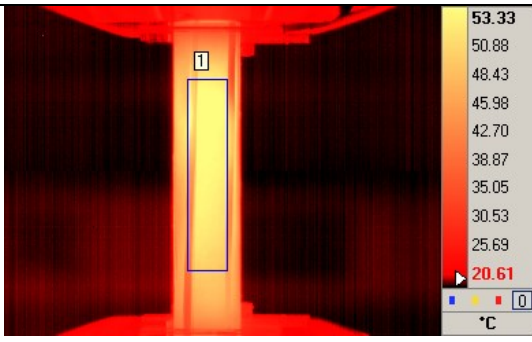
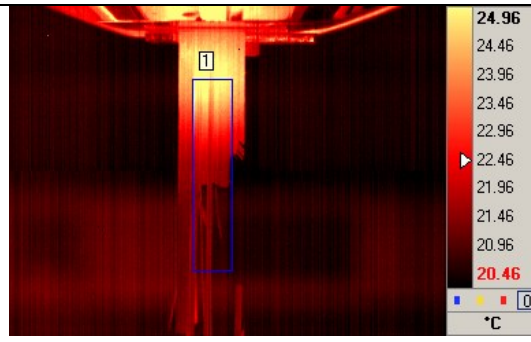
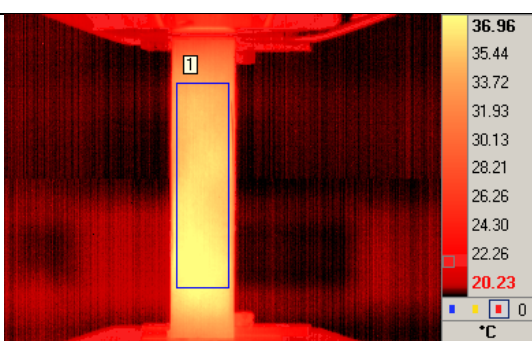
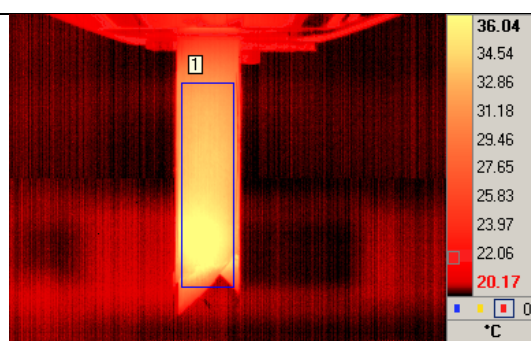


Figure 10.4: Moduli of multi-axial CFRP lay-up measured in cyclic tensile tests.

Marks 1 to 4 listed in table 10.2 illustrate the behaviour of specimen 14 (number of cycles to failure: 1,233,644). After 30,000 cycles the stiffness progression in figure 10.4 showed a rapid change which corresponds to thermographic photograph number 1 on which a starting crack at the surface is visible. The following alternating stiffness course could be dedicated to growth of this first crack (thermographic photograph 2 after 80,000 cycles). The next rapid stiffness change was detected after 100,000 cycles. As illustrated in thermographic picture no. 3 a second crack was monitored there. The decrease of the dynamic modulus at this point of the fatigue test might also be an indicator for delamination. The following alternating signal could be dedicated to further crack growth which resulted in failure after 1,233,644 cycles (thermographic picture 4). Specimen 13 showed smoother stiffness decrease compared to specimen 14. No rapid stiffness changes or sections with alternating courses could be detected which indicated a different failure mode. In specimen 13 no cracks could be detected with thermography until 57,000 cycles. At 59,297 cycles the specimen failed.

Table 10.2: Correlation between stiffness changes and by thermographic camera photographs.

Picture No.: 1, Specimen: 14 Number of cycles: 30,000	Picture No.: 2, Specimen: 14 Number of cycles: 80,000
	
Picture No.: 3, Specimen: 14 Number of cycles: 100,000	Picture No.: 4, Specimen: 14 Number of cycles: 1,233,644
	
Picture No.: 5, Specimen: 13 Number of cycles: 57,000	Picture No.: 6, Specimen: 13 Number of cycles: 59,297
	

The comparisons of stiffnesses from cyclic tensile tests and thermography analysis showed the possibility of correlating damage with stiffness degradation. The number of cycles at which damage occurs according the stiffness courses fitted very well to the thermographic records. Moreover, the results of cyclic tensile tests showed a difference in fatigue behaviour between specimens tested at high stress levels and tested at low stress levels. The same differences were detected with thermography analysis.

10.6. Summary and Outlook

Two methods for calculation of cyclic stiffnesses were compared by the example of a multiaxial lay-up consisting of 8 layers and made of carbon fibres and epoxy resin with focus on potential to monitor fatigue damage. The first method, where secant moduli were calculated from stress-strain-hysteresis, did not show significant stiffness changes that could be related with characteristic damage mechanisms monitored by thermography analysis. The second method applied was a new method called cyclic tensile tests. In these tests, the servo-hydraulic test machine conducted displacement controlled tensile tests with a defined speed after a certain number of load controlled sinusoidal cycles. In the quasi-static tests in between the cyclic load blocks, strains were measured with an optical measurement system. Results show that this new test method provides similar stiffness results compared to the dynamic moduli calculated from stress-strain-hysteresis. This indicates that for stiff materials such as CFRP which do not show much strain-rate dependence, the slope of the stress-strain-hysteresis is similar to the slope of stress-strain curves under quasi-static loading. The superimposition of dynamic moduli and moduli from cyclic tensile tests emphasize that the absolute level is reasonable. Additionally, cyclic tensile tests provide the possibility of monitoring surface cracks which is not possible when analysing stress-strain-hystereses only. Because cracks at the surface disturb optical measurement they can be determined by measurement artefacts.

The first results of the cyclic tensile test method seem promising. Further damage characterisation will be done by detecting stiffness changes and stopping specimens at certain number of cycles prior to failure. Microscopic investigations may allow correlation between stiffness changes and

delamination inside the specimens. The potential of this testing method lies within the possibility of detecting surface cracks and by evaluating mechanical properties measured under loading conditions comparable to quasi-static moduli and Poisson's ratios. Mechanical stiffnesses of single UD laminates will be determined as well under fatigue loading. The attempt will be made to use those cycle-dependent stiffnesses as input parameters for FE simulation and possibly fatigue life prediction.

10.7. References

- [1] Reifsnider KL. Damage and damage mechanics. In: Reifsnider KL, editor. Fatigue of composite materials. Amsterdam, New York: Elsevier; 1991, p. 11–77.
- [2] Stinchcomb W, Bakis CE. Fatigue behaviour of composite materials. In: Reifsnider KL, editor. Fatigue of composite materials. Amsterdam, New York: Elsevier; 1991, p. 105–80.
- [3] DIN Deutsches Institut für Normung e.V. Aerospace series - Carbon fibre reinforced plastics - Unidirectional laminates, Tensile tests parallel to fibre direction;;49.040.10(2561). Berlin: Beuth Verlag GmbH; 1995.
- [4] ASTM International. Standard Test Method for Tensile Properties of Polymer Matrix Composite Materials(ASTM D3039/D3039M-00). West Conshohocken, PA, United States: ASTM International; 2000.
- [5] Schürmann H. Konstruieren mit Faser-Kunststoff-Verbunden: Mit 39 Tabellen. 2nd ed. Berlin, Heidelberg, New York, NY: Springer; 2007.
- [6] Zahnt B. Ermüdungsverhalten von diskontinuierlich glasfaserverstärkten Kunststoffen: Charakterisierungsmethoden, Werkstoffgesetze und Struktur-Eigenschafts-Beziehungen. Dissertation. Leoben; 2003.
- [7] Altstädt H. Hysteresismessungen zur Charakterisierung der mechanischen Eigenschaften von R-SMC. Ph.D. Dissertation. Kassel; 1987.
- [8] Pinter G, Ladstätter E, Billinger W, Lang R. Characterisation of the tensile fatigue behaviour of RTM-laminates by isocyclic stress–strain-diagrams. International Journal of Fatigue 2006;28(10):1277–83.

- [9] Philippidis TP, Vassilopoulos AP. Fatigue design allowables for GRP laminates based on stiffness degradation measurements. *Composite Science and Technology* 2000(60):2819–28.

11. Publication 5

11.1. Bibliographic information

- Title: Technological approach to fatigue-life prediction of CFRP
- Authors and relevant contributions to this publication:
 - Julia BRUNBAUER¹
Experimental testing, data evaluation, preparation of the publication
 - Gerald PINTER¹
Discussion of experimental results
- Affiliation:
 1. Institute of Materials Science and Testing of Polymers, Montanuniversitaet Leoben, Otto Glöckel-Strasse 2, 8700 Leoben, Austria
- Periodical: ECCM16 – 16th European Conference on Composite Materials, Sevilla, Spain, 22-26 June 2014, Proceedings
- DOI: -

Statement with regard to this publication: The manuscript presented here is an adapted accepted manuscript in order to fit the formatting of the thesis and does not necessarily reflect exactly the actually published version.

11.2. Abstract

In this paper the issue of adequate stiffness measurement and use of fatigue stiffnesses for fatigue life prediction is investigated. Studies on the experimental measurement of stiffness properties of unidirectional carbon/epoxy laminates under tension-tension fatigue loads are presented. Moduli are calculated from stress-strain hystereses. Results differ from quasi-static scales because of the different load speeds and strain rate dependent material behaviour. A new test procedure for measuring adequate stiffness properties in fatigue tests is presented. This method can be used to determine adequate cycle-dependent material properties for implementation in classical laminate theory or software based fatigue life prediction.

11.3. Introduction

Continuously fibre reinforced composites offer great possibilities for lightweight construction due to their outstanding mechanical properties in relation to weight. This material class has found an increasing number of applications in structural parts in the aircraft and in the automotive industry. To assure both weight reduction and safety material utilisation has to be optimized. As a result, composite parts are load-tailored and need to be designed individually. Stress analysis is therefore of tremendous importance. In contrast to most metal materials, highly anisotropic material behaviour has to be taken into account.

The most well-known approach to simple but effective stress analysis of composite materials under quasi-static loads is the classical laminate theory (CLT) [1]. CLT can be used to calculate stresses and strains in each layer of laminates or multiaxial lay-ups and provide information about resulting linkages which could lead to bending, shear or other deformations. Therefore, stresses in different multiaxial lay-ups can be compared and applications can be improved. Preconditions for accurate use of CLT are small deformations, ideal bonding between fibre and matrix material and linear elastic material behaviour. Voids, cracks or pores, which can cause complicated stress states, are not taken into account [1]. These

simplifications make CLT an effective and fast tool for application-oriented estimation. Minimal required input parameters for CLT as well as for much more complex finite element based software tools are the anisotropic stiffness parameters of the material. These stiffnesses are usually determined in quasi-static tests with constant load speeds.

The issue of fatigue life estimation of continuously fibre reinforced materials is many times more sophisticated than the quasi-static load case. For fatigue loads as well, stiffnesses are very important information about material behaviour. Though, the common definition of stiffnesses in fatigue tests calculated from stress-strain hysteresis does not provide satisfying results for further calculation. The test speed under fatigue tests with e.g. 10 Hz is higher than in quasi-static tests with 0.5 mm/min cross-head speed. Especially for polymeric materials, effects such as strain-rate dependence or cyclic creep have major influence on the slopes and on the shape of hysteresis. Usually dynamic moduli of polymeric materials are higher than respective quasi-static moduli during the entire fatigue test. Secant moduli decrease during fatigue tests because of creep effects in the materials [2]. As a consequence, the interpretation of dynamic and secant moduli calculated from stress-strain hysteresis in relation to quasi-static moduli is very difficult. It seems very unlikely that materials possess higher stiffnesses under fatigue than under quasi-static loads. Under quasi-static conditions Young's moduli measured in and transverse to fibre direction can be used in combination with Poisson's ratios for calculation of further material parameters such as shear modulus [3]. Under fatigue loads, secant and dynamic moduli cannot be used in theories developed for quasi-static parameters because they describe a different aspect of fatigue behaviour and are not measured under load conditions comparable to classical quasi-static material parameters.

In this work, experimental measurements of fatigue stiffnesses which can be used for known theories such as CLT are presented. Measuring under comparable load conditions is a necessary prerequisite for further use of cycle-dependent material properties in theories developed for quasi-static parameters. Therefore, a test procedure called "cyclic tensile tests" was implemented [4]. The Young's modulus of the material could be monitored with progressing number of cycles starting at the quasi-static value. This

approach is considered technological, because all effects occurring in the specimen under fatigue loading such as crack growth, delamination, fibre matrix debonding etc. are included in the measured material parameters and further calculation with these measured parameters. It is shown, that stiffnesses are material parameters but that they depend highly on the measurement and the strain range used for calculation. The parameters measured in cyclic tensile tests allow the extension of calculation tools such CLT for fatigue loads.

11.4. Experimental work

In this work unidirectional laminates made of carbon fibres and epoxy resin and the stacking sequences $[0^\circ]_4$, $[45^\circ]_8$ and $[90^\circ]_8$ were investigated. The fibre volume content was 55 % (measured by thermo-gravimetric analysis). The specimens' geometry was 200x10x1 mm for $[0^\circ]_4$ and 200x20x2 mm for $[45^\circ]_8$ and $[90^\circ]_8$ specimens. Aluminium-tabs with 1 mm thickness were glued on both sides of the specimens. Gauge length for all specimens was 100 mm. Mechanical extensometers with 50 mm gauge length were used for strain measurement longitudinal to fibre direction. Quasistatic and cyclic tests were performed at room temperature on a servo-hydraulic testing machine equipped with a 100 kN load cell by MTS Systems Corporations. Quasi-static tests were evaluated according to ASTM D 3039 [5]. All fatigue tests were performed with the R -value (=minimum load / maximum load) of 0.1. Specimens were tested on four different stress levels, at least three specimens were tested per stress level. Stress-strain hystereses were recorded locally with a mechanical extensometer by MTS Systems Corporations with a fixing length of 50 mm. The test procedure of cyclic tensile tests is illustrated in figure 11.1. The servo-hydraulic test machine started the testing procedure with a defined number of sinusoidal cycles under load control. After that, the servo-hydraulic test machine unloaded the specimen to 0 N, switched to displacement control and performed a tensile test with a speed of 0.5 mm / min. The tensile tests were performed up to the mean displacement of the respective fatigue tests to avoid additional damaging [4].

Recorded stress-strain hystereses were used for calculation of the secant and the dynamic modulus [2,6]. The secant modulus is defined as maximum stress of hysteresis divided by maximum strain (11.1). The dynamic modulus is calculated from delta values of the stress and strain values of the hysteresis (11.2). The moduli from cyclic tensile tests were calculated between 0.1 % and 0.3 % strain according to ASTM D 3039 [5] (11.3).

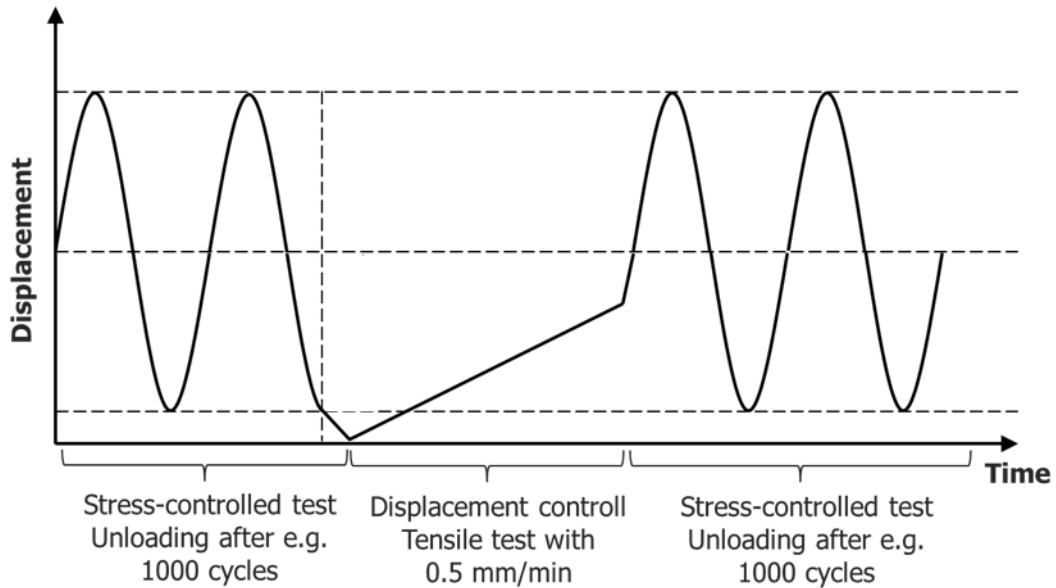


Figure 11.1: Test procedure for cyclic tensile tests [4].

$$E_s = \frac{\sigma_{max}}{\varepsilon_{max}} \quad (11.1)$$

$$E_{dyn} = \frac{\sigma_{max} - \sigma_{min}}{\varepsilon_{max} - \varepsilon_{min}} \quad (11.2)$$

$$E_{cyclic\ tensile\ tests} = \frac{\sigma_{0.003} - \sigma_{0.001}}{0.003 - 0.001} \quad (11.3)$$

11.5. Results and Discussion

For all results presented in this work it was assured in pre-tests that the inclusion of quasi-static tensile tests in the fatigue test did not influence the number of cycles to failure of the specimens. The stiffnesses measured in quasi-static tests according to ASTM D 3039 [5] are presented in table 11.1.

Table 11.1: Stiffnesses measured in quasi-static tests.

	[0°] ₄ [GPa]	[45°] ₈ [GPa]	[90°] ₈ [GPa]
Young's modulus	105 ± 3.7	7.8 ± 0.1	6.3 ± 0.1

Stress-strain hystereses and cyclic tensile tests measured after 10,000, 100,000, 200,000 and 400,000 cycles with [45°]₈ specimens are illustrated in figure 11.2. Stress-strain hystereses were steeper than the respective tensile tests. The moduli calculated from both stress-strain hystereses and tensile tests showed that dynamic moduli for strain-rate dependent polymeric materials were usually higher than the respective quasi-static moduli (figure 11.3).

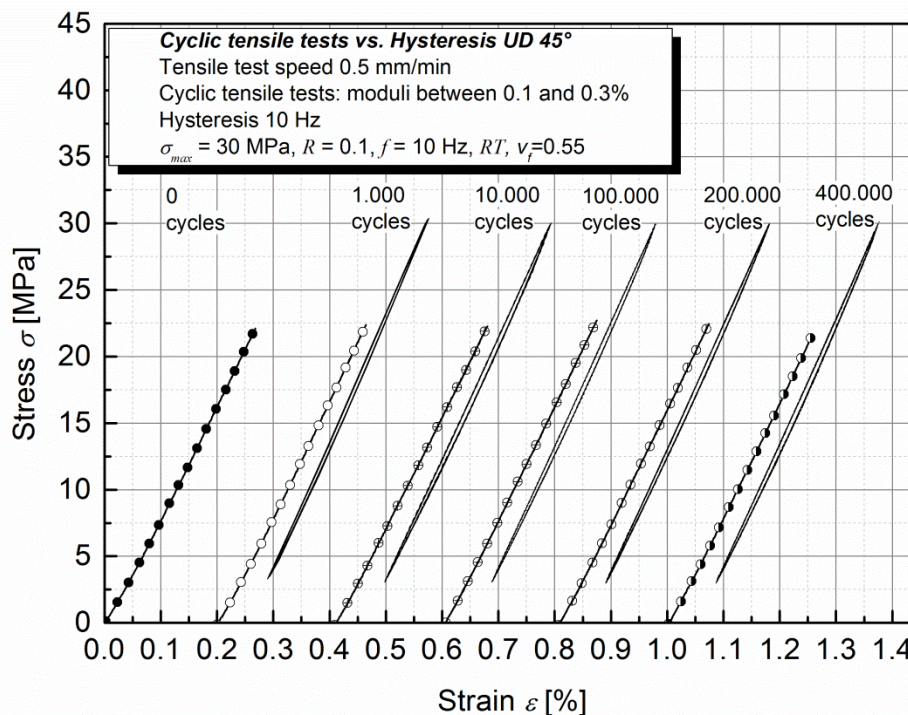


Figure 11.2: Cyclic tensile tests compared to stress strain hysteresis measured at defined numbers of cycles: [45°]₈ laminate, $\sigma_{max} = 30$ MPa, $R = 0.1$, 10 Hz, 0.5 mm/min in cyclic tensile tests.

Moduli measured in cyclic tensile tests corresponded accurately to the Young's modulus of 7.8 GPa, whereas the absolute value for dynamic modulus was 9.6 GPa. Dynamic moduli and moduli from cyclic tensile tests stayed on a constant level during the entire test time. The secant modulus did not decrease, either, which indicated that the specimen did not tend to creep during the fatigue test. When having a closer look at the results of cyclic tensile tests, it could be found that moduli increased at the end of the fatigue tests. Because not only local measurement systems such as extensometer recorded this effect but the piston displacement too, it seemed that this was not a measuring artefact but effects actually happening in the specimen. Fibres in 45° were probably aligning in load direction with increasing number of cycles. Though, fibre movement was too small to be monitored with cameras recording the surface during fatigue tests.

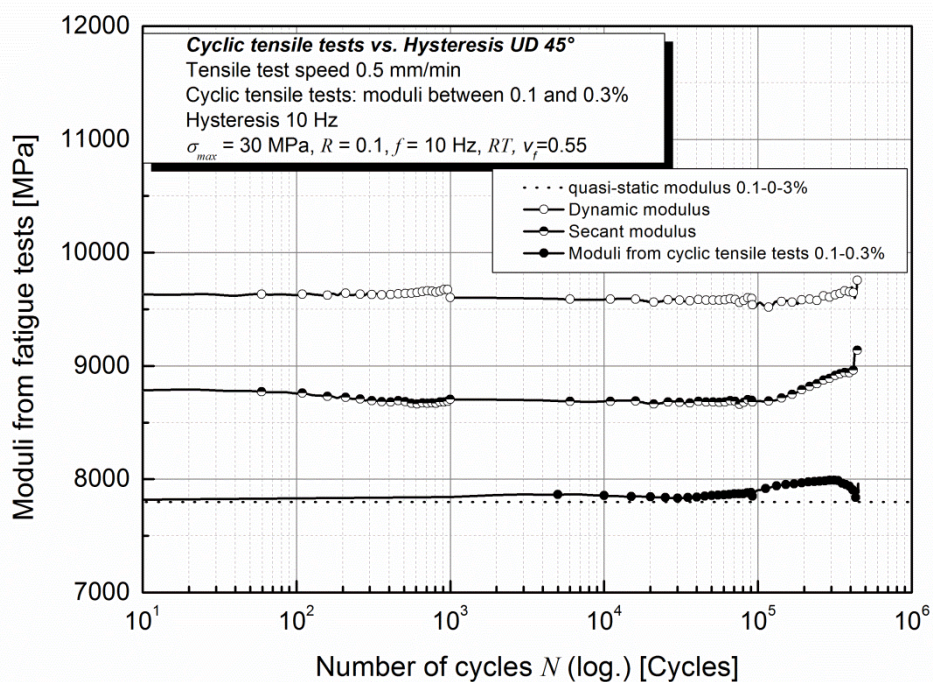


Figure 11.3: Moduli calculated from cyclic tensile tests compared to dynamic and secant modulus calculated from stress-strain hystereses: $[45^\circ]_8$ laminate, $\sigma_{max} = 30$ MPa, $R = 0.1$, 10 Hz, 0.5 mm/min in cyclic tensile tests.

Matrix dominated $[90^\circ]_8$ specimens behaved non-linear in cyclic tests (figure 11.4). As a result of non-linear material behaviour, absolute stiffness values

became somehow a matter of definition depending on the interpretation of stress-strain curves (figure 11.5). Again, moduli were calculated from the stress-strain hystereses as well as from cyclic tensile tests. The dashed lines in figure 11.5 represent the Young's moduli evaluated from quasi-static tensile tests. The deviation between 6300 MPa and 6900 MPa depending on the strain range used for calculation of the Young's modulus emphasized the non-linear material behaviour. Consequently, moduli from quasi-static tensile tests as well as cyclic tensile tests were calculated from linear part of measured stress-strain curves only, which equalled modulus calculation between 0.05 and 0.175 % strain. This observation showed clearly the strain-rate dependent material behaviour when testing unidirectional laminates transverse to fibre direction and the importance of measuring fatigue material parameters under load conditions comparable to quasi-static tests. $[0^\circ]_4$ laminates did not show significant differences between dynamic modulus and moduli calculated from cyclic tensile tests. This resulted from the high fibre dominance in 0° -direction and non-speed dependent behaviour.

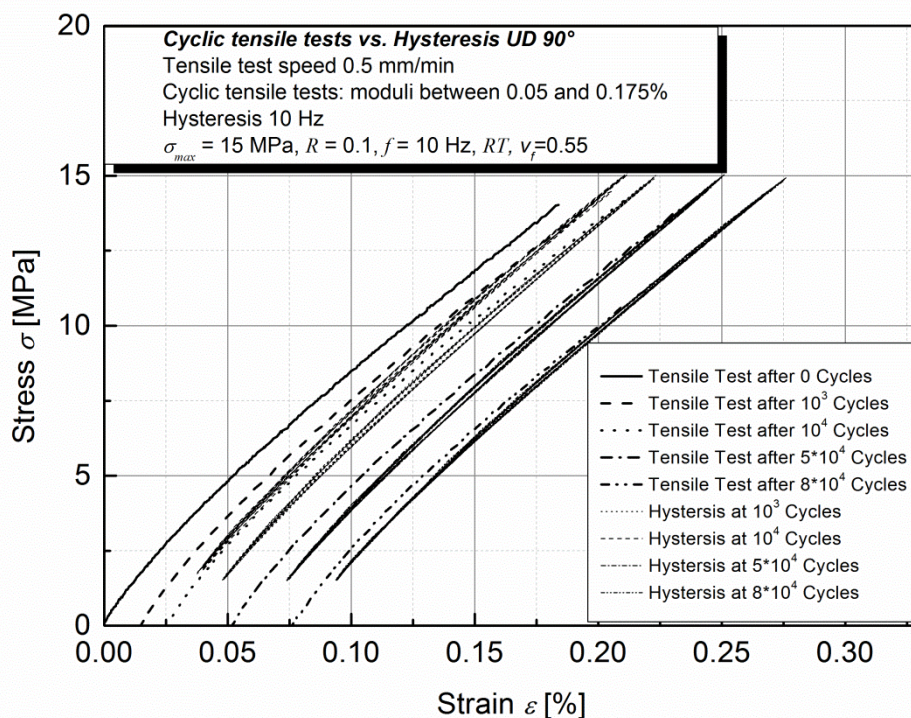


Figure 11.4: Cyclic tensile tests compared to stress strain hystereses: $[90^\circ]_8$ laminate, $\sigma_{max} = 15$ MPa, $R = 0.1$, 10 Hz, 0.5 mm/min in cyclic tensile tests.

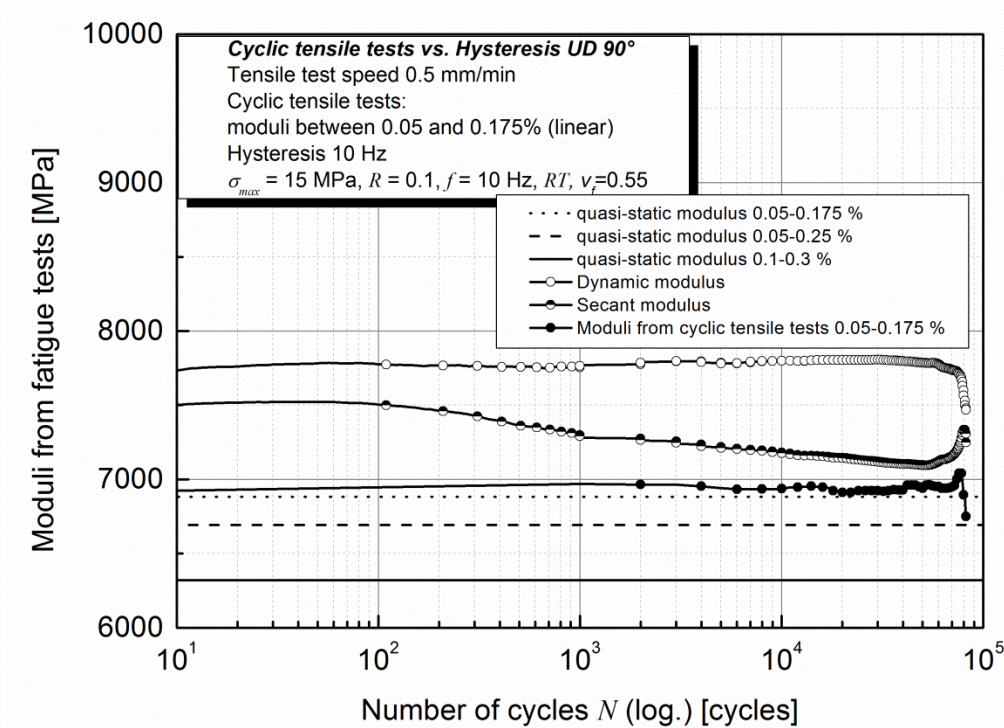


Figure 11.5: Moduli calculated from cyclic tensile tests compared to dynamic and secant modulus calculated from stress-strain hystereses: $[90^\circ]_8$ laminate, $\sigma_{max} = 15$ MPa, $R = 0.1$, 10 Hz, 0.5 mm/min in cyclic tensile tests.

Results produced by using the cyclic tensile test procedure for unidirectional plies in 0° , 45° and 90° in fatigue tests are presented in Figure 11.6. The cycle-dependent moduli for $[0^\circ]_4$, $[45^\circ]_8$ and $[90^\circ]_8$ are illustrated with their respective quasi-static values (dashed lines). Moduli measured with this method started at the respective value of the Young's moduli at 0 cycles. Moduli transverse to fibre direction $[90^\circ]_8$ and $[45^\circ]_8$ stayed on a constant level during the entire test time. This could be related to the damage mechanisms of sudden failure of these laminates. Beyond that, applied load level did not have influence on the progress of moduli. In contrast to that, $[0^\circ]_4$ decreased as a consequence of delamination and damage progress in the specimens. Moduli processes of $[0^\circ]_4$ were dependent on applied stress level (in figure 11.6 one representative stress level is illustrated).

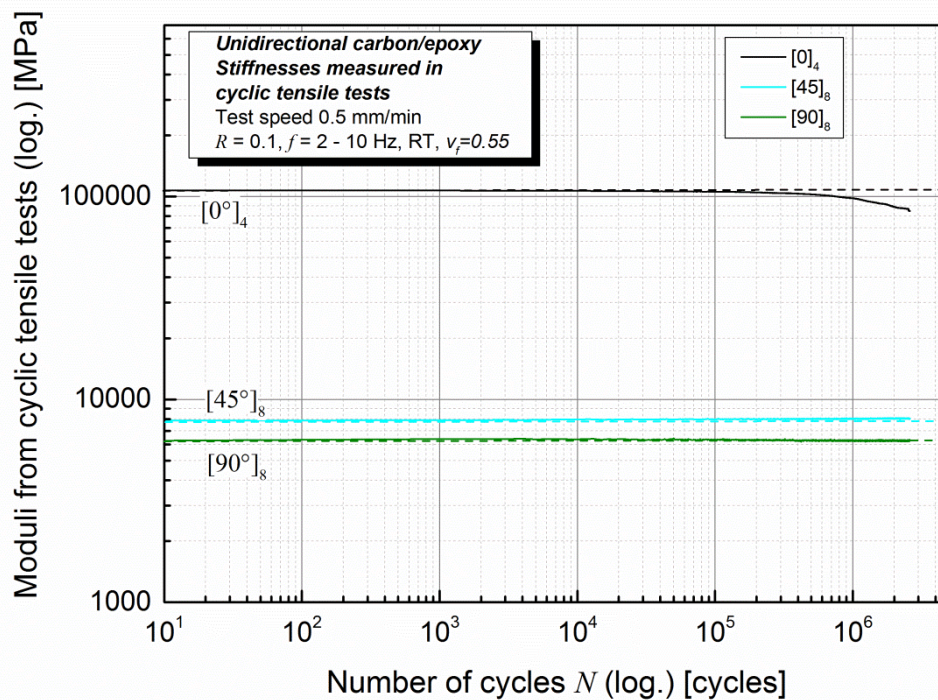


Figure 11.6: Moduli of $[0^\circ]_4$, $[45^\circ]_8$ and $[90^\circ]_8$ laminates measured in cyclic tensile tests compared to the respective Young's moduli from quasi-static tests.

11.6. Conclusions and Outlook

In this work, a test procedure for determination of fatigue stiffnesses has been developed. The cyclic tensile tests procedure provides fatigue parameters measured under quasi-static conditions. It has been shown, that, in contrast to stress-strain analysis, strain-rate dependency of unidirectional plies measured under angles different from fibre direction can be excluded from fatigue results by using this new procedure. Cycle-dependent moduli measured in cyclic tensile tests can be correlated reasonably with the respective quasi-static Young's moduli which is often not the case when analysing stress-strain hystereses. Besides, this test procedure can be easily implemented in conventional Wöhler tests because it does not influence number of cycles to failure in cyclic tests.

Furthermore, cyclic tensile tests can be used to measure cycle-dependent Poisson's ratios and, in combination with cycle-dependent moduli in and transverse to fibre direction, to calculate cycle-dependent shear modulus of the UD layer in the same way as known for quasi-static parameters [3]. Subsequently, the cycle-dependent material parameters of the UD layer can be implemented in classical laminate theory to calculate $E_x(N)$, $E_y(N)$, $G_{xy}(N)$, $\nu_{xy}(N)$ and $\nu_{yx}(N)$ of any multiaxial stack. The results will be validated experimentally with a [0/+45/-45/90/90/-45/+45/90] CFRP multiaxial stack and published elsewhere.

11.7. References

- [1] Schürmann H. Konstruieren mit Faser-Kunststoff-Verbunden: Mit 39 Tabellen. 2nd ed. Berlin, Heidelberg, New York, NY: Springer; 2007.
- [2] Altstädt H. Hysteresismessungen zur Charakterisierung der mechanischen Eigenschaften von R-SMC. Ph.D. Dissertation. Kassel; 1987.
- [3] Tuttle ME. Structural analysis of polymeric composite materials. New York: Marcel Dekker; 2004.
- [4] Brunbauer J, Arbeiter F, Stelzer S, Pinter G. Stiffness Based Fatigue Characterisation of CFRP. AMR 2014;891-892:166–71.
- [5] ASTM International. Standard Test Method for Tensile Properties of Polymer Matrix Composite Materials (ASTM D3039/D3039M-00). West Conshohocken, PA, United States: ASTM International; 2000.
- [6] Pinter G, Ladstätter E, Billinger W, Lang R. Characterisation of the tensile fatigue behaviour of RTM-laminates by isocyclic stress–strain-diagrams. International Journal of Fatigue 2006;28(10):1277–83.

12. Publication 6

12.1. Bibliographic information

- Title: Fatigue-life prediction of carbon fibre reinforced laminates by using cycle-dependent classical laminate theory
- Authors and relevant contributions to this publication:
 - Julia BRUNBAUER¹
Experimental testing, data evaluation, programming of software tool, fatigue-life predictions, preparation of the publication
 - Gerald PINTER²
Discussion of the results
- Affiliations:
 1. Institute of Materials Science and Testing of Polymers, Montanuniversitaet Leoben, Otto Glöckel-Strasse 2, 8700 Leoben, Austria
 2. Polymer Competence Center Leoben GmbH, Roseggerstrasse 12, 8700 Leoben, Austria
- Periodical: Composites Part B
- DOI: 10.1016/j.compositesb.2014.11.015

Statement with regard to this publication: The manuscript presented here is an adapted accepted manuscript in order to fit the formatting of the thesis and does not necessarily reflect exactly the actually published version.

12.2. Abstract

In this work a study about the adaption of the classical laminate theory for fatigue loads is presented. Cycle dependent stiffnesses of single UD 0°, UD 45° and UD 90° plies are implemented in order to calculate the fatigue-induced stiffness decrease of a multidirectional lay-up with the stacking sequence [0°/+45°/-45°/90°/90°/-45°/+45°/0°]. As second input alternative, UD 0°, UD 90° and ±45° plies are used. The calculated cycle-dependent stiffness parameters are compared to experimentally measured fatigue data of the multidirectional lay-up. The experimental test procedure used for the measurement of cycle-dependent stiffness parameters has been published previously. Results show that the experimentally measured stiffness decreases of the multidirectional lay-up can be estimated accurately based on the cyclic unidirectional input parameters.

12.3. Introduction

Carbon/epoxy laminates are increasingly used because of their outstanding mechanical properties and light weight potential in the aircraft and automotive industry. Assuring the life-time of structural parts in such applications is a very important issue. Nowadays there are basically two approaches to technological life-time estimation of composites based on mechanical properties describing different aspects of fatigue life: fatigue strength represented by S-N curves as known from classical metal fatigue and fatigue stiffness. It is well known in literature that mechanical properties in composites decrease during fatigue life because of complex damage mechanisms such as matrix cracking, fibre-matrix debonding, delamination or fibre fracture which have been investigated extensively in variety of studies e.g. [1–5]. Computational models describing fatigue induced damage, especially matrix cracking, have been developed [5,6]. The progressing physical damage mechanisms on microscopic level can be reflected in the decreasing macroscopic stiffness properties and depend on the amplitude of the applied cyclic load [1,2]. Consequently, stiffness decreases can offer information about the physical behaviour of the material at each point of the fatigue test. In addition to that, S-N curves contain information about the

failure strength at the end of the stiffness decrease in dependency of the applied load level.

Unidirectional and multidirectional continuously fibre reinforced composites are among the easiest but most widely spread fibre architectures. Especially material tests of unidirectional laminates are important for the creation of basic material data, under quasi-static as well as fatigue loads. In many cases, multidirectional lay-ups made of the same material have to be characterised as well. Even if the fatigue properties of the unidirectional plies used in the multidirectional lay-up are known, the time consuming fatigue tests usually have to be started again. Consequently, a way to reduce testing time would be beneficial. One established possibility for calculating multidirectional properties based on unidirectional input parameters under quasi-static loads is the classical laminate theory (CLT). CLT is a powerful tool for the design and dimensioning of composite parts. By using stiffnesses and Poisson's ratios of single plies, the properties of multidirectional lay-ups can be estimated very accurately under quasi-static loads [7–9]. Necessary input parameters are the Young's modulus in fibre direction E_{11} , the Young's modulus transverse to fibre direction E_{22} , the shear modulus G_{12} and the major and minor Poisson's ratios ν_{12} and ν_{21} . It has to be considered that all physical effects such as fibre-matrix adhesion, interfaces and delaminations are already included in the mechanical parameters on ply level and taken on the next, multidirectional level by the classical laminate theory. This basic assumption of the CLT makes it a mechanical approach rather than a micromechanical one. CLT has been used and adapted for a variety of materials and applications e.g. [10–12]. However, the CLT is not applicable to fatigue so far.

In this paper, the classical laminate theory has been adapted in order to calculate the stiffness properties of a multidirectional lay-up under fatigue loads $E_x(N)$, $E_y(N)$, $G_{xy}(N)$ and $\nu_{xy}(N)$ based on the cycle-dependent properties of the unidirectional ply $E_{11}(N)$, $E_{22}(N)$, $G_{12}(N)$ and $\nu_{12}(N)$. To measure these input parameters, an experimental procedure had to be developed which could ensure measuring cycle-dependent linear elastic material properties under conditions comparable to the quasi-static Young's and shear moduli already published in [13]. This new cyclic test procedure was mainly

necessary because the commonly used method for calculating fatigue moduli from stress-strain hystereses was not useful for further life-time estimation. Because of the strain rate dependent behaviour of the epoxy matrix, absolute values of moduli calculated from stress-strain hystereses were not in the same scales as quasi-static moduli usually used in CLT [13,14]. Consequently, the “cyclic tensile test” procedure was used for the experimental tests in this work which includes displacement controlled quasi-static tensile tests within force controlled tension-tension fatigue tests [13]. By evaluating the included quasi-static tensile tests, cycle-dependent Young’s and shear moduli could be calculated. These cycle-dependent input parameters of the unidirectional ply were implemented in a programmed software routine which repeated the CLT for a defined number of cycles. Shear moduli were implemented in two different ways. Fatigue stiffness properties of a quasi-isotropic multidirectional lay-up [$0^\circ/+45^\circ/-45^\circ/90^\circ/\text{symm.}$] were calculated. Results were compared to the experimentally measured stiffness progresses at three different load levels. Additionally, multidirectional specimens were stopped after certain numbers of cycles and investigated by light microscopy to get qualitative insight in the damage mechanisms responsible for the stiffness degradation.

12.4. Experimental work

Unidirectional (UD) lamina made of carbon fibres and epoxy resin were tested at angles of 0° , 45° and 90° . Multidirectional specimens consisting of $\pm 45^\circ$ and [$0^\circ/+45^\circ/-45^\circ/90^\circ/\text{symm.}$] layers build in a symmetric way referring to the middle plane were investigated as well. The fibre volume content of all specimens was 55 % (measured by thermo gravimetric analysis as published in [15]). UD 0° plies consisted of 4 layers, all other specimens were made of 8 layers. The specimens’ geometry was 200x10x1 mm (length x width x thickness) for UD specimens in fibre direction and 200x20x2 mm for all other specimens. Aluminium tabs of 1 mm thickness were glued on both sides of the specimens.

Quasi-static tensile as well as tension-tension fatigue tests were performed on a servo-hydraulic test machine equipped with a load frame and load cell

for 100 kN by MTS Systems Corporations (Minnesota, USA). Gauge length for all performed tests was 100 mm. Hydraulic wedge pressure of 5 MPa was chosen in order to prevent slipping without damaging the specimens. Good adhesion between aluminium tabs and CFRP specimen was assured in preliminary tests. Quasi-static tensile tests were performed with a test speed of 0.5 mm/min until failure. A digital image correlation (DIC) system by GOM (Braunschweig, Deutschland) was used for strain measurement in and transverse to fibre direction. Tensile moduli were calculated between 0.001 and 0.003 absolute strain according to [16]. Fatigue tests were performed at four different stress levels. A minimum of three specimens was tested on each stress level. Constant test frequencies between 2 and 10 Hz were applied in the fatigue tests with different lay-ups. The choice of frequency depended on expected number of cycles to failure and on the specimens' tendency for hysteretic heating which was examined in preliminary tests [17]. Specimens' temperatures were controlled by infrared (IR) sensors in all tests. All fatigue tests were performed with the R -value (= minimum force / maximum force) 0.1.

Conventional sinusoidal tests with constant load amplitude as well as cyclic tensile tests were performed on different stress levels for comparison of numbers of cycles to failure. In tests according to cyclic tensile test procedure presented in [13], the servo-hydraulic test machine started the test procedure by performing a displacement controlled tensile test with a test speed of 0.5 mm/min. Displacements in these quasi-static tensile tests were always smaller than the respective, locally measured sinusoidal displacement of the specimens to avoid additional damaging as illustrated in figure 12.1. After a tensile test, the test machine switched to load control and performed 1000 sinusoidal cycles with $R = 0.1$. Subsequently, the servo-hydraulic test machine unloaded the specimen to 0 N, switched to displacement control and performed another quasi-static tensile test (figure 12.1). The tensile tests measured between the cyclic loads were used to calculate moduli and Poisson's ratios in exactly the same way as known for quasi-static tensile tests by means of the computer language matlab by MathWorks (Ismaning, Germany). Fatigue results were analysed statistically according to [18] in addition.

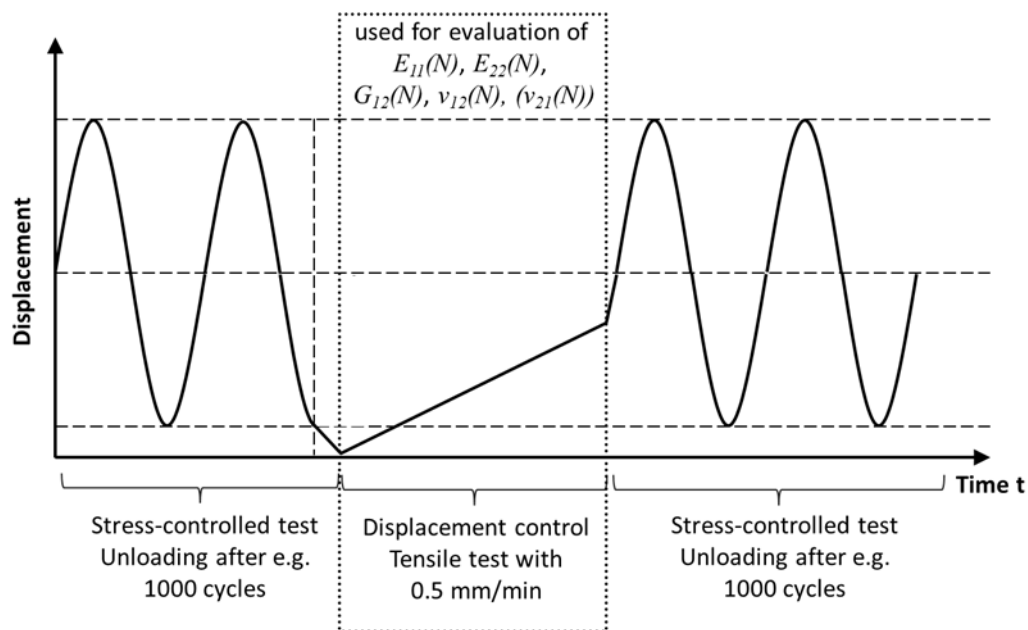


Figure 12.1: Experimental test procedure “cyclic tensile tests” and evaluation of cycle-dependent stiffness properties.

12.4.1. Shear moduli in quasi-static and fatigue tests

Different possibilities for the measurement of the shear stress-strain behaviour of composite materials are known. For woven or multidirectional materials, the rail shear test is a popular method [19,20]. However, the rail shear test cannot be recommended for unidirectional laminates because the measured properties do not correspond to reality [20]. There are basically two methods if the shear behaviour of unidirectional plies has to be characterised with rectangular specimens: First, the shear modulus G_{12}' can be calculated if the moduli in fibre direction E_{11} , transverse to fibre direction E_{22} , the modulus of a UD 45° ply E_{45} and the Poisson's ratio ν_{12} are known (12.1) [21]. Second, the in-plane shear behaviour can be evaluated in tensile tests with $\pm 45^\circ$ specimens. Tensile stresses are used to calculate shear stresses τ_{12} . The shear strain γ_{12} is evaluated as difference between the longitudinal and the transversal strain of the $\pm 45^\circ$ specimen. Finally, the shear modulus G_{12}^* is calculated between 0.002 and 0.006 absolute strain according to (12.2) [22]. Both methods were used for evaluation of shear moduli in quasi-static as well as fatigue tests and for further implementation in cycle-dependent CLT.

$$G'_{12} = \frac{E_{45} * E_{11} * E_{22}}{4 * E_{11} * E_{22} - E_{45} * (E_{22} - 2 * \nu_{12} * E_{22} + E_{11})} \quad (12.1)$$

$$G^*_{12} = \frac{\Delta \tau_{12}}{\Delta \gamma_{12}} \quad (12.2)$$

12.4.2. Poisson's ratios measured in quasi-static and fatigue tests

The two Poisson's ratios provide useful information about the anisotropic strain response of a material under load and are necessary input parameters for the CLT. The major Poisson's ratio ν_{12} can be evaluated from quasi-static tensile or cyclic tensile tests with UD 0° specimens by measuring strains transverse to (22-direction) and in fibre direction (11-direction) (12.3). The minor Poisson's ratio ν_{21} can either be measured in the same way with UD 90° specimens or it can be calculated according to (12.4). Both formula were used for the calculation and validation of ν_{12} and ν_{21} as well as $\nu_{12}(N)$ and $\nu_{21}(N)$.

$$\nu_{12} = \frac{\varepsilon_{22,2} - \varepsilon_{22,1}}{\varepsilon_{11,2} - \varepsilon_{11,1}} \quad (12.3)$$

$$\nu_{21} = \frac{E_{22}}{E_{11}} * \nu_{12} \quad (12.4)$$

12.4.3. Fatigue life prediction with CLT

The known procedure of the CLT [7–9] and its extension for fatigue loads were implemented in the computer language matlab. The schematic progress of the programmed procedure is illustrated in figure 12.2. Because the laminate which should be calculated was symmetric referring to the middle plane, warping could not occur and was therefore neglected in the following calculation [8]. Influences of temperature and humidity were not taken into account in the elasticity laws. The classical laminate theory was used for the creation of the cycle-dependent elasticity laws of the multidirectional lay-up. Further ply-by-ply stress analysis is not included in the results presented herein.

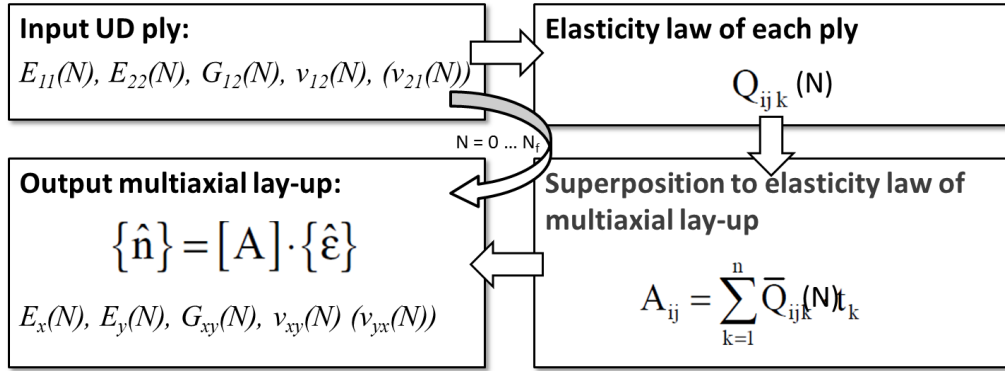


Figure 12.2: Schematic progress of the cycle-dependent classical laminate theory in matlab.

At first, the number of plies k , the angle α and the thickness t_k of each ply of the multidirectional lay-up which should be calculated were requested by the matlab routine. The input parameters $E_{11}(N)$, $E_{22}(N)$, $G_{12}(N)$, $\nu_{12}(N)$ and $\nu_{21}(N)$ were implemented as text file. The cycle-dependent stiffness properties of the unidirectional ply were used to create the elasticity law including the stiffness matrix $[Q_{ij}(N)]$ according to (12.5). To combine the stiffness properties of the single plies in order to create a multidirectional lay-up, the local properties had to be transferred from the plies' coordinate systems into a global coordinate system. Therefore, $[Q_{ij}(N)]$ was extended with the transformation matrix $[T]_{1,2 \rightarrow x,y}$ (12.6) to create the transformed ply stiffness matrix $[\bar{Q}_{ij}(N)]$. By multiplying the transformed plies' stiffness matrixes with the relative ply thicknesses t_k , the elasticity law of the multidirectional lay-up could be created (12.7) [7–9].

$$[Q_{ij}(N)] = \begin{bmatrix} \frac{E_{11}(N)}{1-\nu_{12}(N)\nu_{21}(N)} & \frac{\nu_{21}(N)E_{11}(N)}{1-\nu_{12}(N)\nu_{21}(N)} & 0 \\ \frac{\nu_{12}(N)E_{22}(N)}{1-\nu_{12}(N)\nu_{21}(N)} & \frac{E_{22}(N)}{1-\nu_{12}(N)\nu_{21}(N)} & 0 \\ 0 & 0 & G_{12}(N) \end{bmatrix} \quad (12.5)$$

$$[T]_{1,2 \rightarrow x,y} = \begin{bmatrix} \cos^2 \alpha & \sin^2 \alpha & -\sin 2\alpha \\ \sin^2 \alpha & \cos^2 \alpha & \sin 2\alpha \\ 0.5 * \sin 2\alpha & -0.5 * \sin 2\alpha & \cos 2\alpha \end{bmatrix} \quad (12.6)$$

$$A_{ij}(N) = \sum_{k=1}^n \bar{Q}_{ijk}(N) * t_k \quad (12.7)$$

Finally, the properties of the inverse stiffness matrix $[A(N)]^{-1}$ were used to calculate the stiffness properties of the multidirectional lay-up. Moduli $E_x(N)$ and $E_y(N)$, shear modulus $G_{xy}(N)$, and Poisson's ratios $\nu_{xy}(N)$ and $\nu_{yx}(N)$ were evaluated according to (12.8-12.12). t represents the total thickness of the multidirectional lay-up [8].

$$E_x(N) = \frac{1}{(A^{-1})_{11}(N)*t} \quad (12.8)$$

$$E_y(N) = \frac{1}{(A^{-1})_{22}(N)*t} \quad (12.9)$$

$$G_{xy}(N) = \frac{1}{(A^{-1})_{66}(N)*t} \quad (12.10)$$

$$\nu_{xy}(N) = -\frac{(A^{-1})_{12}}{(A^{-1})_{22}} \quad (12.11)$$

$$\nu_{yx}(N) = -\frac{(A^{-1})_{12}}{(A^{-1})_{11}} \quad (12.12)$$

For the calculation of the stiffness properties of the multidirectional lay-up with CLT, different input parameter sets were used. The first calculations were performed with quasi-static values which were equal to cycle dependent properties measured with cyclic tensile test procedure after 0 cycles ($N_f = 0$). For fatigue loads, it is well known that the progress of stiffness decreases depends on the applied load. Higher applied loads usually cause faster decreases of mechanical properties. To take this aspect into account, three different load levels and consequently three different numbers of cycles to failure were used as input parameters for the cycle-dependent classical laminate theory. The properties of the multidirectional specimen were calculated with different input parameter sets up to $2*10^4$ (N_2), $1*10^5$ (N_3) and $1.5*10^6$ cycles (N_4). Beyond the distinction of number of cycles to failure (N_f to N_4), the shear modulus was implemented in two different ways:

Alternative 1:

- UD 0°, UD 45° and UD 90° specimens were used for the creation of input parameters for CLT.
- G_{12} was calculated by using E_{11} , E_{45} and E_{22} (12.1).

- By analysing only the unidirectional plies used for building the multidirectional lay-up, interactions between the plies when embedded in a composite were entirely neglected.

Alternative 2:

- UD 0°, UD 90° and ±45° specimens were used for the creation of input parameters for CLT.
- G_{12^*} was measured in in-plane shear tests with ±45° specimens (12.2).
- By using ±45° plies as input, the behaviour between the +45° and -45° layers in the multidirectional lay-up might be represented in a more realistic way.

These variations made a total of eight input parameter versions. The parameter sets will be abbreviated in the following. For the eight different input versions the designations “input 1.1” to “input 4.2” were used. The first number of the designations (e.g. Input 1.-) described the applied load level by number of cycles to failure (N_1 to N_4). The second number (e.g. Input -.1) provided information about which of the two alternatives for evaluating the shear moduli were implemented in the CLT. For example, input 4.2 included Young’s moduli and Poisson’s ratios measured on the lowest load level up to $N_4 = 1.5 \cdot 10^6$ cycles. The shear moduli were evaluated from ±45° specimens as described in alternative 2. The respective outputs calculated with the classical laminate theory are abbreviated in the same way.

12.4.4. Damage mechanisms under fatigue loads

In order to contain qualitative information about the dominating damages occurring under fatigue loads, the multidirectional specimens were investigated with light microscopy. Therefore, the cyclic tests were stopped after certain numbers of cycles and the intact specimens were taken out of the servo-hydraulic test machine. On all specimens investigated in this way, the same three locations on the specimens named with mark I to mark III were photographed every time the fatigue tests were stopped (figure 12.3).

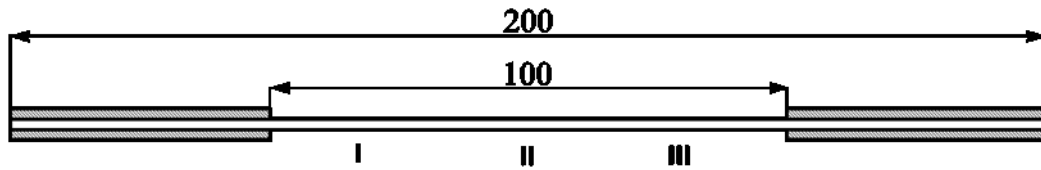


Figure 12.3: Schematic illustration of the specimens' areas investigated with light microscopy during fatigue tests.

12.5. Results

12.5.1. Quasi-static input parameters for CLT

The experimentally measured quasi-static properties of UD 0° , 45° , 90° as well as $\pm 45^\circ$ and $[0^\circ/+45^\circ/-45^\circ/90^\circ/\text{symm.}]$ specimens are presented in table 12.1. Strains were measured with a DIC system. Comments about the exact way of evaluation of the respective properties are included.

Based on the experimentally measured properties presented in table 12.1, the quasi-static input parameters for CLT (which correspond to $N_I = 0$) were created. In table 12.2, the input parameter set 1.1 including the shear modulus G_{12}' calculated by using E_{11} , E_{22} , E_{45} , ν_{12} according to (12.1) is listed. In table 12.3, in-plane shear tests with $\pm 45^\circ$ specimens were used to measure G_{12}^* . The calculated G_{12}' was higher compared to the measured in-plane shear modulus G_{12}^* .

Table 12.1: Young's moduli, shear moduli and Poisson's ratios measured in quasi-static tensile tests ($N_I = 0$).

	Moduli [GPa]	Poisson's ratios [-]	Comments
E_{11}	107.0		Tensile modulus UD 0° specimen
E_{22}	5.5		Tensile modulus UD 90° specimen
E_{45}	9.0		Tensile modulus UD 45° specimen
$E_{\pm 45}$	10.7		Tensile modulus $\pm 45^\circ$ specimen
ν_{12}		0.34	Poisson's ratio measured with UD 0° specimen (12.3)
ν_{21}		0.02	Poisson's ratio measured with UD 90° specimen, verified with (12.4)
G_{12}^*	3.3		Shear modulus from in-plane shear test with $\pm 45^\circ$ specimen according to [22]
E_x , E_y	37.3		Tensile modulus [0°/+45°/-45°/90°/symm.] specimen
ν_{xy}		0.3	Poisson's ratio [0°/+45°/-45°/90°/symm.] specimen

Table 12.2: Input parameter set 1.1 ($N_I = 0$).

	E_{11} [GPa]	E_{22} [GPa]	ν_{12} [-]	ν_{21} [-]	G_{12}' [GPa]
Input 1.1	107.0	5.5	0.34	0.02	3.8

Table 12.3: Input parameter set 1.2 ($N_I = 0$).

	E_{11} [GPa]	E_{22} [GPa]	ν_{12} [-]	ν_{21} [-]	G_{12}^* [GPa]
Input 1.2	107.0	5.5	0.34	0.02	3.3

12.5.2. Cycle-dependent moduli and Poisson's ratios as input for CLT

For cycle-dependent classical laminate theory, input parameters of UD 0°, UD 45°, UD 90° and ±45° specimens were measured with the cyclic tensile test procedure (figure 12.1). The cycle-dependent input parameters $E_{11}(N)$, $E_{22}(N)$, $G_{12}'(N)$, $G_{12}^*(N)$, $\nu_{12}(N)$ and $\nu_{21}(N)$ were evaluated before the beginning of the cyclic loading and then in intervals of 1000 cycles. It was assured in preliminary tests, that the tensile tests included in the fatigue test procedure did not influence the number of cycles to failure. Furthermore, because of loading the specimens in a quasi-static way only up to the displacement of the cyclic tests the embedded tensile tests required only a short period of time. Because of that the temperature of the specimens measured with IR sensors in fatigue tests at different load levels was not influenced by the cyclic tensile test procedure either but was similar to usual fatigue tests with constant load amplitude. Consequently, the numbers of cycles to failure measured with the cyclic tensile test procedure could be used to create conventional S-N curves as well (figure 12.4). Fatigue tests were usually stopped after $2 \cdot 10^6$ cycles. Run outs are marked with arrows in figure 12.4.

Although the S-N curves as such were not required for the classical laminate theory they could provide a good indication of the material behaviour. Each of the data points presented in figure 4 includes one cycle-dependent stiffness decrease. The evaluation of the S-N curves according to [18] is included in table 4. Slopes k of the double-logarithmic S-N curves, scatter width T_s and calculated fatigue strength σ_{max} at $5 \cdot 10^6$ cycles are presented. UD 0° specimens possessed by far the flattest slope, whereas UD 90° showed the steepest among the measured laminates. Consequently, the decrease of fatigue strength was highest for specimens tested transverse to fibre direction. The significant difference between the fatigue behaviour of ±45° and UD 45° specimens was visible in the fatigue strengths. Scatter width T_s of all tested specimens was small which indicated good reproducibility of the tests.

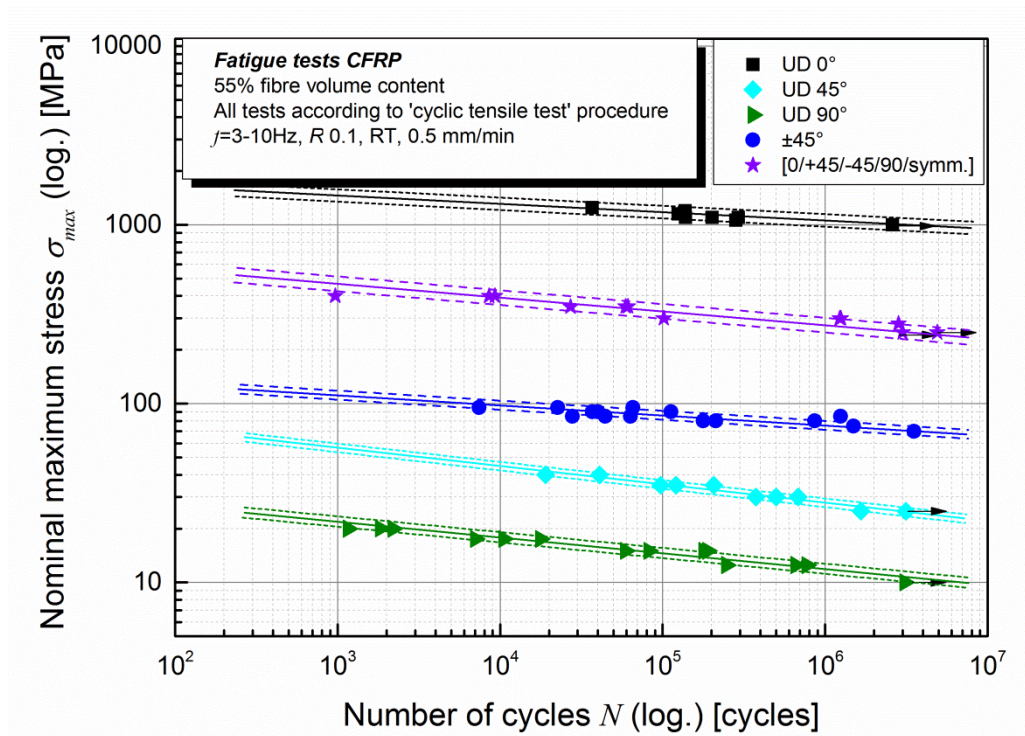


Figure 12.4: S-N curves created simultaneously to stiffness measurement with “cyclic tensile test” procedure. Each data point represents one cycle-dependent stiffness progress.

Table 12.4: Evaluation of fatigue curves: slope k , scatter width T_s and calculated fatigue strength σ_{max} at $5 \cdot 10^6$ cycles of unidirectional specimens tested at 0° , 45° , 90° , of $\pm 45^\circ$ and $[0^\circ/+45^\circ/-45^\circ/90^\circ/symm.]$ specimens, $R = 0.1$, room temperature.

	k [-]	T_s [-]	σ_{max} at $5 \cdot 10^6$ [MPa]
UD 0°	24.9	1/1.14	967.0
UD 45°	9.2	1/1.12	23.6
UD 90°	11.1	1/1.15	10.7
$\pm 45^\circ$	17.0	1/1.13	65.5
$[0^\circ/+45^\circ/-45^\circ/90^\circ/symm.]$	13.0	1/1.21	244.0

The input parameters for cycle-dependent CLT are presented in a double-logarithmic way in figure 12.5. The three different load levels were used to calculate the properties of the multidirectional lay-up up to $2 \cdot 10^4$ (Input 2.1 and 2.2.), $1 \cdot 10^5$ (Input 3.1 and 3.2) and up to $1.5 \cdot 10^6$ cycles (Input 4.1 and 4.2). Moduli decreases in fibre direction $E_{11}(N)$ depended on the level of the applied load. The higher the applied load, the earlier started the stiffness decreases. Moduli transverse to fibre direction $E_{22}(N)$ did not show any significant stiffness decrease on the contrary. This indicated that specimens failed in an abrupt way without previous damage propagation [1].

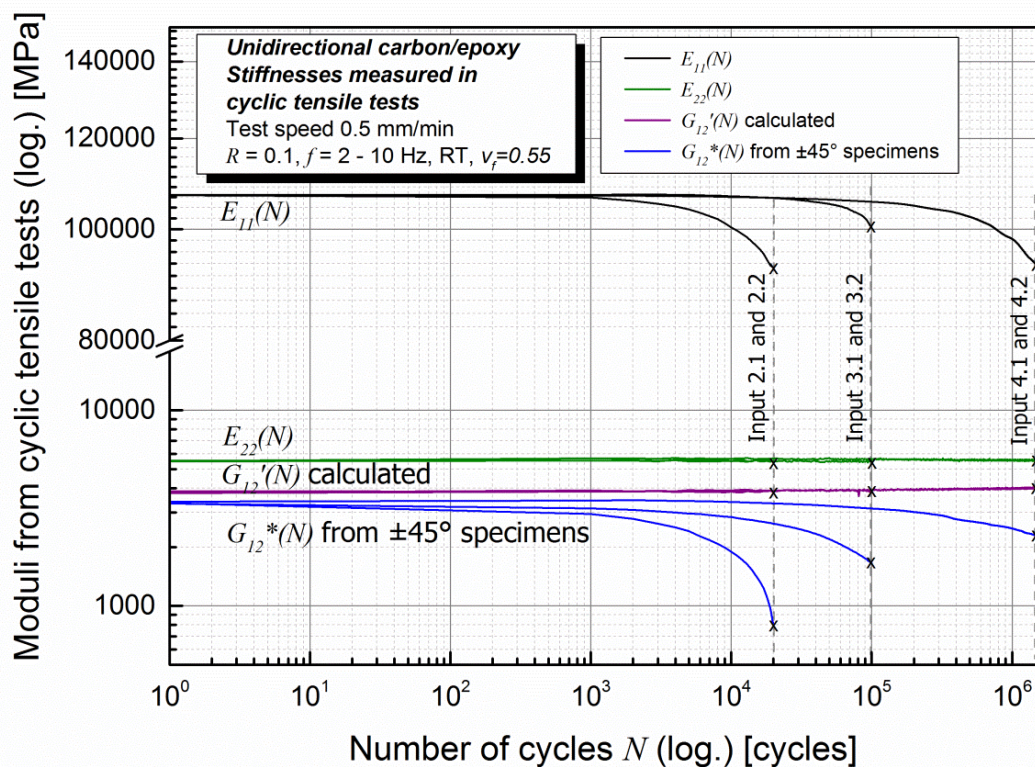


Figure 12.5: Input parameters for stiffness calculation up to $2 \cdot 10^4$, $1 \cdot 10^5$ and $1.5 \cdot 10^6$ cycles of the multidirectional lay-up by using classical laminate theory.

The comparison between $G_{12}'(N)$ and $G_{12}^*(N)$ showed clearly the different fatigue behaviour of UD 45° and $\pm 45^\circ$ specimens. Stiffness properties of UD 45° specimens, which were used for calculation of $G_{12}'(N)$, did not decrease under fatigue loads. Consequently, $G_{12}'(N)$ was almost constant for the illustrated load levels. On the contrary, stiffnesses of $\pm 45^\circ$ specimens, which possessed higher fatigue strengths than UD 45° specimens (figure

12.4), decreased apparently. The stiffness decrease of $\pm 45^\circ$ specimens might result from the possibility of relative movement of the $+45^\circ$ and -45° layers within the specimens [17]. Besides, the progress of stiffness decrease depended distinctively on the applied load level. The higher the applied load level, the faster and decreased the mechanical properties.

The minor Poisson's ratio $\nu_{21}(N)$ was measured in cyclic tensile tests with UD 90° specimens. Similar to the progress of $E_{22}(N)$, $\nu_{21}(N)$ stayed on a constant level during the entire test time. Furthermore, $E_{11}(N)$, $E_{22}(N)$ and $\nu_{21}(N)$ were used to calculate the major Poisson's ratio $\nu_{12}(N)$ (4). Because of the constant behaviour of $E_{22}(N)$ and $\nu_{21}(N)$, the progress of the major Poisson's ratio was similar to the decrease of $E_{11}(N)$ after starting at the quasi-static value.

12.5.3. Calculated stiffness degradation of multidirectional lay-up by CLT vs experiment

Table 12.5 and table 12.6 compare the calculated stiffness properties of the multidirectional lay-up with the experimentally measured E_x (which was equal to E_y because of symmetry reasons) and ν_{xy} after 0 cycles. The properties in table 5 were calculated with shear modulus according to alternative 1. In table 6 the shear modulus measured according to alternative 2 was used. For the quasi-static case ($N_I = 0$), the way of shear modulus evaluation did not have much influence on the calculated stiffness properties. In comparison to the experimentally measured E_x and ν_{xy} , calculation overestimated reality between 7 and 9 %. This might result from the fact that the implemented CLT assumed an "ideal material" and did not take cracks, voids or other imperfections into account which could cause complicated stress states in the material and therefore decrease to mechanical properties [8].

Table 12.5: Stiffness parameters of multidirectional lay-up [$0^\circ/+45^\circ/-45^\circ/90^\circ/\text{symm.}$] calculated with CLT and input parameter version 1 (Output CLT 1.1, $N_I = 0$).

E_x [GPa]	E_y [GPa]	ν_{xy} [-]	ν_{yx} [-]	G_{xy} [GPa]	E_x measured [GPa]	ν_{xy} measured [-]
40.7	40.7	0.31	0.31	1.6	37.3	0.3

Table 12.6: Stiffness parameters of multidirectional lay-up [0°/+45°/-45°/90°/symm.] calculated with CLT and input parameter version 2 (Output CLT 1.2, $N_f = 0$).

E_x [GPa]	E_y [GPa]	ν_{xy} [-]	ν_{yx} [-]	G_{xy} [GPa]	E_x measured [GPa]	ν_{xy} measured [-]
40.2	40.2	0.31	0.31	1.5	37.3	0.3

The comparison between calculated stiffness properties $E_x(N)$ and $G_{xy}(N)$ and measured $E_x(N)$ of the multidirectional lay-up is presented in figure 12.6. The absolute value of the calculated $E_x(N)$ was higher compared to the experimentally measured properties due to overestimation of the real material behaviour as already discussed. Though, the calculated qualitative stiffness decreases corresponded very well to the measured properties.

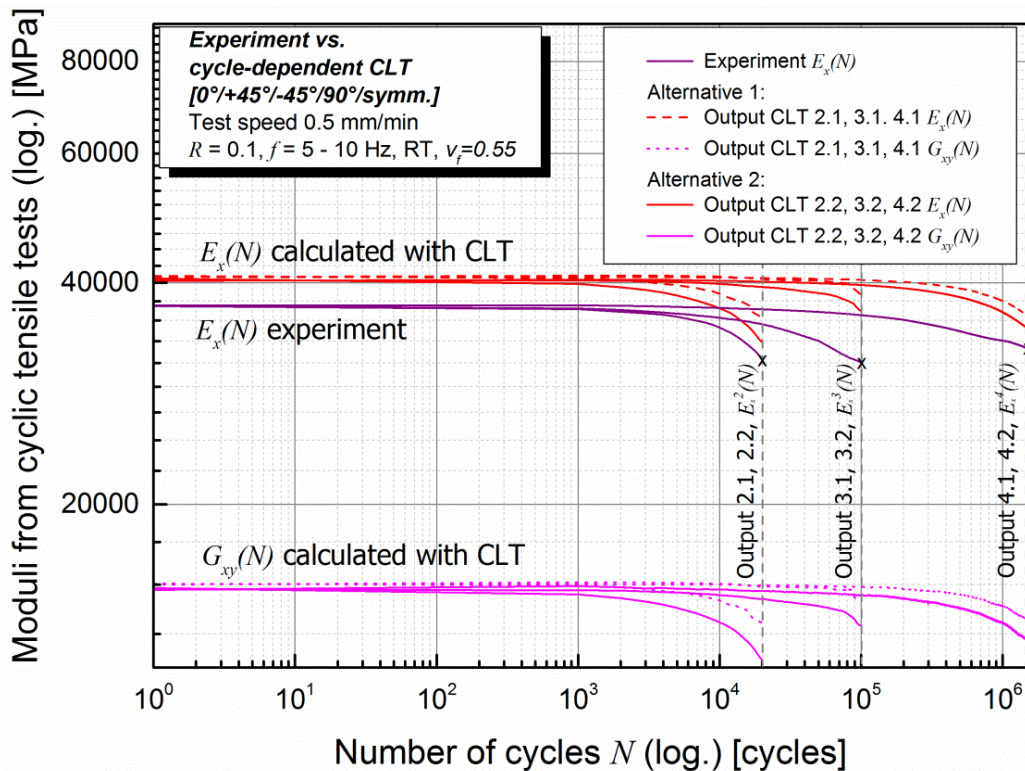


Figure 12.6: Comparison between $E_x(N)$ ($E_x^2(N)$ to $E_x^4(N)$) measured in fatigue tests and $E_x(N)$ calculated with cycle-dependent CLT on three different fatigue load levels.

For all implemented load levels, the input parameter version where $\pm 45^\circ$ specimens were used for the evaluation of the shear modulus was even closer to the reality. This observation emphasised that the mechanisms under fatigue load of unidirectional specimens were very different from the processes in multidirectional specimens. Consequently, predictions could be improved by using $\pm 45^\circ$ instead of UD 45° as input. Shear moduli $G_{xy}(N)$ decreased similarly during fatigue loading. Again, the input alternative using $\pm 45^\circ$ specimens resulted in lower values. $G_{xy}(N)$ could be verified with further experiments.

For better comparability between calculated and measured stiffness properties, table 12.7 to 12.9 list the results on three load levels after certain numbers of cycles. Table 12.7 includes the relative calculated stiffness decreases of output 2.1, 2.2 and the respective experimentally measured $E_x^2(N)$ after 0, $5 \cdot 10^3$, $1 \cdot 10^4$ and $2 \cdot 10^4$ cycles. Starting with 100 % E_x after 0 cycles, the stiffness decreases calculated with input alternative 1 were not as big as the decreases calculated with alternative 2. Alternative 2 was closer or even below the actual measured decreases.

Table 12.7: Comparison between Output 2.1, Output 2.2 and the experiment $E_x^2(N)$.

Cycle no.	E_x Alternative 1 [%]	E_x Alternative 2 [%]	E_x^2 measured [%]
0	100	100	100
$5 \cdot 10^3$	97.5	95.5	96.5
$1 \cdot 10^4$	94.8	92.0	93.3
$2 \cdot 10^4$	88.5	82.6	84.7

The relative stiffness decreases as results of the third input parameter version (output 3.1 and 3.2, $N_3 = 1 \cdot 10^5$) after 0, $1 \cdot 10^4$, $5 \cdot 10^4$ and $1 \cdot 10^5$ cycles are summarised in table 12.8. In this case, both calculation alternatives overestimated the actually measured stiffness decreases. Again, alternative 2, which used $\pm 45^\circ$ as input instead of UD 45° , was closer to reality.

Table 12.8: Comparison between Output 3.1, Output 3.2 and the experiment $E_x^3(N)$.

Cycle no.	E_x Alternative 1 [%]	E_x Alternative 2 [%]	E_x^3 measured [%]
0	100	100	100
$1 \cdot 10^4$	100	99	95.7
$5 \cdot 10^4$	98.8	96.5	88.5
$1 \cdot 10^5$	94.8	91.3	83.9

Finally, table 12.9 presents the results of output 4.1 and 4.2 ($N_4 = 1.5 \cdot 10^6$) in comparison with the respective experimental result $E_x^4(N)$ after 0, $1 \cdot 10^5$, $8 \cdot 10^5$, $1.2 \cdot 10^6$ and $1.5 \cdot 10^6$ cycles. The stiffness decrease at this load level was slower compared to the previous two. Output 4.2 described the actual stiffness decrease very well with only about 2 % deviation between calculation and experiment.

Table 12.9: Comparison between Output 4.1, Output 4.2 and the experiment $E_x^4(N)$.

Cycle no.	E_x Alternative 1 [%]	E_x Alternative 2 [%]	E_x^4 measured [%]
0	100	100	100
$1 \cdot 10^5$	99.3	98.8	96.8
$8 \cdot 10^5$	94.3	92.5	90.1
$1.2 \cdot 10^6$	91.2	88.8	88.7
$1.5 \cdot 10^6$	88.9	86.3	87.1

12.5.4. Damage mechanisms as reasons for stiffness degradation

By investigating the multidirectional specimens with light microscopy after certain numbers of cycles, basic information about occurring damages in the specimens responsible for decreasing stiffnesses could be gained. In figure

12.7, one representative multidirectional specimen which was tested at $\sigma_{max} = 300$ MPa, with a test frequency of 10 Hz and failed after about $1.6 \cdot 10^6$ cycles, which corresponds to input 4, is presented. When comparing the illustrated specimen after 10^5 cycles to the experimentally measured stiffness decreases at the lowest stress level presented in figure 12.6 and table 12.9, delaminations as well as decreased stiffness could be detected.

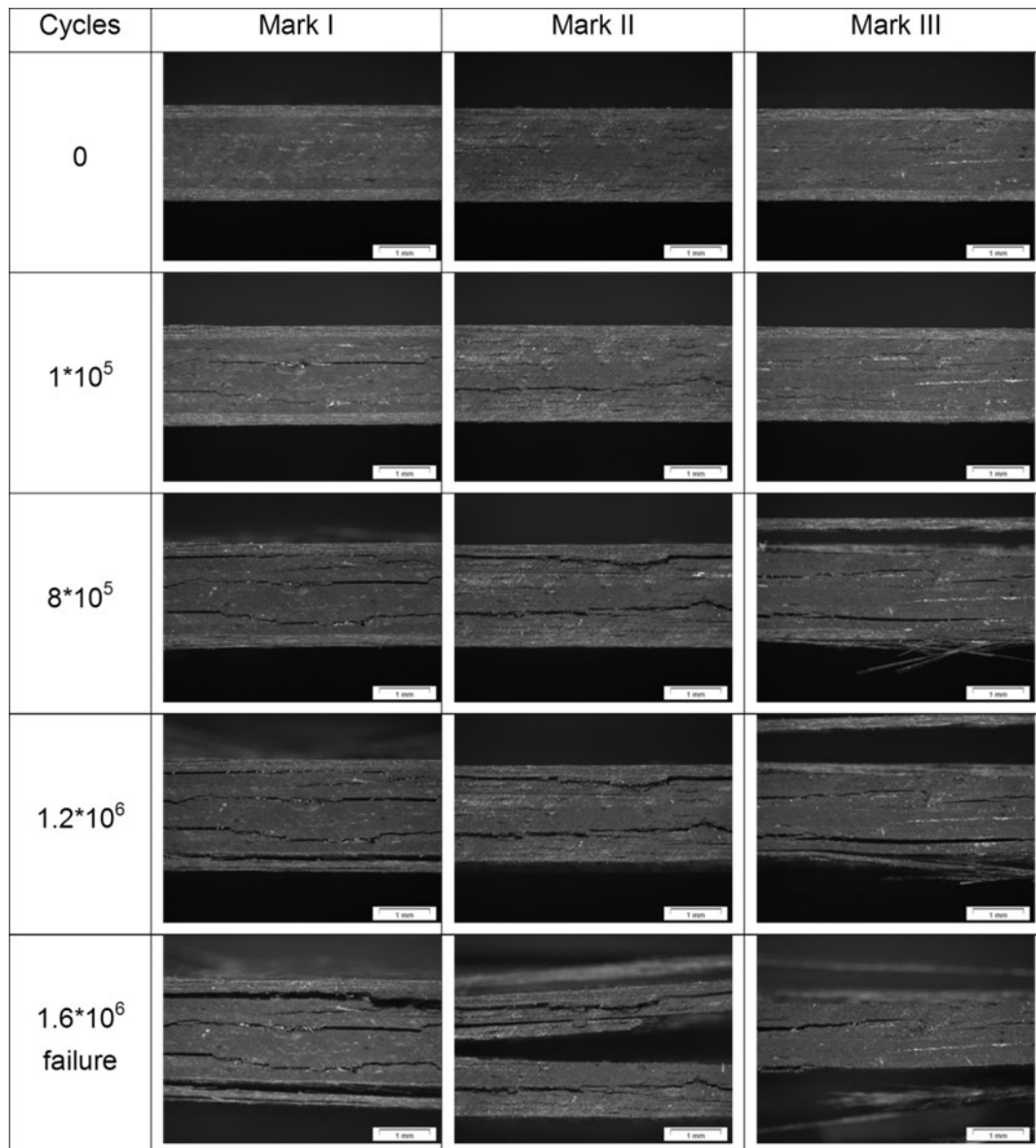


Figure 12.7: Light microscopic photographs of multidirectional specimens taken after certain numbers of cycles at defined positions of the specimens as shown in figure 12.3.

After $8 \cdot 10^5$ cycles, delaminations through the specimen widened which led to a measurable increase of thickness (or more precisely to an increasing distance between the outer layers) and further stiffness decrease. After $1.2 \cdot 10^6$ cycles, in addition to delaminations throughout the specimens, fibre breakage began in the outer layers (0°) which led to further stiffness decrease down to $\sim 88\%$ of the initial stiffness (table 12.9). After final failure of the illustrated specimen after $1.6 \cdot 10^6$ cycles, it seemed that the increasing widened delaminations had led to bending deformations from the inside of the specimen. For more detailed quantification, non-destructive testing techniques will be necessary. Besides, it has to be taken into account that small damages visible at the specimens' surfaces might be caused by edge effects.

12.6. Conclusions and Outlook

In this work, the classical laminate theory was successfully adapted for fatigue loads. The conclusions of this study are as follows:

- By using the experimental test procedure cyclic tensile tests as presented in [13], fatigue properties could be measured under quasi-static conditions and be used for well-known theories such as the CLT.
- The cycle-dependent input parameters of unidirectional plies were used to calculate the stiffness properties of a multidirectional lay-up with the adapted CLT. The fatigue-induced stiffness decreases were calculated accurately. It has been shown that the calculation with $\pm 45^\circ$ layers instead of single UD 45° was even more appropriate for stiffness calculation of the $[0^\circ/+45^\circ/-45^\circ/90^\circ/\text{symm.}]$ lay-up.
- In summary, the introduced method can be used to calculate the fatigue stiffness properties of any multidirectional lay-up once the properties of the unidirectional plies are known. Consequently, the testing time for lay-ups only differing in stacking sequence can be reduced.

In future works, the calculated shear moduli of the multidirectional lay-up G_{xy} need to be compared with experimental results. Non-destructive test

methods could be used for more detailed correlation between measured or calculated stiffness decreases on different load levels and the responsible damage mechanisms. Furthermore, the presented test procedure could be integrated in variable amplitude fatigue tests and the experimental results implemented in the classical laminate theory programmed in this work.

12.7. References

- [1] Talreja R. *Fatigue of Composite Materials*. Pennsylvania, U.S.A: Technomic Publishing Inc; 1987.
- [2] Reifsnider KL (ed.). *Fatigue of composite materials*. Amsterdam, New York: Elsevier; 1991.
- [3] Gamstedt E, Sjögren B. Micromechanisms in tension-compression fatigue of composite laminates containing transverse plies. *Composites Science and Technology* 1999;59(2):167–78.
- [4] Correa E, Gamstedt EK, París F, Mantič V. Effects of the presence of compression in transverse cyclic loading on fibre–matrix debonding in unidirectional composite plies. *Composites Part A: Applied Science and Manufacturing* 2007;38(11):2260–9.
- [5] Ladevèze P, Lubineau G. A computational mesodamage model for life prediction for laminates. In: Harris B, editor. *Fatigue in composites: Science and technology of the fatigue response of fibre-reinforced plastics*. Cambridge: Woodhead; CRC Press; 2003, p. 432–41.
- [6] Lubineau G, Ladevèze P. Towards a micromechanics-based damage mesomodel for CFRP laminates under thermomechanical cyclic loading. *Science and Engineering of Composite Materials* 2005;12(1-2):71–82.
- [7] Jones RM. *Mechanics of composite materials*. 2nd ed. Philadelphia, PA: Taylor & Francis, Inc; 1999.
- [8] Schürmann H. *Konstruieren mit Faser-Kunststoff-Verbunden: Mit 39 Tabellen*. 2nd ed. Berlin, Heidelberg, New York, NY: Springer; 2007.

-
- [9] Altenbach H, Altenbach J, Kissing W. Mechanics of composite structural elements: With 23 tables. Berlin [u.a.]: Springer; 2004.
- [10] Chaphalkar P, Kelkar AD. Classical laminate theory model for twill weave fabric composites. *Composites Part A: Applied Science and Manufacturing* 2001;32(9):1281–9.
- [11] Ng Y. Deriving Composite Lamina Properties from Laminate Properties Using Classical Lamination Theory and Failure Criteria. *Journal of Composite Materials* 2005;39(14):1295–306.
- [12] Park CH, Baz A. Comparison between finite element formulations of active constrained layer damping using classical and layer-wise laminate theory. *Finite Elements in Analysis and Design* 2001;37:35–56.
- [13] Brunbauer J, Arbeiter F, Stelzer S, Pinter G. Stiffness Based Fatigue Characterisation of CFRP. *AMR* 2014;891-892:166–71.
- [14] Brunbauer J, Pinter G. Technological approach to fatigue life prediction of CFRP. In: *ECCM16*, editor. 16th European Conference on Composite Materials; 2014.
- [15] Brunbauer J, Stadler H, Pinter G. Mechanical properties, fatigue damage and microstructure of carbon/epoxy laminates depending on fibre volume content. *International Journal of Fatigue* 2014 // 2015;70:85–92.
- [16] ASTM International. Standard Test Method for Tensile Properties of Polymer Matrix Composite Materials (ASTM D3039/D3039M-00). West Conshohocken, PA, United States: ASTM International; 2000.
- [17] Brunbauer J, Pinter G. On the strain measurement and stiffness calculation of carbon fibre reinforced composites under quasi-static tensile and tension-tension fatigue loads. *Polymer Testing* 2014;40:256–64.
- [18] ASTM International. Standard Practice for Statistical Analysis of Linear or Linearized Stress -Life (S-N) and Strain-Life (e-N) Fatigue Data (ASTM E739-91). West Conshohocken, PA, United States: ASTM International; 1991.

- [19] Baere I de, van Paepegem W, Degrieck J. Comparison of the modified three-rail shear test and the (45,45) ns tensile test for pure shear fatigue loading of carbon fabric thermoplastics. [October 23, 2013].
- [20] ASTM International. Standard Test Method for Shear Properties of Composite Materials by V-Notched Rail Shear Method(ASTM D7078/D7078M-05). West Conshohocken, PA, United States: ASTM International; 2005.
- [21] Tuttle ME. Structural analysis of polymeric composite materials. New York: Marcel Dekker; 2004.
- [22] ASTM International. Standard Test Method for In-Plane Shear Response of Polymer Matrix Composite Materials by Tensile Test of a $\pm 45^\circ$ Laminate(ASTM D3518/D3518M-94). West Conshohocken, PA, United States: ASTM International; 2007.

13. Publication 7

13.1. Bibliographic information

- Title: Computational fatigue-life prediction of continuously fibre reinforced composites
- Authors and relevant contributions to this publication:
 - Julia BRUNBAUER¹
Experimental testing, data evaluation, preparation of the publication
 - Christian GAIER²
Fatigue-life predictions, discussion and preparation of predicted results
 - Gerald PINTER³
Discussion of results
- Affiliations:
 1. Institute of Materials Science and Testing of Polymers, Montanuniversitaet Leoben, Otto Glöckel-Strasse 2, 8700 Leoben, Austria
 2. MAGNA POWERTRAIN, Engineering Centre Steyr GmbH & CoKG, Steyrer Strasse 32, 4300 Sankt Valentin, Austria
 3. Polymer Competence Center Leoben GmbH, Roseggerstrasse 12, 8700 Leoben, Austria
- Periodical: Computers & Structures
- Status: submitted

Statement with regard to this publication: The manuscript presented here is an adapted manuscript in order to fit the formatting of the thesis and does not necessarily reflect exactly the actually submitted version.

13.2. Abstract

The potential of a fatigue-life prediction method for continuously fibre reinforced carbon/epoxy laminates has been investigated. Stress analysis conducted with a finite element solver in combination with the experimentally measured anisotropic S-N curves was used as input parameters. Subsequently, lifetime of a unidirectional and a multidirectional composite was calculated for a cyclic tension-tension load case and validated with experimental fatigue tests. The predicted lifetime of the unidirectional laminate correlated well to the experimental results. For the fatigue-life calculation of multidirectional composites, some adaptations could be made. Results and possible improvements based on the presented calculations are discussed in detail.

13.3. Introduction

Continuously fibre reinforced composites have found an increasing number of applications during the last decades due to the usability in lightweight constructions and the outstanding mechanical properties. To assure both weight reduction and safety, material utilisation has to be optimised by producing load-tailored and individually designed composite parts. Assessing expected stresses and possibly occurring failure is of tremendous importance to achieve these objectives and can be realised by conducting mechanical tests and using predictive theories. In contrast to most metallic materials, highly anisotropic material behaviour has to be taken into account influencing not only the mechanical properties but also damage mechanisms.

Among different theories describing and predicting composite failure, Puck [1–3] characterised failure under quasi-static loads with a stress-based criterion considering five different failure modes. Due to the differentiation between fibre and matrix dominated failure mechanisms, Puck's criterion can consider physically motivated material behaviour rather than criteria by e.g. Hashin or Tsai-Hill [4,5]. Puck's five failure modes are defined as two modes for fibre failure (FF) under tension and compression load and three modes describing inter-fibre failure mechanisms (IFF). The IFF modes distinguish

between matrix failure due to tension (Mode A), compression (Mode B) or combined compression and shear load (Mode C) [3] (figure 13.1). Consequently, Puck's criterion allows not only the prediction of critical stresses but of the expected failure mode as well. Failure criteria are often visualised by fracture surfaces or fracture bodies. Puck's criterion and Tsai-, Hill- or Wu-like global stress criteria for the $(\sigma_1, \sigma_2, \tau_{12})$ -space are compared in a schematic way in figure 13.2 [6].

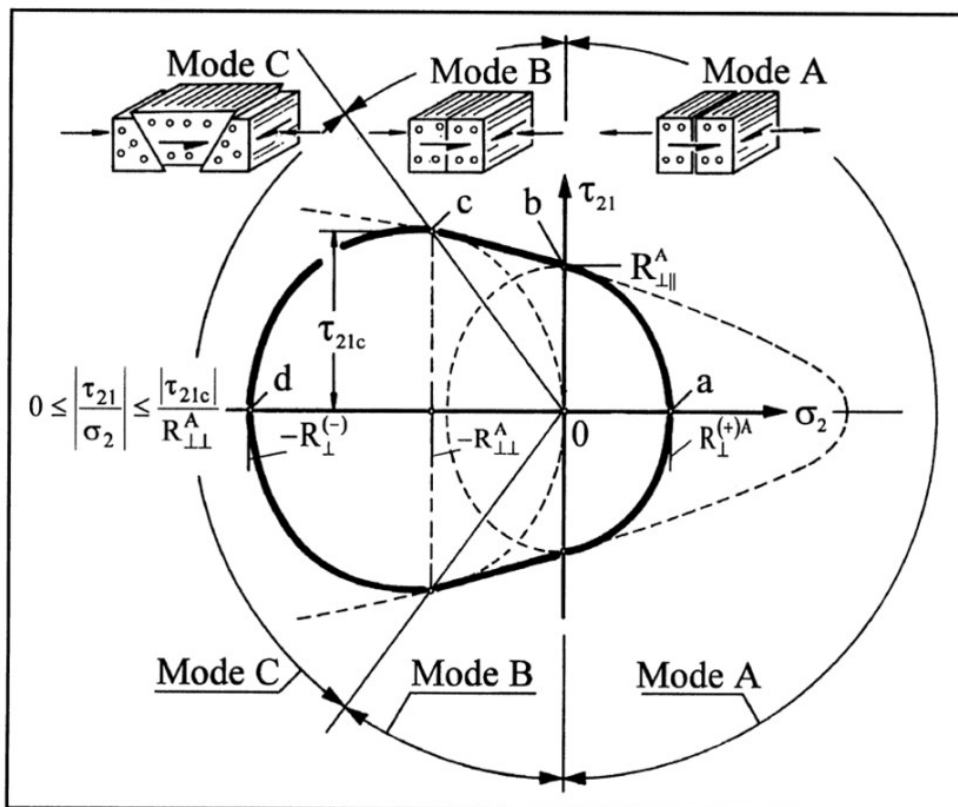


Figure 13.1: Inter-fibre fracture (IFF) modes A,B and C for $\sigma_1 = 0$ [2].

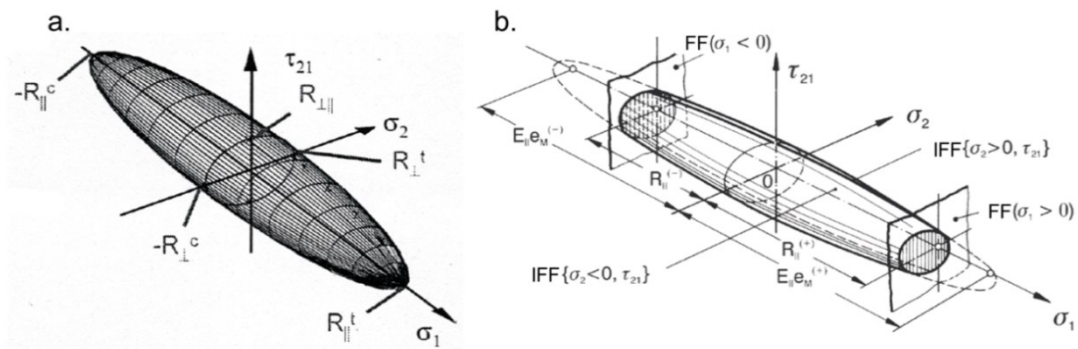


Figure 13.2: Visualisation of fracture criteria for unidirectional fibre reinforced composites: a. Tsai-, Hill- or Wu-like global stress based criteria and b. the 2D representation of Puck's action plane related criteria referring to [6].

If composite structures are exposed to cyclic loads such as mechanical loads or temperature changes, which is a very likely scenario during their operation time, the prediction of the material behaviour becomes even more complex due to the occurring damage mechanisms. Common damage mechanisms in composite materials are matrix cracking, fibre matrix debonding, delamination or fibre fracture. These damage mechanisms may change, progress or interact during fatigue-life and decrease mechanical properties such as stiffness and strength [7–9]. Beyond that, fatigue-induced damage mechanisms depend not only on the direction of fibres in relation to the applied load, but on the amplitude of the cyclic load and on the mechanical mean stress in addition. Due to the described material behaviour, accurate fatigue-life prediction tools considering the variety of aspects of continuously fibre-reinforced materials are still in their early stages. Various studies regarding this issue have been published in the last decades pursuing different approaches e.g. [10–13].

For metallic materials, theories based on fatigue strength, usually represented by stress versus number of cycles curves (S-N curves), are widely spread and have been implemented successfully in commercial software tools. One software tool is Finite Element Fatigue (FEMFAT) developed by Magna Powertrain Engineering Center Steyr GmbH & Co KG (St. Valentin, Austria). In contrast to the studies published for composite

materials so far, a very comprehensive approach is used. The real part geometry, quasi-static and fatigue material data reflecting effects on the material behaviour, the load-time history caused by the application and local stresses calculated by finite element (FE) analysis are taken into account. For each node of the finite element mesh, local S-N curves are predicted [14–16]. Critical damages are calculated according to the critical plane concept [17,18]. Thereby, damage accumulation is performed for all planes at defined angles, at each node. The plane, in which the calculated damage reaches a maximum, is considered as critical. The equivalent stresses occurring in the critical planes are classified by rainflow-counting. Subsequently, damages are calculated based on the local S-N curves and accumulated to the total damage sum. This software tool has been successfully adapted for fatigue-life prediction of orthotropic materials [19]. For injection moulded short fibre reinforced plastics, anisotropic material behaviour and effects caused by the injection moulding process can already be taken into account. The functionality of simulation chains from injection moulding simulation to life-time prediction has been presented and validated in different studies [20–22].

13.4. Fatigue-Life Prediction Method for Laminates

To meet the fatigue characteristics of continuously fibre reinforced composites, FEMFAT has been extended with a tool for lifetime estimation of laminates called FEMFAT laminate recently. Within this software tool for laminates, standard methods for the assessment of metallic parts based on S-N curves have been adapted for laminates. For each ply of the laminate, the lifetime prediction is performed. The two failure modes FF and IFF according to Puck are considered. The ply, in which the damage becomes a maximum, is considered as critical and is expected to fail first. For the assessment of FF, the stress history of the normal stress σ_l longitudinal to the fibre orientation is calculated by linear superimposition of in general multiaxial load channels. A rainflow counting algorithm is applied to obtain an amplitude-mean-rainflow-matrix of closed load cycles. Subsequently, the partial damages are analysed by using experimentally measured material S-N curves and are linearly

accumulated according to Palmgren/Miner [23,24]. For IFF as illustrated in figure 13.1, the same procedure is performed for the normal stress σ_2 transverse to the fibre orientation and for the in-plane shear stress τ_{12} and the respective material S-N curves in the fatigue-life software. To apply Puck's criterion according to figure 13.1 also combinations of σ_2 and τ_{12} have to be considered [1–3]. Nevertheless, for non-proportional loading the stress vector spanned by σ_2 and τ_{12} may change its direction with respect to time. It is difficult to apply a rainflow counting procedure in such a case. To solve this problem a simplified version of the so-called “Critical Plane – Critical Component” approach was developed [17,25,26]. By using this approach, the stress vector is projected onto several fixed directions. For each direction, the rainflow counting and the aspired damage analysis can be performed without any restrictions. The direction, which delivers the maximum damage, is assumed critical for fatigue failure. It can be mathematically interpreted as the critical component of the stress vector and it defines the type of failure mode A, B or C. To assure that each mode is covered by at least one direction, an angle of 30° is used between directions as default, leading to six directions in the σ_2 - τ_{12} -plane as shown in figure 13.3. For the damage analysis of the intermediate directions S-N curves are taken, which are obtained by interpolation between the S-N curves for σ_2 and τ_{12} .

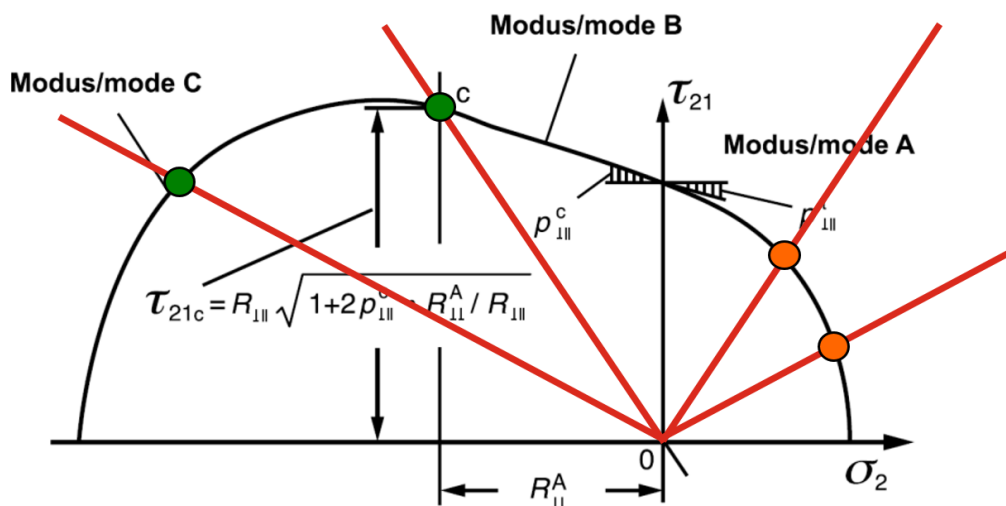


Figure 13.3: Fatigue assessment of different load directions in the laminate plane.

To consider the influence of mechanical mean stress, Haigh-diagrams are constructed from quasi-static and cyclic material parameters such as ultimate tensile strength, ultimate compressive strength, ultimate shear strength, alternating and pulsating fatigue limit for a given number of cycles e.g. $5 \cdot 10^6$ [23,24]. Due to the different strengths under tensile and compressive loads of composite materials caused by the anisotropic macroscopic material behaviour, a highly asymmetric Haigh-diagram for tensile-compressive loading transverse to the fibre direction is obtained. The Haigh-diagram for shear loading appears symmetric. For intermediate directions, which cannot all be covered by experimental tests, the Haigh-diagrams are interpolated with a smooth transition between tensile-compressive loading at an angle of $\varphi = 0^\circ$ and shear loading at $\varphi = 90^\circ$ resulting in a Haigh-surface as schematically illustrated in figure 13.4. The static limitations of the Haigh-surface at the left hand side (yellow line in compressive domain) and right hand side (red line in the tensile domain) are determined by Puck's criterion.

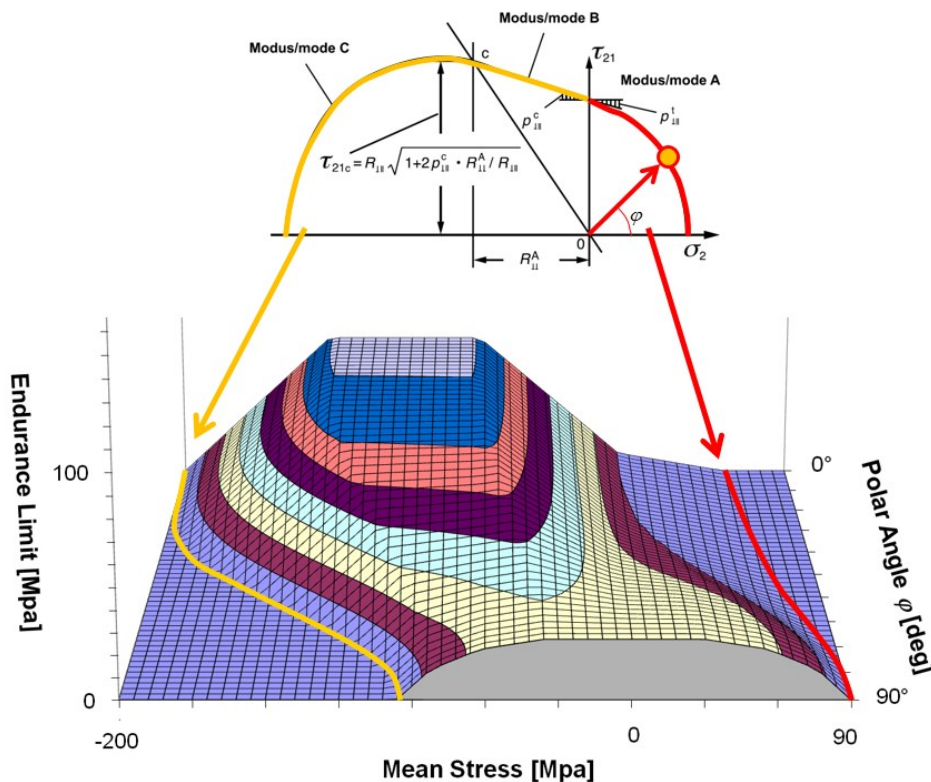


Figure 13.4: Sketch of a Haigh diagram for IFF according to [17,25,26].

13.5. Experimental Work

Unidirectional (UD) lamina made of carbon fibres and epoxy resin were tested at angles of 0° , 45° and 90° . Lay-ups consisting of $\pm 45^\circ$ and $[0^\circ/+45^\circ/-45^\circ/90^\circ/\text{symm.}]$ layers were both symmetric referring to the middle plane. The fibre volume content of all specimens was 55 % (measured by thermo gravimetric analysis as published in [27]). UD 0° plies consisted of four layers; all other specimens were made of eight layers. The specimens' geometry used in quasi-static tensile and tension-tension fatigue tests was 200x10x1 mm (length x width x thickness) for UD specimens in fibre direction and 200x20x2 mm for all other specimens. For quasi-static compression and tension-compression fatigue tests, specimens' geometry was 110x10x2 mm (UD 0°) and 110x20x2 mm, respectively. Aluminium tabs (length: 50 mm, thickness: 1 mm) were glued on both sides of all specimens. The schematic dimensions for UD 0° are illustrated for tension (figure 13.5) and compression tests (figure 13.6).

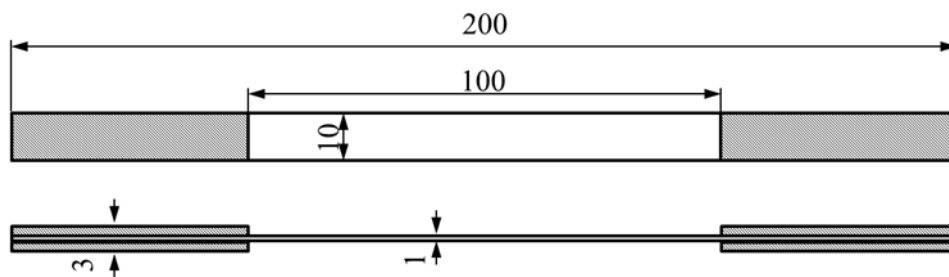


Figure 13.5: Schematic illustration of UD 0° specimens' geometry used for quasi-static tensile and tension-tension fatigue tests (in mm).

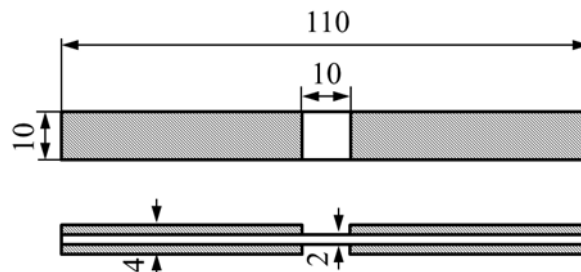


Figure 13.6: Schematic illustration of UD 0° specimens' geometry used for quasi-static compression and tension-compression fatigue tests (in mm).

Quasi-static and fatigue tests were performed on a servo-hydraulic test machine equipped with a load frame and load cell for 100 kN by MTS Systems Corporations (Minnesota, USA) at room temperature. Hydraulic wedge pressure of 5 MPa was chosen in order to prevent slipping without damaging the specimens. Good adhesion between aluminium tabs and carbon/epoxy specimens was assured in preliminary tests. Gauge length was 100 mm for tensile and 10 mm for compression loads. Quasi-static tension and compression tests were performed with a test speed of 0.5 mm/min until failure. During quasi-static tests a digital image correlation (DIC) system by GOM (Braunschweig, Deutschland) was used for strain measurement in and transverse to fibre direction in order to calculate Poisson's ratios. Tensile moduli were calculated according to [28]. Compressive moduli were evaluated between 0.001 and 0.003 absolute strain according to [29]. Shear moduli were evaluated as in-plane shear response in tensile tests with $\pm 45^\circ$ specimens [30]. Tension-tension fatigue tests were performed with the R -value (= minimum force / maximum force) of 0.1, tension-compression fatigue tests with $R = -1$ until failure. If number of cycles exceeded $2 \cdot 10^6$, tests were usually stopped. For the creation of S-N curves, specimens were tested at four different stress levels. A minimum of three specimens were tested on each stress level. Test frequency was chosen between 2 and 10 Hz depending on the test load and the specimens' tendency for hysteretic heating [31]. Specimens' temperatures were controlled by infrared sensors in all tests. Results of fatigue tests were evaluated statistically to calculate the slope of the S-N curves k , scatter with T_s and the nominal stress amplitude after $5 \cdot 10^6$ cycles σ_a at $5 \cdot 10^6$ according to [32].

13.6. Results and Discussion

13.6.1. Test Results for Quasi-Static Loading

The results of quasi-static tensile and compressive tests are presented in the way they were used as input parameters for the software tools. Material parameters in fibre direction are summarised in table 13.1, mechanical properties transverse to fibre direction are presented in table 13.2 and shear properties evaluated with $\pm 45^\circ$ specimens in table 13.3. The shear moduli G_{13}

and G_{23} necessary for FE analysis were not measured experimentally but assumed as 3.3 GPa and 2.0 GPa.

Table 13.1: Quasi-static input parameters evaluated in quasi-static tension and compression tests in fibre direction.

Young's modulus in fibre direction [GPa]	107.0
Elastic Poisson's ratio [-]	0.34
Elongation at rupture [%]	1.35
Ultimate tensile strength [MPa]	1550
Tensile strength at 0.2% strain [MPa]	235
Ultimate compressive strength [MPa]	549

Table 13.2: Quasi-static input parameters evaluated in quasi-static tension and compression tests transverse to fibre direction.

Young's modulus transverse to fibre direction [GPa]	5.5
Ultimate tensile strength [MPa]	33
Tensile strength at 0.2% strain [MPa]	11
Ultimate compressive strength [MPa]	89
Compressive strength at 0.2% strain [MPa]	13

Table 13.3: Quasi-static shear input parameters evaluated in quasi-static tension tests with $\pm 45^\circ$ specimens.

In-plane shear modulus G_{12} [GPa]	3.3
In-plane shear strength [MPa]	74
In-plane shear strength at 0.2% shear strain [MPa]	8

13.6.2. Results of Fatigue Tests

Fatigue data of UD 0° , UD 90° and $\pm 45^\circ$ were used as input parameters for fatigue-life prediction. The experimentally measured S-N curves for $R = 0.1$ and $R = -1$ at room temperature are illustrated as nominal stress amplitudes σ_a versus number of cycles in figure 13.7. Slope k , scatter width T_s and nominal stress amplitude after $5 \cdot 10^6$ cycles σ_a at $5 \cdot 10^6$ of the S-N curves are summarised in detail in table 13.4.

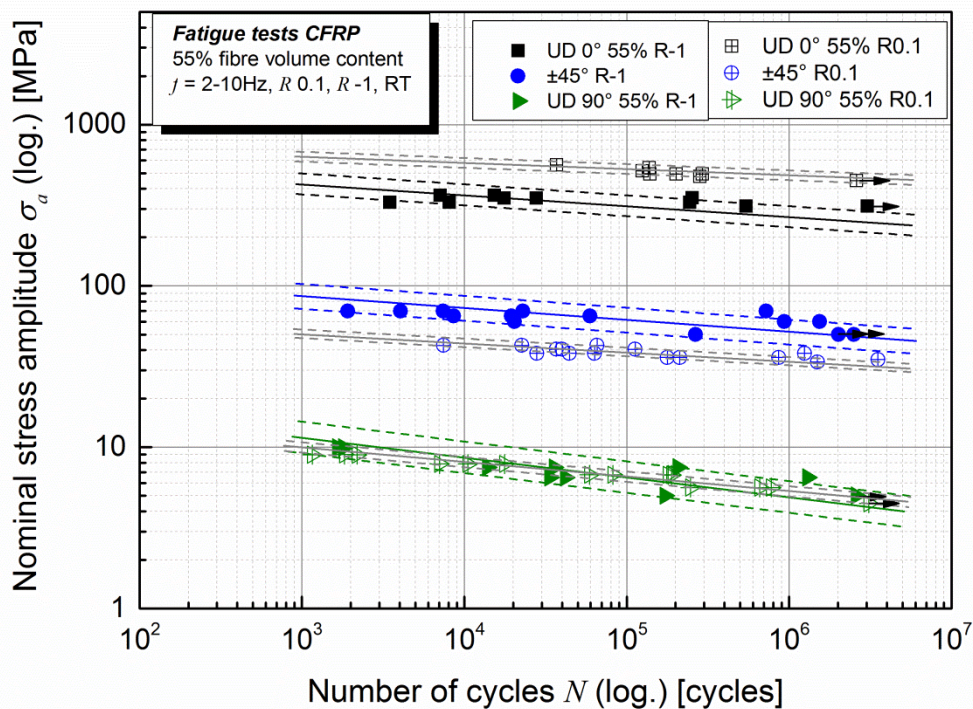


Figure 13.7: S-N curves of unidirectional laminates tested until failure at angles of 0° and 90° as well as $\pm 45^\circ$ specimens with stress ratios $R = 0.1$ and $R = -1$, RT, which were used as input parameters for fatigue-life prediction.

Pulsating fatigue amplitudes ($R = 0.1$) were higher for specimens in fibre direction than alternating amplitudes ($R = -1$) as a result of the quasi-static ultimate compressive strength being approximately 30 % of the ultimate tensile strength (table 13.1). On the contrary, alternating amplitudes were higher than pulsating amplitudes for $\pm 45^\circ$ specimens. For specimens tested

transverse to fibre direction, the mean stress did not significantly influence the fatigue strengths.

Table 13.4: Slope k , scatter width T_s and nominal stress amplitude after $5 \cdot 10^6$ cycles σ_a at $5 \cdot 10^6$ for $R = 0.1$ and $R = -1$ of fatigue tests with UD 0° , UD 90° and $\pm 45^\circ$ specimens used as input parameters for fatigue-life prediction.

Specimen	R [-]	k [-]	T_s [-]	σ_a at $5 \cdot 10^6$ [MPa]
UD 0°	0.1	24.9	1/1.14	435.2
UD 90°	0.1	11.1	1/1.15	4.8
$\pm 45^\circ$	0.1	17.0	1/1.13	29.5
UD 0°	-1	13.4	1/1.41	248.4
UD 90°	-1	8.0	1/1.58	4.2
$\pm 45^\circ$	-1	13.5	1/1.45	43.4

For the implementation in FEMFAT Laminate, the respective maximum cyclic stresses for $R = 0$ and $R = -1$ after $5 \cdot 10^6$ cycles and the slopes of S-N curves were required. Therefore, fatigue data measured at $R = 0.1$ in combination with mean stress effect [23,24] were used to calculate pulsating tension fatigue strength of 928.2 MPa (in fibre direction) and 9.95 MPa (transverse to fibre direction) for $R = 0$. Shear fatigue strength after $5 \cdot 10^6$ required by the software tool were calculated by dividing the fatigue strengths of $\pm 45^\circ$ specimen by two [30]. Consequently, pulsating shear fatigue strength for $R = 0$ was 30.8 MPa. The alternating fatigue strengths were equal to the stress amplitudes σ_a at $5 \cdot 10^6$ measured at $R = -1$ and listed in table 13.4.

For verification of the calculations obtained by the described fatigue analysis method, experimental fatigue tests with pulsating loading ($R = 0.1$) of two additional laminate configurations, UD 45° and a multi-layer composite [$0^\circ/+45^\circ/-45^\circ/90^\circ/\text{symm.}$], were performed. These test results in combination

with S-N curves of UD 0°, UD 90° and ±45° specimens are visualised for tension-tension loading at $R = 0.1$ in figure 13.8.

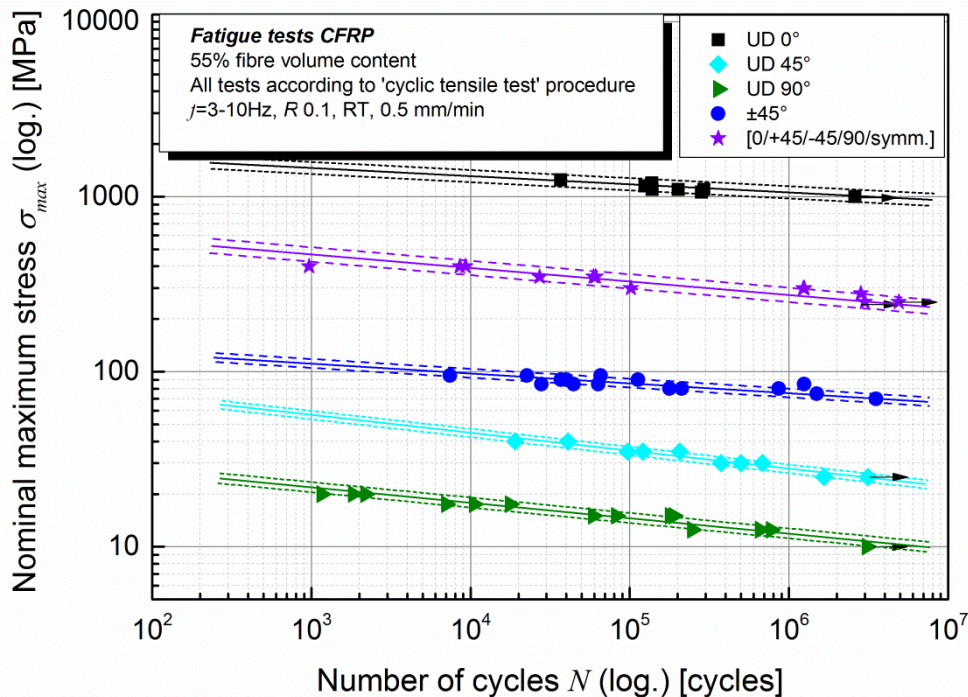


Figure 13.8: S-N curves of unidirectional laminates tested until failure at angles of 0°, 45° and 90° as well as ±45° specimens and [0°/+45°/-45°/90°/symm.] at stress ratios $R = 0.1$ [33].

13.6.3. FE Analysis

For the finite element analysis of deformation and stresses with the FE solver ABAQUS, the specimens were modelled with linear quadrilateral shell elements. In the ABAQUS input file, the thickness and material of each ply and the orientation of the fibres are defined in a shell section with the attribute COMPOSITE. The used stiffness parameters are summarised in tables 13.1 to 13.3. To obtain correct clamping conditions, also the Aluminium tabs were modelled with shell elements and connected to the laminates. For modelling of the Aluminium tabs, tensile modulus of 70 GPa and Poisson's ratio of $\nu = 0.34$ were assumed.

13.6.4. Fatigue-Life Prediction

For fatigue-life prediction with FEMFAT an input material dataset was generated as a first step. Quasi-static material properties as presented in tables 13.1 to 13.3 were implemented. Furthermore, the fatigue strengths for alternating and pulsating loading in and transverse to the fibre orientation and for shear loading were implemented. Based on those data, Haigh-diagrams were constructed (figure 13.9). In contrast to the behaviour known from metallic materials, the tensile mean stresses had a positive effect on the fatigue-life for loading in fibre direction which corresponded to the high quasi-static material properties in fibre direction (table 13.1).

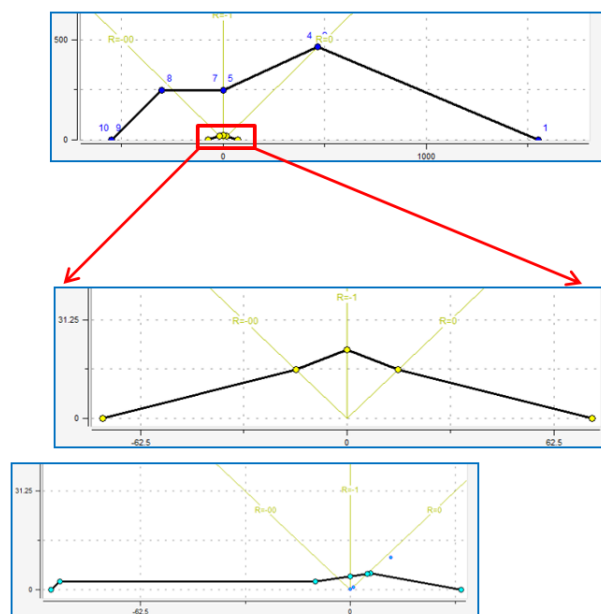


Figure 13.9: Haigh-diagram for loading in fibre direction (top), shear Haigh-diagram (middle) and Haigh-diagram for loading transverse to the fibre orientation (bottom).

Furthermore, fatigue-life predictions were performed for the UD 0°, UD 90° and ±45° specimen in order to check the validity of the input data. The check was assessed successfully if the fatigue simulation produced the same S-N curves as the ones experimentally measured. A perfect fit with experimental test results could be obtained for UD 0° and UD 90° specimens as illustrated with red lines drawn in comparison to the experimental results in figure 13.10. For the two implemented load cases, tension-tension and tension-

compression, the produced input data in and transverse to fibre direction fitted the experimental data very well. For $\pm 45^\circ$, the damage distribution along the specimens calculated by the software was not as homogeneous as for UD 0° and UD 90° specimens. The disturbed damage distribution in the area of the clamping of the specimen is schematically illustrated in figure 13.11. This effect might be caused by the two different directions of layers within the specimen, $+45^\circ$ and -45° , resulting in a stress introduction into the specimen different from uniaxial specimen. However, the obtained damage distribution reflected the lay-up of the laminates and corresponded to the failure locations monitored in fatigue tests. To address this effect, two different input parameter sets were tested, one corresponding to the area of clamping and one to a position in the middle of the specimen. Consequently, the correlation between calculation and experimental results was best in the undisturbed middle region of the specimen which was used as input for subsequent fatigue-life prediction (figure 13.10).

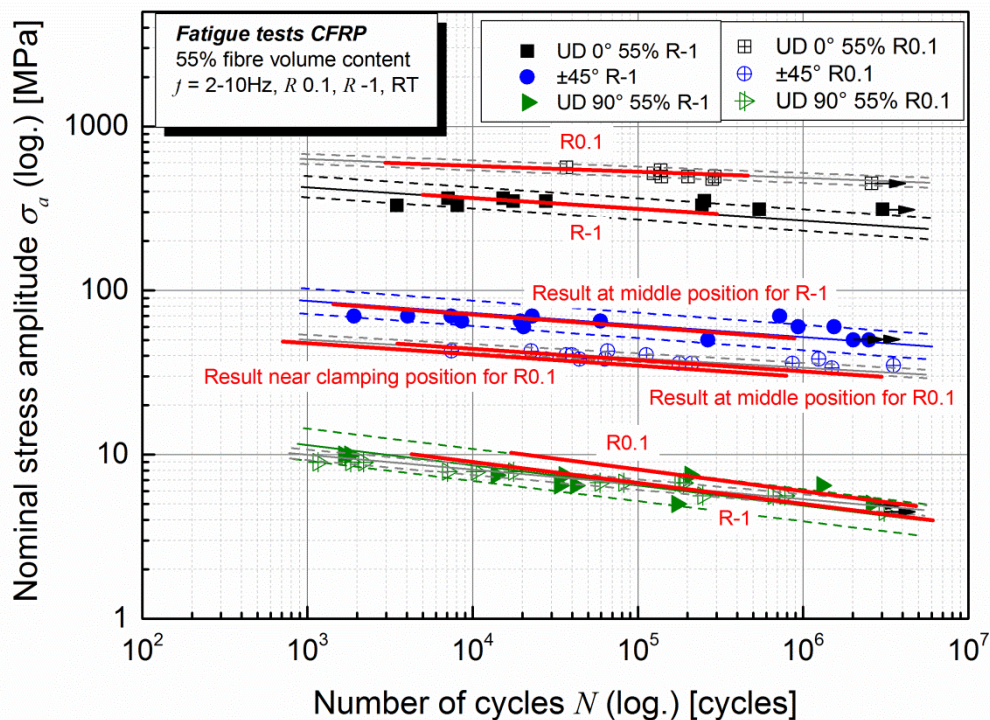


Figure 13.10: Comparison of simulation results (red lines) with test results. For $\pm 45^\circ$ the results depended on the position on the specimen.

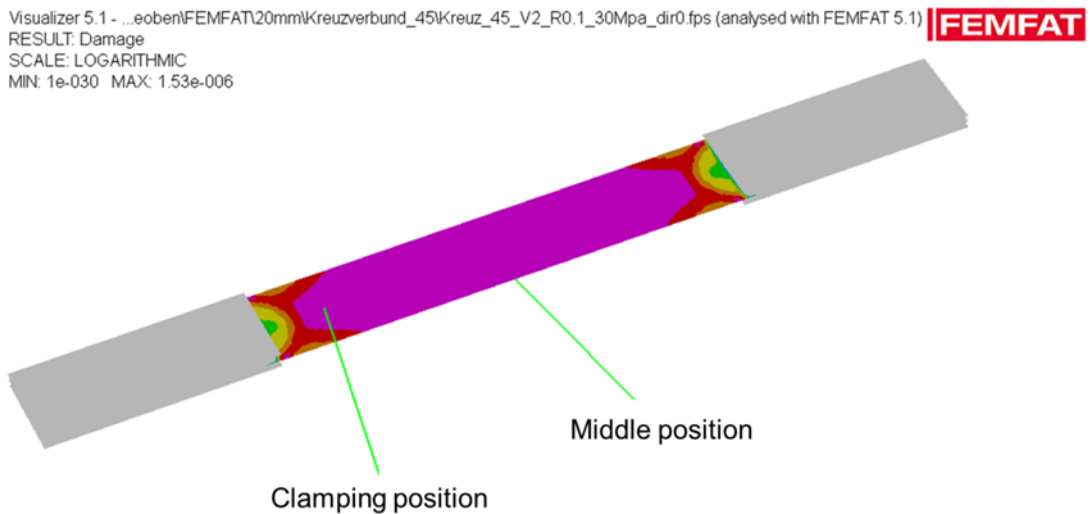


Figure 13.11: Schematic illustration of the inhomogeneous damage distribution near the clamping for the $\pm 45^\circ$ specimen with stress ratio $R = 0.1$.

Based on the input parameter sets validated for $R = 0.1$ and $R = -1$, the fatigue-life of the UD 45° specimens, in which all layers were aligned at the same angle of 45° , and of a multiaxial lay-up with the stacking sequence $[0^\circ/+45^\circ/-45^\circ/90^\circ/\text{symm.}]$ were predicted subsequently. Due to the unidirectional lay-up of the UD 45° specimen and the fixed clamping, asymmetric stress distribution resulting in inhomogeneous damage distribution were obtained (figure 13.12). For this case not the shear stress was responsible for fatigue failure as supposed by intuition, but the normal stress transverse to the fibre direction for both investigated locations at the middle of the specimen and at the clamping position. Consequently, the best correlation with experimental results was again obtained for the middle position as presented in figure 13.13. It can be assumed, that the stresses at the clamping position were too high because of singularity effects at the edges, where Aluminium tabs were connected to the laminate. Only a very detailed modelling of notch radii with finite solid elements may increase the accuracy at such positions, which nevertheless would be too much effort in daily engineering practice.

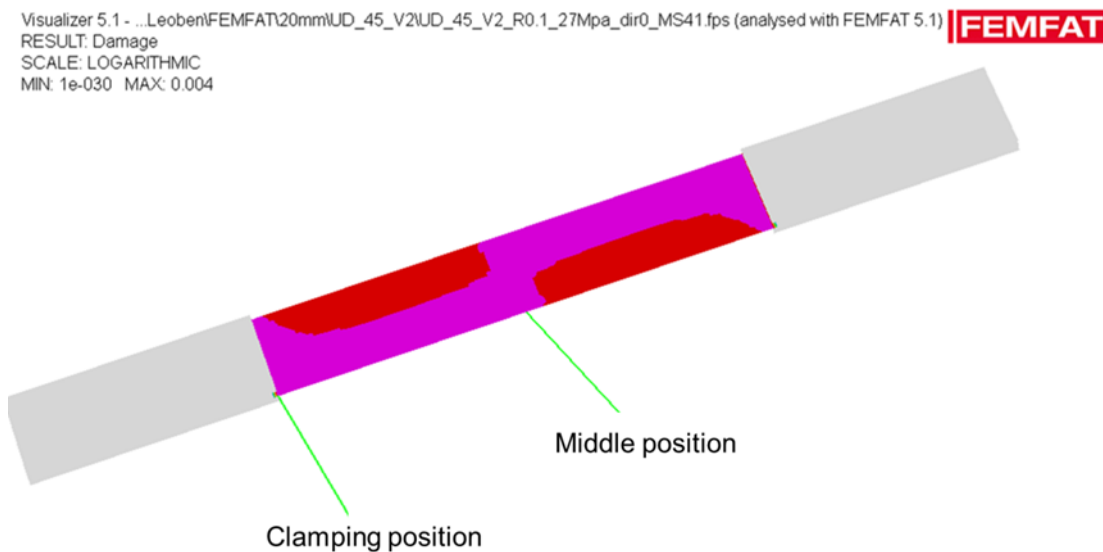


Figure 13.12: Schematic illustration of the inhomogeneous damage distribution for the UD 45° specimen with stress ratio $R = 0.1$.

For the multi-layered composite, the predictive situation was quite different. Due to the functional principle of the fatigue-software tool of analysing the laminate ply by ply, interactions between the plies influencing in the total behaviour of the entire laminate were not taken into account. Consequently, the fatigue-life prediction assuming that the 90° ply at the middle plane of the [0°/+45°/-45°/90°/symm.] specimen was critical for failure which resulted in predictions far beyond the test result for total failure (red line in figure 13.13). If continuing the fatigue-life calculation after the assumed failure of the 90° plies, ±45° and 0° would still carry load until the neighbouring plies with -45° orientation and subsequently the plies with +45° orientation would fail, schematically drawn in figure 13.13. At last, only the 0° plies would carry the load. The stresses in the 0° plies were four times larger than the nominal stress at this point. If this obtained stress was taken for fatigue-life calculation by hand using the measured UD 0° S-N curve, one would obtain almost exactly the test result.

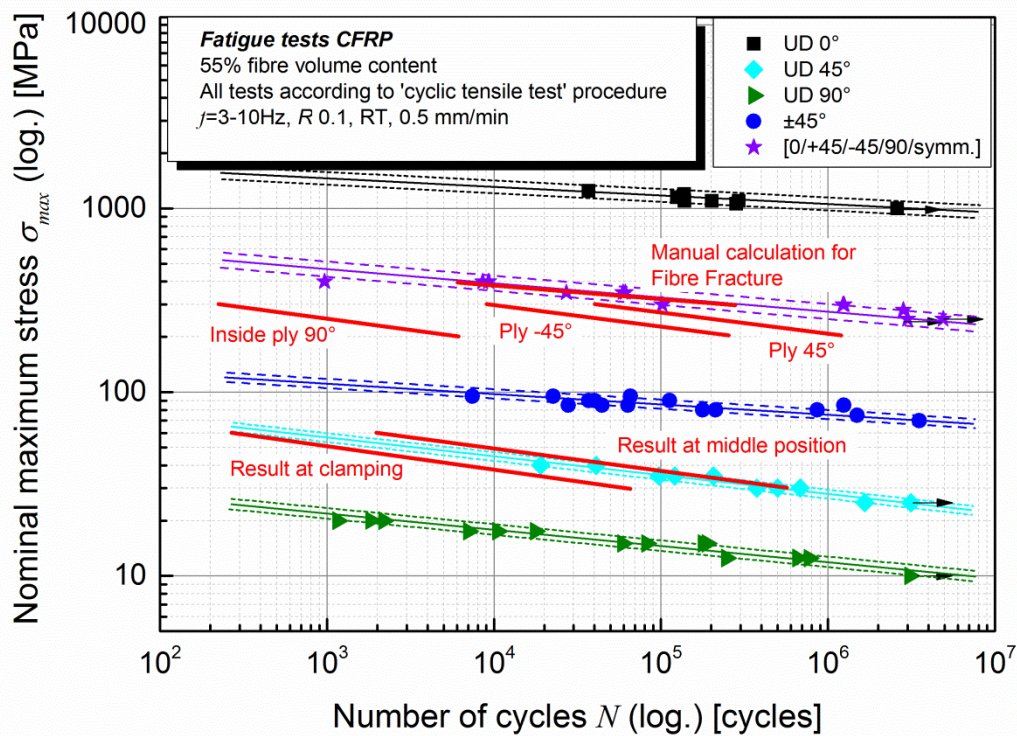


Figure 13.13: Comparison of simulation results (red lines) with test results for UD 45° and multi-layered composite [0°/+45°/-45°/90°/symm.].

13.7. Conclusions and Outlook

In this work, quasi-static and fatigue data of carbon/epoxy laminates were measured longitudinal and transverse to the fibre orientation and also for shear loading to characterise the anisotropic fatigue behaviour of the material. The obtained experimental data were used as input parameters for the commercially available, software-based fatigue-life prediction method FEMFAT Laminate which enables the assessment of fibre and inter fibre fracture even for non-proportional loading. Fatigue-life of a unidirectional 45° laminate and a multi-layer composite were calculated and validated with experimental results.

As a first step, the cyclic input material data were assessed in order to check the validity of the calculations. Good simulation results could be obtained for

UD laminates in and transverse to fibre direction and also for $\pm 45^\circ$ orientation. However, clamping positions should be excluded from fatigue assessment, because finite shell element models could not represent the physical conditions adequately. By considering the influence of clamping on the damage distribution, the fatigue-life of the UD 45° could be predicted very accurately. For the fatigue-life calculation of the multi-layered composites with the stacking sequence $[0^\circ/+45^\circ/-45^\circ/90^\circ/\text{symm.}]$, the functional principle of the software which analysed life until initial cracking of the weakest ply by the current state of the art of fatigue-life prediction (similar to the weakest link concept) influenced the results. As a consequence, the fatigue software assumed failure as soon as the 90° ply became critical. However, it could be shown that considerations beyond the point where 90° layers became critical lead to reasonable predictions even for the multi-axial lay-up.

For the accurate software-based prediction of total failure of the complete composite structure, additional research and development activities will be necessary. Especially stiffness degradation caused by fatigue-induced damage mechanisms [33,34] must be considered in an iterative way. Alternatively stress and fatigue analyses could be conducted with iteratively adapted stiffness parameters. Mathematical models will have to be developed to describe the reduction of stiffness parameters in dependence of the damage evolution. In addition, delamination will have to be considered in the future by stress components perpendicular to the laminate's plane taking into account. However, only finite solid elements will be able to deliver these stress components with sufficient accuracy.

13.8. References

- [1] Puck A. Festigkeitsanalyse von Faser-Matrix-Laminaten: Modelle für die Praxis. München, Wien: Hanser; 1996.
- [2] Puck A, Schürmann H. Failure analysis of FRP laminates by means of physically based phenomenological models. Composites Science and Technology 1998(58):1045–67.

-
- [3] Puck A, Schürmann H. Failure analysis of FRP laminates by means of physically based phenomenological models. *Composite Science and Technology* 2002(62):1633–62.
- [4] Hashin Z. Finite thermoelastic fracture criterion with application to laminate cracking analysis. *J.Mech.Phys.Solids* 1996 (Vol.44 No.7):1129–45.
- [5] Tsai S, Wu E. A General Theory of Strength for Anisotropic Materials. *Journal of Composite Materials* 1971(Vol. 5):58–80.
- [6] Deuschle H. 3D failure analysis of UD fibre reinforced composites: Puck's theory within FEA. Dissertation. Stuttgart; 2010.
- [7] Talreja R. *Fatigue of Composite Materials*. Pennsylvania, U.S.A: Technomic Publishing Inc; 1987.
- [8] Talreja R, Singh CV. *Damage and failure of composite materials*. Cambridge, New York: Cambridge University Press; 2012.
- [9] Reifsnider KL (ed.). *Fatigue of composite materials*. Amsterdam, New York: Elsevier; 1991.
- [10] Kawai M. A phenomenological model for off-axis fatigue behavior of unidirectional polymer matrix composites under different stress ratios. *Composites Part A: Applied Science and Manufacturing* 2004;35(7-8):955–63.
- [11] Ladevèze P, Lubineau G. A computational mesodamage model for life prediction for laminates. In: Harris B, editor. *Fatigue in composites: Science and technology of the fatigue response of fibre-reinforced plastics*. Cambridge: Woodhead; CRC Press; 2003, p. 432–41.
- [12] Lubineau G, Ladevèze P, Violeau D. Durability of CFRP laminates under thermomechanical loading: A micro–meso damage model. *Composites Science and Technology* 2006;66(7-8):983–92.
- [13] Philippidis TP, Vassilopoulos AP. Life prediction methodology for GFRP laminates under spectrum loading. *Composites Part A: Applied Science and Manufacturing* 2004;35(6):657–66.
- [14] Eichlseder W. Fatigue analysis by local stress concept. *Computers & Structures* 2002(80):2109–13.

- [15] Unger B, Dannbauer H, Eichlseder W. Virtual Fatigue Optimisation of Automotive Structures. *Engineering Integrity* 2004;15(1):6–13.
- [16] Gaier C, Dannbauer H. Ein effizientes kritisches Schnittebenenverfahren für duktile, semi-duktiler und spröde Werkstoffe: 1. Leobener Betriebsfestigkeitstage Planneralm, 8.-10. März 2006:145–57.
- [17] Gaier C, Pramhas G, Steiner W. An Extended Critical Plane Criterion for General Load Situations. In: Blom AF, editor. *Proceedings of the 8th International Fatigue Conference June 2-7 2002 Stockholm Sweden // Fatigue 2002: Proceedings of the Eighth International Fatigue Congress held 3-7 June, 2002, Stockholm, Sweden*. Heath, West Midlands, UK: Engineering Materials Advisory Services; 2002, p. 259–66.
- [18] Gaier C, Unger B, Dannbauer H. Multiaxial fatigue analysis of orthotropic materials. *Rev. Metall.* 2010;107(9):369–75.
- [19] Guster C, PINTER G, Mösenbacher A, Eichlseder W. Evaluation of a Simulation Process for Fatigue Life Calculation of Short Fibre Reinforced Plastic Components. *Procedia Engineering* 2011;10:2104–9.
- [20] Mösenbacher A, Brunbauer J, Pichler PF, Guster C, Pinter G. Modelling and validation of fatigue life calculation for short fibre reinforced injection moulded parts. In: *ECCM16, editor. 16th European Conference on Composite Materials*; 2014.
- [21] Gaier C. Investigations on a statistical measure of the non-proportionality of stresses. *International Journal of Fatigue* 2004;26(4):331–7.
- [22] Gaier C, Fleischer H, Guster C, Pinter G. Influence of Fiber Orientation, Temperature and Moisture on the Fatigue Behavior of Injection Molded Fiber Reinforced Thermoplastics // Einfluss von Faserorientierung, Temperatur und Feuchtigkeit auf das Ermüdungsverhalten von kurzfaserverstärkten Thermoplasten*. *MP* 2010;52(7-8):534–42.
- [23] Radaj D. *Ermüdungsfestigkeit: Grundlagen für Leichtbau, Maschinen- und Stahlbau*. 3rd ed. Berlin [u.a.]: Springer; 2007.

-
- [24] Haibach E. Betriebsfestigkeit: Verfahren und Daten zur bauteilberechnung. Berlin: Springer; 2006.
- [25] Orth M, Butz M, Gaier C. Durability Assessment of CFRP Components with Static Failure Criteria // Betriebsfestigkeitsanalyse von CFK-Bauteilen mit statischen Versagenskriterien*. MP 2014;56(7-8):559–66.
- [26] Orth M, Butz M, Gaier C. Entwicklung einer Methode zur Betriebsfestigkeitsanalyse von Strukturbauteilen aus CFK unter Zuhilfenahme verschiedener statischer Versagenskriterien. In: DVM, editor. 40. Tagung DVM Arbeitskreis Betriebsfestigkeit; 2013.
- [27] Brunbauer J, Stadler H, Pinter G. Mechanical properties, fatigue damage and microstructure of carbon/epoxy laminates depending on fibre volume content. International Journal of Fatigue 2014 // 2015;70:85–92.
- [28] ASTM International. Standard Test Method for Tensile Properties of Polymer Matrix Composite Materials (ASTM D3039/D3039M-00). West Conshohocken, PA, United States: ASTM International; 2000.
- [29] ASTM International. Standard Test Method for Compressive Properties of Polymer Matrix Composite Materials with Unsupported Gage Section by Shear Loading (ASTM D3410/D3410M-03). West Conshohocken, PA, United States: ASTM International; 2008.
- [30] ASTM International. Standard Test Method for In-Plane Shear Response of Polymer Matrix Composite Materials by Tensile Test of a $\pm 45^\circ$ Laminate (ASTM D3518/D3518M-94). West Conshohocken, PA, United States: ASTM International; 2007.
- [31] Brunbauer J, Pinter G. On the strain measurement and stiffness calculation of carbon fibre reinforced composites under quasi-static tensile and tension-tension fatigue loads. Polymer Testing 2014;40:256–64.
- [32] ASTM International. Standard Practice for Statistical Analysis of Linear or Linearized Stress -Life (S-N) and Strain-Life (e-N) Fatigue Data (ASTM E739-91). West Conshohocken, PA, United States: ASTM International; 1991.

- [33] Brunbauer J, Pinter G. Fatigue life prediction of carbon fibre reinforced laminates by using cycle-dependent classical laminate theory. *Composites Part B: Engineering* 2015;70:167–74.
- [34] Reifsnider KL, Talug A. Analysis of fatigue damage in composite laminates. *International Journal of Fatigue* 1980;2(1):3–11.
- [35] Talreja R. Damage Characterization. In: Reifsnider KL, editor. *Fatigue of composite materials*. Amsterdam, New York: Elsevier; 1991, p. 79–103.

Part VI.

Summary, Conclusions and Outlook

Summary

Carbon fibre reinforced plastics offer a variety of high-performance applications thanks to their extraordinary mechanical properties in relation to their weight. However, prior to any application, expected failure loads and location of damage have to be verified. If cyclic loads are applied and fatigue occurs, the demands on failure criteria and fatigue-life prediction are even more complex. Various studies have been performed and appropriate failure criteria for quasi-static load cases have been developed since the 1960s. Due to the complexity of fatigue propagation in composite materials, the interaction of damage mechanisms and their decreasing effect on mechanical properties, the prediction of not only expected fatigue load but also of time to failure is complicated.

In the presented thesis, the applicability of different fatigue-life prediction approaches was investigated. To be able to build calculations on reliable fatigue input parameters measured under known conditions, a comprehensive experimental study was conducted prior to the experimental evaluation of material parameter which was presented in publication 1. During these preliminary tests, the effect of test parameters on the investigated carbon/epoxy laminates such as the test frequency was evaluated in dependency of the stacking sequence. It could be shown that for unidirectional laminates the test frequency was not critical but that especially specimens with symmetric stacking sequence such as $\pm 45^\circ$ were very sensitive to the effect of hysteretic heating probably due to inner friction between the layers. To address the observed effects, frequencies for further material tests were defined. In addition to that, the issue of strain measurement in fatigue tests for subsequent strain measurement was investigated. Strain gauges, mechanical extensometers, optical systems and

the piston displacement were used to measure quasi-static stress-strain curves and stress-strain hysteresis loops. The effect of each strain measurement system on the evaluated stiffnesses was assessed. Results showed that strain gauges did not deliver reliable or reproducible strains and were very sensitive to misalignment and surface cracks. Mechanical extensometers were perfectly suitable for unidirectional specimens tested in and transverse to fibre direction and also for symmetric lay-ups. If specimens with tendency to surface cracks were tested, which occurred in specimens tested in fibre direction as well, all systems were limited. Consequently, strain measurement with optical systems or mechanical extensometers could be used to evaluate locally measured stiffnesses until the formation of first surface cracks. To measure the stress-strain hysteresis loops until fracture, the piston displacement could be used by being calibrated with the previously measured local strains. Furthermore, the experimental tests showed that the piston displacement, although it had to be considered as global strain measurement since the stiffness of the test machine was included in the measurement, could provide reasonable results.

Since the fatigue-induced damage mechanisms depend on the unique properties of each material such as the stacking sequence and may vary due to external influences, the combined effect of mechanical mean stress and fibre volume fraction was studied. The effect of fibre volume fraction might be of interest because of two reasons. First, in big structures it is likely that the fibre volume fraction is not constant along the entire component due to production influences and complex geometries. Second, because it is well-known in literature that damage mechanisms are usually induced by matrix-cracking as illustrated in chapter 1, the increasing amount of matrix material with decreasing fibre volume fraction might influence the damage behaviour as well. To address these effects, carbon/epoxy laminates with two different fibre volume fractions were produced. The plate quality and the aspired fibre volume contents were monitored with different thermo-mechanical and thermo-analytical methods as discussed in publication 2. Unidirectional laminates were tested at angles of 0° , 45° and 90° in relation to the fibre direction in fatigue tests with different mechanical mean stresses. Fracture surfaces were investigated comprehensively with scanning electron microscopy. The load cases, whether tension-tension or tension-compression

loads were applied, resulted in different damage mechanisms caused by the fibre content. While in tension-tension fatigue tests the damage behaviour of specimens with low fibre content tested transverse to fibre direction was dominated by matrix-cracking and interfacial debonding, specimens with high fibre fraction showed fibre pull-out resulting in increased fatigue strengths. With an increase of the applied load amplitude, the damage mechanisms in specimens tested transverse to fibre direction became similar and the influence of fibre volume content decreased. In tension-compression fatigue tests on the contrary, the fibre volume content had no significant influence on the fatigue strengths of specimens tested transverse to fibre direction. This observation could be ascribed to the damage mechanisms of broken fibres and fibre bundles within the fracture plane. All fatigue results were correlated with the investigated damage mechanisms and explanations, not only for specimens transverse to fibre direction but also for the other investigated angles as discussed in publications 2 and 3.

Based on the found insights in mechanical behaviour and damage mechanisms, fatigue-life prediction tools were investigated. Two different approaches were presented in this thesis. The first approach focused on fatigue-life prediction based on mechanical stiffness decreases. This approach is especially interesting because it is known that the decrease of stiffness can be correlated with the responsible damage mechanisms. To realise a fatigue-life prediction tool, the well-known classical laminate theory, which was initially developed for stiffness calculation of multidirectional composites and ply-by-ply stress analysis under quasi-static loads, was adapted for fatigue loads. Since any prediction is decisively dependent on the quality of input parameters, the experimental stiffness measurement had to be considered first. Therefore, in publications 4 and 5 the combined effect of strain-rate dependency, anisotropy and stacking sequence on the stiffness evaluation in tension-tension fatigue tests was characterised. It could be shown that especially matrix-dominated specimens such as off-axis specimens or specimens tested transverse to fibre direction tended to behave strain-dependently. As a consequence, stiffnesses calculated from stress-strain hysteresis loops measured in fatigue tests were higher than the stiffnesses measured in quasi-static tests due to the lower load speed in quasi-static tests. However, stiffnesses measured under quasi-static

conditions such as the Young's modulus or the well-known five engineering constants E_{11} , E_{22} , G_{12} , ν_{12} and ν_{21} are used to perform calculations with e.g. the classical laminate theory or Finite Element analysis. To address the strain-rate dependency, a new experimental test procedure called "cyclic tensile tests" was developed and implemented in the fatigue test software. Within this procedure, the servo-hydraulic tests machine applied a sinusoidal, cyclic tension-tension load. After a certain number of cycles, the test machine unloaded the specimen, switched to displacement control and performed a tensile test under quasi-static conditions. Subsequently, the load-controlled cyclic loading continued. By evaluating these included tensile tests, which reflect the damage due to the already applied load cycles, cycle-dependent stiffness properties measured under quasi-static conditions could be generated. Furthermore it could be validated that the included tensile tests did not influence the hysteretic behaviour or numbers of cycles to failure, which makes this test implementable in conventionally performed fatigue tests for the creation of S-N curves. The cycle-dependent stiffnesses generated in "cyclic tensile tests" with specimens at angles of 0° , 90° , 45° and $\pm 45^\circ$ were implemented in the adapted classical laminate theory presented in publication 6. The fatigue-induced stiffness decreases of a multidirectional lay-up with the stacking sequence $[0^\circ/+45^\circ/-45^\circ/90^\circ/\text{symm.}]$ were calculated on different load levels. Validation with experimental results showed good correlation and the potential of this method. Based on the measured input parameters, carbon/epoxy laminates with any stacking sequence could be predicted.

As second approach to fatigue-life prediction, the strength-based concept of S-N curves or Wöhler lines known from classical fatigue of metallic materials was adapted for composite materials. Of course, this kind of approach was initially developed for a material class with a fatigue behaviour and damage mechanisms very different from composite materials. However, due to the long experience in fatigue of metallic materials commercial software tools are available. The advantages of such software tools are that e.g. complex geometries are considered by prior Finite Element analysis or the load-time history, which is tremendous importance, can be taken into account for life-time prediction. To address the properties of composite materials beyond the already implemented tools, the Finite Element FATigue (FEMFAT) developed

by Magna Powertrain, Engineering Center Steyr, has been extended with Puck's failure criterion appropriate for anisotropic composite materials. By using this newly developed software tools designed for composite materials, the S-N curves of carbon/epoxy laminates were calculated and presented in publication 7. As a first step, the input parameters of S-N curves measured longitudinal and transversal to the fibre direction and under shear load were validated with the experimentally measured curves. These first assessments proved the good correlation of fitted and measured S-N curves. Subsequently, the fatigue-life of a unidirectional and a multidirectional composite was predicted. The calculations for the unidirectional laminate were promising and fitted the experimental results very well, especially when excluding the clamping influence. In the fatigue-life predictions of the multidirectional composite, the functional principle of the software influenced the results. Since the software assumed fracture as soon as the weakest ply failed, which was not consistent with reality where other layers were still able to carry the applied loads, reality was underestimated by the predictions. However, it could be shown that by continuing the fatigue-life prediction beyond the point of first failure, the experimentally measured fatigue behaviour could be predicted.

Conclusions and Outlook

The results and findings regarding the fatigue behaviour of carbon/epoxy composites presented in this thesis show tools for fatigue-life prediction. Both approaches applied in this thesis, stiffness and strength based models, provided reasonable results when predicting the fatigue behaviour of multidirectional carbon/epoxy composites. To be able to extend and combine the two approaches for more complex and real-life applications, the following issues need to be addressed in the future.

As basic prerequisite for any fatigue-life prediction, it has to be considered that the test parameters used for the experimental measurement of input parameters might impact the mechanical properties and consequently the performed predictions. The unique damage behaviour of each composite material influencing the decrease of properties and performance has always to be taken into account by critically reflecting the measured results and adapting the respective test parameters and test equipment if necessary.

Non-destructive test methods will be necessary in order to assess the characteristic damage mechanisms responsible for the measured stiffness decreases of the respective material in detail. Methods will have to be developed to correlate specific stiffness decreases, which should be ideally measured online during tests, with the occurring damage mechanisms. This would offer the possibility of using stiffness decreases as non-destructive test method for damage mechanisms on the one hand. On the other hand, defined stiffness decreases could be used as fatigue-life criteria for applications which are strain critical such as aircrafts. Consequently, this would allow the utilisation of the material's properties in an optimum way.

The effect of fibre volume content on the properties and damage mechanisms was investigated in this thesis. It was shown that the fibre volume content significantly influences both the mechanical performance and the damage behaviour. However, the fibre volume content is not included in the presented fatigue-life predictions so far. This inclusion would be beneficial in order to make the fatigue-life prediction tools independent from the specific material and applicable to carbon/epoxy laminates with variable fibre fractions. A possibility to realise this extension for both of the approaches pursued, stiffness and strength, could be the combination with software tools creating material models e.g. Digimat.

To make fatigue-life prediction more efficient, mathematical descriptions of the stiffness decreases measured in this thesis will be necessary. The experimentally measured stiffness data until failure are available now. However, mathematical descriptions of the measured stiffness decreases as function of anisotropy, fibre volume content, number of cycles and the applied load amplitudes will have to be developed. Based on functions describing the cyclic material behaviour, the presented stiffness based fatigue-life prediction tool could be extended for more general tasks.

Furthermore, these aspired mathematical functions describing the stiffness degradations could be included in the software-based fatigue-life prediction tool based on fatigue strengths and S-N curves as discussed in publication 7. Additionally, the inclusion of delamination modelling will have to be addressed. Since delamination is mainly driven by stresses acting perpendicular to the laminate plane, taking into account this third direction will be necessary. However, for the reproduction of three-dimensional stress states in fatigue-life prediction and in the previous stress analysis, the adaption of solid elements, which are able to transport these stresses, will have to be conducted. Beyond that, the characterisation of input parameters will have to be extended in order to take the influences of e.g. temperature, humidity, notches or variable load amplitudes on the fatigue behaviour into account. For the cyclic tests necessary to reflect these effects, the cyclic tensile test procedure developed in this thesis should be included. By performing cyclic tests with this procedure, both fatigue-induced stiffness

decreases measured under quasi-static conditions and number of cycles to failure can be evaluated with one coupon.

The consideration of the suggestions made and a combination of the two presented approaches could lead to the development of a comprehensive, software-based approach towards fatigue-life prediction. By including geometry influences, finite element analysis, load-time history, material S-N curves, anisotropic failure criteria and prospectively also stiffness degradation, delamination and material models describing the properties in dependency of fibre volume fraction, the fatigue-life of composite materials might become predictable even for complex applications.

Appendix

Symbols

Designation	Unit	Description
v_f , %	[%]	Fibre volume fraction
σ_1	[MPa]	Normal stress longitudinal to fibre direction
σ_2	[MPa]	Normal stress transversal to fibre direction
σ_3	[MPa]	Normal stress perpendicular to the $\sigma_1 - \sigma_2$ plane
τ_{13}, τ_{12}	[MPa]	Shear stresses acting perpendicular to σ_1
τ_{21}, τ_{23}	[MPa]	Shear stresses acting perpendicular to σ_2
τ_{31}, τ_{32}	[MPa]	Shear stresses acting perpendicular to σ_3
σ_{11}	[MPa]	Normal stress longitudinal to direction of the applied load
σ_{22}	[MPa]	Normal stress transversal to the direction of the applied load
ε_{11}	[%]	Strain longitudinal to load direction
ε_{22}	[%]	Strain transversal to load direction
ε_{Break}	[%]	Strain at failure

SYMBOLS

γ_{12}	[%]	Shear strain caused by shear stress τ_{12}
E_{11}	[MPa] or [GPa]	Young's modulus of a UD lamina longitudinal to fibre direction
E_{22}	[MPa] or [GPa]	Young's modulus of a UD lamina transversal to fibre direction
E_{45}	[MPa] or [GPa]	Young's modulus of a UD 45° lamina
G_{12}	[MPa] or [GPa]	Shear modulus of a UD lamina
ν_{12}, ν_{21}	[-]	Major and minor Poisson's ratio of a UD lamina
E_x	[MPa] or [GPa]	Young's modulus of a composite longitudinal to load direction
E_y	[MPa] or [GPa]	Young's modulus of a composite transversal to load direction
G_{xy}	[MPa] or [GPa]	Shear modulus of a composite
ν_{xy}, ν_{yx}	[-]	Major and minor Poisson's ratio of a composite
$[A]$	[MPa] or [GPa]	Matrix of the extensional stiffnesses of a composite
$[Q]$	[MPa] or [GPa]	Stiffness matrix of a material element in the lamina coordinate system
$[T]$	[-]	Transformation matrix from lamina to composite coordinate system
E_s	[MPa] or [GPa]	Secant modulus evaluated from a stress-strain hysteresis loop
$ E^* $ or E_{dyn}	[MPa] or [GPa]	Dynamic modulus evaluated from a stress-strain hysteresis loop
R	[-]	Ratio of minimum force to maximum force in a cyclic test

σ_a	[MPa]	Nominal stress amplitude
σ_m	[MPa]	Nominal mean stress
σ_{max}	[MPa]	Nominal maximum stress, highest stress in a cyclic test
σ_{min}	[MPa]	Nominal minimum stress, lowest stress in a cyclic test
$\sigma_a \text{ at } 5*10^6$	[MPa]	Nominal stress amplitude after $5*10^6$ cycles
$\sigma_{max} \text{ at } 5*10^6$	[MPa]	Nominal maximum stress after $5*10^6$ cycles
N	[-]	Number of cycles
N_f	[-]	Number of cycles to failure
k	[-]	Slope of a S-N curve
T_s	[-]	Scatter width of a S-N curve